Sustainably dyed and functionalized biobased poly (lactic acid) fibers for textile applications

Sustainably dyed and functionalized biobased Poly (Lactic Acid) fibers for textile applications

An in-depth Investigation of the effect of multifunctional colorants on the properties of PLA

by ***Naveen Kumar Balakrishnan***

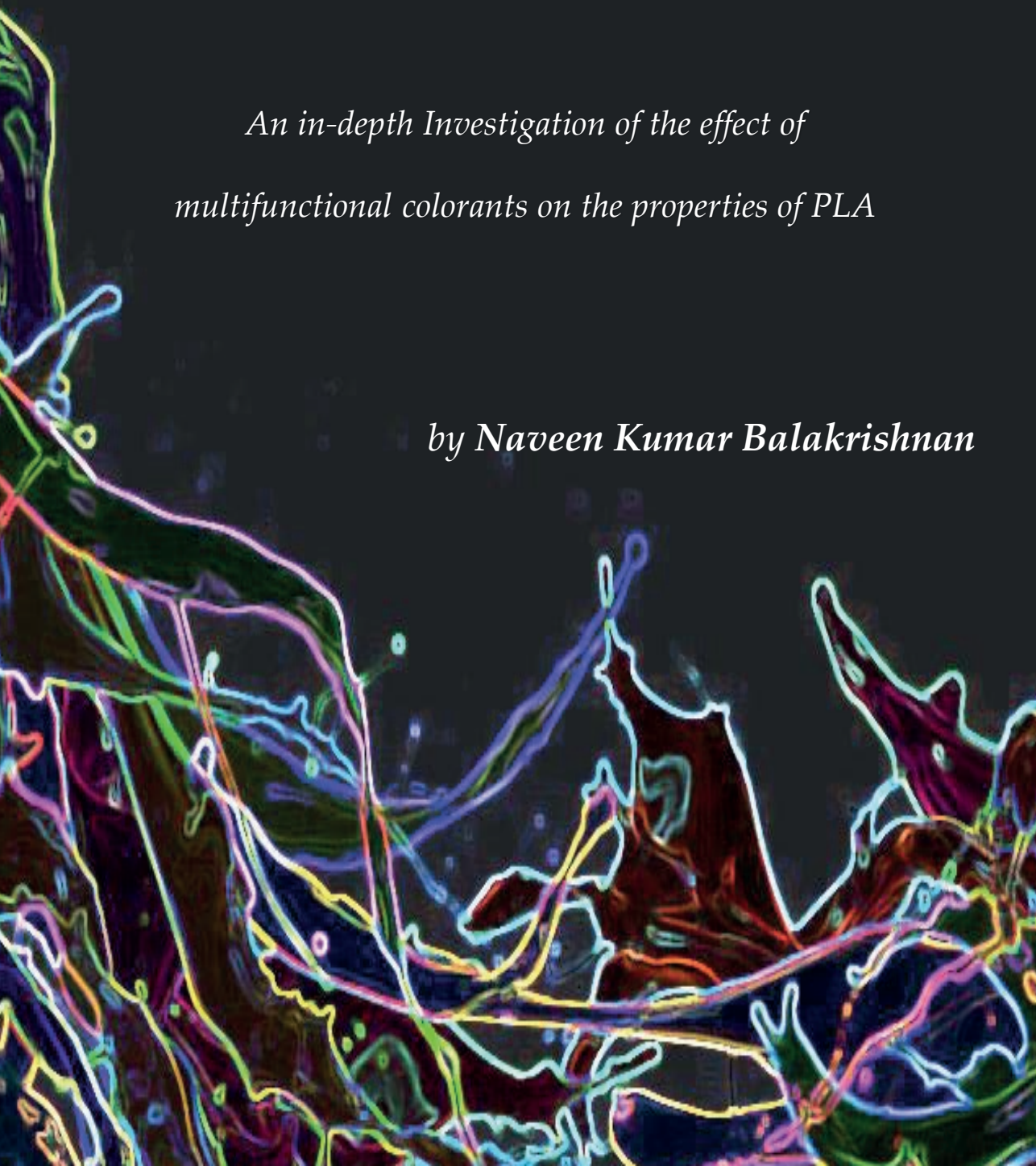

Sustainably dyed and functionalized biobased Poly (Lactic Acid) fibers for textile applications

An in-depth Investigation of the effect of multifunctional colorants on the properties of PLA

Naveen Kumar Balakrishnan

Sustainably dyed and functionalized biobased Poly (Lactic Acid) fibers for textile applications

An In-depth Investigation of the effect of multifunctional colorants on the properties of PLA

Balakrishnan, N.K.

Maastricht University, 2023

Cover design: © Sandhiya Srinivasan

Printing: ProefschriftMaken (www.proefschriftmaken.nl)

ISBN: 978-94-6469-640-0

Sustainably dyed and functionalized biobased

Poly (Lactic Acid) fibers for textile applications

An in-depth Investigation on the effect of multifunctional colorants on the properties of PLA

DISSERTATION

to obtain the degree of Doctor at the Maastricht University,

on the authority of the Rector Magnificus,

Prof. dr. Pamela Habibović

In accordance with the decision of the Board of Deans,

to be defended in public

on Monday 06th November 2023 at 13:00 hours

by

Naveen Kumar Balakrishnan

Supervisor

Prof. dr.–Ing. habil. Dipl.–Wirt. Ing. G.H. (Gunnar) Seide

Co-Supervisor

Prof. dr. rer. nat. R. (Robert) Groten, Hochschule Niederrhein

Assessment Committee

Prof. dr. med. Stefan Jockenhövel (Chair)

Dr. Roy Dolmans, Oerlikon Manmade Fibres & Co.KG

Prof. dr. Christian Hopmann, RWTH University

Prof. dr. Kim Ragaert

This project is as a part of the Beauti-fully Biobased Fibers Project granted by RAAK-PRO program with project number 02.107, which is partly funded by the Dutch Agency for Applied Research (SIA).

Abbreviations

% (w/w)	Percentage by weight
AMIBM	Aachen-Maastricht Institute for Biobased Materials
ANOVA	Analysis of variance
DSC	Differential scanning calorimetry
DF	Drawn filament
DIN	Deutsches Institut für Normung
FPV	Filter pressure value
GPC	Gel permeation chromatography
MFI	Melt flow index
MDR	Melt draw ratio
PDI	Polydispersity index
LF	Low-oriented filament
POM	Polarized optical microscopy
RCS	Relative color strength
SD	Standard deviation
SSD	Solid-state draw ratio
SEM	Scanning electron microscopy
TGA	Thermogravimetric analysis

Material abbreviations

A	Materials containing alizarin
B	Materials containing blue pigment 15:1
G	Materials containing green pigment 7
H	Materials containing hematoxylin
HFIP	Hexafluor-2-isopropanol
I	Materials containing indigo
LA	Compounds containing alizarin and liquid plasticizer
LH	Compounds containing hematoxylin and liquid plasticizer
LQ	Compounds containing quercetin and liquid plasticizer
P	Materials containing pink pigment PR122
PET	Polyethylene terephthalate
PLA	Polylactic acid
PP	Polypropylene
Q	Materials containing quercetin
Y	Materials containing yellow pigment 155

Physical variables

F_C	Coulombic force
F_{EF}	Electrical field strength
F_G	Gravitation
ℓ	Distance/length
M, α	Mark-Houwink constants
M_n	Number-average molar mass
M_w	Weight-average molar mass
T_{cc}	Cold crystallization temperature
T_g	Glass transition temperature
T_m	Melting temperature/point
X, Y, Z	Charges in the jet
X_c	Percentage crystallinity
$\dot{\gamma}$.	Shear rate
η	Effect strength
η'	Shear viscosity
η^*	Complex viscosity
σ	Electrical conductivity
V_i	Extrusion velocity
V_f	Take up velocity

Contents

Chapter 1

Introduction, aim, scope, and outline

1.1 Introduction

The global textile industry holds a significant position in the economy, playing a crucial role in our daily lives. This versatile sector has a wide range of applications, from clothing and household textiles to industrial and technical textiles, as well as medical filters and membranes. The textile industry is highly globalized, with production chains spanning the world. In 2020, the European textile and clothing industry consisted of 160,000 companies, employed 1.5 million people, and generated a revenue of €162 billion [1]. The diverse sectors that utilize textile fibers are outlined in Figure 1.1 below [2].

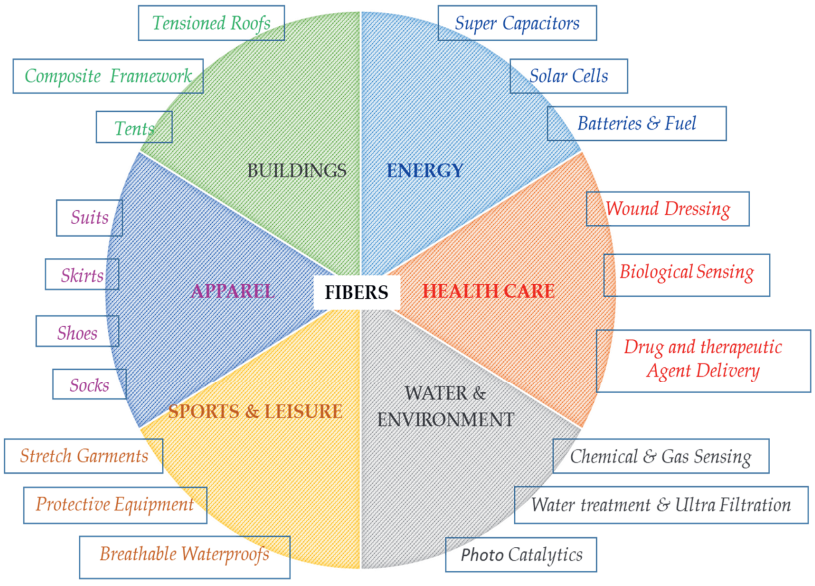

Figure 1.1: Fiber applications (qualitatively observed) in different textile sectors [2]

Among the various textile sectors, the apparel sector is one of the largest, with a market size of around €1.41 trillion in 2021 [3]. Synthetic or man-made fibers make up about 70% of the material used in the textile industry, with production reaching 80.9 million tons in 2020 and expected to grow even more in the coming years with polyethylene terephthalate (PET) being the primary player accounting for 48 million tons [4]. However, the textile sector's dependence on fossil resources contributes to global warming, and CO_2 emission making it unsustainable. To meet the sustainability goals

set by the European Union, the European textile market is shifting towards sustainable materials that has low CO_2 emissions. Biobased materials such as Polylactic acid (PLA) is a good alternative for that. It can be synthesized from sustainable sources like cornstarch, potatostarch and is compostable under industrial composting conditions. Despite being made from cornstarch, it only uses less than 0.02% of the crop production and requires half the fossil resources required by other fossil-based polymers [5]. The market size of PLA reached 2.11 million tons in 2019 and continues to grow [6]. In Table 1.1, the properties of PLA are compared to other commonly used polymers such as PET, polyamide 6 (PA6), and polypropylene (PP).

Table 1.1: Properties of PLA, PET, and PP [7-10]

Properties	**PLA**	**PET**	**PP**	**PA6**
Glass transition temperature (°C)	55-60	70-80	-10	57-65
Melting point (°C)	170-180	255-260	155-165	220-225
Density (g/cm^3)	1.24	1.38	0.92	1.14
Tensile modulus (GPa)	3.83	1.40	11.01	1.10-15.86
Elongation at break (%)	6	2-70	400	2-67
Flexural Modulus (GPa)	3.69	1.38-8.27	1.50	1.17-13.79
Limiting oxygen index (%)	24	19	20	20

As observed from Table 1, PLA's mechanical properties are a little subpar to the conventionally used polymers but PLA offers superior moisture management and flame retardance compared to PET making it a promising sustainable alternative polymer for textile applications [11-13]. Adding color to polymer materials is fundamental for various textile applications because appearance is one of the first things that influences consumer's buying decisions. The global market of colorants is expected to reach €98 Billion until 2030. Conventionally textile products are dyed by exhaust dyeing and exhaust dyeing of PLA can be hindered by its hydrolytic degradation and low thermal stability [14-16]. Besides, in exhaust dyeing, a water bath is used to dye the yarn or fabric, with auxiliary chemicals added to aid dye fixation. These chemicals are also fossil-based, toxic in most cases and apart from this, up to 25% of the dye is wasted in the dyeing bath

and ends up polluting water bodies, making textile industries one of the largest water polluters [17,18]. Since exhaust dyeing of PLA is challenging because of its hydrolytic degradation, low thermal stability and is not feasible from the sustainability perspective, an alternative dyeing process is required to fully embrace the shift towards a greener future. Dope dyeing, where the colorant is added to the polymer before melt spinning eliminating the need for auxiliary chemicals and water, is a potential candidate [19].

Colorants are multifunctional and the utilization of colorants in polymer materials has the potential to provide more than just color. For ex., these colorants can offer additional functionalities such as being antimicrobial and nucleating. For example, the addition of certain pigments to polypropylene (PP) has been shown to promote crystallization [20]. Similar to PP, PLA has a low crystallization rate. By adapting the dope dyeing process for polylactic acid (PLA), it not only eliminates the issue of hydrolytic degradation that occurs during exhaust dyeing, but it may also improve the crystallization rate, potentially leading to higher productivity. Furthermore, colorants such as carbon black and copper phthalocyanine have been used in electronics because of their favorable electrical properties. They can be added to the PLA to enhance its electrical performance [21]. In addition, biobased colorants such as curcumin and alizarin offer antibacterial properties against various microbes, making them ideal for developing antimicrobial textiles [22].

With the Covid-19 pandemic, the demand for masks skyrocketed and the global filtration market was estimated to reach €32 billion in 2022, dominated by fossil-based PP and polyethylenesulfone [23]. Melt blowing is a process commonly used to produce such filter materials but the machine design is complex and would need to be optimized for each material and is also limited to low micrometer ranges. In contrast, electrospinning can be more versatile. A charged electric field to draw a polymer liquid here to produce fibers with diameter in the submicro and nano range. Polymer liquid with low viscosity and high electrical conductivity are preferred for this process. So solution electrospinning, which uses a polymer solution, is more commonly used due to low viscosity and high electrical conductivity of polymer solutions. However, the solvents for PLA, such as chloroform and dichloromethane, are toxic, making the process unsustainable and environmentally harmful [24-27]. On the other hand, melt electrospinning can be more sustainable, but the unfavorable viscosity and poor electrical conductivity of polymers make it challenging to produce fibers with diameters

in the submicro and nanorange. Additionally, to provide even antimicrobial properties to filters, extra additives remain necessary [23].

Incorporating multifunctional colorants into PLA can lead to the improvement of electrical and antimicrobial properties of PLA leading to production of thinner fibers in melt electrospinning for potential filtration applications. Dope dyeing of PLA can be a potential sustainable alternative to produce PLA based apparels and the suggested approaches can advance the production of sustainable textile products.

To get a deeper understanding surrounding the production of PLA fibers, this chapter aims to provide a brief overview of the current knowledge and understanding of PLA, with a specific focus on its manufacturing methods, namely spinning, dyeing, and electrospinning. Finally the chapter will be concluded with a discussion of scope, objectives and outline of the thesis, providing a clear roadmap of the research.

1.2 Fiber manufacturing techniques

The functional requirements of fibers vary based on the application they are used for. In the apparel industry, factors such as breathability, haptic, and color are crucial, while mechanical properties such as tensile strength, creep, shrinkage, and density play a more significant role in reinforcement applications. For filtration applications, the pore size and specific surface area of the fiber are critical factors. The fiber diameter and the processing are adapted to meet the specific requirements. For example, fibers with a diameter range of 10 - 100 μm are commonly used in the apparel sector, while submicro (fibers with a diameter less than 1 μm) and nanofibers with a diameter less than 100 nm are preferred for filters to achieve the required filtration efficiency [28]. The dependency of specific surface area of the fibers on the fiber diameter and the common range of diameters used in different applications are presented are shown in Figure 1.2.

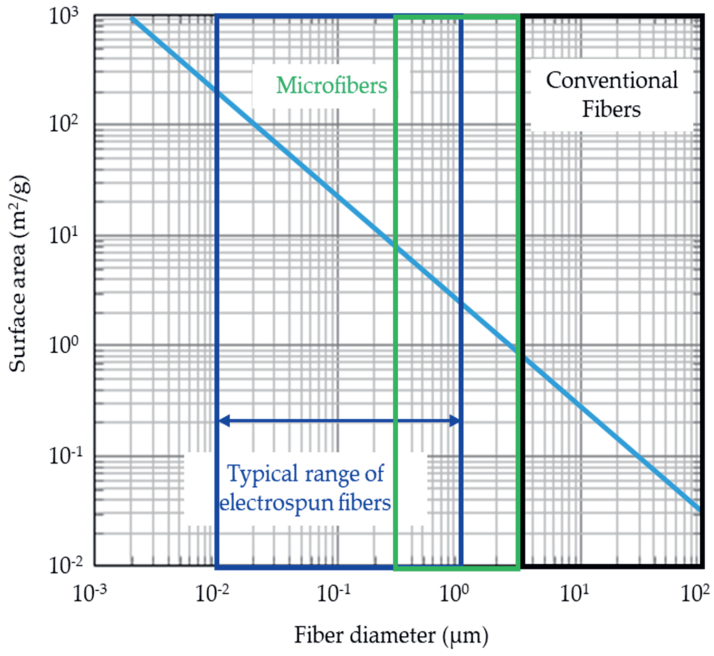

Figure 1.2: Effect of fiber diameter on specific surface area and common range of diameter used for different textile applications [29]

As different applications require different fiber sizes and functionalities, various technologies are necessary to fabricate such fibers. In Figure 1.3, a brief overview of the different techniques used to produce different fiber diameters is shown [30]. These technologies include electrospinning, melt spinning, solution spinning, dry-jet wet spinning, and more. The selection of the appropriate technology depends on the desired fiber diameter, fiber functionality, production rates, quantities and target application. With advancements in technology, new techniques and methods are being developed to produce fibers with even smaller diameters and improved functionalities.

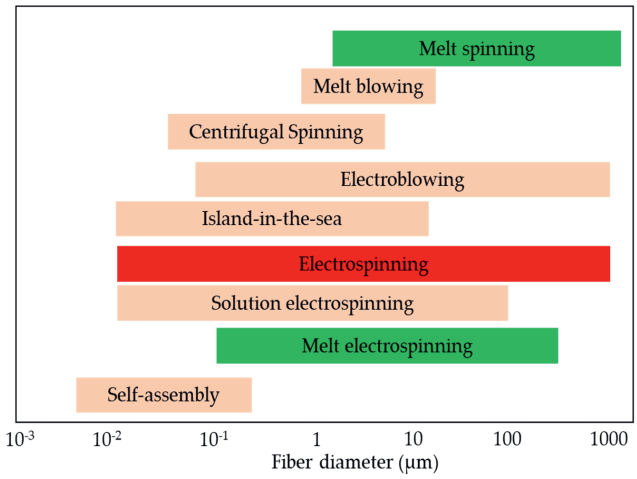

Figure 1.3: Fiber fabrication techniques [31-35]

To better understand the current state of fiber fabrication, it is important to consider the different techniques available and how they are utilized based on the desired application. Though there are multiple methods, melt spinning is the most commonly used for apparel fibers due to its high production rates and versatility [36]. Melt blowing is used to produce fibers with diameters in the low micrometer range but is limited, when producing fibers in the submicro and nano range. Furthermore, it can be expensive because of the complex machine design and would need to be optimized for each material. To overcome these shortcomings, electrospinning is widely researched for submicro and nanometer fibers because of its straightforward machine design and its full potential is yet to be unveiled [31]. In the next sections, we will delve into the technicalities of both melt spinning and electrospinning to gain a deeper understanding of their principles, process factors, and current advancements made for processing PLA in the field.

1.3 Production of conventional textiles through melt spinning

The value chain of man-made textile garment production is presented below in Figure 1.4. Among the different steps involved in production of a textile garment, melt spinning and dyeing are considered here.

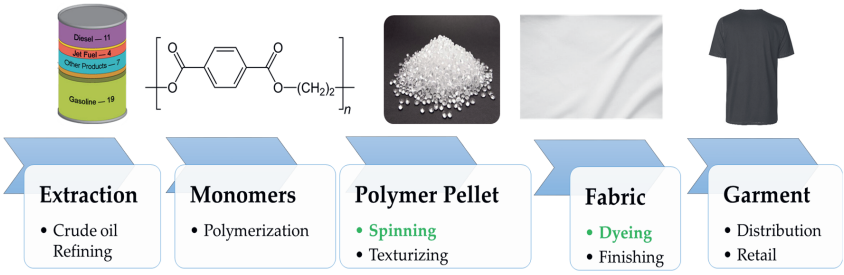

Figure 1.4: Conventional value chain of garments [37]

1.3.1 Melt spinning process

Melt spinning is a process used to produce filaments from polymer granules. The polymer is melted with the help of shear and heat inside a single-screw extruder, then transported under high pressure to the spinning head via a melt pump. At the spinning head, the melt is forced through small orifices in the spinneret, creating the desired shape of the filaments. The filaments are cooled with air in a quenching chamber and treated with spin finish (oil) for lubrication. They are then drawn with rolls or godets and wound onto bobbins using a winder [36]. The process is depicted in Figure 1.5 below.

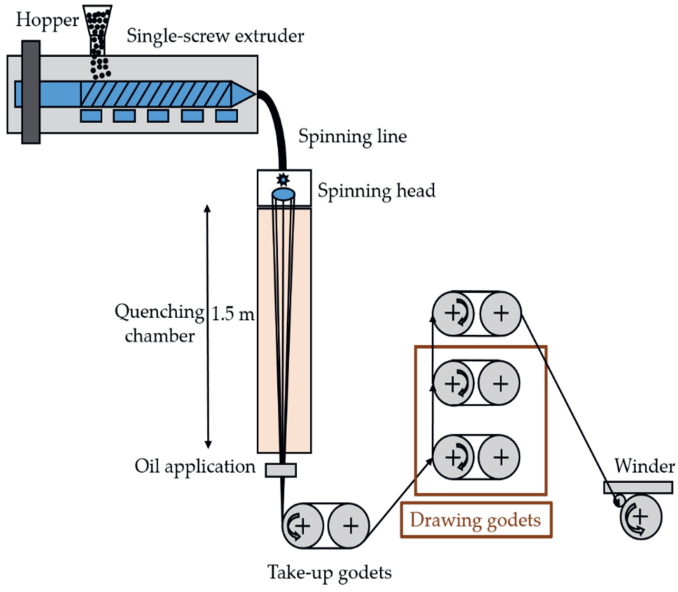

Figure 1.5: Melt spinning proces schematic [38]

The speed at which the polymer melt leaves the spinneret is called the extrusion speed (V_i). There is close to no molecular orientation before this in the polymer melt. When the polymer melt is drawn with the help of godets, strain is applied on it and this induces orientation in the polymer chains promoting crystallization. The speed at which the take up godet runs is called take up speed (V_f). The ratio between the filament take up speed and the extrusion sped is called the melt draw ratio (MDR) as shown below in Eq. 1.1. It is typically between 40 and 600 depending on the type of filament yarn being spun [39].

$$MDR = {V_f}/{V_i} \qquad \textbf{Eq. 1.1}$$

The second parameter that can affect orientation and crystallinity is the strain rate, i.e., the rate at which drawing is applied. This depends on the overall throughput (extrusion speed) and take up speed used during processing. The drawing force and drawing rate applied together act as an external stimulus and accelerates the formation of crystalline region (Figure 1.6).

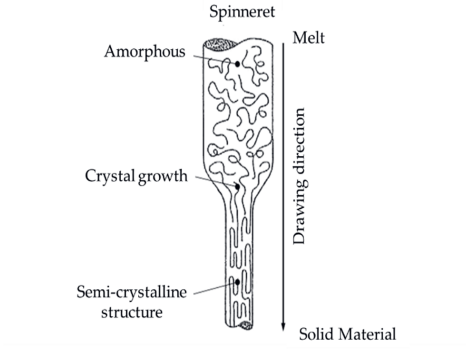

Figure 1.6: Structure development in melt spinning [36,40-42]

The filaments can also be heated after taken up and drawn between godets running at different speeds leading to more orientation. The ratio with which this is performed is called solid-state draw ratio (DR) and this can be calculated from the take up speed (V_f) and the winder speed (V_2) as shown in Eq. 1.2. It is normally between 2 and 5.

$$DR = {V_2}/{V_f} \qquad \textbf{Eq. 1.2}$$

In addition to the extrusion and take up speeds, a number of machine and material parameters impact the properties of the multifilament produced through the melt

spinning process. These parameters include the spinning temperature, cooling rate, and the inherent material properties like crystallization rate, viscosity and molecular weight [36,40]. For applications such as apparel, low-oriented yarns (LOY) and partially-oriented yarns (POY) are usually used, where these yarns are drawn directly from the melt and then wound. LOYs are produced with winder speeds between 800 m/min and 1300 m/min, resulting in low orientation and mechanical properties. POYs are produced with winder speeds between 3000 m/min and 5000 m/min, resulting in stronger stress-induced orientation of the yarn. The LOYs or POYs can then be draw texturized and turned into textile products. A summary of the key parameters affecting the melt spinning process is provided in Table 1.2.

Table 1.2: Parameters affecting the melt spinning process

Polymer parameters	**Process parameters**
Molecular weight and distribution	Temperature
Viscosity	Spinneret nozzle diameter, L/D ratio
Stereochemical purity (in case of PLA)	Melt draw ratio
Crystallization rate	Solid-state draw ratio
Glass transition/ melt/ degradation temperature	Humidity & quenching rate

1.3.2 Dyeing Technology

Color is the first thing that comes into a customer's mind when purchasing new clothing. Colorants (classified as dyes and pigments) are used for coloring textiles. The global textile colorant market reached €8 billion in 2021 and was expected to grow at 6.57% annually [43]. It has been estimated that around 3600 different dyes and 8000 different chemicals are being used by textile industry today [44]. Biobased dyes, extracted from various parts of plants, were used in the ancient times. However, the yield was low and the stability was also poor in some colorants. Therefore, with the development of fossil-based dyes, they are used more commonly for dyeing the fabrics [45]. They are more stable and form more brilliant colors. Exhaust dyeing is the conventionally used dyeing

method to dye textiles and dyes are used here. A schematic of exhaust dyeing is presented below in Figure 1.7.

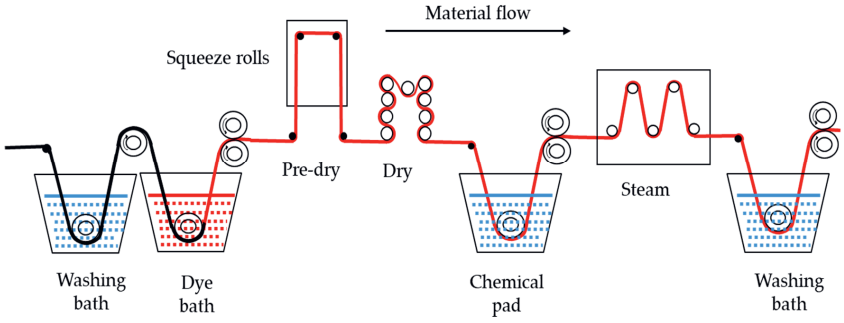

Figure 1.7: Schematic of exhaust dyeing [46]

In exhaust dyeing, the yarn or a fabric is dipped in a bath containing dye and other auxiliary chemicals. The dyeing works by transfer of dyes from bath to the textile material. The dyeing process takes place in two steps: Preparation, and dyeing. In the first step, the impurities in the fabric are removed using alkaline water solution and detergent. Depending on the type of material used, an additional bleaching step may be necessary to ensure whiteness of the fabric [46]. In the second dyeing step, the dyes are applied to the fabric. The size of dye molecule, the temperature of the dye bath and the crystallinity of the polymer are major factors affecting the dye take up. A large dye particle size, low dye bath temperature, and high crystallinity of the fabric are harmful for the exhaust dyeing process. Although dyes diffuse into the fabric during the dyeing process, auxiliary chemicals are required to fix them in the fabric [46]. After this step, the dyed fabric is washed and rinsed to remove the excess non-fixed dyes.

Although widely used, exhaust dyeing is reported to be environmentally unfavorable. During the dyeing process, about 10-25% of the dye can be lost, 2–20% of which is directly discharged into rivers and streams along with the toxic fixatives [17]. This is one of the reasons behind textile industry being the second greatest polluter of water resources [18]. A more sustainable alternative to this is the mass coloration or dope dyeing process, where the colorant (dyes and pigments can be used here) is incorporated into the polymer melt during fiber production. A comparison of dope dyeing and exhaust dyeing of polyamide 6 revealed that dope dyeing reduces water use by ~40%,

chemical use by 97%, waste by ~50%, and the overall number of processing steps [19]. A schematic overview of the dope dyeing process is presented below in Figure 1.8.

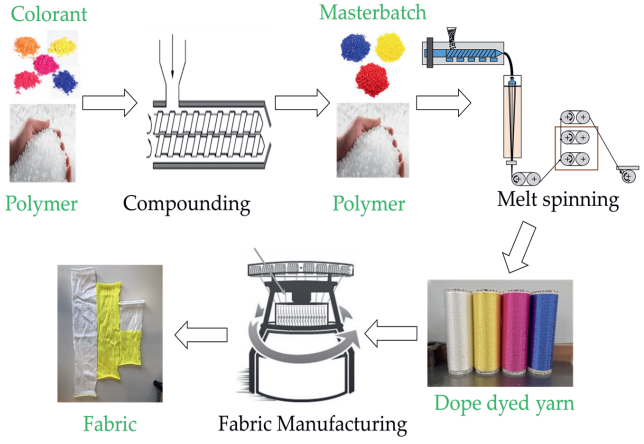

Figure 1.8: Overview of dope dyeing process [97]

A masterbatch is created by compounding a colorant at a concentration ranging from 5-40% using a twin-screw extruder. This masterbatch is then added to the polymer to achieve the desired color shade in the final product - the colored filaments. Proper dispersion of the colorant in the polymer is crucial for achieving an even color distribution [47]. Dyes are easier to disperse because they can be soluble in the polymer, unlike pigments which do not dissolve. Improper mixing can cause the colorant particles to form clumps, known as agglomerates and aggregates [48]. The degree of dispersion and the tendency of the pigments to agglomerate depend on the physical properties of the particles [49]. For optimal results, it is important to minimize the number of clumps, as shown in Figure 1.9.

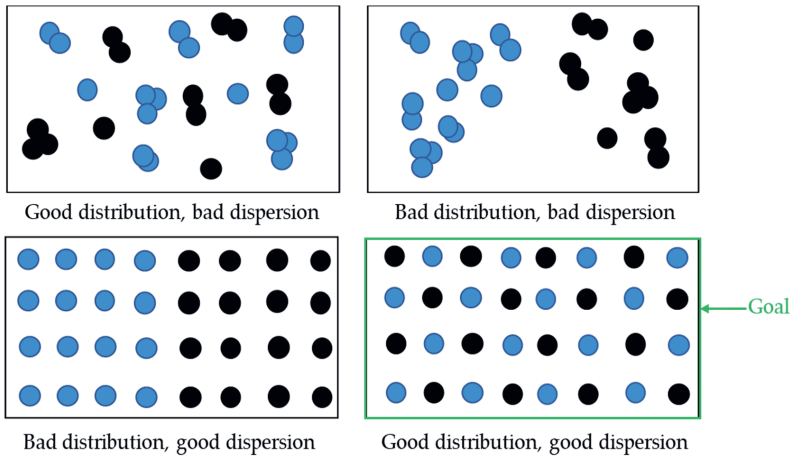

Figure 1.9: Dispersive and distributive mixing of colorants in polymer matrix [50]

Aggregation not only hinders proper dispersion but also can lead to technological limitations such as weakened mechanical strength in fibers, breakage during spinning, and difficulties in achieving the desired color of the final product. This can result in increased production time and waste, causing economic disadvantages [50]. To address this issue, researchers have focused on improving colorant dispersion in polymer matrices. For example, Deshmukh et al. compared pigment dispersion in a low-density polyethylene matrix using two types of masterbatches. Buccella et al. explored the impact of processing parameters on the dispersion and coloration of a green organic pigment masterbatch [52]. The best way to obtain fine pigment dispersion was found to be a compounding process involving three extrusions without filtration, resulting in a reduction in filter pressure and an increase in relative color strength (RCS) [53]. In Table 1.3 below, a comparative analysis between exhaust dyeing and dope dyeing is presented.

Table 1.3: Comparison of exhaust and dope dyeing [46, 51]

Exhaust Dyeing	**Dope dyeing**
Most popular and common	Not as commonly practiced
Lots of colorants currently in use are compatible	Thermal stability of colorants (especially biobased colorants) is a limitation

Adding multiple shades or colors is easier	Getting multiple shades is not possible
Changing the color of the dye bath is easy. More suitable for production in smaller quantities.	Changing color of the multifilament spinning line is challenging. Lots of material is required for changing color. Therefore, production starts with darker shade and gradually moves towards lighter shades. More suitable for production in large quantities.
High water and chemical usage	Close to no water and chemical usage
Effluents lead to water pollution	Does not lead to water pollution
A large amount of dye used can stick to the bath and become wastage	Close to no dye wastage but lot of material is required when color needs to be changed
Additional chemical treatments are required to improve fastness properties	Since colorants are mixed directly into the polymer melt, fastness properties are good even in the absence of additional chemical treatments
Preferred for dyeing materials in lower quantities	Preferred for dyeing materials in larger quantities
Only the outer shell is dyed	Textile material is dyed, color is scratch/abrasion proof

Previously we looked into technical aspects of melt spinning and dyeing. In the next subchapter, melt spinning and dyeing of PLA is discussed.

1.3.3 Melt spinning and dyeing of PLA

- **Melt spinning of PLA**

Polylactic acid (PLA) is a highly sought-after biobased polymer, and its suitability for melt spinning has been studied for over a decade. While PLA has excellent fiber-forming properties, it is prone to thermal and hydrolytic degradation. To mitigate this, proper

drying of PLA before melt spinning and proper spinning temperature are crucial in determining the properties of the yarn. In addition, PLA is brittle and has low crystallization rate. Blending with other polymers or additives have been attempted as ways to solve this. Table 1.4 provides a brief overview of selected attempts in the melt spinning of PLA.

Table 1.4: Overview of literature on melt spinning of PLA

Publication	**Short description**	**Findings**
Siebert et. Al [52]	Investigation of effect of nucleating agents [Talc and Bis(hydroxyethyl)terephthalate (BHET)] on the crystallinity of industrially melt spun PLA.	It was observed that the take up velocity and solid-state draw ratios influenced the crystallinity of the filaments spun and the nucleating agents did not affect the crystallinity significantly.
Maqsood et. Al [7]	A PLA based sock was developed by melt spinning, texturizing, and knitting. The thermophysiological properties of the socks were measured and statistically modelled.	It was observed that the thermal conductivity was better when knitting socks containing single jersey structure with single jersey structure. Single jersey structure also led to better vapor diffusion, air permeability but had lower thermal resistance compared to rib structure.
Wiessner et. Al [53]	PLA/PCL blends were produced with the help of reactive processing induced by electrons. Melt spinning was carried out with the resulting blend. The goal was to	The melt strength and elastic recovery of the blend were improved. The toughness of PLA

	use PCL to improve the toughness and crystallization speed of PLA.	could be increased up to 2.4 times.
King et. Al [54]	Melt spinning was carried out with various parameters and its effect on properties of PLA was investigated. The process parameters that were varied included melt temperature, throughput, take up speed, winding speed, solid-state draw ratio.	The mechanical properties could be increased from 3 cN/tex to about 40 cN/tex by optimizing the processing conditions. The degree of crystallinity also increased from 14.6% to 62.2%. However, molecular weight was observed to decrease due to processing.
Kikutani et. Al [55]	The fiber structure development during melt spinning of PLA was investigated. Several PLA grades with varying optical purity were melt spun and effect of increasing D-content on the properties of melt spun PLA were investigated.	High take up speeds of upto 10000 m/min were achieved. It was observed that the birefringence and crystallinity of the fiber obtained reduced with increasing D-content and the mechanical properties increased with increasing take up speed.
Maqsood et. Al [56]	Intumescent flame retardant and biobased carbonization agents were compounded with PLA. Melt spinning was later carried out with the composites and the effect of the additives on the flame retardancy and melt spinnability of PLA was examined.	The flame retardancy of PLA improved with increasing weight percentage of additives. However, this reduced the stability of the melt spinning process and led

		to filaments with low mechanical properties.
Aoutat et. Al [57]	Composites of PLA/cellulose nanowhiskers and PLA/ microcrystalline cellulose were prepared by melt compounding. A compatibilizer based on PLA-grafted maleic anhydride was added during compounding. The composites were melt spun and the properties of the as-spun filaments were tested.	Incorporation of microcrystalline cellulose resulted in reducing the spinnability because the dispersion was poor despite the use of compatibilizer. However, thermal stability, flame retardancy, improved with the addition of cellulose nanowhisker.
Youngblood et. Al [58]	Nanocellulose was used as reinforcing agents to improve the stiffness and strength of melt spun PLA filaments. Polyethylene glycol was used as a compatibilizing agent.	Melt spinning of the PLA nanocellulose composite was possible with the help of compatibilizing agent. The strength was not affected much by the addition of nanocellulose but the stiffness increased upto 600%.
Srisawat et. Al [59]	PLA was blended with another biopolymer polybutylene succinate (PBS) at different weight percentages. PBS is a ductile material and the goal of blending was used to improve the brittleness of PLA.	It was observed above 10% (w/w), PBS is not miscible in PLA and phase separation occurred. When added in lower quantities, PBS improved the elasticity of PLA but this led to reduction in crystallinity.

Fritz et. Al [60]	Various grades of PLA were melt spun with different winding speeds between 2000-5000 m/min. The influence of winding speed on the tensile properties and crystallinity of the fibers were determined.	The maximum tenacity of 300 MPa, elongation of 30% were achieved. The stereo purity of PLA also affected the crystallinity obtained.
Zinn et. Al [61]	Bicomponent fibers were melt spun using Poly[(3-hydroxybutyrate)-co-(3-hydroxyvalerate) (PHBV) and PLA. PHBV is a slow crystallizing biopolymer and this makes its melt spinning challenging. To overcome this hinderance, core/sheath bicomponent spinning was carried out with PHBV and PLA.	The bicomponent fibers could be melt spun. Tensile strength of 0.34 GPa was achieved. It was observed that PLA was responsible for the tensile strength and the fibers were also biocompatible.

- **Dyeing of PLA**

Polyesters, such as PLA, are typically dyed with disperse dyes, which are sparingly soluble in water. Polyethylene terephthalate (PET) is the most widely used polyester in textiles and its dyeing process is well established. PET is typically dyed at high temperatures of around 130°C, and in some cases, carriers are used to aid dye diffusion into the substrate [62,63]. Nakpathom et al. found that dyeing PET fabric with natural colorants extracted from annatto seeds at 130°C for 30 minutes provided the best results [64]. However, high-temperature dyeing can cause dye liquor to evaporate, so alternative methods such as using ionic liquids as dye carriers or dyeing in pressured vessels have been proposed [65]. Lindström et. Al investigated the chemical and physical changes in PET fibers due to exhaust dyeing and found that the dyeing process resulted in changes in tensile strength, crystallinity, and moisture-related properties [63]. Since PLA is also a type of polyester, disperse dyes are expected to be effective for dyeing it. However, dyeing PLA at same conditions as PET led to hydrolytic degradation of PLA and loss of mechanical strength. Therefore, researchers started looking into dyeing of PLA and in the Table 1.5 below, some of the key findings are reported.

Table 1.5: Overview of current progress in dyeing of PLA

Publication	Short description	Findings
Tavanie et. Al [66]	PLA produced from disposal packages were melt recycled and melt spun. The melt spun fibers were exhaust dyed at low dyeing temperature with three disperse dyes (C.I. Dispersse Yellow 3, C.I. Disperse Yellow 64, and C.I. Disperse Red 167).	Dyeing of recycled PLA at low temperature was possible using disperse dyes with low molecular weight. The washing fastness was assessed to be very good.
Khoddami et. Al [67]	The influence of irradiation with UV/Ozone on the dyeing behavior of PLA and PET fabrics were investigated. Pretreatment with sodium silicate solutions, distilled water, and hydrogen peroxide were applied prior to irradiation and their influence on dyeing performance was studied.	The color depth increased after irradiation with all three pretreatments. It was hypothised that it came from roughening of the surface of the fabric induced by irradiation.
Khoddami et. Al [9]	The dyeing, washing, and finishing performance of dyed PLA fibers was compared with PET fibers.	The dye shades obtained on PLA are brighter than PET. The color yield of PLA was higher than PET. However, the color and wash fastness of dyes in PLA was observed to be lower.
Wilding et. Al [68]	Several disperse dyes were used to dye PET and PLA fabrics. Various finishing conditions were applied and their effect on the wet fastness of the dyes was investigated. Furthermore,	All the tested properties except thermal migration appeared to be similar between PLA and PET fabrics. Thermal migration of dye occurred in PLA during heat

	perspiration and rubbing fastness of the dyed fabric was inspected.	treatment and this led to lower color fastness.
Farrington et. Al [69]	The colorfastness and thermal migration of 5 different disperse dyes with differing hydrophobicity was investigated in softened PLA and PET fabrics. 5 different softeners were also used in the study to investigate the change in properties.	The wash fastness, alkaline perspiration, and wet-rub fastness of PLA fabrics was poorer than PET. It was observed that hydrophobicity of the dyes and the softener did not affect the wash and wet-rub fastness of PLA. However, the dyes with higher hydrophobicity led to reduction in alkaline perspiration fastness. Hydrophobic nature of the dye may have had a slight influence on the alkaline perspiration fastness.
Freeman et. Al [70]	Yellow azo-anthraquinone disperse dyes were synthesized and used for dyeing polylactide fibers. Azo-anthraquinone dyes were made from 1-aminoanthraquinone. The structure of the extracted dye was confirmed with mass spectroscopy and its dyeing performance on PLA fabric was assessed.	It was observed that the anthraquinone dyes have high affinity towards PLA. Dyeing at 90 °C with a pH of 5.0 and a dyeing time of 60 min was found to be optimal. The wash and light fastness of the dyed fabric were good.
Yang et. Al [16]	When the dye has a structure similar to PLA, it is considered to have good affinity to PLA. Several model dyes were synthesized with hydrophobic chains similar to PLA and their	The synthesized model dyes had exhaustions over 85% at 110 °C on PLA. This was significantly better than the conventional disperse dyes. The light fastness of the dyes

	performance as dyes was investigated.	was satisfactory and it increased upon addition of halogen atoms but the exhaustion reduced.
Baig et. Al [15]	The hydrolytic stability of fabrics made with PLA was investigated by subjecting PLA fabrics to scouring, bleaching, and dyeing under different conditions of temperature, time, and pH.	It was observed that scouring had to be performed close to glass transition temperature. Bleaching with hydrogen peroxide was detrimental to the fiber structure and led to loss of mechanical property. Dyeing at higher temperature and high processing times also led to degradation and loss of mechanical properties.
Yiqi et. Al [71]	The effect of repeated cleaning at different pH levels, washing temperatures and drying were investigated. 50 cleaning cycles at pH level of 8 and 10, washing temperatures of 35 °C and 55 °C and drying at 21 °C and 50 °C was applied and the breaking tenacity, elongation, and modulus of the PLA yarns were measured after every 10 cycles.	It was observed that increasing the pH led to greater loss of tenacity, elongation, and modulus. The mechanical property retention was good when PLA was washed at 35 °C and air dried.
Yang et. Al [14]	A solvent dyeing process was proposed as an alternative to the exhaust dyeing process normally carried out using water. Since dyeing PLA in a water bath at high temperature leads to degradation, reduction of mechanical properties, and changes in crystallinity, an	PLA fabric dyeing was successful and the color fastness was comparable to PLA dyed in a water bath. However, there was a mechanical strength loss induced by thermal disorientation. Nevertheless,

	alternative approach is proposed with the use of a liquid paraffin bath.	the strength could be improved by post heating treatment.
Fu et. Al [72]	Polylactic acid grafted carbon black (PLA-g-CB) was synthesized and used as black pigment to produce dyed PLA fibers. Carbon blacks with different particle sizes were used to synthesize the grafted PLA and the influence of particle size and amount of grafted pigment on color, strength, and crystallization of dope dyed PLA fiber were studied.	The dope dyed PLA fiber was reported to have good color property, good color levelling, high tensile strength, good crystallinity, and fastness. Water and ethanol migration resistance was found to be very good.

Short summary:

- PLA shows a lot of promise for melt spinning but its low thermal stability, brittleness, and slow crystallization rates limits its application in textile field.
    - Increasing the crystallinity of the fibers can lead to partial improvement in thermal and blending with other polymers is a potential approach to improve the brittleness.
    - Nucleating agents have shown to improve its crystallization rate but not in melt spinning.
- Polyesters such as PET have been conventionally dyed by exhaust dyeing at high temperatures.
- Dyeing PLA under similar conditions lead to hydrolytic degradation and loss of mechanical strength.
    - Attempts to optimize the dyeing conditions has given promising results but the dyeability is still not as good as PET.
    - Cold crystallization can also occur during dyeing leading to changes in mechanical strength and physical properties.
- Although practiced since ancient times, exhaust dyeing is not very sustainable since it uses large amounts of water and chemicals, which in turn leads to water pollution.

1.4 Fabrication of submicro and nanofibers using electrospinning

Melt spinning is an efficient production method for a broad variety of filaments, well known and the main process to produce fibers. A limitation of melt spinning is the production of thin filaments in submicro- or even nano-range. The limitation of the minimal achievable filament diameter lies in the application of mechanical force to draw the fibers [28,72]. The rotation of the godets is transferred into strain in the filaments by means of adhesion and friction. Hence, the influence on the filaments is high. Below a material specific drawing speed, the filament is stretched and undergoes viscoelastic deformation without fracture. Above this threshold value, the filament exhibits a more rigid behavior leading to breakage under this type of load application. High drawing speeds and ratios are necessary to achieve very low diameters [73]. Melt spinning is effective in achieving low diameters up to 10 μm but it is challenging to achieve lower diameters [28]. Therefore, other means of force application become necessary to achieve diameters in the submicro and nano range.

Electrospinning is an interesting method for producing ultra-fine fibers with diameters in the submicrometer range. It involves three key components: a high voltage source, a spinneret nozzle, and a collector plate. In electrospinning, a polymer solution or melt is pushed through a syringe and a charged electric field is applied. This causes the polymer to form a charged droplet, known as a Taylor cone [74]. If the viscosity of the polymer is low, it forms droplets but if it is high enough, the electrostatic repulsion will cause the droplet to form a charged laminar jet, which is then stretched into a fiber [31]. The polymer liquid used in this process can either be the polymer solution or a polymer melt. In case of a solution, the solvent evaporates leading to the formation of fiber and in case of a polymer melt, the solidification of the melt leads to the formation of fiber [75].

During electrospinning, two charged poles are used to create the electric field. This can be achieved either by charging the needle or collector or rarely both. They can also be positively or negatively charged. In Figure 1.10, the various electrospinning setups are shown [76,77].

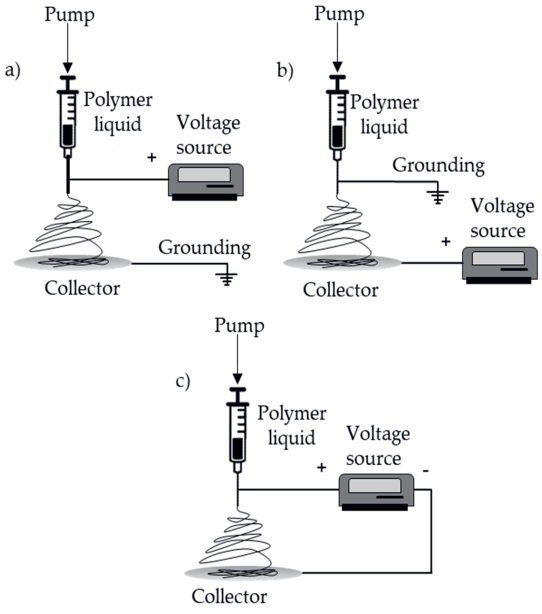

Figure 1.10: Electrospinning setups [77]

In solution electrospinning, since syringes are used to hold the polymer solution, all three setups can be used. However, in melt electrospinning, extruders are typically required for processing the polymer melt since the polymer melt viscosity is higher. In this case, if the nozzle is charged, the integrated extruder can also be affected by this causing irreversible electronic damage [32]. Depending on the type of charge applied, the forces acting on the fiber also changes, affecting the fiber diameter. Irrespective of the setup, the electric field strength (F_{EF}) and the gravitation (F_G) are the same but the polymer liquid jet is polarized to different extents and therefore the corresponding Coulombic forces (F_C) also differ, as shown in Figure 1.11. Charging the nozzle directly charges the polymer, whereas, when the collector is charged, the polymer needs to be charged indirectly through the gap between the nozzle and collector. Therefore, the charge density is low since the surface area of the collector is much higher than the nozzle's and the nozzle-collector distance also influences the charge density. This in turn leads to formation of thicker fibers [78].

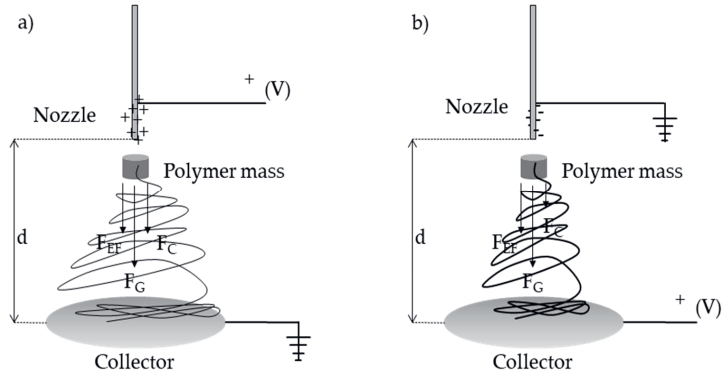

Figure 1.11: Forces acting in different electrospinning setups: a) charged syringe with a grounded collector b) charged collector with a grounded syringe [78]

When the polymer jet gets influenced by the applied electric field, various instabilities such as axisymmetric Rayleigh instability, and non-axisymmetric bending instability affect the drawing of the jet [79]. Rayleigh instability refers to the disintegration of the polymer jet into droplets. This leads to reduction of free surface energy. However, this is not beneficial for electrospinning since this disrupts fiber formation. The non-axisymmetric instability occurs when charged jets are exposed to an electric field. This is known as whipping and is preferred in electrospinning since it leads to formation of fibers without breakage and with every loop, the diameter of the loop gets larger leading to thinner fibers, which can also be oriented [80,81]. The whipping process is chaotic and the movement of the jet is uncontrolled. More whipping is experienced when the jet is highly charged. Therefore, higher electrical conductivity of the polymer liquid is preferred. The schematic of the instabilities is presented below in Figure 1.12.

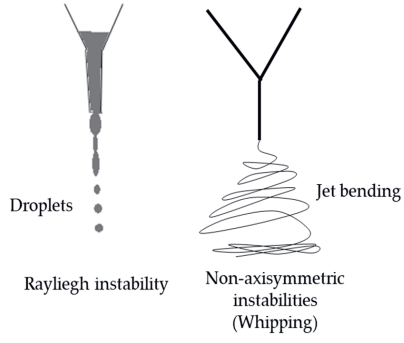

Figure 1.12: Different modes of jet instabilities [82]

The diameter of an electrospun fiber depends on several factors. The factors affecting the electrospinning process are presented below in Table 1.6.

Table 1.6: Parameters affecting electrospinning

Material characteristics	Machine parameters
Molecular weight	Temperature
Electrical conductivity	Electrical field strength
Viscosity	Flow rate
Crystallization	Nozzle diameter
Solution concentration	Air temperature and humidity
Surface energy	Nozzle to collector distance

- **Material characteristics**

Viscosity of the polymer liquid jet influences the fiber formation and whipping. Viscosity of a polymer depends on its molecular weight and the dependency is explained by the Mark-Houwink equation (Eq. 1.3) below [83].

$$[\eta] = KM^{\alpha} \qquad \textbf{Eq. 1.3}$$

Where η refers to the intrinsic polymer viscosity, M is the molecular weight, K and α are known as Mark-Houwink constants and are fixed for each polymer. During electrospinning, when the polymer jet is stretched, if the viscosity is too low, the jet breaks into droplets. However, if the viscosity is too high, the electric field applied might not be strong enough to influence the jet [84]. Therefore, low viscosity of polymer liquid is preferred to get fibers with small diameters.

- **Machine parameters**

The temperature of electrospinning affects the polymer liquid jet viscosity and also the electrical conductivity. The viscosity reduces with increasing processing temperature and above a certain point, the polymer starts to degrade. Therefore, the temperature of processing used should be high enough to have low viscosity but at the same time

should not lead to material degradation. A high electric field strength is expected to interact better with the polymer jet. However, if the electric field strength is too high, it could lead to flashes forming in the device and damage the device. The nozzle to collector distance needs to be optimum since with very high nozzle to collector distance, the effect of electric field will be very low on the polymer liquid jet, whereas if the collector is too close, there won't be any time for whipping to take place [31].

Solution electrospinning has been widely used currently. This is because in the solution form, the process functions at a lower temperature, and lower electrical voltage. Most of the polymers used commercially such as PET, PLA, and PP are not electrically conductive. When dissolved in a solvent, they become ionized and more conductive. Furthermore, the viscosity of polymer solution is very low compared to the viscosity of polymer melt. These two properties combined make solution electrospinning more favorable [85]. Fiber diameters of lower than 100 nm have been achieved with this process. However, in comparison, melt electrospinning is relatively new and more challenging. Compared to PP, that has no functional groups, PLA and PET have functional groups coming from ester linkage. These functional groups can act as dipoles and interact with the electric field leading to some whipping. However, additives that improve electrical conductivity and reduce viscosity of polymer melt are still necessary since the effect is not the same as solution electrospinning. So, low production rates are also used to achieve low diameters in melt electrospinning. Although, studies show the fabrication of fibers below 100 nm, this is very uncommon and typical the fiber diameter lies in the lower micrometer ranges [86]. While larger fibers are formed by melt electrospinning, toxic solvents that are used in solution electrospinning are not necessary here. This makes the process potentially more sustainable.

1.4.1 Electrospinning of PLA

PLA has recently become a very important material for electrospinning because of its biodegradability and biocompatibility [87]. They are very interesting for biomedical applications such as scaffolds, wound dressing, and filters. Since the nonwoven market currently is heavily dependent on fossil-based resources and the search for alternative sustainable materials is taking shape, PLA pops up as a potential alternative for applications such as filtration [9,88]. PLA based submicro and nano fibers have been fabricated through solution electrospinning, whereas submicro fibers have been produced using melt electrospinning. Furthermore, most of these studies have been

performed in lab scale devices and in the Table 1.7 below, a short overview on the electrospinning of PLA is presented.

Table 1.7: Overview of electrospinning of PLA

Publication	Short description	Findings
Georgiadou et. Al [89]	Solution electrospinning of PLA was carried out with several non-hazardous solvents and solvents effect on the diameter of fiber and its morphology was determined.	Fibers could be produced only with 10 % (w/w) concentration of PLA in acetone. The process was more stable when binary solvent system was used. Fibers with lowest mean diameter of 223 nm were produced.
Rashid et. Al [24]	Influence of polymer concentration and electrospinning conditions on jet formation and production of beaded PLA fibers was investigated. The solvent used for solution electrospinning was Dimethylformamide (DMF).	It is observed that Taylor cone formation occurred at voltages of 10 and 12.8 kV. 12.5% (w/w) and 15% (w/w) of PLA were identified to be effective to produce electrospun fibers with diameter in the lower micrometer range. Even though, PLA fibers electrospun with DMF as a solvent normally contains a lot of beads, it was reduced to less than 35 beads.
Kaynak et. Al [90]	Taguchi optimization for process parameters was applied to optimize solution electrospinning of PLA and Polyhedral Oligomeric Silsequioxane (POSS) particles filled PLA.	A solution with a PLA concentration of 8%, throughput of 1.8 mL/h, and a 18 cm nozzle to collector distance at 15 kV voltage were found to be the most optimal process parameter. Lowest average

		diameter of about 208 nm was obtained.
Kostopoulos et. Al [91]	Scaffolds were made from solution electrospun PLA. Multi-walled carbon nanotubes, and hydroxyapatite nanoparticles were used to modify PLA prior to spinning. The porosity, physical and mechanical properties of the scaffolds were investigated.	Fabrication of cylindrical structures containing dense networks of non-woven was possible with solution containing the 1% (w/w) of MWCNT. At higher amounts, nanofillers formed more agglomerates. The scaffolds became less hydrophobic upon modification but the mechanical properties improved.
Daniels et. Al [92]	Birch Bark Triterpene Extract (TE) loaded PLA fiber was fabricated using solution electrospinning with DCM and DMSO and characterized.	It was observed that the TE was entrapped in the electrospun PLA fibers. An initial burst release of TE occurred in vitro and in due time, more than 90% was released.
Wen et. Al [25]	A review was performed on recent developments in fabrication of electrospun PLA nanofibers for food packaging applications.	Electrospinning proves to be versatile and facilitates fabrication of PLA-based nanomaterials with a multitude of properties. The encapsulation efficiency and controlled release of bioactive agents was especially good and this led to higher shelf life.
Long et. Al [93]	Melt electrospinning of PLA was carried out at different spinning temperatures to control the	Increasing the melt spinning temperature from 200 °C to 240 °C led to a reduction in average diameter of the PLA

	morphology of the fabricated PLA microfibers and spheres.	fibers. Upon increasing the spinning temperature to over 250 °C, microspheres were obtained.
Ahmadi et. Al [94]	Melt electrospinning process of PLA was optimized. Various melt electrospinning parameters, such as molecular weight, electric field strength, flow rate and temperature on the morphology were varied and their effect on the fiber diameter of was studied.	Molecular weight had the most influence on the diameter of the fiber obtained. Mean fiber diameter increased when the molecular weight increased. The throughput had the lowest impact. By optimizing the process, fibers with diameter of below 100 nm were achieved.
Long et. Al [95]	A hand operated Wimshurst generated was used to apply electric field in the melt electrospinning of PLA and polycaprolactone microfibers.	Fabrication of PLA and polycaprolactone microfibers with diameter in the range of 15-45 μm was achieved. The fibers could directly be melt electrospun onto a pork liver. The proposed approach gives a possibility of melt electrospinning fibers for wound dressing.
Konig et. Al [96]	Pilot-scale melt electrospinning of PLA was carried out with a 600-nozzle melt electrospinning device. The findings of melt electrospinning in lab scale were transferred to pilot scale. PLA grades with different melt flow rates were melt electrospun and the influence of spinning parameters on diameter of the fiber obtained	Pilot-scale melt electrospinning was successful and fibers with lowest individual diameter of 420 nm was achieved at a pump speed of 5 rpm and a temperature of 230 °C. The results from lab scale could be transferred to pilot scale.

	was investigated. Salts were also used as conductive additives.	Addition of salts led to degradation of PLA.

Short summary:

- Solution electrospinning is well developed and yield fibers with diameter in nanorange.
    - However, toxic solvents are used making the process unsustainable.
- Melt electrospinning can be a more sustainable alternative.
    - The low electrical conductivity and high viscosity of polymer melt poses challenges.
- Melt electrospinning of PLA has been studied largely on lab scale.
    - Achieving diameters in the sub micrometer is still challenging.
    - Material modification or expensive machine modifications are necessary to achieve low diameters.

1.5 Problem statement

In the previous sections, different textile application and the methods used to produce corresponding fibers were introduced and the commonly used methods for producing fibers for conventional textiles, and submicro and nanofibers for filtration and biomedical applications were discussed. Yarns for conventional textiles are predominantly melt spun in industries. Fossil-based PET is the most commonly used material and exhaust dyeing is the preferred dyeing process. Due to its high dependence on fossil resources, the market is leaning towards sustainable biobased materials such as PLA. Polyesters such as PET have been conventionally dyed by exhaust dyeing at high temperatures, which can be challenging in case of PLA. In extreme cases, it has led to hydrolytic degradation and loss of mechanical properties. Majority of the studies have focused on improving the exhaust dyeing of PLA but exhaust dyeing is not very sustainable since it uses large amounts of water and chemicals, which in turn leads to water pollution. Dope dyeing is potentially a more sustainable alternative to dye PLA since water bath and auxiliary chemicals are not necessary here but has not been studied thoroughly yet.

Electrospinning is becoming the preferred method for fabricating submicro and nano fibers. It can either be carried out using a polymer solution or a polymer melt and electric field is applied to draw the fiber. Compared to polymer melt, polymer solutions have

lower viscosity and higher electrical conductivity. Both these favor formation of thinner fibers in solution electrospinning. So solution electrospinning is more industrially applied. Although nanofibers have been achieved with solution electrospinning, the solvents for PLA such as chloroform, dichloromethane are toxic making the process unsustainable and environmentally unfriendly. Additionally, it leads to production difficulties because of blocked nozzles if the solvent evaporates too fast. In contrast, melt spinning is more sustainable but the unfavorable viscosity and poor electrical conductivity of polymers makes it challenging to achieve fibers with diameters in the submicro and nanorange without further modifications. Majority of the studies have focused on optimizing solution electrospinning of PLA and making machine modification to improve melt electrospinning of PLA. Apart from imparting color, colorants such as carbon black, copper pthalocyanine have other functionalities such as conductivity and have been used in electronics making them potential conductive additives for PLA. Furthermore, biobased colorants such as curcumin, alizarin have antibacterial properties, which are beneficial for filtration applications. Yet this has not been used in melt electrospinning.

1.6 Aim and Scope

The goal of this thesis is to evaluate the potential of multifunctional colorants for production of eco-friendly PLA based textiles. To achieve this, the thesis is split into two parts. The aim of first part of the thesis is to develop dope dyed PLA knitted fabrics through melt spinning and the following aspects are looked into:

- Investigation of the effect of multifunctional colorants on the degradation, mechanical, rheological, physical, and thermal properties of PLA.
- Assessment of the efficiency of multifunctional colorants as nucleating agents for PLA in melt spinning.
- Examination of the use of dope dyeing as a dyeing method to dye PLA.

A mix of fossil-based, potential biobased and biobased colorants were used in the study. The colorants were mixed with PLA and dope dyed PLA filaments were produced, which were later knitted into tubular fabrics and the effect of the colorants on the properties of dope dyed PLA yarn and fabric was investigated. Furthermore, among the colorants used, there are biobased and potential biobased colorants. The performance of biobased and potential biobased colorants were compared to the fossil-based colorants.

The aim of the second part of the thesis is to investigate the use of multifunctional colorants for production of melt electrospun PLA nonwoven fiber webs for potential biomedical and filtration applications. During this study, the following characteristics are reflected:

- Investigation the effect of multifunctional colorants on degradation, electrical, rheological, and thermal properties of PLA and the diameter of the fibers fabricated.
- Development a fiber web (nonwoven) prototype by pilot scale melt electrospinning of PLA with multifunctional colorants.

To attain these goals, PLA compounds were made in lab scale and electrospinning was carried out. The influence of colorants and their amount on the diameter of the PLA fiber was measured. A scale up using pilot scale melt electrospinning device was then performed with the most promising colorants and the properties of the nonwovens were tested. The thesis is divided into 5 chapters to explain the outcomes of the research work and the outline is described in the next section.

1.6 Outline of the thesis

The research work carried out to achieve the above-mentioned goals is described in the following chapters. The work carried out is intended to give deeper insights into dope dyeing and melt electrospinning of PLA with multifunctional colorants to enable production of sustainable fibers for various textile applications.

In **Chapter 1**, an overview of the fibers used for textile applications and two of the commonly used fabrication techniques was presented. Furthermore, insight into the latest research on processing of PLA using these techniques were discussed and the shortcomings were listed. Later the aim of the research work and the outline is shown.

Chapter 2 focuses on the dope dyeing of PLA. We used five different colorants for the study. We analyzed the colorants and produced a masterbatch containing 5% (w/w) of each colorant. The effect of the colorants on degradation, thermal, and rheological properties of PLA was then investigated. Then melt spinning was carried out using pure PLA and the masterbatch to produce multifilament yarn containing three different weight percentages of the colorants. During melt spinning, three different draw ratios were applied and the impact of colorants and process parameters on thermal, physical and mechanical properties of PLA yarn were investigated respectively. Knitted fabrics

were made out of dope dyed PLA yarn and the stability of the colorants and the effect of colorants on the properties of PLA fabric were examined.

With the Covid-19 pandemic, the demand for masks skyrocketed and melt electrospinning is currently being studied as a potential technique for the manufacture of fibers with low diameters. However, the low electrical conductivity, and high viscosity of the polymer melt make it challenging to realize it. Since some of the colorants are semi-conductive and antibacterial in nature, they can be called multifunctional. In **Chapter 3,** the influence of colorants on PLA's electrical conductivity and melt electrospun fiber diameter was investigated. We used three potential biobased dyes and a plasticizer in the study. The effect of the additives on viscosity, conductivity, thermal, and degradation behavior of PLA was examined. The morphology and crystallinity of melt electrospun fibers were compared to melt spun fibers with different draw ratios.

Chapter 3 was a proof of principle study for the use of multifunctional colorants for melt electrospinning. In **Chapter 4,** we looked deeper into this and investigated the influence of dyes and pigments on the melt electrospinning performance of PLA was investigated. Dyes have a tendency to dissolve and disperse better in the polymer melt but pigments remain as particles inside and are harder to disperse in the polymer but pigments such as copper pthalocyanine are more electrically conductive than biobased dyes. Therefore, we both type of colorants were used and the effects of the colorants on the electrical conductivity, viscosity, thermal properties and degradation of PLA and the fiber diameters obtained were examined.

Chapter 5 examines the effect of potential biobased dyes on melt electrospinning of PLA in the 600-nozzle pilot scale device. Curcumin, alizarin, and quercetin were the dyes used since they are antibacterial in nature. All the dyes were tested against a gram positive and a gram-negative bacterium. Since melt electrospinning is carried out at high temperatures, it can degrade leading to loss of antibacterial functionality. Therefore, the dyes underwent heat treatment at spinning temperatures and the antibacterial properties were tested again to determine the influence of thermal treatment. We carried out melt electrospinning at pilot scale with three different weight percentage of the dyes. The influence of dyes on the rheological, electrical, and thermal properties of PLA were investigated. Furthermore, the effect of dyes on the diameter and the antibacterial properties of the fiber webs were examined.

In **Chapter 6,** an insight into similarities and differences between melt spinning and melt electrospinning is discussed. The important process parameters affecting the processes

such as draw ratio were calculated and a comparative study between the values obtained from melt spinning and melt electrospinning carried out in this thesis was performed to identify the current status of novel melt electrospinning process and suggest future optimization steps.

The schematic overview of different chapters in this thesis is presented below in Figure 1.13.

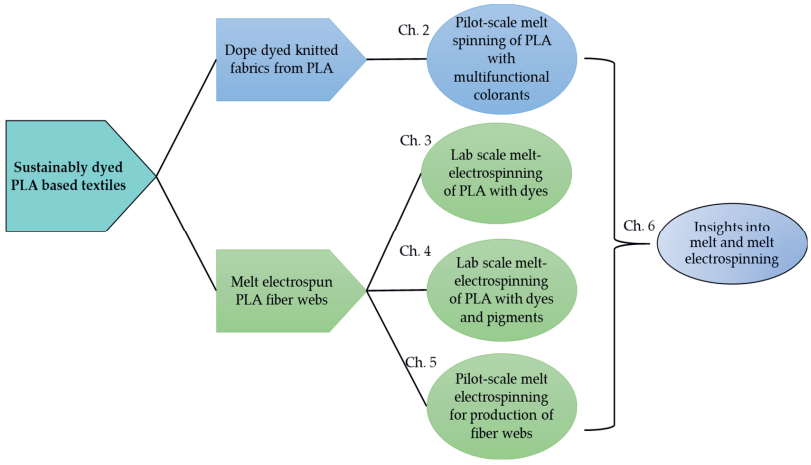

Figure 1.13: Schematic overview of different chapters in this thesis

References

1. EURATEX, E.a.S. Facts & Key Figures of the European Textile and Clothing Industry. 2020.
2. Islam, S. Development of automotive textiles with antiodour/antimicrobial properties. Masters, RMIT University, Melbourne, Australia, 2008.
3. Tighe, D. Global apparel market - statistics & facts. Available online: https://www.statista.com/topics/5091/apparel-market-worldwide/#dossierKeyfigures (accessed on 28.12.2022).
4. Pulidini, K.B., S. Polyester Fiber Market Size. Available online: https://www.gminsights.com/industry-analysis/polyester-fiber-market (accessed on 02.05.).
5. Hussain, T.; Tausif, M.; Ashraf, M. A review of progress in the dyeing of eco-friendly aliphatic polyester-based polylactic acid fabrics. Journal of Cleaner Production 2015, 108, 476-483, doi:10.1016/j.jclepro.2015.05.126.
6. Bioplastics Market Development Update 2020. Available online: chrome-extension://efaidnbmnnnibpcajpcglclefindmkaj/https://docs.european-bioplastics.org/conference/Report_Bioplastics_Market_Data_2020_short_version.pdf (accessed on 02.05).
7. Maqsood, M.; Seide, G. Development of biobased socks from sustainable polymer and statistical modeling of their thermo-physiological properties. Journal of Cleaner Production 2018, 197, 170-177, doi:10.1016/j.jclepro.2018.06.191.
8. Dorgan, J.R.; Lehermeier, H.; Mang, M. Thermal and Rheological Properties of Commercial-Grade Poly(Lactic Acid)s. Journal of Polymers and the Environment 2000, 8.
9. Avinc, O.; Khoddami, A. Overview of Poly(lactic acid) (PLA) Fibre. Fibre Chemistry 2010, 41, 391-401, doi:10.1007/s10692-010-9213-z.
10. Material Properties Database. Available online: https://www.makeitfrom.com/compare/Polyethylene-Terephthalate-PET-PETE/Polylactic-Acid-PLA-Polylactide (accessed on
11. Abdrabbo, A.; El-Dessouky, H.M.; Fotheringham, A.F. Treatment of polylactic acid fibre using low temperature plasma and its effects on vertical wicking and surface

characteristics. Journal of the Textile Institute 2013, 104, 28-34, doi:10.1080/00405000.2012.693699.

12. Baig, G.A.; Carr, C.M. Kawabata evaluation of PLA-knitted fabric washed with various laundering formulations. The Journal of The Textile Institute 2014, 106, 111-118, doi:10.1080/00405000.2014.960249.

13. Bax, B.; Müssig, J. Impact and tensile properties of PLA/Cordenka and PLA/flax composites. Composites Science and Technology 2008, 68, 1601-1607, doi:10.1016/j.compscitech.2008.01.004.

14. Xu, S.; Chen, J.; Wang, B.; Yang, Y. Sustainable and Hydrolysis-Free Dyeing Process for Polylactic Acid Using Nonaqueous Medium. ACS Sustainable Chemistry & Engineering 2015, 3, 1039-1046, doi:10.1021/sc500767w.

15. Baig, G.A. Hydrolytic stability of PLA yarns during textile wet processing. Fibers and Polymers 2013, 14, 1912-1918, doi:10.1007/s12221-013-1912-7.

16. He, L.; Zhang, S.F.; Tang, B.T.; Wang, L.L.; Yang, J.Z. Dyes with high affinity for polylactide. Chinese Chemical Letters 2007, 18, 1151-1153, doi:10.1016/j.cclet.2007.07.031.

17. Carmen, Z.; Daniela, S. Textile Organic Dyes – Characteristics, Polluting Effects and Separation/Elimination Procedures from Industrial Effluents – A Critical Overview. In Organic Pollutants Ten Years After the Stockholm Convention, Puzyn, T., Mostrag-Szlichtyng, A., Eds.; InTech: 2012; Volume 1, pp. 55-86.

18. Carmichael, A. Man-Made Fibers Continue To Grow. Available online: https://www.textileworld.com/textile-world/fiber-world/2015/02/man-made-fibers-continue-to-grow/ (accessed on 02.05).

19. Reinhardt, D. Vergleichende Sachbilanz im Textilbereich – Spinnfärbung versus Flottenfärbung; Friedrich-Schiller-Universität Jena: 2003; p. 5.

20. Hossein Tavanai, M.M., M. Zarebini, A.S. Rezve. A Study of the Nucleation Effect of Pigment Dyes on the Microstructure of Mass Dyed Bulked Continuous Filament Polypropylene. Iranian Polymer Journal 2005, 14, 267-276.

21. Gsanger, M.; Bialas, D.; Huang, L.; Stolte, M.; Wurthner, F. Organic Semiconductors based on Dyes and Color Pigments. Adv Mater 2016, 28, 3615-3645, doi:10.1002/adma.201505440.

22. Roy, S.; Rhim, J.W. Preparation of bioactive functional poly(lactic acid)/curcumin composite film for food packaging application. Int J Biol Macromol 2020, 162, 1780-1789, doi:10.1016/j.ijbiomac.2020.08.094.

23. Pleated Membrane Filtration Market Size, Share, Growth and Industry Analysis by Type, Application. Available online: https://www.businessresearchinsights.com/market-reports/pleated-membrane-filtration-market-100964 (accessed on 28.12.2022).

24. Zubir, A.A.M.; Khairunnisa, M.P.; Surib, N.A.; NorRuwaida, J.; Ali, A.H.M.; Rashid, M. Electrospinning of PLA with DMF Effect of polymer concentration on the bead diameter of the electrospun fibre. In Proceedings of the 26th Regional Symposium on Chemical Engineering, Kuala Lumpur, Malaysia, 2020.

25. Wu, J.H.; Hu, T.G.; Wang, H.; Zong, M.H.; Wu, H.; Wen, P. Electrospinning of PLA Nanofibers: Recent Advances and Its Potential Application for Food Packaging. J Agric Food Chem 2022, 70, 8207-8221, doi:10.1021/acs.jafc.2c02611.

26. Pavezi, K.J.P.; Rocha, A.; Bonafé, E.G.; Martins, A.F. Electrospinning-electrospraying of poly(acid lactic) solutions in binary chloroform/formic acid and chloroform/acetic acid mixtures. Journal of Molecular Liquids 2020, 320, doi:10.1016/j.molliq.2020.114448.

27. Buschle-Diller, G.; Cooper, J.; Xie, Z.; Wu, Y.; Waldrup, J.; Ren, X. Release of antibiotics from electrospun bicomponent fibers. Cellulose 2007, 14, 553-562, doi:10.1007/s10570-007-9183-3.

28. Hacker, C. Anlagenentwicklung für das Elektroschmelzspinnen für die Feinfaservliesstoffen für die Abwasseraufbereitung. PhD, RWTH Aachen University, Aachen, Germany, 2014.

29. Wang, L. Functional Nanofibre: Enabling Material for the Next Generation Smart Textiles. Journal of Fiber Bioengineering and Informatics 2008, 1, 81-92, doi:10.3993/jfbi09200801.

30. Koenig, K. Melt electrospinning towards industrial scale nanofiber production: An in-depth material and parameter study based on polypropylene and polylactic acid. PhD, Maastricht University, Maastricht, The Netherlands, 2020.

31. Koenig, K.; Beukenberg, K.; Langensiepen, F.; Seide, G. A new prototype melt-electrospinning device for the production of biobased thermoplastic

submicrofibers and nanofibers. Biomater Res 2019, 23, 10, doi:10.1186/s40824-019-0159-9.

32. Brown, T.D.; Dalton, P.D.; Hutmacher, D.W. Melt electrospinning today: An opportune time for an emerging polymer process. Progress in Polymer Science 2016, 56, 116-166, doi:10.1016/j.progpolymsci.2016.01.001.

33. Badrossamay, M.R.; McIlwee, H.A.; Goss, J.A.; Parker, K.K. Nanofiber assembly by rotary jet-spinning. Nano Lett 2010, 10, 2257-2261, doi:10.1021/nl101355x.

34. Mishimashi, M.M.; Otsushi, F.J. Island-in-sea fiber, combined filament yarn and textile product. 2013.

35. Biswas, A.; Bayer, I.S.; Biris, A.S.; Wang, T.; Dervishi, E.; Faupel, F. Advances in top-down and bottom-up surface nanofabrication: techniques, applications & future prospects. Adv Colloid Interface Sci 2012, 170, 2-27, doi:10.1016/j.cis.2011.11.001.

36. Ziabicki, A. Fundamentals of Fibre Formation; Wiley Interscience Publishers: Cambridge, UK, 1976.

37. Palacios-Mateo, C.; van der Meer, Y.; Seide, G. Analysis of the polyester clothing value chain to identify key intervention points for sustainability. Environ Sci Eur 2021, 33, 2, doi:10.1186/s12302-020-00447-x.

38. Nakajima, T.; JKajiwara, K.; McIntyre, J.E. Advanced Fiber Spinning Technology; Woodhead Publishing: Sawston, USA, 1994.

39. Xu, R.; Chen, X.; Xie, J.; Cai, Q.; Lei, C. Influence of Melt-Draw Ratio on the Crystalline Structure and Properties of Polypropylene Cast Film and Stretched Microporous Membrane. Industrial & Engineering Chemistry Research 2015, 54, 2991-2999, doi:10.1021/acs.iecr.5b00215.

40. Walczak, Z.K. Process of Fiber Formation; Elsevier: Oxford, UK, 2002.

41. Fourne, F. Synthetic Fibers Machines and Equipment, Manufacture, Properties Carl Hanser Verlag: Munich, Germany, 1998.

42. Kikutani, T. Handbook of textile fibre structure; Woodhead Publishing Limited: Cambridge, UK, 2009; Volume 1.

43. Global Textile Dyes Market. Available online: https://finance.yahoo.com/news/textile-dyes-global-market-report-

113800418.html?guccounter=1&guce_referrer=aHR0cHM6Ly93d3cuZ29vZ2xlLmNvbS8&guce_referrer_sig=AQAAALdw4i3f2liPIzo2Gci39Oenr2lvFFSz3OhAHESc5NgTPToyH3aDxPQ_7izJbJpWUJ0MAVzwpAS28WRUYpUPnS0KZK0Cw_KVtnxNxUGxSkqS00Io9v4yTXznKauK3dhlzMSUdDBGaOk2zO67bs61oRfzXEUCv8-kp8IET3a9tNVC (accessed on 28.12.2022).

44. Notten, P. Sustainability and Circularity in the Textile Value Chain; 2020.

45. Moore, S.B.; Ausley, L.W. Systems thinking and green chemistry in the textile industry: concepts, technologies and benefits. Journal of Cleaner Production 2004, 12, 585-601, doi:10.1016/s0959-6526(03)00058-1.

46. Choudhury, A.K.R. Handbook of textile and industrial dyeing; Woodhead Publishing: Cambridge, UK, 2011; Volume 2.

47. Marcincin, A. Modification of fiber-forming polymers by additives. Progress in Polymer Science 2002, 27, 61.

48. Christie, R.M. Pigments, dyes and fluorescent brightening agents for plastics: An overview. Polymer International 1994, 34, 11.

49. Haastrup, S.; Yu, D.; Broch, T.; Larsen, K.L. Comparison of the performance of masterbatch and liquid color concentrates for mass coloration of polypropylene. Color Research & Application 2016, 41, 484-492, doi:10.1002/col.21987.

50. Fakirov, S. Polymer nanocomposites: Why their mechanical performance does not justify the expectation and a possible solution to the problem? Express Polymer Letters 2020, 14, 436-466, doi:10.3144/expresspolymlett.2020.36.

51. Perkins, W.S. A Review of Textile Dyeing Processes. In Proceedings of the American Association of Textile Chemists and Colorists, North Carolina, USA, 1991.

52. Siebert, S.; Berghaus, J.; Seide, G. Nucleating Agents to Enhance Poly(l-Lactide) Fiber Crystallization during Industrial-Scale Melt Spinning. Polymers (Basel) 2022, 14, doi:10.3390/polym14071395.

53. Huang, Y.; Brünig, H.; Müller, M.T.; Wießner, S. Melt spinning of PLA/PCL blends modified with electron induced reactive processing. Journal of Applied Polymer Science 2021, 139, doi:10.1002/app.51902.

54. Gajjar, C.R.; Stallrich, J.W.; Pasquinelli, M.A.; King, M.W. Process-Property Relationships for Melt-Spun Poly(lactic acid) Yarn. ACS Omega 2021, 6, 15920-15928, doi:10.1021/acsomega.1c01557.

55. Takasaki, M.; Ito, H.; Kikutani, T. Structure Development of Polylactides with Various d-Lactide Contents in the High-Speed Melt Spinning Process. Journal of Macromolecular Science, Part B 2007, 42, 57-73, doi:10.1081/mb-120015750.

56. Maqsood, M.; Langensiepen, F.; Seide, G. The Efficiency of Biobased Carbonization Agent and Intumescent Flame Retardant on Flame Retardancy of Biopolymer Composites and Investigation of their Melt-Spinnability. Molecules 2019, 24, doi:10.3390/molecules24081513.

57. Aouat, T.; Kaci, M.; Devaux, E.; Campagne, C.; Cayla, A.; Dumazert, L.; Lopez-Cuesta, J.-M. Morphological, Mechanical, and Thermal Characterization of Poly(Lactic Acid)/Cellulose Multifilament Fibers Prepared by Melt Spinning. Advances in Polymer Technology 2018, 37, 1193-1205, doi:10.1002/adv.21779.

58. Clarkson, C.M.; El Awad Azrak, S.M.; Chowdhury, R.; Shuvo, S.N.; Snyder, J.; Schueneman, G.; Ortalan, V.; Youngblood, J.P. Melt Spinning of Cellulose Nanofibril/Polylactic Acid (CNF/PLA) Composite Fibers For High Stiffness. ACS Applied Polymer Materials 2018, 1, 160-168, doi:10.1021/acsapm.8b00030.

59. Jompang, L.; Thumsorn, S.; On, J.W.; Surin, P.; Apawet, C.; Chaichalermwong, T.; Kaabbuathong, N.; O-Charoen, N.; Srisawat, N. Poly(Lactic Acid) and Poly(Butylene Succinate) Blend Fibers Prepared by Melt Spinning Technique. Energy Procedia 2013, 34, 493-499, doi:10.1016/j.egypro.2013.06.777.

60. Schmack, G.; Tändler, B.; Optiz, G.; Vogel, R.; Komber, H.; Häußler, L.; Voigt, D.; SWeinmann, S.; Heinemann, M.; Fritz, H.-G. High-Speed Melt Spinning of Various Grades of Polylactides. Journal of Applied Polymer Science 2004, 91, 7.

61. Hufenus, R.; Reifler, F.A.; Maniura-Weber, K.; Spierings, A.; Zinn, M. Biodegradable Bicomponent Fibers from Renewable Sources: Melt-Spinning of Poly(lactic acid) and Poly[(3-hydroxybutyrate)-co-(3-hydroxyvalerate)]. Macromolecular Materials and Engineering 2012, 297, 75-84, doi:10.1002/mame.201100063.

62. Clark, M. Handbook of textile and industrial dyeing; Clark, M., Ed.; Woodhead Publishing Limited: Cambridge, UK, 2011; Volume 1.

63. Lindström, F. Chemical and physical changes in PET fibres due to exhaust dyeing. Master Thesis, University of Boras, Borås, 2018.

64. Nakpathom, M.; Somboon, B.; Narumol, N.; Mongkholrattanasit, R. High temperature dyeing of PET fabric with natural colourants extracted from annatto seeds. Pigments & Resin Technology 2019, 48, 8.

65. Opwis, K.; Benken, B.; Knittel, D.; Gutmann, J.S. Dyeing of PET Fibers in Ionic Liquids. International Journal of New Technology and Research 2017, 3, 9.

66. Fattahi, F.; Izadan, H.; Khoddami, A. Investigation into the Effect of UV/Ozone Irradiation on Dyeing Behaviour of Poly(Lactic Acid) and Poly(Ethylene Terephthalate) Substrates. Progress in Color, Colorants and Coatings 2012, 5, 8.

67. Avinc, O.; Phillips, D.; Wilding, M. Influence of different finishing conditions on the wet fastness of selected disperse dyes on polylactic acid fabrics. Coloration Technology 2009, 125, 288-295, doi:10.1111/j.1478-4408.2009.00209.x.

68. Avinc, O.; Wilding, M.; Bone, J.; Phillips, D.; Farrington, D. Evaluation of colour fastness and thermal migration in softened polylactic acid fabrics dyed with disperse dyes of differing hydrophobicity. Coloration Technology 2010, 126, 353-364, doi:10.1111/j.1478-4408.2010.00269.x.

69. He, L.; Lu, L.; Zhang, S.; Freeman, H.S. Synthesis and application of yellow azo-anthraquinone disperse dyes for polylactide fibres. Coloration Technology 2010, 126, 92-96, doi:10.1111/j.1478-4408.2010.00232.x.

70. Karst, D.; Hain, M.; Yang, Y. Mechanical properties of polylactide after repeated cleanings. Journal of Applied Polymer Science 2008, 108, 2150-2155, doi:10.1002/app.27897.

71. Zhang, L.; Dong, H.; Li, M.; Wang, D.; Liu, M.; Wang, C.; Fu, S. Synthesis and characterization of carbon black modified by polylactic acid (PLA-g-CB) as pigment for dope dyeing of black PLA fibers. Journal of Applied Polymer Science 2019, 137, doi:10.1002/app.48784.

72. Beyreuther, R.; Brünig, H. Dynamics of Fibre Formation and Processin; Springer: Berlin, Heidelberg, 2007.

73. Hegemann, B. Deformationsverhalten von Kunststoffen beim Thermoformen. PhD Thesis, Stuttgart University, Stuttgart, Germany, 2004.

74. Bhattarai, R.S.; Bachu, R.D.; Boddu, S.H.S.; Bhaduri, S. Biomedical Applications of Electrospun Nanofibers: Drug and Nanoparticle Delivery. Pharmaceutics 2018, 11, doi:10.3390/pharmaceutics11010005.

75. Xue, J.; Wu, T.; Dai, Y.; Xia, Y. Electrospinning and Electrospun Nanofibers: Methods, Materials, and Applications. Chem Rev 2019, 119, 5298-5415, doi:10.1021/acs.chemrev.8b00593.

76. Ostheller, M.E.; Balakrishnan, N.K.; Groten, R.; Seide, G. The Effect of Electrical Polarity on the Diameter of Biobased Polybutylene Succinate Fibers during Melt Electrospinning. Polymers (Basel) 2022, 14, doi:10.3390/polym14142865.

77. Kilic, A.; Oruc, F.; Demir, A. Effects of Polarity on Electrospinning Process. Textile Research Journal 2008, 78, 532-539, doi:10.1177/0040517507081296.

78. SalehHudin, H.S.; Mohamad, E.N.; Mahadi, W.N.L.; Muhammad Afifi, A. Multiple-jet electrospinning methods for nanofiber processing: A review. Materials and Manufacturing Processes 2017, 33, 479-498, doi:10.1080/10426914.2017.1388523.

79. Shin, Y.; Hohman, M.M.; P., B.M. Electrospinning: A whipping fluid jet generates submicron polymer fibers. Applied Physics Letters 2001, 78, doi:https://doi.org/10.1063/1.1345798.

80. Reneker, D.H.; Yarin, A.L. Electrospinning jets and polymer nanofibers. Polymer 2008, 49, 2387-2425, doi:10.1016/j.polymer.2008.02.002.

81. Kim, G.-M. Verstärkungsmechanismen auf Makro-, Mikro- und Nano-Längenskalen in heterogenen Polymerwerkstoffen. PhD, Martin-Luther-Universität, 2007.

82. Bagchi, S.; Brar, R.; Singh, B.; Ghanshyam, C. Instability controlled synthesis of tin oxide nanofibers and their gas sensing properties. Journal of Electrostatics 2015, 78, 68-78, doi:10.1016/j.elstat.2015.11.001.

83. Colby, R.H.; Fetters, L.J.; Graessley, W.W. The melt viscosity-molecular weight relationship for linear polymers. Macromolecules 2002, 20, 2226-2237, doi:10.1021/ma00175a030.

84. Ostheller, M.E.; Balakrishnan, N.K.; Groten, R.; Seide, G. Detailed Process Analysis of Biobased Polybutylene Succinate Microfibers Produced by Laboratory-Scale Melt Electrospinning. Polymers (Basel) 2021, 13, doi:10.3390/polym13071024.

85. Faccini, M.; Amantia, D.; Vázquez-Campos, S.; Vaquero, C.; Ipiña, J.M.L.d.; Aubouy, L. Nanofiber-based filters as novel barrier systems for nanomaterial exposure scenarios. Journal of Physics: Conference Series 2011, 304, doi:10.1088/1742-6596/304/1/012067.

86. Canetta, C.; Guo, S.; Narayanaswamy, A. Measuring thermal conductivity of polystyrene nanowires using the dual-cantilever technique. Rev Sci Instrum 2014, 85, 104901, doi:10.1063/1.4896330.

87. Davachi, S.M.; Kaffashi, B. Polylactic Acid in Medicine. Polymer-Plastics Technology and Engineering 2015, 54, 944-967, doi:10.1080/03602559.2014.979507.

88. Jafari, M.; Shim, E.; Joijode, A. Fabrication of Poly(lactic acid) filter media via the meltblowing process and their filtration performances: A comparative study with polypropylene meltblown. Separation and Purification Technology 2021, 260, doi:10.1016/j.seppur.2020.118185.

89. Casasola, R.; Thomas, N.L.; Trybala, A.; Georgiadou, S. Electrospun poly lactic acid (PLA) fibres: Effect of different solvent systems on fibre morphology and diameter. Polymer 2014, 55, 4728-4737, doi:10.1016/j.polymer.2014.06.032.

90. Meyva-Zeybek, Y.; Kaynak, C. Electrospinning of PLA and PLA/POSS nanofibers: Use of Taguchi optimization for process parameters. Journal of Applied Polymer Science 2020, 138, doi:10.1002/app.49685.

91. Kotrotsos, A.; Yiallouros, P.; Kostopoulos, V. Fabrication and Characterization of Polylactic Acid Electrospun Scaffolds Modified with Multi-Walled Carbon Nanotubes and Hydroxyapatite Nanoparticles. Biomimetics (Basel) 2020, 5, doi:10.3390/biomimetics5030043.

92. Fan, T.; Daniels, R. Preparation and Characterization of Electrospun Polylactic Acid (PLA) Fiber Loaded with Birch Bark Triterpene Extract for Wound Dressing. AAPS PharmSciTech 2021, 22, 205, doi:10.1208/s12249-021-02081-z.

93. Yu, S.-X.; Zheng, J.; Yan, X.; Wang, X.-X.; Nie, G.-D.; Tan, Y.-Q.; Zhang, J.; Sui, K.-Y.; Long, Y.-Z. Morphology control of PLA microfibers and spheres via melt electrospinning. Materials Research Express 2018, 5, doi:10.1088/2053-1591/aab9f4.

94. Doustgani, A.; Ahmadi, E. Melt electrospinning process optimization of polylactic acid nanofibers. Journal of Industrial Textiles 2015, 45, 626-634, doi:10.1177/1528083715610297.

95. Qin, C.C.; Duan, X.P.; Wang, L.; Zhang, L.H.; Yu, M.; Dong, R.H.; Yan, X.; He, H.W.; Long, Y.Z. Melt electrospinning of poly(lactic acid) and polycaprolactone microfibers by using a hand-operated Wimshurst generator. Nanoscale 2015, 7, 16611-16615, doi:10.1039/c5nr05367f.

96. Koenig, K.; Langensiepen, F.; Seide, G. Pilot-scale production of polylactic acid nanofibers by melt electrospinning. e-Polymers 2020, 20, 233-241, doi:10.1515/epoly-2020-0030.

97. Balakrishnan, N. K.; Siebert, S.; Richter, C.; Groten, R.; Seide, G. Effect of Colorants and Process Parameters on the Properties of dope dyed Polylactic Acid Multifilament Yarns. Polymers 2022, 14, doi:https://doi.org/10.3390/polym14225021

Chapter 2

Effect of colorants and process parameters on the properties of dope dyed polylactic acid multifilament yarns

This chapter is based on the following publication:
Balakrishnan, N. K.; Siebert, S.; Richter, C.; Groten, R.; Seide, G. Effect of Colorants and Process Parameters on the Properties of dope dyed Polylactic Acid Multifilament Yarns. Polymers 2022, 14, doi: https://doi.org/10.3390/polym14225021.

Abstract

The color of textile fibers is typically imparted by submersion in a high-temperature dye bath. However, the treatment of the effluent is challenging and the textile industry is therefore a major source of water pollution. Current fashion trends favor biobased polymers such as polylactic acid (PLA) but exhaust dyeing at high temperatures causes hydrolytic degradation, reducing the crystallinity and tenacity of the yarn. To preserve the mechanical properties of PLA-based textiles, an alternative to exhaust dyeing called dope dyeing can be used, wherein colorants are incorporated into the polymer matrix during melt spinning. We evaluated this process by dope dyeing PLA with several colorants, then testing the thermal, physical, and mechanical properties of the yarn and the physical properties of circular-knitted fabrics. Although the colorants affected the crystallization behavior at lower cooling rates, during the melt spinning process, the drawing speed had a greater effect on the crystallinity and mechanical properties of the dyed yarn. Scanning electron microscopy revealed that the colorants were well dispersed in the PLA matrix. We found that the colorants did not affect the physical properties of the knitted fabric. Our results can be used to develop more environmentally beneficial dope dyed PLA yarn with improved mechanical properties.

Keywords: fiber spinning; dope dyeing; nucleating agent; crystallinity; sustainability; biobased.

Graphical Abstract

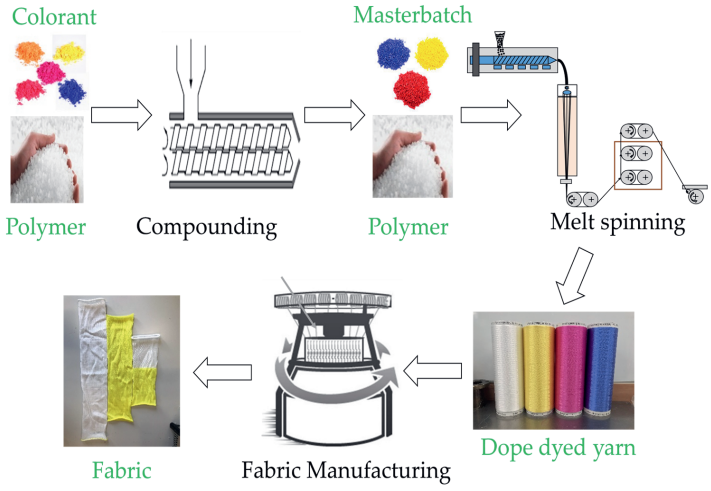

2.1 Introduction

Synthetic fiber production has doubled in the last two decades, reaching 80.9 million tons in 2020, and the most common material is polyethylene terephthalate (PET), accounting for 48 million tons [1]. Because PET is a fossil-based polymer, its production from nonrenewable raw material, and its ultimate disposal contribute to climate change. The textile industry is therefore shifting towards more sustainable and biobased and/or biodegradable polymers, which reached a production volume of 2.11 million tons in 2020, with polylactic acid (PLA) accounting for 18.7% of this total [2]. PLA can be produced from renewable resources such as corn, sugar beet, and wheat, and it currently accounts for less than 0.03% of global corn production, thus representing negligible competition with food crops. Although often described as biodegradable, PLA is only compostable under industrial conditions [3]. The production of 1 tons of PLA consumes 42 GJ of energy and releases 1.3 tons of CO_2, ~40% less than PET [4]. Furthermore, PLA fibers are characterized by inherently better moisture management, a higher limiting oxygen index (LOI), and enhanced wicking properties com-pared to PET fibers, making them suitable for use in sustainable clothing [5].

Despite the advantages of PLA, its commercial production is limited by its thermolability and low heat resistance due to its glass transition temperature (Tg) of ~55 °C [6]. The heat resistance of PLA can be improved by increasing its crystallinity, but the inherent low crystallization rate of the polymer leads to products with low

130 °C without loss of integrity, but PLA is hydrolyzed under these conditions, weakening the fibers [9]. However, dyeing at lower temperatures results in poor dye take up compared to PET [3,10,11]. The exhaust dyeing of PLA with indigoid compounds is possible at 110 °C [11,12]. Furthermore, PLA fibers modified with polyhedral oligomeric silsesquioxane nanoparticles also showed better dyeability than pure PLA [13]. The dyeing of recycled PLA fibers using selected disperse dyes achieved satisfactory exhaustion rates at 80 °C, but the light fastness of the fibers was poor [10]. Natural dye from flowers has also been used to produce yellow PLA films [14]. The tensile strength of PLA declines with increasing dyeing time, probably reflecting the impact on fiber crystallinity [6,15].

Despite its widespread use, conventional exhaust dyeing is unsustainable because toxic chemicals are needed to fix colorants to the polymer and on top of it, 10–25% of the dye is lost during the process, 2–20% of which is directly discharged into rivers and streams along with the toxic fixatives [16]. The textile industry is therefore the second greatest global polluter of water resources [17]. Exhaust dying at high temperatures also consumes energy, and the high temperatures not only cause the degradation of labile fibers such as PLA but also affect crystallinity and lead to shrinkage, disrupting the fiber orientation [6]. In comparison, mass coloration or dope dyeing involves the incorporation of colorants into the polymer melt during fiber production [18]. The dope dyeing of PLA with carbon black was shown to improve the mechanical proper-ties of the fibers [19]. A comparison of dope dyeing and exhaust dyeing of polyamide 6 revealed that dope dyeing reduces water use by ~40%, chemical use by 97%, and waste by ~50% and also reduces the overall number of processing steps [20].

Although dope dyeing has many advantages, only 5% of polyester fibers are dope dyed, and the proportion is even lower for PLA [18]. Like PLA, polypropylene (PP) is also characterized by slow crystallization, but this has been controlled and optimized by using colorants as nucleating agents [21]. We recently reported a similar nucleating effect when using selected pigments in PLA [22]. However, the effect of colorants on the mechanical, rheological, and thermal properties of PLA during dope dyeing has not been studied in detail. Herein, we describe the dope dyeing of PLA with fossil-based and biobased colorants. We compared the biobased pigment pink PR122 and the potential biobased colorant alizarin to the fossil-based pigments green 7, blue 15:1, and yellow 155. We incorporated different weight percentages of the colorants into PLA melts and determined their effect on the rheological and thermal properties of yarn, including their

propensity for degradation. We also used different draw ratios to investigate the influence of additives and process parameters on the mechanical proper-ties and crystallinity of the PLA yarns. Finally, we prepared circular-knitted fabrics from the melt spun yarns and investigated their air permeability, water vapor permeability, and Martindale abrasion resistance. We compared the performance of the different colorants to assess the potential of biobased colorants for the development of environmentally beneficial dope dyed PLA yarns with improved properties.

2.2 Materials and Methods

2.2.1 Materials

PLA grade L130 (TotalEnergies-Corbion, Gorinchem, Netherlands) was used for all experiments and has the following manufacturer-specified properties: L-content ≥ 99%, T_g ~60 °C, and melt flow index = 24 g/10 min at 210 °C/2.16 kg. We purchased alizarin (Sigma-Aldrich, St Louis, MO, USA), whereas the pigments blue 15:1, green 7, pink PR122, and pigment yellow 155 were kindly donated by Clariant (Muttenz, Switzerland). The chemical structure of the colorants are presented below in Table 2.1.

Table 2.1: Chemical structure of the colorants [23-27].

Additive	Chemical Structure
Alizarin	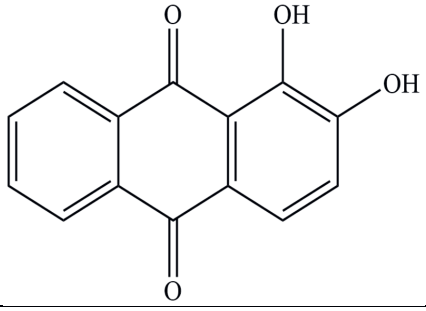

Pigment blue 15:1	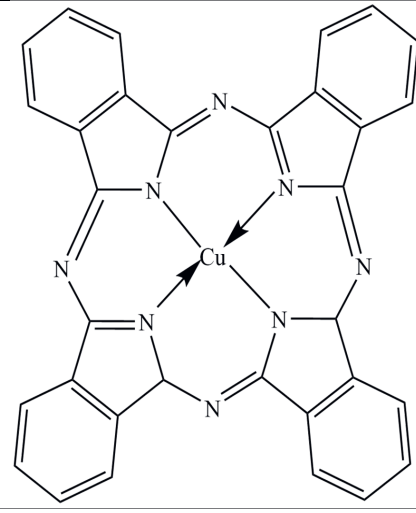
Pigment green 7	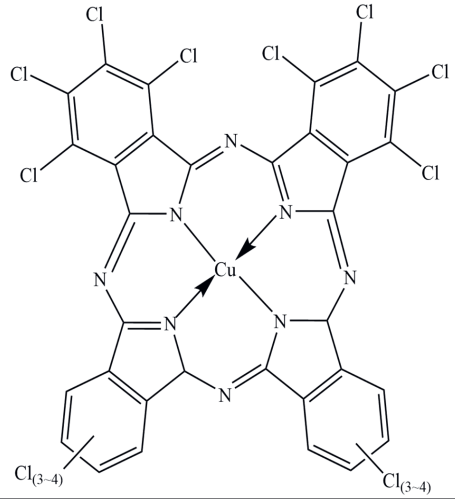
Pink PR122	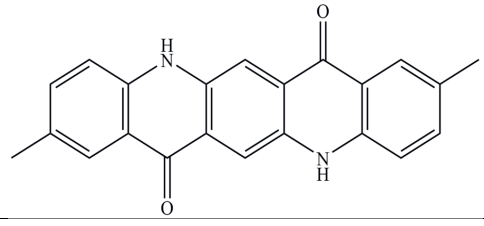

Pigment yellow 155	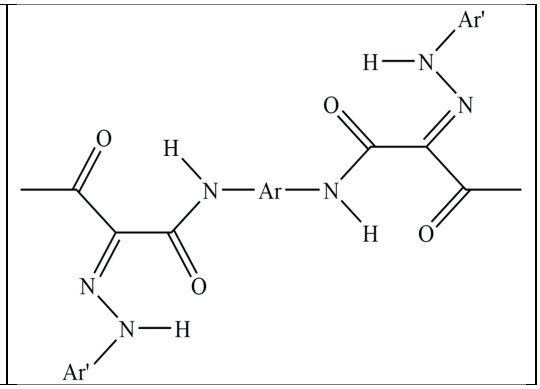

2.2.2 Compounding

We dried PLA and the colorants under a vacuum at 80 °C overnight to reduce the moisture content (<100 ppm). The materials were compounded using a KETSE 20/40 twin-screw compounder (Brabender, Duisburg, Germany) with a screw diameter (D) of 20 mm and a length of 40D. Masterbatches containing 5% (w/w) of each colorant were prepared (named A5, B5, G5, P5, and Y5). The extrudates were cooled in a water bath before granulation.

2.2.3 Melt Spinning

Fibers were prepared using an FET-100 series pilot-scale melt spinning machine (Fiber Extrusion Technology, Leeds, UK) featuring a spinneret with 48 holes (diameter 0.25 mm) and an L/D ratio of 2 (Figure 2.1). The materials were dried again at 80 °C overnight under vacuum before spinning at a temperature of 200 °C (The water content was maintained below 100 ppm). We maintained a constant extruder pressure of 60 bars and a constant throughput of 36 g/min at a winding speed of 1200 m/min, but we applied three different draw ratios.

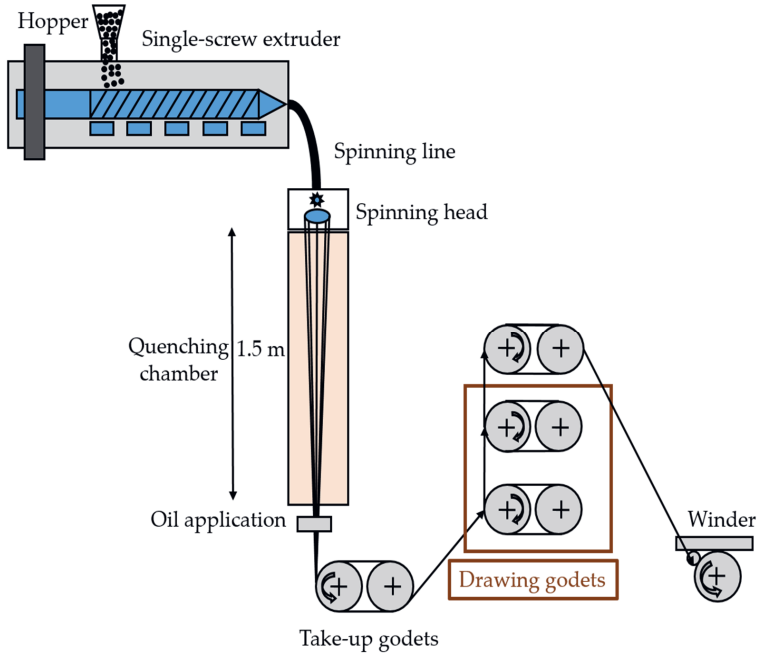

Figure 2.1: Schematic illustration of the pilot-scale melt spinning device.

The masterbatch granules were diluted with pure PLA to achieve weight-percentages of 0.1%, 0.2%, and 0.3% for melt spinning. The first yarn was drawn fully from the melt, and no solid-state drawing (SSD) was applied. The second yarn was semi-drawn from the melt (medium SSD). The third yarn was only slightly drawn from the melt and was primarily drawn by SSD. We compared yarns produced with the highest weight percentage of colorants (0.3%) because, if no significant effects were observed at this concentration, we could rule out effects at lower concentrations without testing. The yarns were named using the convention C0x.y, wherein C is the first letter of the colorant name, x is the weight percentage, and y is the SSD ratio. For example, PLA.1 refers to the pure PLA yarn drawn with an SSD ratio of 1, and A03.2 refers to the yarn dyed with 0.3% (*w*/*w*) alizarin and drawn with an SSD ratio of 2. The complete set of yarns is presented in Table 2.2.

Table 2.2: Complete set of yarns produced under different experimental parameters.

Abbreviation	Material: Colorants Shown as % (*w*/*w*)	Take Up (m/min)	Melt-Drawing Ratio	Winding Speed (m/min)	SSD Ratio
PLA.1	PLA	1100	72	1200	1
PLA.2	PLA	600	39	1200	2
PLA.3	PLA	400	26	1200	3
A03.1	PLA + 0.3% alizarin	1100	72	1200	1
A03.2	PLA + 0.3% alizarin	600	39	1200	2
A03.3	PLA + 0.3% alizarin	400	26	1200	3
B03.1	PLA + 0.3% blue 15:1	1100	72	1200	1
B03.2	PLA + 0.3% blue 15:1	600	39	1200	2
B03.3	PLA + 0.3% blue 15:1	400	26	1200	3
G01.1	PLA + 0.3% green 7	1100	72	1200	1
G02.2	PLA + 0.3% green 7	600	39	1200	2
G03.3	PLA + 0.3% green 7	400	26	1200	3
P03.1	PLA + 0.3% pink PR122	1100	72	1200	1
P03.2	PLA + 0.3% pink PR122	600	39	1200	2
P03.3	PLA + 0.3% pink PR122	400	26	1200	3
Y03.1	PLA + 0.3% yellow 155	1100	72	1200	1
Y03.2	PLA + 0.3% yellow 155	600	39	1200	2
Y03.3	PLA + 0.3% yellow 155	400	26	1200	3

2.2.4 Knitting

The melt spun yarn was knitted using a TK-83 circular knitting machine (Harry Lucas, Neumünster, Germany). A knitted fabric with a single jersey structure was produced on gauge E24/gg using 264 needles with a cylinder diameter of 3½ inches. A knitted fabric

colorant content of 0.3% (w/w). All fabrics were prepared using the same knit-ting parameters (stitch, take-off, and knitting speed).

2.2.5 Characterization of Colorants

Differential scanning calorimetry (DSC) was used to reveal any thermal transitions during processing. We applied one heating and one cooling cycle from 25 °C and 250 °C at a heating rate of 10 °C/min using a SC 214 device (Netzsch, Selb, Germany). The morphology of the colorants was determined by scanning electron microscopy (SEM) using a JSM-IT200 device (Jeol, Freising, Germany). The images were acquired in secondary electron mode with an acceleration tension of 15 kV and are presented at 1000× magnification.

2.2.6 Characterization of Masterbatches

The masterbatches of PLA with 5% (w/w) of colorants were analyzed by DSC from 25 °C to 200 °C to investigate the effect of colorants on thermal transition temperatures. We applied two heating cycles and one cooling cycle. We used the second heating cycle to determine the effect of colorants on any change in thermal transition, and we used the first cooling cycle to investigate any change in crystallization temperature (T_c). The T_g, melting point (T_m) and cold crystallization temperature (T_{cc}) were also compared.

Rheological analysis was carried out using a Discovery Hybrid Rheometer (DHR1) from TA Instruments (New Castle, DE, USA). Angular frequencies were applied over the range 1 to 624 rad/s using a 25 mm plate plate setup to investigate the effect of colorants on the viscosity of PLA, and complex viscosity values were compared at the same angular frequency (10 rad/s).

Fourier-transform infrared (FTIR) spectroscopy was used to investigate interactions between PLA and the colorants. FTIR spectra were recorded on a PerkinElmer 400 FT(N)IR device (Massachusetts, USA) in transmission mode by completing 64 scans between 4000 and 500/cm with a resolution of 2/cm.

The cross-section of the masterbatches was analyzed by SEM as described above to determine the distribution of colorants. The samples were frozen in liquid nitrogen, fractured, and sputtered with gold prior to the measurements.

The average molecular weight (M_n), weight average molecular weight (M_w), and polydispersity index (PDI) of PLA and its masterbatches were determined by gel permeation chromatography (GPC) using a 1260 Infinity device (Agilent Technologies,

Santa Clara, CA, USA). The mobile phase was hexafluoro-2-isopropanol (HFIP) containing 0.19% sodium trifluoroacetate. We prepared filtered solutions containing 5 mg samples and injected them into a 7 µm modified silica column. We used a standard polymethyl methacrylate polymer (1.0×10^5 g/mol) for calibration.

2.2.7 Characterization of Yarn

DSC over the range 35 to 200 °C was used to determine the effect of colorants, their weight percentage, and the drawing parameters on the thermal transitions of PLA yarn. We measured the T_g, T_m, and T_{cc} and the degree of crystallinity (X_c) of pure PLA and dyed PLA yarns. The melting enthalpy of 100% crystalline PLA is 93.7 J/g. X_c was calculated using Eq. 2.1. [28-30].

$$X_c = {\Delta H_m - \Delta H_c * 100}\Big/{\Delta H_m^0} \qquad \textbf{Eq. 2.1}$$

H_m^0 is the melt enthalpy of the material at 100% crystallinity, H_m is the melting enthalpy at T_m and H_c is the enthalpy of cold crystallization at T_{cc}.

The yarn linear density (weight per length) was measured according to DIN EN ISO 1973, and mechanical properties (tenacity and elongation) were measured using a ZwickLine Z2.5 instrument (Zwick Roell, Ulm, Germany) according to DIN EN ISO 2062. A starting length (L_0) of 200 mm was used, and the test was carried out at 200 mm/min. All tests were carried out in triplicate.

Commission Internationale de l'Eclairage (CIE) L*a*b* color coordinates were measured using a PCE CSM 7 colorimeter (PCE Instruments, Palm Beach, FL, USA) according to EN ISO 11664-4. An aperture size of 4 mm was used. L* is the lightness index and can vary from 0 (black) to 100 (white); a higher negative a* value indicates a stronger green color; a higher positive a* value indicates a stronger red color. Similarly, a higher negative b* value indicates a stronger blue color, and a higher positive b* value indicates a stronger yellow color.

The ultraviolet (UV) light stability of the colorants in dyed yarns was measured using a blue wool scale (BWS) test according to ISO 105-B02. We exposed the samples to UVA light (0.68 W/m^2) at 340 nm and 50 °C. We prepared sample swatches from the yarn dyed with 0.3% (*w*/*w*) of each colorant, and the CIE L*a*b* coordinates were measured on the left, middle, and right. The middle part of the sample was always covered to prevent UV exposure. Samples showing a visual change at level 4 of the grayscale were given a preliminary score. The left part was then covered. The test was continued, and a final

score was given when the right part matched level 3 of the grayscale. After 130 h, we evaluated the effect of the UV on the samples. At this point, we graded light-fastness against the BWS and assigned a score between 1 (very poor) and 8 (excellent).

2.2.8 Characterization of Knitted Fabric

The effect of the colorants on the air permeability and water vapor permeability of knitted fabrics was investigated using an FX 3300 tester (Textest Instruments, Schwerzenbach, Switzerland) and Permetest (Sensora, Liberec, Czech Republic). Air permeability was measured on all knitted fabrics with an air pressure of 200 Pa and a test area of 20 cm2 according to DIN EN ISO 9237. Water vapor permeability was measured according to DIN EN ISO 11092. Abrasion resistance was measured using an AquAbrasion 1819 Martindale abrasion test device (James Heal, Sterling, VA, USA). The test was carried out according to DIN EN ISO 12947-2 with 15,000 cycles. After 1000, 2000, 3000, 4000, 5000, 7500, and 10,000 cycles, the test was stopped, and images were captured to record the abrasion of the knitted fabric. The CIE L*a*b* color coordinates of the fabric were also measured, according to the procedure mentioned above, before, and after the Martindale test to determine the abrasion resistance of the colorants. Five samples of each knitted fabric were tested at a nominal pressure of 12 kPa.

2.3 Results and Discussion

2.3.1 Analysis of the Colorants

2.3.1.1 Thermal Characteristics

Most colorants showed little to no thermal transition under our experimental conditions, as anticipated because their Tm lay beyond the tested temperature range (Figure 2.2). Even so, we observed a broad endothermic peak between 50 and 100 °C for the blue 15:1 and green 7 colorants and alizarin. Given that the two inorganic colorants were not dried before DSC and are based on copper complexes, this could indicate the evaporation of residual water. Similarly, the peak observed in the alizarin thermogram was assumed to represent water evaporation because the colorant is not expected to undergo other thermal transitions within this temperature range. Similar observations have been reported for TiO_2 [31]. No significant peak was observed for any of the colorants during the cooling cycle. We used a temperature of 200 °C for the melt spinning of PLA, and no thermal transition was observed for any of the colorants below 200 °C, so no change in the physical state of the colorants was anticipated during melt spinning.

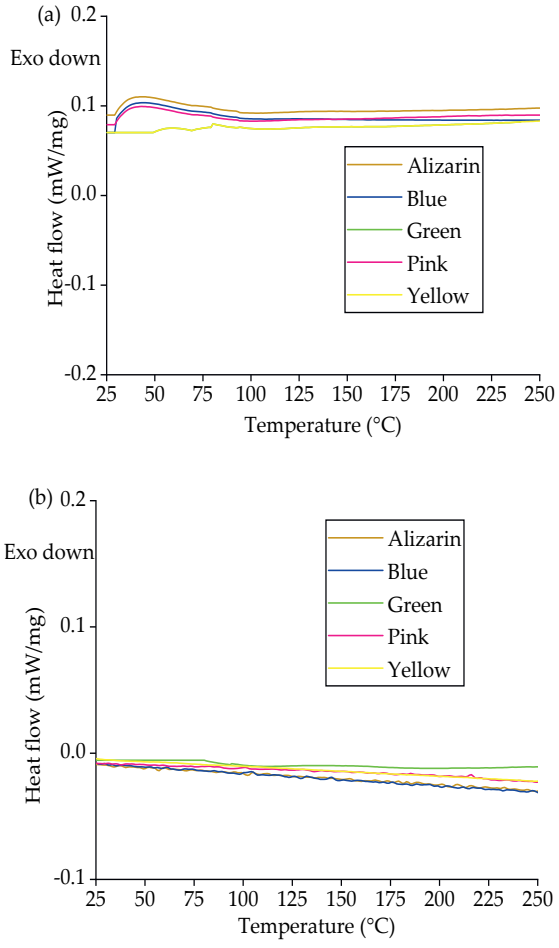

Figure 2.2: DSC thermograms of five colorants during (a) the heating cycle and (b) the cooling cycle.

2.3.1.2 Morphological Characteristics

The colorants are supplied as tiny crystals in the shape of bricks, rods, or plates, but this structure can break down during processing due to the high temperature and/or shear forces, and the crystals can dissolve in the surrounding medium [32]. SEM images revealed that alizarin has a needle-like structure, whereas the blue 15:1, green 7, and yellow 155 pigments have a plate-like structure, and pigment pink PR122 has a spherical morphology (Figure 2.3). All five colorants formed agglomerates, ranging in size from ~2 µm (blue 15:1, green 7 and yellow 155) to 2–5 µm (pink PR122) and 10–20 µm (alizarin).

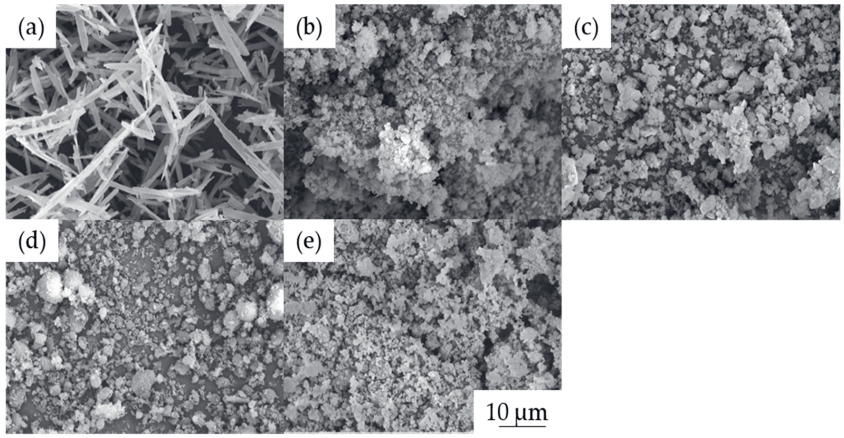

Figure 2.3: SEM images of the colorants (a) alizarin, (b) pigment blue 15:1, (c) pigment green 7, (d) pigment pink PR122, and (e) pigment yellow 155.

2.3.2 Analysis of PLA Masterbatches

2.3.2.1 Thermal Characteristics

The DSC thermograms of PLA and its masterbatches containing 5% (w/w) of each colorant (A5, B5, G5, P5, and Y5) are presented in Figure 2.4. PLA and all five masterbatches showed a major melting peak at ~175 °C. However, masterbatches G5 and P5 also showed a second, minor melting peak at ~165 °C, which may indicate a defective crystal structure. The defective crystals melt and re-crystallize, then melt again at 175 °C [33]. During the cooling cycle, the Tc remained constant at ~100 °C for PLA as well as masterbatches G5 and P5, but the Tc of A5, B5, and Y5 was higher, with B5 showing the highest Tc of ~140 °C. These data indicate that these colorants have a nucleating effect on PLA and thus promote crystallization. Similar nucleating effects have been observed in the past for compounds containing small amounts of pigment in a PP matrix and by talc and bis(hydroxyethyl)terephthalate in the case of PLA [34,35].

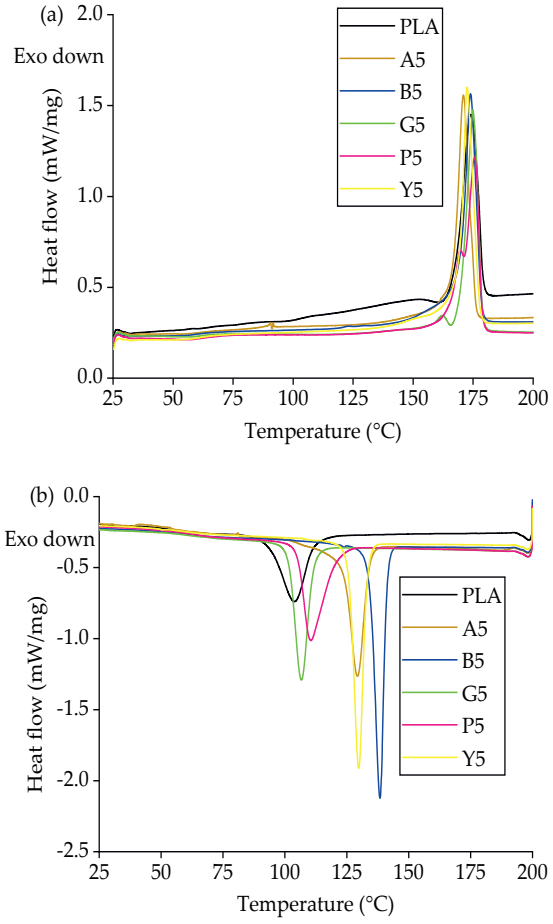

Figure 2.4: DSC thermograms of PLA and its masterbatches containing 5% (w/w) of each colorant during (a) the heating cycle and (b) the cooling cycle.

2.3.2.2 Rheological Characteristics

The rheograms of PLA and its masterbatches containing 5% (*w*/*w*) of each colorant are presented in Figure 2.5. All six materials showed non-Newtonian shear thinning behavior, in which the viscosity declines with increasing shear rate. This behavior is typical of polymers at high temperatures [36-38]. To facilitate a visual comparison, the complex viscosity of PLA and its masterbatches are shown at an angular frequency of 10/s in Figure 2.5b.

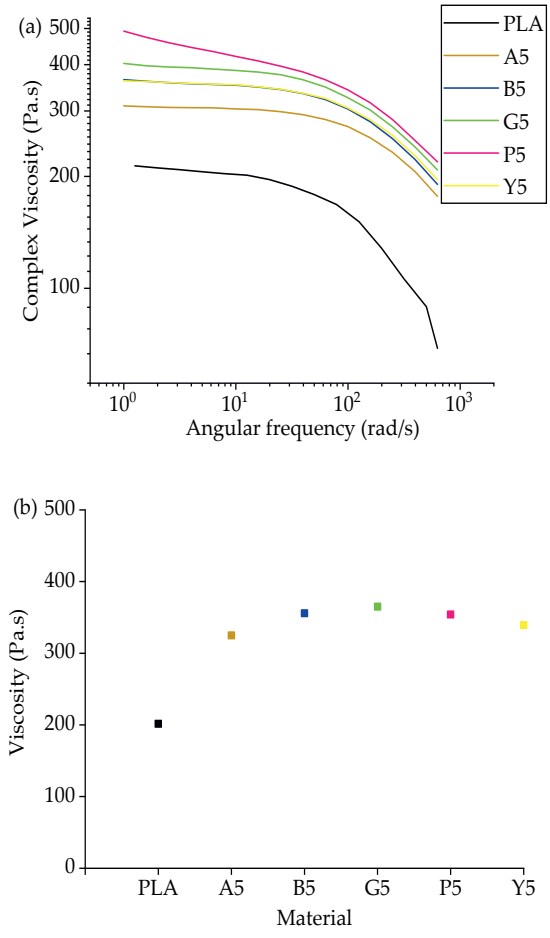

Figure 2.5: Rheological analysis of PLA and its masterbatches containing 5% (w/w) of each colorant. (a) Rheogram of PLA and the five masterbatches. (b) Complex viscosity of PLA and the five masterbatches at an angular frequency of 10/s.

The complex viscosity of PLA at an angular frequency of 10 rad/s was 201 Pa.s, but the value increased in the presence of each colorant. The highest increase of 47% was observed for masterbatch G5. Given that the colorants do not melt below 200 °C, they must act as anchors for the PLA chains, leading to an increase in melt viscosity. Furthermore, the polar groups in the colorants can interact with the polar groups in the PLA chain, hindering chain slippage and increasing the viscosity even further, as pre-viously reported [22]. A similar increase in viscosity was reported when PLA was grafted with carbon black [39]. However, given the much lower weight percentage of colorants used

for melt spinning (0.1–0.3%), we did not expect a substantial increase in viscosity or any effect on the behavior of the polymer.

2.3.2.3 Molecular Interactions between the Colorants and PLA

The FTIR spectra of PLA and its masterbatches were very similar (Figure 2.6). They all featured the characteristic C-H stretching peaks at 2993/cm and 2939/cm and C-O bending at 1184/cm. However, the peak at 1747/cm, representing the C=O stretching of PLA, shifted to 1750/cm in all of the masterbatches. This may signify an interaction between the hydroxyl groups of PLA and the functional groups of colorants, which could promote the distribution of colorant molecules in the PLA matrix. A similar shift in the C=O stretching peak of PLA was also observed when PLA was mixed with Kenaf fibers, indicating the possibility of hydrogen bonding between the components [40]. The hydrogen bonding observed in our FTIR spectra may explain the increase in the viscosity of the PLA masterbatches. In the case of the P5 masterbatch, we observe additional peaks between wavenumbers of 1650/cm and 1580/cm. This can be attributed to the bending vibration of the amine (N-H) group present in the pigment [41,42].

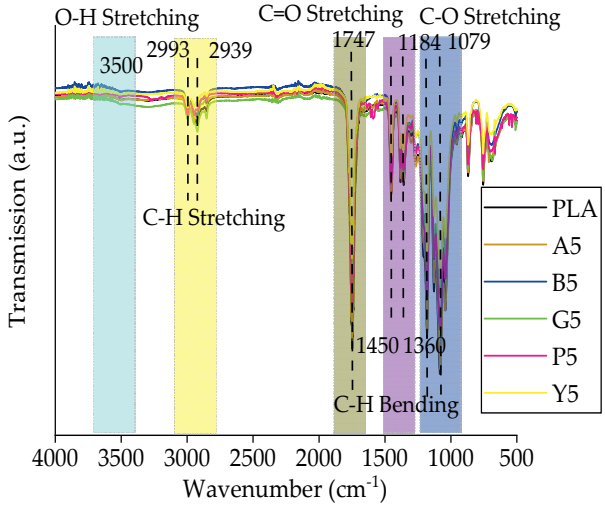

Figure 2.6: FTIR spectra of PLA and its masterbatches containing 5% (w/w) of each colorant.

2.3.2.4 Morphological Analysis

The dispersion of colorants in the PLA matrix was investigated by SEM. Cross-section images of PLA (after the compounding simulation step) and the masterbatches revealed that three colorants (alizarin, pigment blue 15:1, and pink PR122) were well dispersed

including the pure PLA, suggesting that they represented additives introduced by the manufacturer. However, we find more agglomerates in case of the masterbatches made with green 7 and yellow 155. In Section 3.1.2, we observed that these two pigments have plate-like structure, and this leads to the hypothesis that these structures are harder to disperse in PLA. Still, this contrasts with our previous study, in which we observed more abundant aggregates for almost all colorants [22]. However, in the previous study, a glass syringe with a plunger was used for spinning. The compounds were filled and melted inside the syringe barrel, and no shear was applied to break down the aggregates. In contrast, we applied shear during the preparation of our masterbatches and melt spinning to improve the mixing of the colorants. Furthermore, the colorants used here (and PLA) dissolve in solvents such as chloroform and dimethyl formamide, suggesting the Hansen solubility parameter of the colorants and PLA matrix are similar. FTIR spectroscopy provided evidence for the formation of hydrogen bonds, which also supports the compatibility of the colorants with PLA [43].

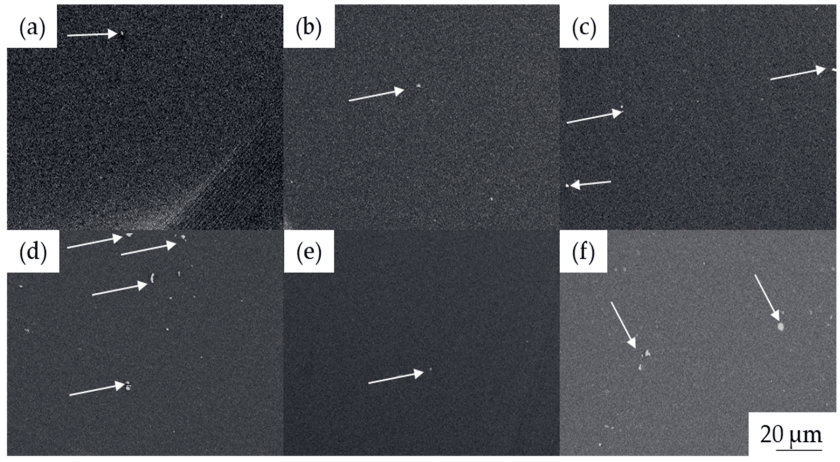

Figure 2.7: SEM images of cross-sectioned PLA and masterbatch granules: (a) pure PLA, (b) A5, (c) B5, (d) G5, (e) P5, and (f) Y5. Arrows indicate the position of aggregates.

2.3.2.5 GPC Analysis

GPC analysis revealed no significant difference in the molecular weight or PDI of PLA and its masterbatches (Figure 2.8). The relative M_w of PLA was 145,690 Da; the M_n was 83,016 Da; and the PDI was 1.76. A5 had the lowest M_w (131,950 Da) and M_n (78,316 Da), whereas P5 had the highest M_w (147,060 Da) and M_n (83,355 Da). The PDI of all samples was ~1.70. These data confirmed that the addition of colorants did not lead to the

degradation of PLA and that dope dyeing therefore avoids the polymer chain degradation that is typically observed during conventional exhaust dyeing.

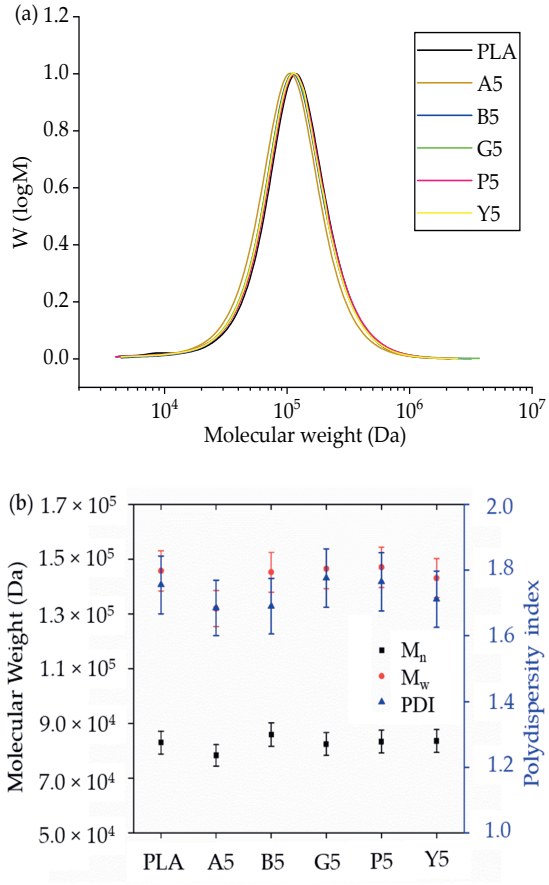

Figure 2.8: GPC analysis of PLA and its masterbatches containing 5% (w/w) of each colorant. (a) GPC elugram with normalized intensity on the y-axis. (b) Mean Mw, Mn, and PDI values ± SE (n = 3).

2.3.3 Characterization of Yarns

2.3.3.1 Mechanical Properties

The linear density of all yarns was measured to be 300 ± 5 dtex and was therefore considered 300 dtex for the tests. The tensile force vs. elongation graphs of PLA were compared at different SSD ratios (Figure 2.9a). We also compared PLA and dyed yarns containing 0.3% (w/w) of each colorant at SSD ratios of 1, 2, and 3 (Figure 2.9 b–d).

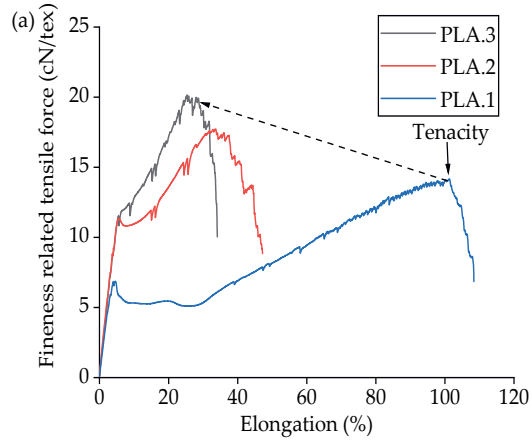
(a)
Fineness related tensile force (cN/tex)
Elongation (%)
PLA.3
PLA.2
PLA.1
Tenacity
0
5
10
15
20
25
0
20
40
60
80
100
120

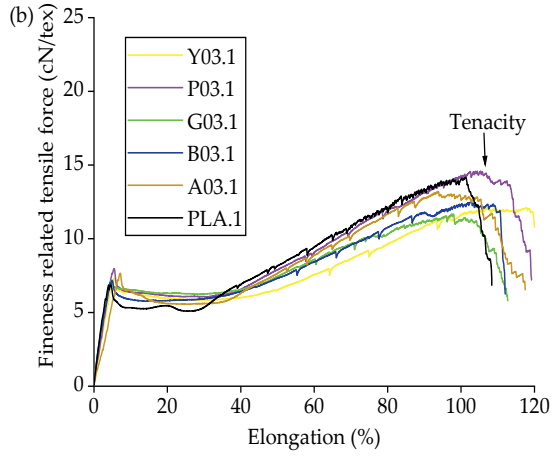
(b)
Fineness related tensile force (cN/tex)
Elongation (%)
Y03.1
P03.1
G03.1
B03.1
A03.1
PLA.1
Tenacity
0
5
10
15
20
25
0
20
40
60
80
100
120

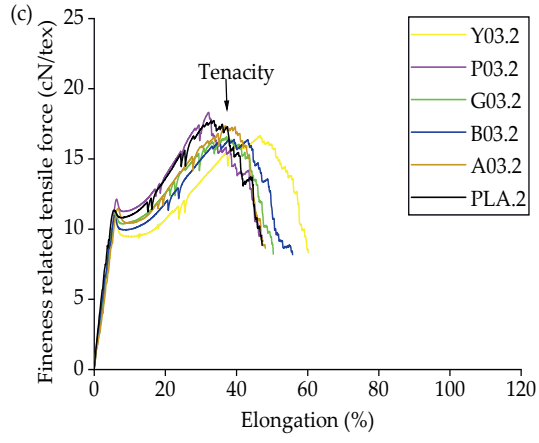
(c)
Fineness related tensile force (cN/tex)
Elongation (%)
Y03.2
P03.2
G03.2
B03.2
A03.2
PLA.2
Tenacity
0
5
10
15
20
25
0
20
40
60
80
100
120

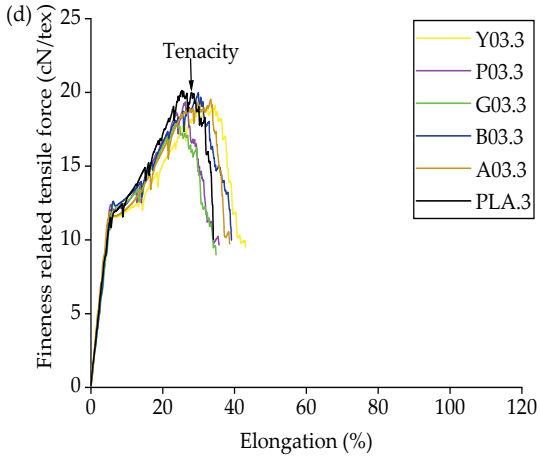

Figure 2.9: Tensilegrams of PLA and dyed yarns containing 0.3% (w/w) of each colorant at different SSD ratios. (a) Mean values of PLA yarns drawn at different SSD ratios. (b–d) Mean values of PLA and dyed yarns containing 0.3% (w/w) of each colorant drawn at SSD ratios of (b) 1, (c) 2, and (d) 3. Data are means of n = 5 samples.

The tenacity (tensile strength) of PLA yarns increased at higher SSD ratios (Figure 2.9a). The tenacity increased by almost 50% (from 14 to 20 cN/tex) when the SSD ratio increased from 1 to 3. At the same time, the elongation declined by 72% (from 94% to 26%). Increasing the SSD ratio was previously shown to increase tenacity and reduce elongation by stretching and orienting the polymer chains, leading to strain-induced crystallization [44,45]. The mechanical properties obtained from melt spun PLA yarn are similar to the values obtained by researchers in the past, when a maximum tenacity of about 30 cN/tex was reported [46,47]. There was no significant change in the mechanical properties of the yarn in the presence of colorants (Table 2.3). For example, at an SSD ratio of 3, pure PLA yarns showed the highest tenacity (20.03 cN/tex) and Y03.3 yarns the lowest (18.30 cN/tex), whereas A03.3 yarns showed the greatest elongation (31%) and Y03.3 yarns the lowest (25%). The properties of all of the other yarns produced also fall in the same range. This is a significant advantage compared to conventional exhaust dyeing, in which the higher temperature and prolonged dyeing time reduce the mechanical integrity of PLA fabrics [6,48].

Table 2.3: Tenacity and elongation of PLA and dyed yarns containing 0.3% (*w*/*w*) of each colorant with standard deviations (SD).

Material	Tenacity (cN/tex)	Elongation at Maximum Force (%)
PLA.1	13.90 ± 0.57	94.33 ± 5.08
PLA.2	17.53 ± 0.32	36.33 ± 1.75

PLA.3	20.03 ± 0.17	26.33 ± 1.22
A03.1	13.20 ± 0.08	95.67 ± 2.50
A03.2	17.60 ± 0.20	39.33 ± 1.74
A03.3	19.97 ± 0.41	31.00 ± 1.63
B03.1	11.97 ± 0.37	97.33 ± 1.14
B03.2	17.03 ± 0.17	40.33 ± 1.12
B03.3	19.60 ± 0.51	27.33 ± 1.72
G01.1	13.07 ± 0.18	100.00 ± 4.23
G02.2	16.17 ± 0.40	39.67 ± 2.34
G03.3	19.33 ± 0.24	29.33 ± 0.98
P03.1	14.10 ± 0.37	100.00 ± 1.09
P03.2	16.63 ± 0.72	32.33 ± 0.42
P03.3	19.67 ± 1.18	25.00 ± 2.13
Y03.1	11.77 ± 0.16	95.00 ± 0.94
Y03.2	16.27 ± 0.34	34.00 ± 3.11
Y03.3	18.30 ± 0.38	25.33 ± 2.25

2.3.3.2 Physical Properties

Increasing the SSD ratio did not change the Tm of the yarns (Figure 2.10). However, although the Tg remained constant at SSD ratios of 1 and 2, no Tg peak was observed at an SSD ratio of 3 (Figure 2.10). The tenacity of the yarns increased by 20% when the SSD ratio increased from 1 to 2, but the increase in crystallinity was negligible (Table 2.4). This suggests that drawing during spinning was sufficient to orient the polymer chains but insufficient to induce crystallization. However, at an SSD ratio of 3, the increase in tenacity was accompanied by a >1.5-fold increase in the degree of crystallinity, reaching 51.7% for the pure PLA fibers. Such an increase in drawing leading to increased crystallinity, to a maximum of 67%, was also reported by Mai et al. [44,49] and was also anticipated because higher SSD ratios orient the polymer chains, creating a more ordered structure that induces crystallization during processing. We also observed a shoulder in the melting peak for PLA fibers at an SSD ratio of 3, probably reflecting the formation of imperfect α' crystals during drawing, which melt at a temperature lower than α crystals. Similar melting behavior has previously been observed for drawn PLA chains [44,49].

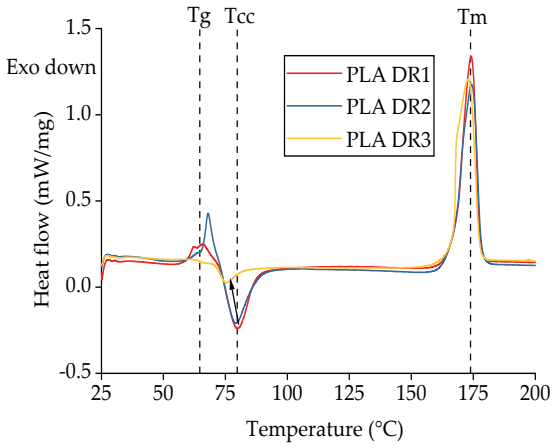

Figure 2.10: DSC thermogram of PLA yarns drawn at different ratios.

The higher crystallinity at an SSD ratio of 3 was also accompanied by a lower Tcc. Cold crystallization occurs due to rapid quenching, when amorphous polymer chains that cannot crystallize during spinning relax and crystallize to form a more ordered structure. Two hypotheses could explain the lower Tcc. First, the crystallinity of the yarns may be higher in PLA.3, limiting cold crystallization and therefore reducing the peak crystallization temperature. Second, the polymer chains are already oriented in yarns drawn with higher SSD ratios, so less energy is needed for crystallization, and cold crystallization is therefore accelerated. If the first hypothesis were correct, the onset of cold crystallization would remain constant regardless of the SSD ratio. We therefore tested for the onset of crystallization and found that the temperature declined from 75.7 °C (PLA.1) to 72.1 °C (PLA.2) and 70.8 °C (PLA.3) as the SSD ratio increased. Because the onset of crystallization also changes, the first hypothesis is rejected and the second hypothesis becomes more plausible. This leads to the conclusion that, among the parameters considered, the orientation resulting from SSD is higher than that resulting from melt drawing.

The DSC thermograms of pure PLA yarns and dyed yarns containing 0.3% (w/w) of each colorant produced at different SSD ratios are presented in Figure 2.11, and the corresponding T_g, T_m, T_{cc}, T_c and X_c values are summarized in Table 4. The DSC curves for dyed yarn containing 0.1% and 0.2% (w/w) of each colorant were very similar and are provided in the appendix (Figure 2.A1 and Figure 2.A2). As described above for the masterbatches (Section 2.3.2.1), the Tc increased in the presence of 0.3% (w/w) of the blue 15:1 pigment and yellow 155 pigments because they act as strong nucleating agents. The

T_c remained constant at 133 °C for the blue 15:1 pigment and 127 °C for the yellow 155 pigment, regardless of the weight percentage. Interestingly, although alizarin acted as a nucleating agent in masterbatch A5, the effect was not observed in the yarns, indicating that the nucleation effect only occurs at >0.3% (w/w) alizarin.

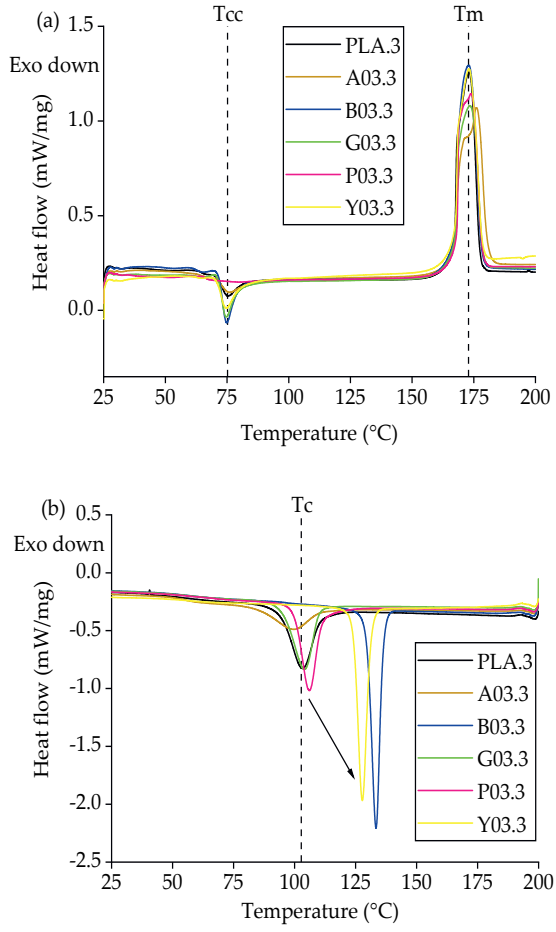

Figure 2.11: DSC thermogram of PLA and dyed yarns containing 0.3% (*w/w*) of each colorant at an SSD ratio of 3 during (**a**) the heating cycle and (**b**) the cooling cycle.

Table 2.4: The thermal transition values of PLA and dyed yarns drawn at different SSD ratios with SD (n = 3).

Sample	T_g (°C)	T_{cc} (°C)	T_m (°C)	X_c (%)	T_c (°C)
PLA.1	60.8 ± 0.2	79.5 ± 0.5	174.2 ± 0.9	29.8 ± 2.1	100.2 ± 0.5
PLA.2	60.5 ± 0.5	79.3 ± 0.6	174.3 ± 0.6	29.9 ± 1.3	100.2 ± 1.3
PLA.3	-	75.0 ± 0.1	173.0 ± 1.0	51.7 ± 3.1	100.2 ± 0.9
A03.1	60.1 ± 0.3	82.7 ± 1.2	175.2 ± 0.6	27.6 ± 3.0	101.0 ± 0.7
A03.2	60.5 ± 0.1	81.3 ± 1.7	174.9 ± 1.0	29.7 ± 1.7	97.7 ± 1.5
A03.3	-	75.8 ± 0.4	176.0 ± 1.5	51.5 ± 5.3	99.1 ± 1.0
B03.1	60.2 ± 1.5	84.3 ± 0.8	174.4 ± 0.3	30.7 ± 0.8	133.1 ± 0.4
B03.2	61.2 ± 0.7	80.6 ± 2.0	173.9 ± 0.7	27.1 ± 1.5	133.8 ± 0.6
B03.3	-	74.8 ± 0.3	172.8 ± 0.4	48.5 ± 3.1	133.4 ± 0.8
G03.1	59.8 ± 1.8	82.5 ± 0.2	173.8 ± 0.4	29.3 ± 0.9	104.7 ± 0.2
G03.2	60.2 ± 1.9	79.8 ± 1.3	174.6 ± 0.6	30.4 ± 0.9	105.2 ± 0.2
G03.3	-	74.7 ± 0.3	173.3 ± 0.7	44.9 ± 1.2	104.0 ± 0.2
P03.1	60.0 ± 0.5	79.9 ± 0.7	174.6 ± 0.1	29.9 ± 1.9	108.7 ± 1.4
P03.2	61.1 ± 0.2	78.4 ± 1.1	176.0 ± 0.8	29.1 ± 0.9	108.0 ± 0.9
P03.3	-	-	173.7 ± 0.2	52.1 ± 0.1	106.2 ± 0.6
Y03.1	60.2 ± 3.2	82.8 ± 0.5	174.6 ± 0.1	29.7 ± 0.3	127.2 ± 1.0
Y03.2	61.8 ± 0.3	79.9 ± 1.5	174.3 ± 0.8	30.0 ± 1.3	127.5 ± 0.9
Y03.3	-	74.8 ± 0.5	173.1 ± 0.2	48.47 ± 2.1	127.7 ± 1.0

Table 2.4 also shows that the T_g, T_m, T_{cc}, and X_c values were unaffected by the presence of most colorants, but green 7 was an exception, with slightly lower values at an SSD of 3. However, the mechanical properties of the yarn were unchanged. This is probably because the colorant affects the crystallization process but does not interfere with polymer chain orientation. The degree of crystallinity of the yarns dyed with all other colorants drawn at an SSD ratio of 3 was 48–50%. This seems to be the case even for the blue 15:1 pigment and yellow 155 pigment showing nucleating effects. This is perhaps because DSC was carried out at lower cooling speeds of 10 °C/min, whereas higher cooling rates of >200 °C/s were applied during melt spinning. This suggests that, although some colorants act as strong nucleating agents at lower cooling rates, they do not have sufficient time to influence the crystallinity of the yarn during spin-ning. This differs from conventional dyeing, wherein changes in crystallinity are ob-served depending on the dyeing protocol. Only the green 7 colorant affected yarn crystallinity, but the effect was marginal and not enough to reduce mechanical strength. Dope dyeing is therefore advantageous because it offers better control over the crystallinity of the yarn.

2.3.3.3 Color and UV Stability

The CIE L*a*b color values and BWS of the PLA and dyed yarns revealed that in-creasing the weight percentage of colorant resulted in a darker shade of yarn (Table 2.5). This was indicated either by the L value (whiteness index), for example, in yarns containing alizarin, or by both the L and a values in the case of the green 7 colorant, because lower L values indicate darker colors and negative a values represent greener hues. All five colorants were stable on exposure to UV light, scoring ≥ 7 in the BWS test. Although the color obtained by the exhaust dyeing of PLA with natural colorants like alizarin and indigo was good, the light fastness of PLA exhaust dyed with alizarin was reported to be low in the past even when PLA was modified with nanoparticles, whereas the dope dyeing approach used herein led to improved light fastness [13,50,51].

Table 2.5: CIE L*a*b color values and blue wool scale (BWS) of PLA and dyed yarns.

Material	L	a	b	BWS
PLA-3	84.25	–0.42	2.23	≥7
A01-3	84.46	–2.8	22.19	-
A02-3	83.71	–4.12	41.78	-
A03-3	80.13	–2.67	53.66	≥7
B01-3	41.30	7.53	–31.81	-
B02-3	47.00	8.18	–32.21	-
B03-3	37.09	3.31	–25.22	≥7
G01-3	80.13	–25.83	1.66	-
G02-3	73.19	–43.85	3.44	-
G03-3	71.64	–51.32	3.62	≥7
P01-3	69.17	29.29	–14.61	-
P02-3	60.85	41.12	–19.52	-
P03-3	54.07	49.1	–22.34	≥7
Y01-3	85.06	–5.62	41.44	-
Y02-3	84.37	–4.94	30.93	-
Y03-3	85.77	–5.45	54.75	≥7

2.3.4 Characterization of Knitted Fabrics

2.3.4.1 Water Vapor Permeability

Fabrics with greater water vapor permeability are considered more comfortable for daily use because they allow perspiration to evaporate [52]. The stitch density was kept constant in the knitting tests to avoid this parameter affecting the water vapor permeability [53]. We found that water vapor permeability was unaffected by the presence of colorants (Table 2.6). This agrees with previous studies of pigments added to silicone resin-based paints [54]. Water vapor permeability is affected by changes in

the chemical structure, morphology, and surface characteristics of the fabric, which often occur during conventional dyeing because dye molecules needed to be fixed to the surface of fibers, thus ensuring color fastness. For example, a significant difference in water vapor permeability was reported, following the dyeing of cotton [55]. In contrast, dope dyeing involves the mixing of colorants with the polymer melt, causing the colorant to be distributed throughout the polymer matrix [18]. The absence of surface modification means that the water vapor permeability of knitted fabrics made from dyed PLA yarns is almost identical to that of pure PLA. It is also observed that the water vapor permeability of PLA fabric produced here is better than that of PET (reported to be 40%) and other PLA yarn (about 60%) reported in the past [56,57].

Table 2.6: Relative and absolute water vapor permeability of knitted fabrics made from PLA and dyed PLA yarns containing 0.3% (*w*/*w*) of colorants. Data are means ± SD (*n* = 5).

Material	Relative Water Vapor Permeability (%)	Absolute Water Vapor Permeability ($Pa/m^2/W^{-1}$)
PLA	71.34 ± 3.04	2.60 ± 0.32
A03.1	70.30 ± 1.54	2.46 ± 0.19
B03.1	71.76 ± 3.16	2.72 ± 0.46
G03.1	73.56 ± 2.85	2.46 ± 0.35
P03.1	75.36 ± 2081	2.22 ± 0.32
Y03.1	74.60 ± 2.60	2.38 ± 0.31

2.3.4.2 Air Permeability

The flow of air through a knitted fabric is described as air permeability. Most colorants did not affect the air permeability of the knitted fabric, but the blue 15:1 colorant was an exception (Table 2.7). The blue 15:1 colorant reduced the air permeability slightly, although the change was not significant. The observed change could also reflect the use of laboratory-scale knitting equipment, which may introduce small irregularities. Our results differ from previous reports involving exhaust dyeing, wherein surface modifications that improve the incorporation of dyes in knitted fabrics can affects the air permeability of fabrics more significantly because the dyes form covalent bonds with the polymer chains [18,58]. Colorant molecules interact with the polymer via a different mechanism during dope dyeing, so we did not observe a similar effect. Dope dying therefore offers more scope to control the comfort properties of fabrics, including air permeability.

Table 2.7: Absolute air permeability of knitted fabrics made from PLA and dyed PLA yarns containing 0.3% (*w*/*w*) of each colorant. Data are means ± SD (*n* = 5).

Material	Air Permeability (L/m²/s)
PLA	3848 ± 332
A03.1	3406 ± 65
B03.1	3026 ± 208
G03.1	3890 ± 116
P03.1	3506 ± 257
Y03.1	3906 ± 297

2.3.4.3 Martindale Abrasion Test

The first signs of abrasion were observed after 5000 cycles in the pure PLA fabrics, whereas more cycles (up to 10,000) were required to abrade the dyed fabrics (Figure 2.12 and Table 2.8). As stated above, these differences may reflect irregularities in the knitted surface introduced by the laboratory-scale knitting equipment. A value between 5000 and 10,000 cycles suggests that the fabrics produced here are more suited for decorative use (e.g., in cushions) than general use, which would require the fabrics to withstand >20,000 cycles [59]. Fabrics made from PLA blends have been reported to have low abrasion resistance, being destroyed after 2250 cycles, but the yarn developed in this study was observed to have better abrasion resistance [60]. This can be the case because the yarn produced here had better mechanical properties compared to the PLA blend yarn used in the previous study. The processing conditions should therefore be optimized further to improve the abrasion resistance.

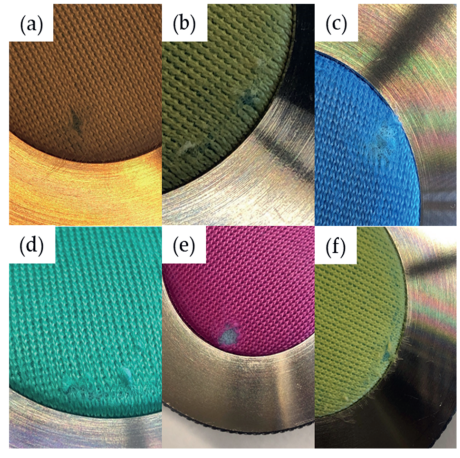

Figure 2.12: First signs of abrasion in knitted PLA fabrics: (**a**) PLA.1, (**b**) A03.1, (**c**) B03.1, (**d**) G03.1, (**e**) P03.1, and (**f**) Y03.1.

Table 2.8: Abrasion resistance and color fastness of PLA and dyed fabrics containing 0.3% (*w*/*w*) of each colorant, determined using the Martindale abrasion test.

Material	Abrasion Resistance (Number of Cycles)	Before Martindale			After Martindale		
		L	a	b	L	a	b
PLA	5000	78.50	−0.21	1.02	72.66	−1.47	3.67
A03.1	10,000	76.80	−2.15	45.20	63.36	−1.00	25.51
B03.1	7500	31.09	3.22	26.22	30.22	5.13	28.66
G03.1	10,000	65.22	−38.22	2.12	63.11	−35.56	2.25
P03.1	7500	44.94	50.05	−13.27	42.91	38.06	−13.23
Y03.1	7500	73.97	−11.13	40.77	70.23	−9.48	33.64

It is observed from Table 2.8 that the color fastness of PLA and the fabrics containing blue, green, pink, and yellow pigment is good. There was minimal color change after the Martindale abrasion test. However, in the case of fabric containing alizarin, a significant color change was observed and the fabric change from yellow to a light yellow color. The overall L,a,b values obtained herein are a little different from the values obtained from the yarn values. This could be the case because of the difference in the measurement method. In the case of yarn, the yarn was bundled into a ball, and the color was measured, and in the case of fabric, the color was measured directly from the reflection of light. This is hypothesized to lead to the small difference in color observed.

2.4 Conclusions

We investigated the effect of colorants on the structure and properties of dope dyed PLA yarn and fabric. We produced masterbatches of PLA containing 5% (w/w) of each colorant using a twin-screw compounder and generated PLA yarns containing up to 0.3% (w/w) of the colorants using a pilot-scale melt spinning machine. This is a more efficient and less environmentally harmful approach to dye thermolabile biopolymers such as PLA. During spinning, we kept the winding speed constant but varied the melt composition and SSD ratio to investigate the effect of these parameters on the properties of PLA yarns. First, we analyzed the thermal properties and morphology of the colorants and found that no thermal transition occurred below the spinning temperature of 200 °C. We then analyzed the masterbatches to investigate the effect of colorants on the rheological and thermal properties of PLA, including its degradation. We observed that the presence of 5% (w/w) of the colorants led to an increase in viscosity. Furthermore, alizarin and the blue 15:1 and yellow 155 pigments showed nucleating activity. No change in molecular weight was observed in the masterbatches, suggesting the absence of PLA degradation. FTIR spectra revealed the possibility of hydrogen bonding between

PLA and the colorants, which facilitated their distribution in the PLA matrix, as confirmed by SEM.

The mechanical testing of pure PLA yarns and yarns containing up to 0.3% (w/w) of the colorants spun at different drawing speeds revealed that the mechanical properties were affected most by the drawing speed, while the colorant had a negligible effect. Increasing the SSD ratio from 1 to 3 at a constant winding speed caused the tenacity of the yarn to increase by ~50%. DSC also revealed that drawing had a stronger influence on the degree of crystallinity of the yarns, but the colorant had no effect even if it acted as a nucleating agent. This may reflect the slow cooling rate during DSC (10 °C/min) compared to >200 °C/s during melt spinning, which is too rapid for nucleation to affect crystallization. Interestingly, the Tcc declined with increasing SSD ratio, suggesting that crystallization accelerates when there is already inherent orientation pre-sent in the processed yarn.

The BWS test revealed that all five colorants are UV-resistant. Furthermore, the incorporation of colorants had no effect on air permeability or water vapor permeability. The Martindale abrasion test revealed that the fabrics were suitable for decorative use. In conventional exhaust dyeing, the dyeing temperature and duration influence the mechanical properties, crystallinity, and the other physical aspects of knitted fabrics. In contrast, dope dyeing had little impact, allowing a greater degree of control over the yarn and fabric properties by modifying the process parameters. We also found that the potentially biobased colorant alizarin and the biobased pink PR122 pigment perform as well as the commercial colorants. We conclude that dope dyeing with colorants can be a sustainable alternative to conventional exhaust dyeing and offers better control of yarn properties.

Acknowledgments

We would like to thank our laboratory technician Henri Becker for the maintenance and modification of our equipment and our student Konrad Beukenberg for supporting the experimental trial preparations. We would like to extend our gratitude to Richard M Twyman for his extensive support with language corrections. We would also like to thank Dorien Derksen and Eric Mattheussens for offering assistance with color measurements.

References

1. Pulidini, K.B.S. Polyester Fiber Market Size. Available online: https://www.gminsights.com/industry-analysis/polyester-fiber-market. (accessed on 2 May 2022).
2. Carus, M. Nova-Institute Announces New Market Study on Bioplastics with Latest Data for 2018. Available online: https://renewable-carbon.eu/news/nova-institute-announces-new-market-study-on-bioplastics-with-latest-data-for-2018/. (accessed on 18 November 2022)
3. Hussain, T.; Tausif, M.; Ashraf, M. A review of progress in the dyeing of eco-friendly aliphatic polyester-based polylactic acid fabrics. J. Clean. Prod. 2015, 108, 476–483. Doi: https://doi.org/10.1016/j.jclepro.2015.05.126.
4. Chen, G.Q.; Patel, M.K. Plastics derived from biological sources: Present and future: A technical and environmental review. Chem. Rev. 2012, 112, 2082–2099. Doi: https://doi.org/10.1021/cr200162d.
5. Abdrabbo, A.; El-Dessouky, H.M.; Fotheringham, A.F. Treatment of polylactic acid fiber using low temperature plasma and its effects on vertical wicking and surface characteristics. J. Text. Inst. 2013, 104, 28–34. Doi: https://doi.org/10.1080/00405000.2012.693699.
6. Xu, S.; Chen, J.; Wang, B.; Yang, Y. Sustainable and Hydrolysis-Free Dyeing Process for Polylactic Acid Using Nonaqueous Medium. ACS Sustain. Chem. Eng. 2015, 3, 1039–1046. Doi: https://doi.org/10.1021/sc500767w.
7. Ma, P.; Xu, Y.; Wang, D.; Dong, W.; Chen, M. Rapid crystallization of poly(lactic acid) by using tailor-made oxalamide derivatives as novel soluble-type nucleating agents. Ind. Eng. Chem. Res. 2014, 53, 12888–12892. Doi: https://doi.org/10.1021/ie502211j.
8. Wang, L.; Wang, Y.-n.; Huang, Z.-g.; Weng, Y.-x. Heat resistance, crystallization behavior, and mechanical properties of polylactide/nucleating agent composites. Mater. Des. (1980–2015) 2015, 66, 7–15. Doi: https://doi.org/10.1016/j.matdes.2014.10.011.
9. Baig, G.A. Hydrolytic stability of PLA yarns during textile wet processing. Fibers Polym. 2013, 14, 1912–1918. Doi: https://doi.org/10.1007/s12221-013-1912-7.

10. Bayati, S.; Tavanaie, M.A. Dyeing of recycled Poly(lactic acid) fibers from disposable packages flake with low energy consumption and effluent. J. Clean. Prod. 2018, 176, 382–390. Doi: https://doi.org/10.1016/j.jclepro.2017.12.038.

11. Fattahi, F.; Izadan, H.; Khodammi, A. Investigation into the Effect of UV/Ozone Irradiation on Dyeing Behaviour of Poly(Lactic Acid) and Poly(Ethylene Terephthalate) Substrates. Prog. Color Color. Coat. 2012, 5, 7.

12. Sidarkote, R.; Suwanruji, P.; Suesat, J. Exhaust Dyeing Poly(Lactic Acid) Fabrics with Indigo Dye Obtained from Indigofera Tinctoria. Adv. Mater. Res. 2014, 1025–1026, 531–534. Doi: https://doi.org/10.4028/www.scientific.net/AMR.1025-1026.531.

13. Baykuş, O.; Tugce Celik, I.; Dogan, S.D.; Davulcu, A.; Dogan, M. Enhancing the dyeability of poly(lactic acid) fiber with natural dyes of alizarin, lawsone, and indigo. Fibers Polym. 2017, 18, 1906–1914. Doi: https://doi.org/10.1007/s12221-017-6636-7.

14. Fajraoui, A.; Ben Nasr, J.; Lacoste, C.; Amar, M.B.; Dony, P.; Odof, S.; El Halouani, F. Coloration of the polylactic acid with the natural dye extracted from acacia cyanophylla flowers. Polym. Test. 2019, 78, 105988. Doi: https://doi.org/10.1016/j.polymertesting.2019.105988.

15. Mogi, K.; Kubokawa, H.; Hatakeyama, T. Effect of dyeing on melting behavior of poly(lactic acid) fabirc. J. Therm. Anal. Calorim. 2002, 70, 867–875.

16. Carmen, Z.; Daniela, S. Textile Organic Dyes—Characteristics, polluting effects and separation/elimination procedures from industrial effluents—A critical overview. In Organic Pollutants Ten Years After the Stockholm Convention; Puzyn, T., Mostrag-Szlichtyng, A., Eds.; InTech: Rang-Du-Fliers, France, 2012; Volume 1, pp. 55–86.

17. Carmichael, A. Man-Made Fibers Continue To Grow. Available online: https://www.textileworld.com/textile-world/fiber-world/2015/02/man-made-fibers-continue-to-grow/ (accessed on 2 May 2022).

18. Choudhury, A.K.R. Handbook of Textile and Industrial Dyeing; Woodhead Publishing: Cambridge, UK, 2011; Volume 2.

19. Zhang, L.; Dong, H.; Li, M.; Wang, D.; Liu, M.; Wang, C.; Fu, S. Synthesis and characterization of carbon black modified by polylactic acid (PLA-g-CB) as pigment

for dope dyeing of black PLA fibers. J. Appl. Polym. Sci. 2019, 137, 48784. Doi: https://doi.org/10.1002/app.48784.

20. Reinhardt, D. Vergleichende Sachbilanz im Textilbereich—Spinnfärbung versus Flottenfärbung; Friedrich-Schiller-Universität: Jena, Germany, 2003; p. 5.

21. Tavanaei, H.; Morshed, M.; Zarebini, M.; Salehi, R.A. A Study of the Nucleation Effect of Pigment Dyes on the Microstructure of Mass Dyed Bulked Continuous Filament Polypropylene. Iran. Polym. J. 2005, 14, 267–276.

22. Balakrishnan, N.K.; Koenig, K.; Seide, G. The effect of dye and pigment concentrations on the diameter of melt electrospun polylactic acid fibers. Polymers 2020, 12, 2321. Doi:https://doi.org/10.3390/polym12102321.

23. Pigment Blue 15. Available online: https://www.tcichemicals.com/NL/nl/p/P0655 (accessed on 12 November 2022).

24. Henan Tianfu Chemical Co., L. Pigment Green 7. Available online: https://www.chemicalbook.com/ProductChemicalPropertiesCB7399460_EN.htm# MSDSA (accessed on 12 November 2022).

25. Pigment Red 122. Available online: https://www.additivesforpolymer.com/portfolio/pigment-red-122/ (accessed on 12 November 2022).

26. Pigment Yellow 155. Available online: https://pubchem.ncbi.nlm.nih.gov/compound/Pigment-Yellow-155 (accessed on 12 November 2022).

27. Alizarin. Available online: https://www.sigmaaldrich.com/catalog/product/sial/122777?lang=en&region=NL (accessed on 12 November 2022).

28. Jia, S.; Yu, D.; Zhu, Y.; Wang, Z.; Chen, L.; Fu, L. Morphology, crystallization and thermal behaviors of PLA-based composites: Wonderful effects of hybrid GO/PEG via dynamic impregnating. Polymers 2017, 9, 528. Doi: https://doi.org/10.3390/polym9100528.

29. Pyda, M.; Bopp, R.C.; Wunderlich, B. Heat capacity of poly(lactic acid). J. Chem. Thermodyn. 2004, 36, 731–742. Doi: https://doi.org/10.1016/j.jct.2004.05.003.

30. Zhang, H.; Bai, H.; Liu, Z.; Zhang, Q.; Fu, Q. Toward high-performance poly(l-lactide) fibers via tailoring crystallization with the aid of fibrillar nucleating agent.

ACS Sustain. Chem. Eng. 2016, 4, 3939–3947. Doi: https://doi.org/10.1021/acssuschemeng.6b00784.

31. Sohn, J.R.; Han, J.S. NiO-TiO2 Catalyst Modified with WO3 for Ethylene Dimerization. In New Developments and Application in Chemical Reaction Engineering; Rhee, H.K., Nam, I.S., Park, J.P., Eds.; Studies in Surface Science and Catalysis; Elsevier B.V.: Amsterdam, The Netherlands, 2006; Volume 159, pp. 269–272.

32. Marzec, A. The effect of dyes, pigments and ionic liquids on the properties of elastomer composites. Ph.D. Thesis, Technical university of Lodz, Łódź, Poland, University Claude Bernard-Lyon 1, Villeurbanne, France, 2014.

33. Gracia-Fernández, C.A.; Gómez-Barreiro, S.; López-Beceiro, J.; Naya, S.; Artiaga, R. New approach to the double melting peak of poly(l-lactic acid) observed by DSC. J. Mater. Res. 2012, 27, 1379–1382. Doi: https://doi.org/10.1557/jmr.2012.57.

34. Lee Wo, D.; Tanner, R.I. The impact of blue organic and inorganic pigments on the crystallization and rheological properties of isotactic polypropylene. Rheol. Acta 2009, 49, 75–88. Doi: https://doi.org/10.1007/s00397-009-0388-2.

35. Yu, F.; Liu, T.; Zhao, X.; Yu, X.; Lu, A.; Wang, J. Effects of talc on the mechanical and thermal properties of polylactide. Journal of Applied Polymer Science 2012, 125, E99-E109. Doi: https://doi.org/10.1002/app.36260.

36. Dorgan, R.J. Poly(lactic acid): Synthesis, Structures, Properties, Processing, Applications, and End of Life, 2nd ed.; Grossman, F.R.N.D., Ed.; John Wiley & Sons, Inc.: Hoboken, NJ, USA, 2022.

37. Bourg, V.; Valette, R.; Le Moigne, N.; Ienny, P.; Guillard, V.; Bergeret, A. Shear and extensional rheology of linear and branched polybutylene succinate blends. Polymers 2021, 13, 652. Doi: https://doi.org/10.3390/polym13040652.

38. Fang, Q.; Hanna, M.A. Rheological properties of amorphous and semicrystalline polylactic acid polymers. Ind. Crops Prod. 1999, 10, 47–53.

39. Zhang, L.; Dong, H.; Li, M.; Wang, L.; Liu, Y.; Wang, L.; Fu, S. Fabrication of polylactic acid-modified carbon black composites into improvement of levelness and mechanical properties of spun-dyeing polylactic acid composites membrane. ACS Sustain. Chem. Eng. 2018, 7, 688–696. Doi: https://doi.org/10.1021/acssuschemeng.8b04264.

40. Kamarudin, S.H.; Chuah, A.L.; Aung, M.M.; Ratnam, C.T.; Jusoh, E.R. A study of mechanical and morphological properties of PLA based biocomposites prepared with EJO vegetable oil based plasticiser and kenaf fibers. Mater. Res. Express 2018, 5, 085314.

41. Zhu, H.; Peng, S.; Jiang, W. Electrochemical properties of PANI as single electrode of electrochemical capacitors in acid electrolytes. Sci. World J. 2013, 2013, 940153. Doi: https://doi.org/10.1155/2013/940153.

42. LibreTexts. Infrared Spectroscopy Absorption Table. Available online: https://chem.libretexts.org/Ancillary_Materials/Reference/Reference_Tables/Spectroscopic_Reference_Tables/Infrared_Spectroscopy_Absorption_Table (accessed on 12 November 2022).

43. David, D.J.; Sincock, T.F. Estimation of miscibility based on solubility parameter concept. Polymer 1991, 33, 4506–4514.

44. Siebert, S.; Berghaus, J.; Seide, G. Nucleating agents to enhance poly(l-Lactide) fiber crystallization during industrial-scale melt spinning. Polymers 2022, 14, 1395. Doi: https://doi.org/10.3390/polym14071395.

45. Baird, D.G.; Collias, D.I. Polymer Processing: Principles and Design, 2rd ed.; John Wiley & Sons, Inc.: Hoboken, NJ, USA, 2014.

46. Naeimirad, M.; Zadhoush, A.; Esmaeely Neisiany, R.; Salimian, S.; Kotek, R. Melt-spun PLA liquid-filled fibers: Physical, morphological, and thermal properties. J. Text. Inst. 2018, 110, 89–99. Doi: https://doi.org/10.1080/00405000.2018.1465336.

47. Olmen, R.V. Biobased PLA Yarns with High Mechanical Properties. Available online: https://www.centexbel.be/en/news/biobased-pla-yarns-with-high-mechanical-properties (accessed on 18 November 2022).

48. Phillips, D.; Suesat, J.; Wilding, M.; Farrington, D.; Sandukas, S.; Sawyer, D.; Bone, J.; Dervan, S. Influence of different preparation and dyeing processes on the physical strength of the Ingeo† fiber component in an Ingeo fiber/cotton blend. Part 1: Scouring followed by dyeing with disperse and reactive dyes. Color. Technol. 2004, 120, 35–40.

49. Mai, F.; Tu, W.; Bilotti, E.; Peijs, T. The Influence of Solid-State Drawing on Mechanical Properties and Hydrolytic Degradation of Melt-Spun Poly(Lactic Acid) (PLA) Tapes. Fibers 2015, 3, 523–538. Doi: https://doi.org/10.3390/fib3040523.

50. Ujjin, S.; Jantip, S. Study on the dyeing properties of poly(lactic acid) and silk yarns with natural dyes. Adv. Mater. Res. 2012, 486, 384–387. https://doi.org/10.4028/www.scientific.net/AMR.486.384.

51. Drivas, I.; Blackburn, R.S.; Rayner, C.M. Natural anthraquinonoid colorants as platform chemicals in the synthesis of sustainable disperse dyes for polyesters. Dye. Pigment. 2011, 88, 7–17. Doi: https://doi.org/10.1016/j.dyepig.2010.04.009.

52. Prahsarn, C.; Barker, R.L.; Gupta, B.S. Moisture vapor transport behavior of polyester knit fabrics. Text. Res. J. 2016, 75, 346–351. Doi: https://doi.org/10.1177/0040517505053811.

53. Gupta, D.; Kothar, V.K.; Jhanj, Y. Heat and moisture transport in single jersey plated fabrics. Indian J. Fiber Text. Res. 2013, 39, 7.

54. Lisowski, J.; Szadkowski, B.; Marzec, A. Effects of selected pigments on the properties of silicone resin-based paints. Materials 2022, 15, 4961. Doi: https://doi.org/10.3390/ma15144961.

55. Shu, D.; Fang, K.; Liu, X.; Cai, Y.; An, F.; Qu, G.; Liang, Y. Cleaner pad-steam dyeing technology for cotton fabrics with excellent utilization of reactive dye. J. Clean. Prod. 2019, 241, 118370. Doi: https://doi.org/10.1016/j.jclepro.2019.118370.

56. Demiryürek, O.; Uysaltürk, D. Thermal comfort properties of Viloft/cotton and Viloft/polyester blended knitted fabrics. Text. Res. J. 2013, 83, 1740–1753. Doi: https://doi.org/10.1177/0040517513478458.

57. Maqsood, M.; Seide, G. Development of biobased socks from sustainable polymer and statistical modeling of their thermo-physiological properties. J. Clean. Prod. 2018, 197, 170–177. Doi: https://doi.org/10.1016/j.jclepro.2018.06.191.

58. Ho-Jin, N.; Dong-Won, J.; Jong-Jun, K. Effect of Mordanting, Dyeing, Rinsing, and Fiber Characteristics on the Air-permeability and Color of Fabrics Dyed using Cochineal Dyestuff. J. Fash. Bus. 2005, 9, 114–124.

59. Alice. The Martindale Test: Fabric Rub Count. Available online: https://www.justfabrics.co.uk/inspiration/the-martindale-test-fabric-rub-count/ (accessed on 18 November 2022).

60. Huang, X.X.; Tao, X.M.; Zhang, Z.H.; Chen, P. Properties and performances of fabrics made from bio-based and degradable polylactide acid/poly

(hydroxybutyrate- co-hydroxyvalerate) (PLA/PHBV) filament yarns. Text. Res. J. 2016, 87, 2464–2474. Doi: https://doi.org/10.1177/0040517516671128.

Chapter 3

Biobased dyes as conductive additives to reduce the diameter of polylactic acid fibers during melt electrospinning

This chapter is based on the following publication:
Koenig, K. †; Balakrishnan, N. K. †, Hermanns, S.; Langensiepen, F.; Seide, G. Biobased dyes as conductive additives to reduce the diameter of polylactic acid fibers during melt electrospinning. Materials 2020, 13 (5), doi: 10.3390/ma13051055

† Both authors contributed equally to the work

Abstract

Electrospinning is widely used for the manufacture of fibers in the low micrometer to nanometer range, allowing the fabrication of flexible materials with a high surface area. A distinction is made between solution and melt electrospinning. The former produces thinner fibers but requires hazardous solvents, whereas the latter is more environmentally sustainable because solvents are not required. However, the viscous melt requires high process temperatures and its low conductivity leads to thicker fibers. Here we describe the first use of the biobased dyes alizarin, hematoxylin and quercetin as conductive additives to reduce the diameter of polylactic acid (PLA) fibers produced by melt electrospinning, combined with a biobased plasticizer to reduce the melt viscosity. The formation of a Taylor cone followed by continuous fiber deposition was observed for all PLA compounds, reducing the fiber diameter by up to 77% compared to pure PLA. The smallest average fiber diameter of 16.04 μm was achieved by adding 2% (w/w) hematoxylin. Comparative analysis revealed that the melt electrospun fibers had a low degree of crystallinity compared to drawn filament controls, resembling partially oriented filaments. Our results form the basis of an economical and environmentally friendly process that could ultimately provide an alternative to industrial solution electrospinning.

3.1 Introduction

Electrospinning is a simple, versatile, and cost-effective method to produce fibers in the low micrometer to nanometer range, thus making a significant contribution to the booming nanotechnology industry [1-3]. The beneficial properties of such fibers include their flexibility and enormous surface area, leading to applications in medicine [4-8], filtration and separation [9,10], electronics and energy [11,12], and textile manufacturing [13-15].

Electrospinning involves the exposure of liquids to strong electric fields. When a large potential difference (tens of kilovolts) is applied to a liquid flowing through a capillary, the liquid forms a jet that may undergo whip-like movements, stretching the fluid and yielding microscale or nanoscale fibers that are deposited on a collector [15]. The two principal types of electrospinning are solution electrospinning, where the polymer is dissolved in a solvent that evaporates to produce the fibers, and melt electrospinning, where a molten polymer is cooled to produce the fibers [1]. Solution electrospinning is easier to implement, has been studied more widely, and is favored by industry, despite the environmental hazards posed when toxic solvents are required. In contrast, research and technology uptake in the field of melt electrospinning has been held back by complex equipment requirements [16], the problem of electric discharge [17], and the high temperature, high viscosity and low conductivity of the polymer melt [18]. Accordingly, parameters that affect the viscosity, conductivity, thermal and structural properties of solution electrospun fibers are well understood, allowing the production of finer fibers, whereas equivalent studies focusing on melt electrospinning are still at an early stage [1,19].

The wider adoption of melt electrospinning could help to reduce the environmental footprint of current industrial electrospinning processes, which require an expensive solvent recovery process and present a high risk of toxic solvent carryover into the final product. For example, one of the commonly used materials in industrial electrospinning process is polylactic acid (PLA) because it is a sustainable polymer made from renewable agricultural resources and is reported to be industrial compostable. Commercial low molecular weight PLA was reported to have a biodegradation degree of 72% after 110 days under aerobic conditions [20]. However, PLA submicrofibers are usually prepared using the toxic solvents dichloromethane, chloroform or *N*,*N*-dimethyl-formamide [21]. It is therefore desirable to improve melt electrospinning technology, aiming to reduce the fiber diameter by overcoming the limitations described above. One promising

approach is the use of additives to increase the conductivity of polymer melts, and plasticizers to reduce their viscosity, in order to produce thinner fibers [22-24]. PLA is the most commercially available biobased and biodegradable thermoplastic polymer with increasing use in the textile sector to replace petroleum-based polymers [25]. It is therefore an important substrate for melt electrospinning technology. PLA fibers produced by melt electrospinning have been modified by adding a plasticizer [21,26], and by adjusting the device during fabrication to facilitate airflow [27] or incorporate laser heating [17]. These approaches led to the production of fibers with diameters in the range 0.2–50 μm [17,18,21,27-33]. However, most of the additives used thus far are unsustainable chemicals that offset the environmental advantages of biobased polymers. They are difficult to disperse in the polymer melt, or they adsorb water and therefore interfere with high-temperature melt electrospinning processes [21,26,34].

Sustainable colorants are used extensively in the textile industry, offering a promising alternative to conventional additives [35]. Colorants can be classified as dyes or pigments. Dyes are molecules that can be solubilized in a polymer substrate, they have good chemical affinity for the polymer, and therefore retain transparency; in contrast, pigments are insoluble in the polymer substrate and are dispersed as very fine particles (Figure 3.1).

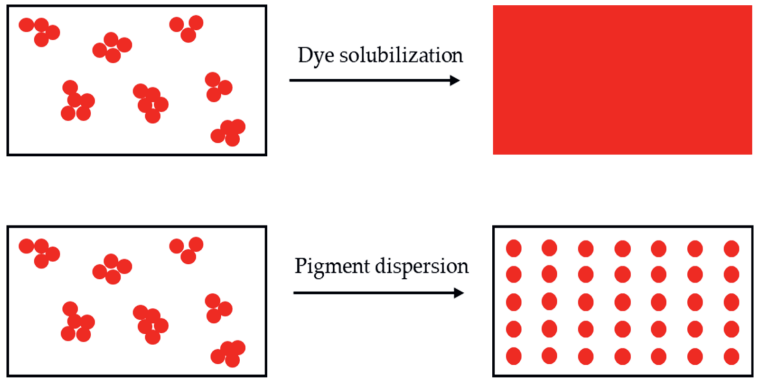

Figure 3.1: Schematic representation of dye solubilization and pigment dispersion.

Common organic textile dyes include alizarin and curcuma, whereas common pigments include copper phthalocyanine and carbon black [36]. Colorants such as alizarin, purpurin and phthalocyanine have already been used to manufacture electronics such as field effect transistors and dye-sensitized solar cells [37] because the presence of

functional groups and/or π-conjugation improves conductivity, and charge carrier mobility may exceed 1 cm^2/Vs [38].

The aim of this study was to investigate the ability of three biobased dyes to increase the conductivity of molten PLA during melt electrospinning, combined with a biobased plasticizer to reduce melt viscosity for an overall reduction of the obtained fiber diameters. We selected the biobased dyes alizarin, quercetin and hematoxylin, which have not previously been used in a melt electrospinning process, and determined their effect on the diameter of PLA fibers manufactured using a single-nozzle melt electrospinning device. We compared fibers incorporating different weight percentages of dye with or without the biobased plasticizer. We determined the influence of the additives on viscosity, conductivity, degradation and thermal behavior. We also compared the morphology and crystallization behavior of melt electrospun fibers to melt spun fibers with different draw ratios. Our results can be used to develop an environmentally beneficial melt electrospinning process for the manufacture of microscale and nanoscale fibers.

3.2 Experimental

3.2.1 Materials

PLA grade L130 (Total|Corbion, Gorinchem, Netherlands) was used as the base polymer for all experiments. The following specifications were reported by the manufacturer: L-content ≥ 99%, glass transition temperature (T_g) ~60 °C, and melt flow index = 24 g/10 min at 210 °C/2.16 kg. The chemical structures and melting points of the biobased dyes alizarin, quercetin, and hematoxylin (Sigma-Aldrich, Zwijndrecht, Netherlands) are presented in Table 3.1.

Table 3.1: Chemical structures and melting points of the dyes alizarin, hematoxylin and quercetin.

Dye	Chemical structure	Melting point (°C)
Alizarin	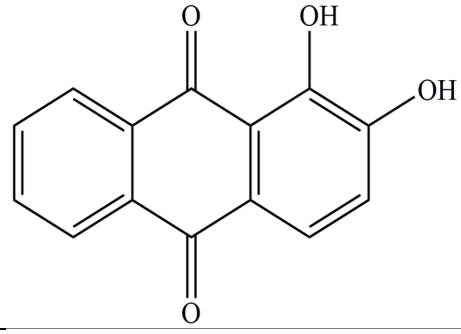	279–283
Hematoxylin	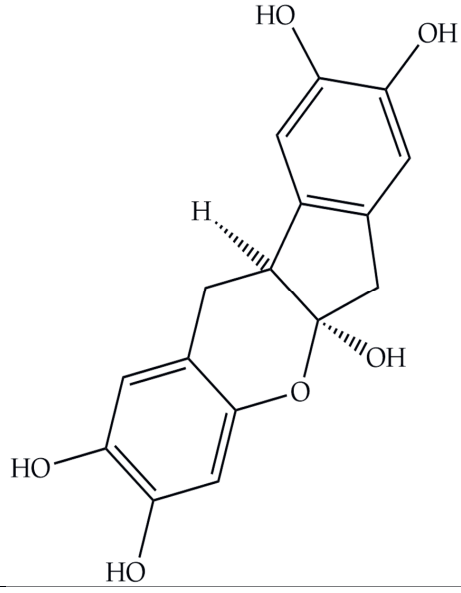	200

Quercetin	0 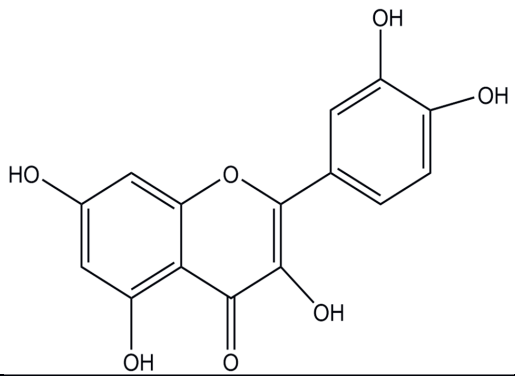	320

Liquid dyes (Rowasol, Pinneberg, Germany) were prepared by stirring 25% (w/w) of the biobased dyes with a plasticizer based on vegetable oil. The dyes were used without plasticizer to test their effect on melt conductivity and with plasticizer to determine the combined effect of increasing the conductivity and reducing the viscosity of the melt.

3.2.2 Micro-compounder

PLA was vacuum dried at 80 °C overnight before compounding to reach a water content of less than 100 ppm. PLA compounds were made by mixing with 1% or 2% (w/w) of each additive in a micro-compounder (Xplore, Sittard, Netherlands) at 200 °C with a screw speed of 100 rpm for 2 min. The list of compounds and their abbreviations are presented in Table 3.2.

Table 3.2: Compound abbreviations according to the dye and weight percent.

Compound abbreviation	Dye	% (w/w) of dye	% (w/w) of plasticizer
A1	Alizarin	1	0
A2	Alizarin	2	0
LA1	Liquid Alizarin	0.25	0.75
LA2	Liquid Alizarin	0.5	1.5
H1	Hematoxylin	1	0

H2	Hematoxylin	2	0
LH1	Liquid Hematoxylin	0.25	0.75
LH2	Liquid Hematoxylin	0.5	1.5
Q1	Quercetin	1	0
Q2	Quercetin	2	0
LQ1	Liquid Quercetin	0.25	0.75
LQ2	Liquid Quercetin	0.5	1.5

In the subsequent evaluation and discussion, it must be taken into account that a direct comparison of results is only feasible between the individual dye compounds or liquid dye compounds due to the changed dye concentration of the liquid dyes.

3.2.3 Melt spinning equipment

Prior to melt spinning PLA was dried the same way it was dried before compoundin. Low-oriented filaments (LOFs) were prepared using a KETSE 20/40 twin-screw extruder (Brabender, Duisburg, Germany) with a spinning head. Melt spinning was performed at 200 °C using a spinneret with 24 holes, each 0.4 mm in diameter, and a length to diameter ratio of two. A constant throughput was maintained and the multifilaments were wound at 150 m/min. The LOFs were post-drawn at 100 °C with a draw ratio of 5 to obtain drawn filaments (DFs). The crystallinity of these filaments was compared to the melt electrospun fibers.

3.2.4 Melt electrospinning equipment

We used a self-configured laboratory-scale single-fiber melt electrospinning device consisting of five major components: temperature controller, high-voltage power supply, heating elements, syringe pump, and collector (Figure 3.2). The device was equipped with JCS-33A temperature process controllers (Shinko Technos, Osaka, Japan) and PT 100 platinum thermocouples (Omega Engineering, Deckenpfron, Germany) to control the melting temperature. The temperature was set to 275 °C for the pure polymer

and polymer with additives. A KNH65 high-voltage generator (Eltex-Elektrostatik, Weil am Rhein, Germany) with a voltage range of 6–60 kV was used. During the melt electrospinning experiments, the voltage was kept constant at 50 kV. A positive voltage was applied to the collector while grounding the spinneret. A flat aluminum plate (6 cm) overlaid with a thin paperboard was used as a collector. The distance between the spinneret and collector was set at 10 cm for all trials. An 11 Plus spin pump (Harvard Apparatus, Cambridge, USA) was used with a constant delivery rate of 4 mL/h. A 2-mL glass syringe (Poulten & Graf, Wertheim, Germany) with a nozzle orifice of 1 mm served as the spinneret. PLA was dried based on previous protocol before spinning.

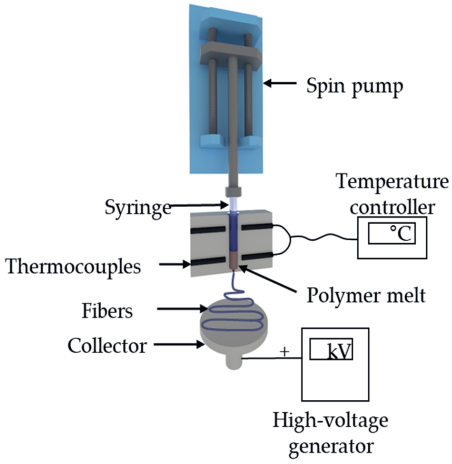

Figure 3.2: Laboratory single-fiber melt electrospinning setup.

3.2.5 Characterization of compounds

Differential scanning calorimetry (DSC) was performed using a Q2000 device (TA Instruments, New Castle, USA) to determine the influence of the additive on the different thermal transition temperatures of PLA. The tests were carried out at a heating rate of 10 °C/min between 25 and 200 °C with a sample size of ~5 mg. The parameters were kept constant for all samples to ensure comparability. TA universal analysis software was used to visualize and compare the data. We compared the T_g, cold crystallization temperature (T_{cc}), melting point (T_m), and percentage crystallinity (X_c). The melt enthalpy of 100% crystalline PLA was considered to be 93.7 J/g [39]. The X_c was determined through the following formula:

$$X_c = {\Delta H_m - \Delta H_c * 100}/{\Delta H_m^0} \qquad \textbf{Eq. 3.1}$$

H_m^0 is the melt enthalpy of the material at 100% crystallinity, H_m is the melting enthalpy at T_m and H_c is the enthalpy of cold crystallization at T_{cc}. Since the reorganization peak prior to melting peak was caused by rearrangement of imperfect crystals, this was not included in calculating overall crystallinity. All compounds as well as the virgin PLA were processed identically and prepared using the same protocol, so any differences in material properties should primarily reflect the nature and quantity of additives.

A Q5000 device (TA instruments) was used to carry out thermogravimetric analysis (TGA) at a heating rate of 10 °C/min under nitrogen flow up to 500 °C. The temperatures at 5% and 50% weight loss were determined using TA universal analysis software and the values were compared to determine the influence of additives on the thermal stability of PLA.

Rheological characterization was carried out using a Discovery HR1 hybrid rheometer (TA Instruments). We performed one flow sweep using a 25-mm plate with an increasing shear rate (0.01–500 rad/s). The gap between the plates was maintained at 1000 μm, and the strain amplitude and environment temperature were maintained at 0.5% and 200 °C, respectively. For better comparability, the viscosity of the pure PLA and all the compounds are presented at a shear rate of 5 rad/s.

The TGA experiment was not isothermal and could only determine the weight loss, so we also measured actual degradation in terms of molecular weight after compounding and melt electrospinning by gel permeation chromatography (GPC) using a 1260 Infinity System (Agilent Technologies, Santa Clara, USA). We used hexafluor-2-isopropanol (HFIP) containing 0.19% sodium trifluoroacetate as the mobile phase at a flow rate of 0.33 mL/min. Solutions were prepared by dissolving 5 mg of pure PLA and the various compounds in HFIP for ~2h, passing the solutions through a 0.2-μm polyetrafluoro-ethylene filter, and injecting them into a modified silica column filled with 7-μm particles (Polymer Standards Service, Mainz, Germany). The experiment was calibrated against a standard polymethyl methacrylate polymer (1.0×10^5 g/mol) and the relative molecular weight (M_w), number average molar mass (M_n), and polydispersity index (PDI) of each polymer were recorded and compared.

The electrical resistance of the pure polymer and compounds was measured at an elevated temperature of 325 °C using a Keithley 617 electrometer (Tektronix Inc.,

Beaverton, USA) as shown in Figure 3.3. The experimental setup has been previously used for conductivity measurements of polymer melts [19]. The polymer granulate was melted using band heaters, and two electrodes, 6 mm apart, were dipped in the melt and connected to the electrometer. The electrical current flowing between the electrodes was measured by applying a constant 10 V.

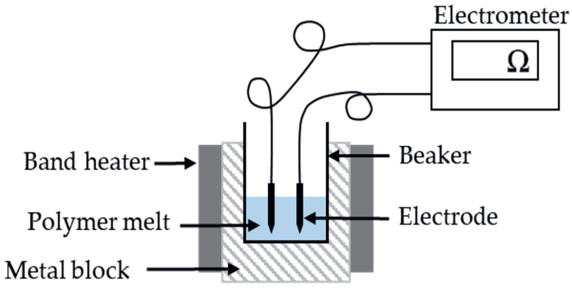

Figure 3.3: Configuration used for the measurement of electrical resistance.

3.2.6 Characterization of the fibers

Fiber diameters were determined by reflected light microscopy using a DM4000 M instrument (Leica Microsystems, Wetzlar, Germany) at 100–200× magnification, and images were captured using Leica Application Suite software. Ten images representing different areas of each nonwoven were used to determine the average fiber diameter. DSC was performed on all melt electrospun fibers to determine the effect of additives and the electrospinning process. DSC was also carried out on the LOFs and DFs, as well as the melt electrospun PLA fibers under the same testing conditions. The thermal transition temperatures and X_c values were compared. Polarized optical microscopy (POM) was used to investigate the crystallinity of the melt electrospun filaments, LOFs and DFs. An Olympus BX53 microscope and DP26 camera (Olympus BV, Leiderdorp, Netherlands) were used to capture the images at 50× magnification. The images were screened for birefringence. The relationship between the electrical resistance, melt viscosity, and average fiber diameter was visualized in surface plots using Minitab19 analysis software.

3.2.7 Cost analysis

Only 2–10% of the liquid processed during solution electrospinning is the polymer (the rest is solvent that evaporates) whereas 100% of the processed liquid solidifies into fibers

during melt electrospinning [1]. The cost of PLA is 2–4 €/kg depending on the grade, and we used a nominal value of 2.1 €/kg in our cost model. In solution electrospinning, PLA is prepared as a 10% solution in chloroform, which costs ~100 €/liter. Accordingly, 10 L of chloroform is required to make 1 kg of PLA fiber. The total material cost of 1 kg of PLA fiber is therefore ~1000 € for the first production cycle without recovery of the solvent and solvent disposal according to standards. For an off-site solvent recovery the cost is estimated to be ~100 € per 200 L of solvent [40]. Considering the case of production of 1 kg of PLA fiber, when 90% of the solvent used can be recovered, 9 L of the solvent can be reused and it would cost ~ 4.5 €. For the remaining 10%, the cost of purchasing new solvent would still be ~100 € and the overall solvent cost would be more than 100 €. In contrast, organic dyes as conductive additives are much less expensive. For example, alizarin costs ~900 €/kg and 1 kg of PLA fiber containing 2% (w/w) of this dye would cost 3 €. Therefore, using organic dyes not only makes the process more sustainable, it is also economical.

3.2.8 Methodology

Our overall workflow is summarized in Figure 3.4. The PLA was characterized and dried before melt electrospinning, and the diameter of the melt electrospun pure PLA fiber was measured. We then tested various combinations of additives (dyes with or without plasticizer) to reduce the viscosity of the melt and increase its conductivity, in order to produce thinner fibers. We prepared 12 compounds in total (Table 3.2) representing each of the three dyes at concentrations of 1% w/w (A1, H1 and Q1) and 2% w/w (A2, H2 and Q2), as well as the liquid dyes in plasticizer also at additive concentrations of 1% w/w (LA1, LH1 and LQ1) and 2% w/w (LA2, LH2 and LQ2). The compound names were based on the initial letter of each dye: A = alizarin, H = hematoxylin and Q = quercetin, with L referring to the liquid form. Melt electrospinning was carried out with the compounds and the diameter of the resulting fibers was measured. All other process parameters (e.g., temperature, throughput, electric field strength) were kept constant.

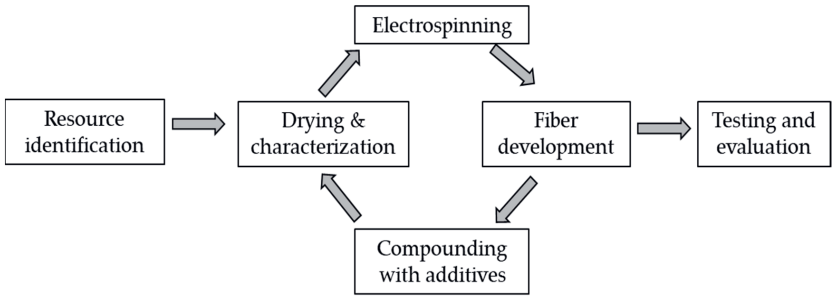

Figure 3.4: Overview of the experimental workflow.

3.3 Results and discussion

3.3.1 Thermal properties of the PLA compounds

The DSC thermograms of PLA and A1 are compared in Figure 3.5 as a representative example of the experiments because all the compounds behaved in a similar manner.

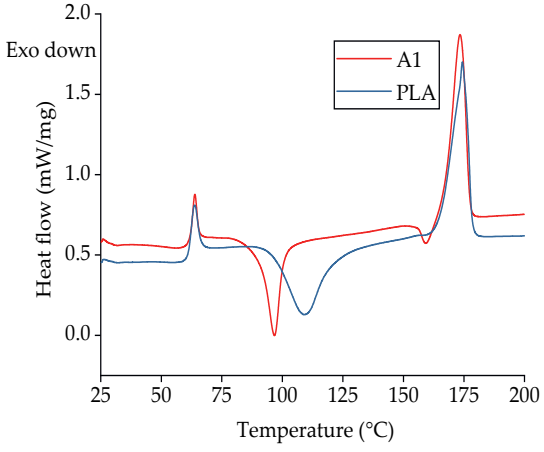

Figure 3.5: DSC thermogram of PLA and compound A1.

The T_g, T_{cc}, T_m and X_c values of each compound are compared visually in Figures 3.6 and 3.7. The T_g and T_m did not change significantly and remained at ~60 °C and ~173 °C, respectively, regardless of the additive and weight percent. The temperature values for PLA are consistent with those previously reported in literature [41,42]. In contrast, the additives had a significant effect on T_{cc}. The T_{cc} of PLA was ~101 °C but this declined to 91.30 °C for A1 and 87.20 °C for A2. Furthermore, the X_c of PLA was 21.47%, but this

increased to 30.72% for A1 and 29.60% for A2. The X_c of the liquid alizarin compounds also increased compared to pure PLA. Although the T_{cc} of the hematoxylin and liquid hematoxylin compounds was not much lower than the value for pure PLA, the X_c of these compounds increased compared to pure PLA. There are two possible explanations for this behavior observed in the cases of these compounds. First, the dye may induce nucleation, as previously reported for polypropylene samples containing colorants [43,44]. Second, the dye may trigger the degradation of PLA, leading to shorter and more mobile polymer chains that are more likely to undergo crystallization. This was explored by GPC analysis (Section 3.3.3). The T_{cc} of compounds Q1 and Q2 was similar to that of PLA, but the X_c decreased from 21.47% to 18.47% and 12.97%, respectively. Also in the case of quercetin, two possible explanations should be considered. The first is that the added quercetin affects the chain mobility and thus disturbs the crystallization process. Similar observations were reported when adding nigrosine dye to polyamide 66 [45]. In case of LQ, since the overall content of quercetin is lower, the hindrance to crystallization is also lower. The second possible explanation is the degradation theory as explained earlier in the case of hematoxylin. This was also explored by GPC analysis (Section 3.3.3).

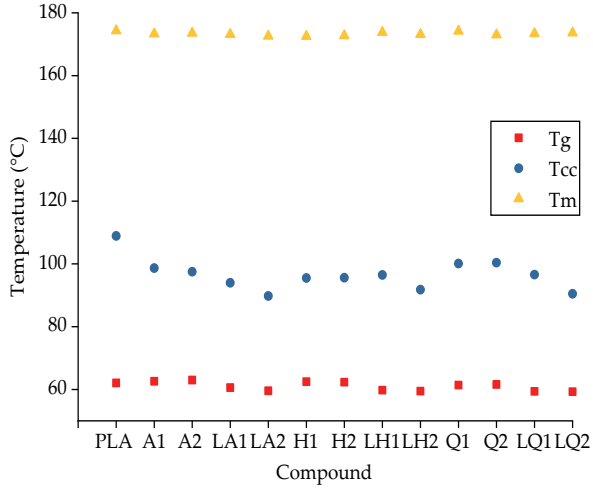

Figure 3.6: Thermal transition temperature of PLA and the PLA/dye compounds.

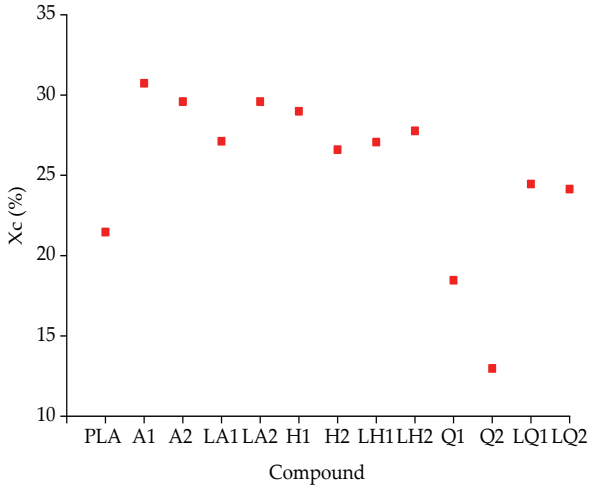

Figure 3.7: Crystallinity (X_c) of PLA and the PLA/dye compounds.

The decomposition temperatures of pure PLA and its compounds were determined by TGA. The temperatures at which 5% and 50% weight loss occurred are compared in Figure 3.8.

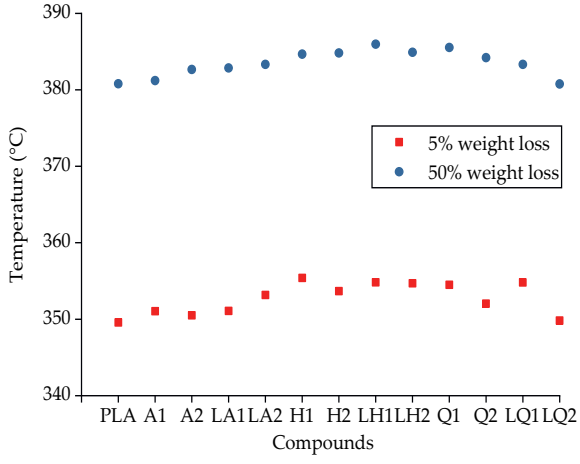

Figure 3.8: Temperature at 5% and 50% weight loss of PLA and the PLA/dye compounds.

The maximum 5% weight loss temperature was observed for compound LH1 at 355 °C and the minimum was observed for pure PLA at 350 °C. Similarly, the maximum 50% weight loss temperature was observed for compound LH1 at 386 °C and minimum was

observed for pure PLA at 381 °C. There was no significant difference in the temperature range over which these weight losses occurred. Since the TGA could only measure the weight loss in the form of the released volatile gases, we characterized the degradation leading to molecular weight reduction and oligomer formation by GPC (Section 3.3.3) and rheological analysis (Section 3.3.2).

3.3.2 Effects of additives on melt viscosity

The shear viscosities of pure PLA and its compounds at a set temperature of 200 °C and a shear rate of 5 rad/s are summarized in Figure 3.9. The viscosity of the polymer melt increased by ~22% following the addition of alizarin, from 493 Pa·s (PLA) to 601 Pa·s (A1) and 595 Pa·s (A2). Higher melt viscosity tends to increase fiber diameters during melt electrospinning, but narrower fibers can still be achieved if the additives increase the electrical conductivity of the melt [19]. The addition of quercetin had a plasticizing effect on the PLA and reduced the melt viscosity by ~37%, from 493 Pa·s (PLA) to 308 Pa·s (Q1) and 312 Pa·s (Q2). However, the addition of hematoxylin achieved the most dramatic effect, reducing the melt viscosity by ~91% at both concentrations, to 42 Pa·s. The melting point of hematoxylin (200 °C) is much lower than that of the other dyes, so the low viscosity of the compounds containing hematoxylin may reflect the melting of the dye along with the polymer. The other possible hypothesis for reducing the viscosity of both hematoxylin and quercetin compounds is polymer degradation. The degradation hypothesis was addressed by GPC analysis (Section 3.3.3).

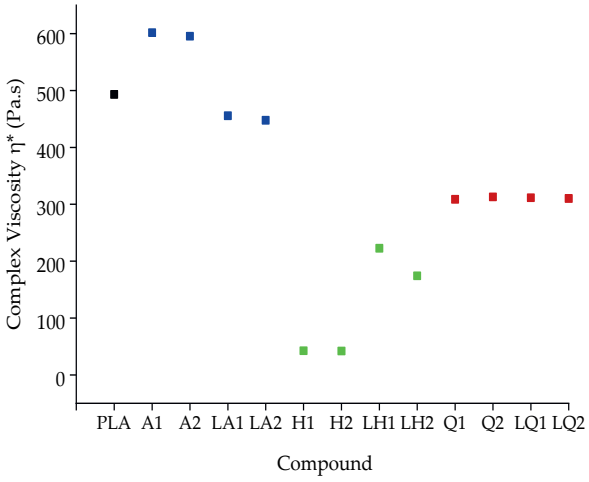

Figure 3.9: Shear viscosity of pure PLA and the PLA/dye compounds, corresponding to a set temperature of 200 °C and a shear rate of 5 rad/s.

Overall, there was little difference in viscosity between compounds containing 1% or 2% (w/w) of a given dye. This was not the case for the liquid dyes, where the plasticizer showed a significant concentration-dependent effect. In the case of alizarin, the dye itself increased the melt viscosity whereas the plasticizer has the opposite effect, so the combination showed only a slight reduction in viscosity compared to pure PLA (7% for LA1 and 9% for LA2). In contrast, because hematoxylin and quercetin reduced the melt viscosity, the addition of plasticizer was expected to enhance this effect. Surprisingly, this was not the case – the viscosity of the liquid hematoxylin and quercetin compounds was significantly higher than the compounds prepared with pure dyes taking into account that also the dye concentration is significantly lower. For example, the viscosity of Q1 was 30% lower than PLA, and the viscosity of H1 was 81% lower than LH1. Normally the polar group of the plasticizer interacts with the polar group of the polymer, swelling the polymer chains and increasing the free volume. Such interactions would reduce intermolecular cohesion and increase polymer chain mobility, thus reducing the viscosity of the melt [46]. The unexpected behavior of the quercetin and hematoxylin compounds may reflect a stronger interaction between these dyes and the plasticizer compared to the interaction between the polymer and plasticizer. The interaction between dye and plasticizer molecules generates bulky particles that could hinder the motion of the polymer chains and ultimate increase the viscosity. Since the three dyes used are chemically different, they interact differently with the plasticizer.

3.3.3 Effect of additives on polymer degradation

GPC analysis of PLA and its compounds (Figure 3.10) revealed M_w, M_n and PDI values of 184,000 g/mol, 107,000 g/mol and 1.72, respectively, for pure PLA. There was no significant change from these values in the alizarin and liquid alizarin compounds. This confirms that the increase in X_c observed for the alizarin and liquid alizarin compounds is a result of the nucleating effect of alizarin. In the quercetin and liquid quercetin compounds, there was a slight reduction in M_w and M_n. A more apparent change was observed in compound Q2, where the M_w and M_n values were 15.12% and 14.01% lower, respectively, compared to pure PLA. The PDI increased for both LQ1 and LQ2, and the highest PDI was observed for LQ2. However, since the change in molecular weight is not as drastic as for the hematoxylin compounds, the viscosity of both quercetin and liquid quercetin compounds was observed to be similar. Hence, in this case, the increase in crystallinity of LQ1 and LQ2 can be attributed to the fact that a lower quantity of quercetin was present compared to Q1 and Q2. In the hematoxylin compounds, the changes were more significant. For example, the M_w and M_n of compound H2 decreased by 40.71% and 40.74%, respectively, compared to pure PLA. As the percentage losses in M_w and M_n were the same, their PDI ratio remained unaffected. The GPC measurements confirmed that the degradation of compounds containing hematoxylin led to the observed reduction in viscosity and increase in X_c (Section 3.3.2). However, in case of the liquid hematoxylin compounds, the M_w and M_n are higher compared to the M_w and M_n of the hematoxylin compounds. The hematoxylin content of LH1 and LH2 compounds is only 25% (w/w) compared to that of H1 and H2 compounds. This could have led to lesser degradation. Furthermore, the interaction between the dye and the plasticizer might have led to bulky particles hindering the flow of polymer chains. This combined effect could have led to higher viscosity reported for these compounds in the previous section.

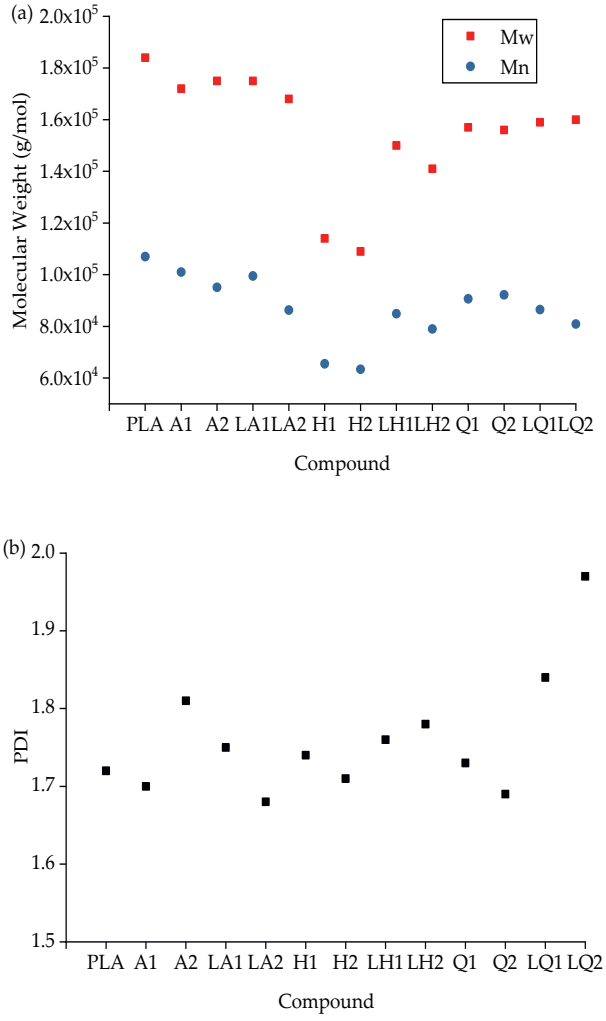

Figure 3.10: Molecular weight (a) and PDI (b) of PLA and the PLA/dye compounds.

GPC analysis was also carried out on the melt electrospun fibers, but no significant reduction of the molecular weight could be detected due the short dwell time of the polymer melt in the syringe of less than less than thirty seconds (Appendix: Figure 3.A1).

3.3.4 Effect of additives on melt conductivity

The electrical resistance of pure PLA its compounds was measured at a set temperature of 325 °C (Figure 3.11). The higher temperature compared to the spinning process was

chosen because more heat energy is lost over the larger surface of the beaker and thus more energy must be supplied to achieve the same melting conditions. However, it should be taken into account that the dyes could melt at the selected temperature and this would most likely influence the electrical conductivity behavior. Electrical conductivity requires freely movable charge carriers, so the electrical resistance of pure PLA (5.0 GΩ) decreased by a factor of five in the presence of any of the additives. In the compounds containing dyes but no plasticizer, the electrical resistance was also inversely related to the dye concentration. Because alizarin increased the viscosity of the melt, the higher conductivity is likely to favor the melt electrospinning process and reduce the fiber diameter. Furthermore, electrical resistance in the liquid alizarin compounds was lower than in compounds containing alizarin but no plasticizer, indicating that the plasticizer also contributes to the higher conductivity, as reported in earlier studies [47, 48]. We observed similar behavior in the liquid hematoxylin and liquid quercetin compounds, although the overall effect of quercetin on electrical conductivity was weakest. The synergetic effects of viscosity and conductivity on fiber diameter are described in more detail in Section 3.3.6.

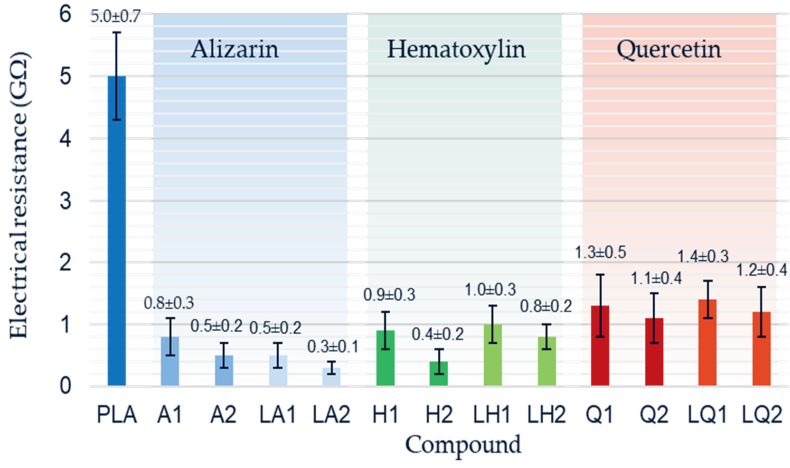

Figure 3.11: Electrical resistances of pure PLA and PLA/dye compounds.

3.3.5 Physical properties of PLA fibers under different processing conditions

The physical properties of the melt spun LOFs and DFs were compared to the melt electrospun PLA fibers by DSC (Table 3.3) and the corresponding thermograms are presented in Figure 3.12.

Table 3.3: Properties of PLA fibers, comparing low orientated and drawn filaments with melt electrospun fibers.

Material	T_g (°C)	T_{cc} (°C)	T_m (°C)	X_c (%)
Low-oriented PLA filament	62.90	95.70	174.10	25.26
Drawn PLA filament	-	-	175.70	58.83
Melt electrospun PLA fiber	62.10	108.90	174.30	8.87

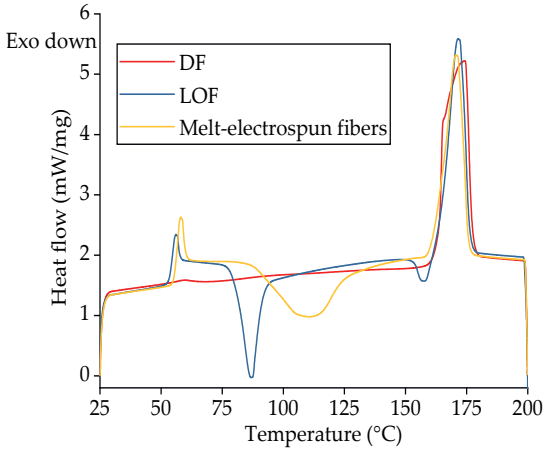

Figure 3.12: DSC thermograms of low-orientated filaments, drawn filaments and melt electrospun PLA fibers.

The T_g, T_m and T_{cc} values were similar for the LOFs and melt electrospun fibers, but we were unable to determine T_g or T_{cc} values after fiber drawing. Furthermore, the X_c of the LOFs and melt electrospun fibers were very low (17.93% and 8.72%, respectively), whereas the X_c after fiber drawing was 58.83%. The absence of a glass transition in DSC thermograms often occurs when the crystalline fraction is more abundant than the amorphous fraction, and the T_{cc} value is absent because the DF is fully drawn, in agreement with previous studies [49]. The melt electrospun fibers are therefore more similar to a LOF than a DF.

POM analysis of the melt electrospun fibers, LOFs and DFs revealed the extent of crystallinity compared to pure PLA fibers produced under different processing conditions (Figure 3.13). Optically anisotropic materials such as crystalline materials

give rise to birefringence due to the difference in their axis length [50]. Although individual crystals could not be observed by POM, very little to no birefringence was detected in the melt electrospun fibers and LOFs, whereas birefringence was observed in the DFs because the degree of crystallinity was increased by drawing. The same technique was previously used to show that the degree of crystallinity in PA66 tensile bars was dependent on the mold temperature [51]. Our combined DSC and POM data therefore indicate that the PLA fibers produced by melt electrospinning are similar to LOFs produced by melt spinning, which have a much lower T_{cc} value than DFs.

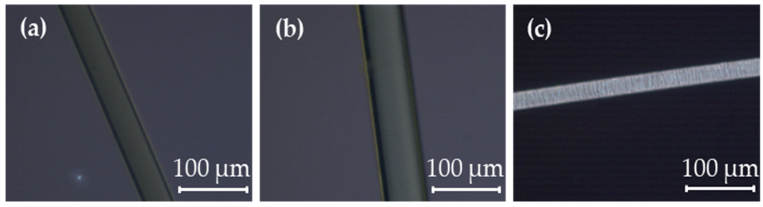

Figure 3.13: POM images. (a) Melt electrospun PLA fiber. (b) Low-oriented PLA filament. (c) Drawn PLA filament.

3.6 Fiber diameters achieved using different PLA compounds

The processability of the compounds and the influence of additives on the fiber diameter were investigated by producing fibers using a single-fiber melt electrospinning device. For pure PLA, the formation of a Taylor cone followed by typical fiber deposition was observed at a set temperature of 275 °C. Fiber formation was possible with all compounds at this temperature and the corresponding fiber diameters could therefore be determined under the same conditions.

The average fiber diameter for pure PLA was 70.6 µm (Figure 3.14). All compounds produced thinner fibers, indicating that all the additives affected viscosity and/or conductivity in a beneficial manner.

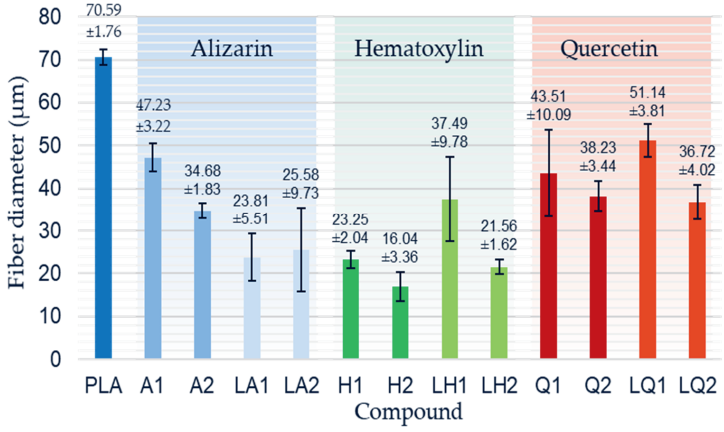

Figure 3.14: Fiber diameters and standard deviations of PLA and the PLA/dye compounds produced by melt electrospinning at 275 °C using a single-nozzle laboratory device.

Despite the increase in viscosity caused by the addition of alizarin, the fiber diameters of compounds A1 and A2 were reduced by 33% and 50% respectively, compared to pure PLA. The increase in electrical conductivity conferred by alizarin therefore compensated for the increase in viscosity and the influence of conductivity was dominant, especially at higher alizarin concentrations. The presence of plasticizer in addition to alizarin reduced the viscosity of the melt, and the smallest fiber diameter of all alizarin compounds was therefore achieved by LA1 (23.8 µm, 63% narrower than pure PLA). There was no significant difference between the fiber diameters of LA1 and LA2.

The addition of hematoxylin led to a significant reduction in viscosity, and the degradation of the polymer (and thus a reduction in M_w) was detected by GPC. As expected, this resulted in the most profound reduction in fiber diameter among all compounds. The finest fibers (16.04 µm, 77% narrower than pure PLA) were achieved for compound H2. The increase in fiber diameter in the presence of the plasticizer matched the unexpected increase in viscosity of liquid hematoxylin compared to hematoxylin compounds without a plasticizer, and the fall in electrical conductivity due to the overall lower concentration of hematoxylin when the plasticizer was present.

Finally, the effect of quercetin on fiber diameter was similar to that of alizarin when each dye was presented in the absence of plasticizer. Interestingly, the dyes had opposite effects in the presence of plasticizer, with the liquid alizarin compounds LA1 and LA2 reducing the fiber diameter further than compounds A1 and A2, but the liquid quercetin

compounds LQ1 and LQ2 producing fibers that were similar in diameter or thicker than those based on compounds Q1 and Q2. As discussed above, this mirrors the opposing effects on viscosity: the plasticizer reduced the viscosity of compounds containing alizarin but increased the viscosity of those containing quercetin. These data also suggest that quercetin has a less significant effect on conductivity than alizarin.

We plotted the relationship between the electrical resistance, melt viscosity and average fiber diameter using Minitab 19 analysis software. Figure 3.15 presents surface plots of fiber diameters in relation to the electrical resistance and viscosity of the alizarin, hematoxylin and quercetin compounds. It has to be considered that the set temperature of the viscosity and resistance measurement deviates from the set temperature of the spinning process, as explained in Section 2.5, so that only a trend can be described. As the temperature increases, the viscosity decreases as well as the resistance [34], so that a further reduction of the fiber diameters is to be expected, The fibers prepared from all three compounds became finer with decreasing melt viscosity and electrical resistance. For the alizarin compounds, the increasing conductivity was the decisive factor controlling fiber diameter because there was little variation in viscosity. The minimum fiber diameter was always achieved using compounds with the lowest viscosity and the lowest electrical resistance.

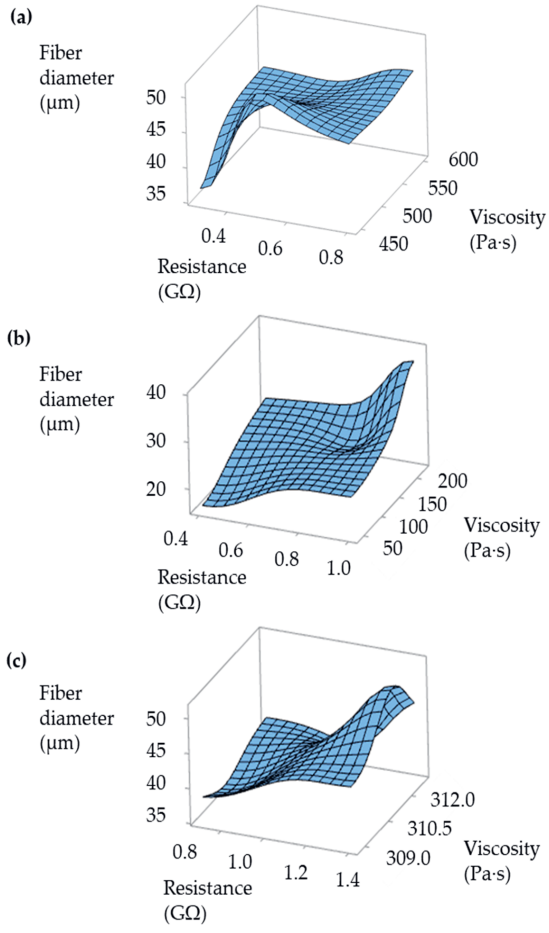

Figure 3.15: Surface plots of fiber diameters in relation to the electrical resistance and viscosity of the melt. (a) PLA/alizarin compounds. (b) PLA/hematoxylin compounds. (c) PLA/quercetin compounds.

The fiber diameters we have achieved are still in the micrometer range, like the majority of fiber diameters previously reported in literature. However, it should be stated that we have not made any device-specific modifications, such as the integration of an accelerated airflow or a heating system as it is already used for other melt electrospinning systems [27]. Furthermore, the fiber diameter is strongly influenced by the flow rate of the polymer [1], so that the use of a nozzle with a smaller orifice can significantly reduce the fiber diameter in future attempts.

3.4 Conclusion and further perspectives

We have successfully tested the biobased dyes alizarin, hematoxylin and quercetin as conductive additives in the melt electrospinning process, and have produced fibers in the micrometer range. All dyes and dye/plasticizer combinations contributed to the desirable reduction of fiber diameter compared to pure melt electrospun PLA fibers, which will facilitate the development of an economical and environmentally friendly process for the production of microfibers and nanofibers that could ultimately replace solution electrospinning. The formation of a Taylor cone followed by continuous fiber deposition was observed for all dyes and dye/plasticizer combinations. The finest fibers (16.04 μm in diameter) were produced by adding 2% (w/w) hematoxylin, reducing the average fiber diameter by 77% compared to pure PLA. However, hematoxylin induced polymer degradation at a spinning temperature of 275 °C, which reduces the M_w and therefore favors the production of finer fibers. In future experiments, the process temperature should be lowered when using hematoxylin to prevent degradation. The addition of alizarin produced finer fibers than pure PLA despite the increase in melt viscosity, indicating that alizarin has a profound effect on the electrical conductivity of the melt. A combination of alizarin (to increase conductivity) and a plasticizer (to reduce viscosity) reduced the fiber diameter to 23.8 μm, which is 63% narrower than the pure PLA fibers. The addition of quercetin reduced the melt viscosity but had a limited effect on electrical conductivity compared to alizarin, and the finest fibers containing this additive (achieved by adding 2% (w/w) liquid quercetin) were 36.72 μm in diameter. The analysis of fibers produced by melt spinning, melt spinning with post-drawing, and melt electrospinning revealed that the melt electrospun fibers had a similar degree of crystallinity to low-oriented filaments and are not comparable to drawn filaments.

Acknowledgements

The authors acknowledge support from the Microscopy Department of the Institute for Textile Technology, RWTH Aachen University, Aachen, Germany. We would also like to thank our laboratory technician Henri Becker for the maintenance and modification of our equipment, and our student Konrad Beukenberg for supporting the experimental trial preparations.

References

1. Brown T, Dalton P, Hutmacher DW. Melt electrospinning today: an opportune time for an emerging polymer process. Elsevier. 2016; 56. Doi: https://doi.org/10.1016/j.jclepro.2018.06.191.
2. Huang Z-M, Zhang YZ, Kotaki M, Ramakrishna S. A review on polymer nanofibers by electrospinning and their applications in nanocomposites. Composites Science and Technology. 2003; 63(15):2223-53.
3. Greiner A, Wendorff JH. Electrospinning: A Fascinating Method for the Preparation of Ultrathin Fibers. Angewandte Chemie International Edition. 2007; 46(30):5670-703.
4. Ma B, Xie J, Jiang J. Rational design of nanofiber scaffolds for orthopedic tissue repair and regeneration. Nanomedicine (Lond). 2013; 8.
5. Shin S-H, Purevdorj O, Castano O. A short review: recent advances in electrospinning for bone tissue regeneration. J Tissue Eng. 2012; 3.
6. McClellan P, Landis WJ. Recent applications of coaxial and emulsion electrospinning methods in the field of tissue engineering. Biores Open Access. 2016; 5.
7. Khajavi R, Abbasipour M, Bahador A. Electrospun biodegradable nanofibers scaffolds for bone tissue engineering. J Appl Polym Sci. 2016; 133.
8. Mani MP, Jaganathan SK, Ismail AF. Appraisal of electrospun textile scaffold comprising polyurethane decorated with ginger nanofibers for wound healing applications. Journal of Industrial Textiles. 2019; 49(5):648-62.
9. Sundarrajan S, Tan KL, Lim SH. Electrospun nanofibers for air filtration applications. Procedia Eng. 2014; 75.
10. Scholten E, Bromberg L, Rutledge GC. Electrospun polyurethane fibers for absorption of volatile organic compounds from air. ACS Appl Mater Interfaces. 2011; 3.
11. Wang J, Li Y, Sun X. Challenges and opportunities of nanostructured materials for aprotic rechargeable lithium–air batteries. Nano Energy. 2013; 2.
12. Wang X, Drew C, Lee S-H. Electrospun Nanofibrous membranes for highly sensitive optical sensors. Nano Lett. 2002; 2.

13. Nan N, He J, You X, Sun X, Zhou Y, Qi K, et al. A Stretchable, Highly Sensitive, and Multimodal Mechanical Fabric Sensor Based on Electrospun Conductive Nanofiber Yarn for Wearable Electronics. Advanced Materials Technologies. 2019; 4(3):1800338.

14. Bhat GS. Advances in polymeric nanofiber manufacturing technologies. J Nanomater Mol Nanotechnol. 2016; 5.

15. Bhardwaj N, Kundu SC. Electrospinning: a fascinating fiber fabrication technique. Biotechnol Adv. 2010; 28.

16. Ogata N, Lu G, Iwata T, Yamaguchi S, Nakane K, Ogihara T. Effects of ethylene content of poly(ethylene-co-vinyl alcohol) on diameter of fibers produced by melt electrospinning. Journal of Applied Polymer Science. 2007; 104(2):1368-75.

17. Ogata N, Yamaguchi S, Shimada N, Lu G, Iwata T, Nakane K, et al. Poly(lactide) nanofibers produced by a melt electrospinning system with a laser melting device. Journal of Applied Polymer Science. 2007; 104(3):1640-5.

18. Zhou H, Green TB, Joo YL. The thermal effects on electrospinning of polylactic acid melts. Polymer (Guildf). 2006; 47.

19. Nayak R, Kyratzis IL, Truong YB, Padhye R, Arnold L. Melt electrospinning of polypropylene with conductive additives. Journal of Materials Science. 2012; 47(17):6387-96.

20. Cadar O, Paul M, Roman C, Miclean M, Majdik C. Biodegradation behaviour of poly(lactic acid) and (lactic acid-ethylene glycol-malonic or succinic acid) copolymers under controlled composting conditions in a laboratory test system. Polymer Degradation and Stability. 2012; 97(3):354-7.

21. Qin Y, Cheng L, Zhang Y, Chen X, Wang X, He X, et al. Efficient preparation of poly(lactic acid) nanofibers by melt differential electrospinning with addition of acetyl tributyl citrate. Journal of Applied Polymer Science. 2018; 135(31):46554.

22. Hacker C, Fourne R, Rübsam U, et al. Challenges of the meltelectrospinning process: an economical and technical window of opportunity [Herausforderungen des Schmelzelektrospinns: wirtschaftliche und technische Potentiale und Möglichkeiten]. Austria: Österreichisches Chemiefaser-Institut, 2013.

23. Nayak R. Polypropylene nanofibers: melt electrospinning versus Meltblowing. Engineering Material: Springer International Publishing; 2017.

24. Nayak R. Effect of viscosity and electrical conductivity on the morphology and fiber diameter in melt electrospinning of polypropylene. Textile Research Journal. 2013; 83(6):606.

25. Maqsood M, Langensiepen F, Seide G. Investigation of melt spinnability of plasticized polylactic acid biocomposites-containing intumescent flame retardant. Journal of Thermal Analysis and Calorimetry. 2020; 139(1):305-18.

26. Yoon YI, Park KE, Lee SJ, Park WH. Fabrication of Microfibrous and Nano-/Microfibrous Scaffolds: Melt and Hybrid Electrospinning and Surface Modification of Poly(L-lactic acid) with Plasticizer. BioMed Research International. 2013; 10.

27. Zhmayev E, Cho D, Joo YL. Nanofibers from gas-assisted polymer melt electrospinning. Polymer. 2010; 51(18):4140-4.

28. Liu Y, Zhao F, Zhang C, Zhang J, Yang W. Solvent-free preparation of poly(lactic acid) fibers by melt electrospinning using an umbrella-like spray head and alleviation of the problematic thermal degradation. J Serb Chem Soc. 2012; 77.

29. Carroll CP, Zhmayev E, Kalra V, Joo YL. Nanofibers from electrically driven viscoelastic jets: modeling and experiments. Korea-Australia Rheology Journal. 2008; 20(3):153-64.

30. Chrzanowska O, Struszczyk M, Krucińska I. Small Diameter Tubular Structure Design Using Solvent-Free Textile Techniques. Journal of Applied Polymer Science. 2014; 131.

31. Mazalevska O, Struszczyk M, Chrzanowski M, Krucińska I. Application of Electrospinning for Vascular Prothesis Design–Preliminary Results. Fibers and Textiles in Eastern Europe. 2011; 19:46-52.

32. Mazalevska O, Struszczyk MH, Krucinska I. Design of vascular prostheses by melt electrospinning—structural characterizations. Journal of Applied Polymer Science. 2013; 129(2):779-92.

33. Zhmayev E, Zhou H, Joo YL. Modeling of non-isothermal polymer jets in melt electrospinning. Journal of Non-Newtonian Fluid Mechanics. 2008; 153(2):95-108.

34. Koenig K, Daenicke J, Langensiepen F, Seide G, Schubert DW. From lab to pilot scale: melt electrospun nanofibers of polypropylene with conductive additives. J Nanomater Mol Nanotechnol. 2019; 8(2).

35. Alves de Lima RO, Bazo AP, Salvadori DMF, Rech CM, de Palma Oliveira D, de Aragão Umbuzeiro G. Mutagenic and carcinogenic potential of a textile azo dye processing plant effluent that impacts a drinking water source. Mutation Research/Genetic Toxicology and Environmental Mutagenesis. 2007; 626(1):53-60.

36. Buccella M. Color masterbatches for polyamide 6 fibers. Optimization of compounding and spinning processes. Physical-chemical characterization of industrial products: University of Trento; 2014.

37. Sun C, Li Y, Qi D, Li H, Song P. Optical and electrical properties of purpurin and alizarin complexone as sensitizers for dye-sensitized solar cells. Journal of Materials Science: Materials in Electronics. 2016; 27(8):8027-39.

38. Gsänger M, Bialas D, Huang L, Stolte M, Würthner F. Organic Semiconductors based on Dyes and Color Pigments. Advanced Materials. 2016; 28(19):3615-45.

39. Jia S, Yu D, Zhu Y, Wang Z, Chen L, Fu L. Morphology, Crystallization and Thermal Behaviors of PLA-Based Composites: Wonderful Effects of Hybrid GO/PEG via Dynamic Impregnating. Polymers. 2017; 9(10):528.

40. Cole D. Bringing Distillation & Solvent Recovery In House: FlexoGlobal; 2019 https://www.flexoglobal.com/blog-articles/2019/daetwyler-01-bringing-distillation-and-solvent-recovery-in-house.html (accessed 21 December 2019).

41. Maqsood M, Seide G. Novel Bicomponent Functional Fibers with Sheath/Core Configuration Containing Intumescent Flame-Retardants for Textile Applications. Materials. 2019; 12(19):3095.

42. Lascano D, Quiles-Carrillo L, Balart R, Boronat T, Montanes N. Toughened Poly (Lactic Acid)—PLA Formulations by Binary Blends with Poly(Butylene Succinate-co-Adipate)—PBSA and Their Shape Memory Behaviour. Materials. 2019; 12(4):622.

43. Broda J. Nucleating activity of the quinacridone and phthalocyanine pigments in polypropylene crystallization. Journal of Applied Polymer Science. 2003; 90(14):3957-64.

44. Mubarak Y, Martin PJ, Harkin-Jones E. Effect of nucleating agents and pigments on crystallisation, morphology, and mechanical properties of polypropylene. Plastics, Rubber and Composites. 2000; 29(7):307-15.

45. Sukata K, Takeuchi H, Shimada M, Agari Y. Influence of the nigrosine dye on the thermal behavior of polyamide 66. Journal of Applied Polymer Science. 2006; 101(5):3270-4.

46. Marcilla A, BeltrÁN M. 5 - MECHANISMS OF PLASTICIZERS ACTION. In: Wypych G, editor. Handbook of Plasticizers (Second Edition). Boston: William Andrew Publishing; 2012. p. 119-33.

47. Yang XQ, Lee HS, Hanson L, McBreen J, Okamoto Y. Development of a new plasticizer for poly(ethylene oxide)-based polymer electrolyte and the investigation of their ion-pair dissociation effect. Journal of Power Sources. 1995;54(2):198-204.

48. Reddy T, Achari V, Sharma A, Rao V. Effect of plasticizer on electrical conductivity and cell parameters of (PVC+KBrO3) polymer electrolyte system. Ionics. 2007; 13:55-9.

49. Walker J, Melaj M, Giménez R, Pérez E, Bernal C. Solid-State Drawing of Commercial Poly(Lactic Acid) (PLA) Based Filaments. Frontiers in Materials. 2019; 6(280).

50. Bergström J. 2 - Experimental Characterization Techniques. In: Bergström J, editor. Mechanics of Solid Polymers: William Andrew Publishing; 2015. p. 19-114.

51. Drummer D, Seefried A, Meister S. Characterization of Material Stiffness on Injection Moulded Microspecimens Using Different Test Methods. Advances in Materials Science and Engineering. 2014.

Chapter 4

The Effect of Dye and Pigment Concentrations on the Diameter of Melt electrospun Polylactic Acid Fibers

This chapter is based on the following publication:
Balakrishnan, N. K.; Koenig, K.; Seide, G. The Effect of Dye and Pigment Concentrations on the Diameter of Melt electrospun Polylactic Acid Fibers. Polymers 2020, 12(10), doi: https://doi.org/10.3390/polym12102321

Abstract

Submicrofibers and nanofibers produce more breathable fabrics than coarse fibers and are therefore widely used in the textiles industry. They are prepared by electrospinning using a polymer solution or melt. Solution electrospinning produces finer fibers but requires toxic solvents. Melt electrospinning is more environmentally friendly, but is also technically challenging due to the low electrical conductivity and high viscosity of the polymer melt. Here we describe the use of colorants as additives to improve the electrical conductivity of polylactic acid (PLA). The addition of colorants increased the viscosity of the melt by >100%, but reduced the electrical resistance by >80% compared to pure PLA (5 GΩ). The lowest electrical resistance of 50 MΩ was achieved using a composite containing 3% (w/w) indigo. However, the thinnest fibers (52.5 μm, 53% thinner than pure PLA fibers) were obtained by adding 1% (w/w) alizarin. Scanning electron microscopy revealed that fibers containing indigo featured polymer aggregates that inhibited electrical conductivity, and thus increased the fiber diameter. With further improvements to avoid aggregation, the proposed melt electrospinning process could complement or even replace industrial solution electrospinning and dyeing.

4.1 Introduction

Electrospinning is a widely used method for the production of microscale and nanoscale fibers, with multiple applications in the field of nanotechnology [1–3]. Such fibers are advantageous due to their flexibility and large surface area, making them suitable for medical applications [4–8], water purification [9,10], and the manufacture of electronic components [11,12] and textiles [13–15]. Submicrofibers are particularly useful in textile applications because of their superior waterproofing properties and breathability compared to thicker fibers [16].

The two main forms of electrospinning are solution electrospinning, in which fibers are produced by evaporating a solvent, and melt electrospinning, in which fibers are drawn from a polymer melt [15]. Both processes are based on the same principle, in which a potential difference is established between the end of a needle capillary and a collector. This creates an electric field that induces a surface charge on the polymer solution or melt, deforming a spherical hanging droplet into a conical shape. When the electrostatic repulsive force of the surface charges overcomes the surface tension, a charged liquid jet is ejected from the tip of the Taylor cone, and the charge density on the jet interacts with the external field to create an instability that stretches the fiber, allowing it to be deposited on the collector as a nonwoven fabric [1,14,15].

Solution electrospinning is currently more economical, and thus a more widespread method for the production of nanofibers and submicrofibers, because the lower viscosity and higher temperature of polymer solutions (compared to polymer melts) allows finer fibers to be produced using much simpler devices [17]. However, the solvents used during this process are expensive and toxic, requiring additional recovery steps to avoid carryover, particularly in biomedical applications [1,18]. For example, the production of polylactic acid (PLA) fibers requires solvents such as chloroform, dichloromethane and N,N-dimethylformamide. For other polymers, such as polypropylene (PP), no solvents are suitable for solution spinning at room temperature [19]. The evaporation of the solvent during electrospinning leaves traces on the fiber, which causes surface roughness or even defects that compromise fiber strength. The concentration of the spinning solution is very low, and evaporation of the solvent reduces the yield and wastes energy. Furthermore, capillaries often become blocked during solution electrospinning, which affects the continuous production of fibers [15,20,21].

The challenges associated with solution electrospinning have focused the efforts of researchers attempting to develop environmentally friendly melt electrospinning processes. Multiple studies have been carried out to improve melt electrospinning technology and thus overcome the limitations caused by the high temperature, high viscosity and/or low conductivity of the polymer melt, with the aim of reducing the fiber diameter [22]. Microfibers and submicrofibers have been produced from several polymers (including polyethylene, PP and PLA) using single-fiber melt electrospinning devices and other configurations [23–29]. Narrower fibers can be produced by integrating a gas stream [30] or by including additives that increase conductivity and or reduce viscosity [18,31–33].

Colorants (dyes and pigments) are often used as additives in the textile industry, including in the dyeing of solution electrospun nanofibers. For example, bath dyeing has been applied to recycled polyester nanofibers [16] and polyamide 66 nanofibers, the latter achieved using acid dyes at lower temperatures compared to regular fibers [34]. Furthermore, dope dyeing has been reported for polyester nanofibers, thus reducing the number of processing steps and avoiding the toxic chemicals required for bath dyeing [35]. However, colorants are not only aesthetic—they can also offer other functionalities, such as better conductivity. For example, the organic semiconductor pigment copper phthalocyanine and dyes such as alizarin have been used for the development of solar cells, but are also suitable as colorants for textiles [36,37]. The π-conjugation present in these colorants is not only responsible for their color, it also improves their electrical conductivity, and it can lead to a charge carrier mobility exceeding 1 cm^2/Vs [38]. The electric and dielectric properties of colorants reveal that conductivity follows a quantum mechanical tunnel model at low temperatures, and a correlated barrier-hopping model at higher temperatures [39].

Most studies of colorants for textiles have involved the solvent electrospinning of unsustainable fossil-based polymers. With depleting oil resources and the threat of climate change, the focus is now shifting towards biobased polymers such as PLA [40]. We previously reported that dyes could be used as conductive additives for the melt electrospinning of PLA, but more work is required to determine the suitability of colorants as conductive additives in melt electrospinning [41]. Both PLA and the colorants have polar functional groups, so their interactions can inhibit the flow of polymer chains, leading to higher viscosity. However, the higher conductivity of the colorants can negate this effect by increasing the overall conductivity of the composite.

Here, we investigated the ability of several colorants (dyes and pigments) to increase the conductivity of molten PLA during melt electrospinning. We compared two potentially biobased dyes (alizarin and indigo), three fossil-based pigments (pigment blue 15:1, pigment green 7, and pigment yellow 155) and the biobased pigment pink PR122 in terms of their effect on the diameter and color of PLA fibers manufactured using a single-nozzle melt electrospinning device. We selected colorants that have a π-conjugation in their structure as a means to increase the conductivity of the polymer melt. No azo dyes were selected, even though they are also conductive, because they are toxic and mutagenic and therefore present an environmental hazard and risk to end-users [42]. We investigated the effects of the additives on the color, viscosity, morphology, thermal properties and degradation of PLA. The use of colorants as multipurpose additives avoids the use of toxic chemicals required for solvent electrospinning and conventional bath dyeing. Our results provide the basis for environmentally friendly melt electrospinning processes for the manufacture of submicrofibers and nanofibers.

4.2 Experimental

4.2.1 Materials

The biopolymer used in the study is PLA L130, with an L-content > 99%, a glass transition temperature (T_g) of 60 °C, and a melt flow index of 24 g/10 min at 210 °C/2.16 kg. It was purchased from Total|Corbion (Gorinchem, Netherlands). The dyes alizarin (A) and indigo (I) were purchased from Sigma-Aldrich (Zwijndrecht, Netherlands). Pigment blue 15:1 (B), pigment green 7 (G), pigment yellow 155 (Y) and biobased pigment pink PR122 (P) were provided by Clariant (Louvain-la-Neuve, Belgium). The chemical structures of the colorants are shown in Table 4.1.

Table 4.1: Chemical structures and melting points of the colorants used in this study [43,44]

Additive	Chemical Structure	Melting Point (°C)
Alizarin	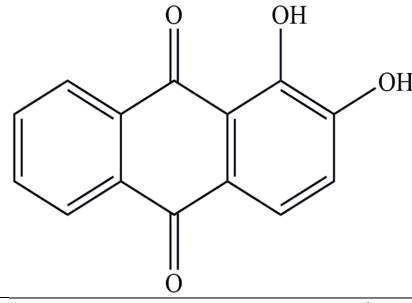	279–283
Blue pigment 15:1	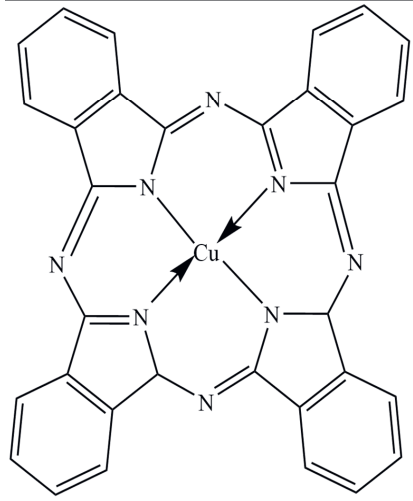	350

Green pigment 7	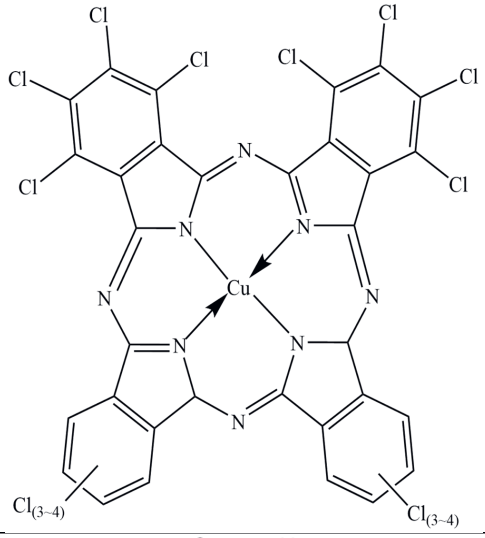	480
Indigo	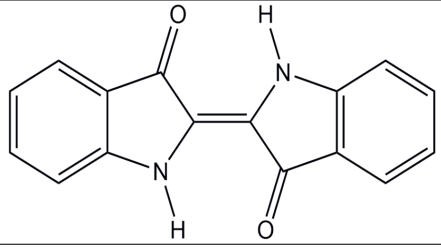	>300
Pink pigment PR122	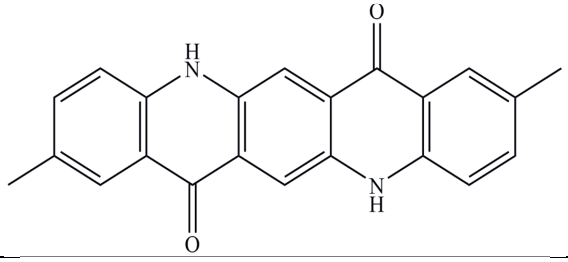	Not available
Yellow pigment 155	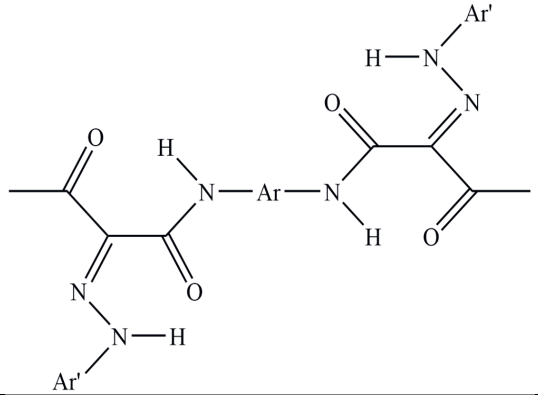	>280

The presence of copper ions is likely to make the inorganic pigments more conductive, but also more difficult to disperse in the polymer matrix. In contrast, although the dyes and organic pigments may have a lower conductivity, they should be easier to disperse.

4.2.2 Methods

4.2.2.1 Microcompounder

PLA undergoes degradation by hydrolysis at high temperatures, so we avoided this by drying PLA and the plasticizer at 80 °C overnight in a vacuum before compounding (to reach a water content of less than 100 ppm). The colorants were dried at 50 °C in a vacuum for 2 h prior to compounding trials, which were carried out using a co-rotating microcompounder from Xplore (Sittard, Netherlands). We prepared three 5 g batches of each composite at 200 °C with a screw speed of 100 rpm and a mixing time of 2 min. Rheometer plates were molded in an IM 5.5 injection molding machine (Xplore). The composites and their abbreviations are listed in Table 4.2.

Table 4.2: List of the 18 composites produced for this study. The composite names were based on the initial letter of each additive and the weight percentage of the additive.

Composite Abbreviation	Colorant Name	% (w/w) of Colorant
A1	Alizarin dye	1
A2		2
A3		3
B1	Blue pigment	1
B2		2
B3		3
G1	Green pigment	1
G2		2
G3		3

I1	Indigo dye	1
I2		2
I3		3
P1	Pink pigment	1
P2		2
P3		3
Y1	Yellow pigment	1
Y2		2
Y3		3

4.2.2.2 Melt electrospinning equipment

We used a single-fiber melt electrospinning device, comprising a temperature controller, high-voltage power supply, heating elements, syringe pump and collector (Figure 4.1). The device was equipped with JCS-33A temperature process controllers (Shinko Technos, Osaka, Japan) and PT 100 platinum thermocouples (Omega Engineering, Deckenpfron, Germany) to maintain the melting temperature at 275 °C. We used a KNH65 high-voltage generator (Eltex-Elektrostatik, Weil am Rhein, Germany) to maintain a constant +50 kV on the collector (a 6 cm aluminum plate overlaid with a thin paperboard) while grinding the spinneret, which was a 2 mL glass syringe (Poulten and Graf, Wertheim, Germany) with a nozzle orifice of 1 mm, and this was placed at a distance 10 cm from the collector. An 11 Plus spin pump (Harvard Apparatus, Cambridge, MA, USA) was used with a constant delivery rate of 4 mL/h. PLA was dried based on same protocol mentioned above before melt electrospinning.

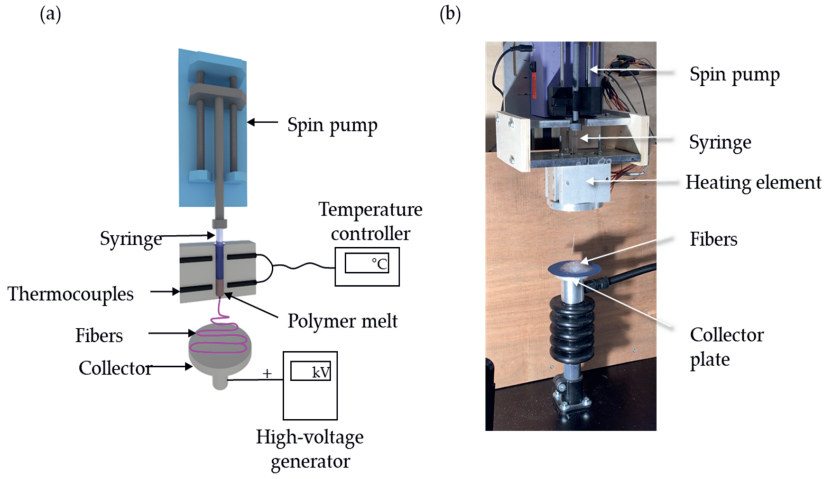

Figure 4.1: Schematic illustration (a) and picture (b) of our melt electrospinning equipment

4.2.2.3 Characterization of Composites

The thermal properties of the composites were analyzed by differential scanning calorimetry (DSC) and thermogravimetric analysis (TGA). For DSC, we used a Q2000 device (TA Instruments, New Castle, DE, USA) for two heating cycles between 25 and 200 °C at a rate of 10 °C/min in a nitrogen atmosphere, and analyzed the data obtained from the second cycle. We compared the T_g, crystallization temperature (T_c) and melting point (T_m) from the second cycle. The percentage crystallinity (X_c) of PLA and its composites was calculated by taking 93.7 J/g as the melt enthalpy of 100% crystalline PLA [45].

$$X_c = \Delta H_m - \Delta H_c * 100 \Big/ \Delta H_m^0 \qquad \textbf{Eq. 4.1}$$

H_m^0 is the melt enthalpy of the material at 100% crystallinity, H_m is the melting enthalpy at T_m and H_c is the enthalpy of cold crystallization at T_{cc}.

The same experimental protocol was used to prepare all the composites, so any differences in the properties would depend on the additive and its quantity. The effect of additives on the thermal degradation of PLA was assumed most evident at the highest additive concentration, so TGA was applied to composites containing 3% (w/w) of each additive. PLA and its composites were heated from room temperature to 500 °C at a rate

of 10 °C/min in a nitrogen atmosphere, and the temperatures at which 5% and 50% weight loss occurred were determined and compared.

We measured changes in PLA viscosity using a Discovery HR1 hybrid rheometer (TA Instruments, Asse, Belgium) fitted with a 25 mm plate (gap = 1000 μm) and a shear rate increasing from 0.01 to 500 1/s. We maintained the strain amplitude at 1% in a constant environment with a nitrogen atmosphere at 200 °C, and used an equilibration time of 5 min. For more relatability, we compared the viscosity of PLA and its composites at a shear rate of 5 1/s.

A 1260 Infinity gel permeation chromatography (GPC) system (Agilent Technologies, Santa Clara, USA) was used to measure molecular degradation in pure PLA and its composites. We used hexafluoro-2-isopropanol (HFIP) containing 0.19% sodium trifluoroacetate as the solvent and mobile phase. We prepared solutions containing 5 mg PLA and its composites, passed them through a polytetrafluoroethylene filter, and injected them into a silica column. Calibration was performed using a standard polymethyl methacrylate polymer (1.0×10^5 g/mol), and we compared the weight average molecular weight (M_w), number average molecular weight (M_n) and polydispersity index (PDI).

The electrical resistance of PLA and its composites was measured at 325 °C using a Keithley 617 electrometer (Tektronix Inc., Beaverton, OR, USA), as shown Figure 4.2. The polymer granulate was melted using band heaters, and two electrodes (6 mm apart) were dipped in the melt and connected to the electrometer. The electrical current flowing between the electrodes was measured by applying a constant 10 V.

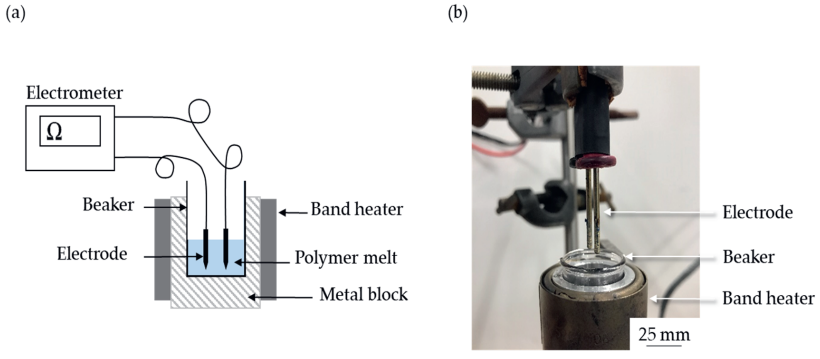

Figure 4.2: Schematic illustration (a) and picture (b) of our electrometer setup

4.2.2.4 Characterization of fibers

We measured fiber diameters by reflected light microscopy using a DM4000 M instrument (Leica Microsystems, Wetzlar, Germany) at 100–200× magnification, and images were captured using Leica Application Suite software. In total, 10 images representing different areas of each nonwoven were used to determine the average fiber diameter.

The dispersion of the colorant was determined by scanning electron microscopy (Leo 1450 VP from Zeiss, Oberkochen, Germany) at an acceleration tension of 15 kV. The samples were freeze-fractured after immersion in liquid nitrogen and then sputtered with gold and mounted on SEM stubs. Cross-section and surface images were acquired in secondary electron mode and at different magnifications depending on the amount of additive.

Color measurements were collected by spectrophotometry in the range 400–800 nm according to ISO 11664-4:2008 using a UV3600 spectrophotometer device (Shimadzu, Kyoto, Japan). A 50 W halogen lamp was used as the light source, and a photomultiplier tube and PbS were used as the detector. The spectrum was recorded in the reflectance mode after white and black calibrations. Spectrophotometric data were transferred from the instrument to CIELab software to define the color coordinates of each sample.

4.2.2.5 Experimental Methodology

Our experimental methodology is summarized in Figure 4.3. We compounded PLA with the additives first, and divided the resulting composites into two parts. The first was injection molded into plates and used for rheological analysis. The second was cut into small granules for characterization and melt electrospinning. Our goal was to reduce the diameter of the fibers by increasing the electrical conductivity and/or reducing the viscosity of the melt. The other process parameters (e.g., temperature, electrical field, and throughput) were kept constant so that any change in fiber diameter could be attributed to the type and quantity of additive.

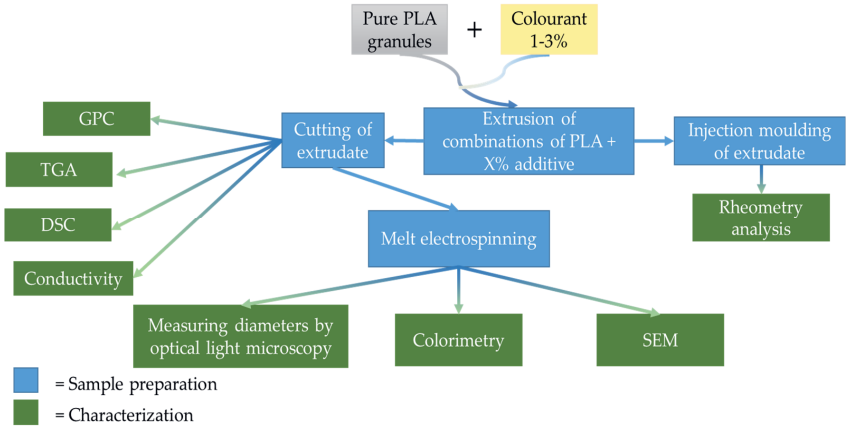

Figure 4.3: Methodology for the preparation and analysis of electrospun PLA fibers.

4.3 Results and discussion

4.3.1 Thermal Properties of the PLA Composites

The DSC thermograms of PLA and the composites containing 2% (w/w) of each additive are presented in Figure 4.4. These are representative results because the other composites followed the same trend, and are therefore included in appendix (Figure 4.A1 and Figure 4.A2).

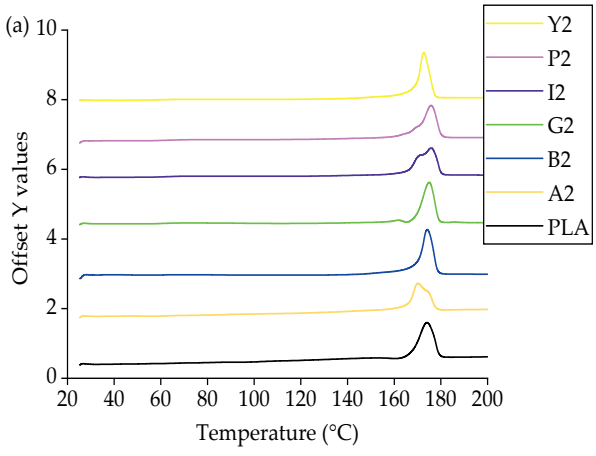

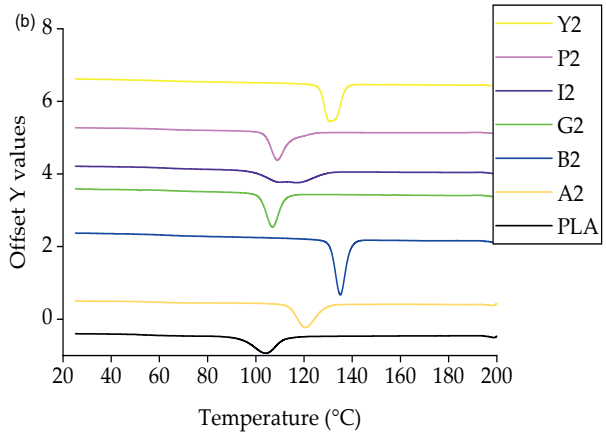

Figure 4.4: DSC thermograms of PLA and composites containing 2% (w/w) of each additive during (a) the heating phase and (b) the cooling phase.

The DSC thermograms indicate the Tg, Tc and Tm. In most cases, we observed a single melting peak during the heating phase, although the composites with alizarin, indigo and pink pigment featured a doublet around the same Tm. This may reflect the formation of imperfect crystals during the first cooling phase, which melt and fuse together to form perfect crystals, and then melt again at the higher temperature. A similar phenomenon was reported for the PLA and carbon black composites [46]. The Tg, Tc and Tm of PLA and its composites are summarized in Figure 4.5.

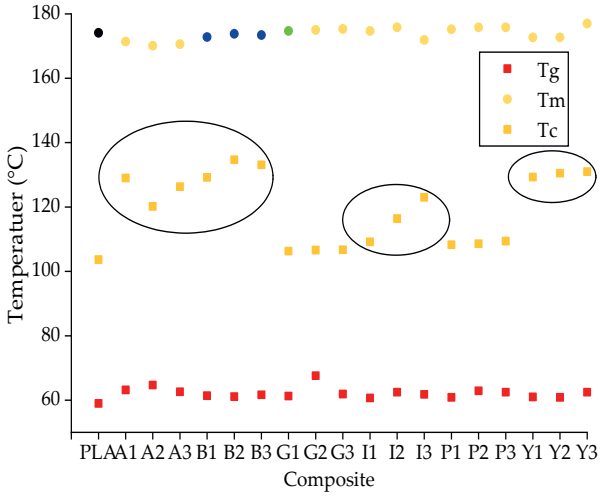

Figure 4.5: The Tg, Tc and Tm of PLA and its composites. The three rings indicate the relationship between Tm and weight percentage for alizarin, indigo, and the blue and yellow pigments. (The composites having a different TC have been circled for easy identification)

The DSC results showed that the Tg of PLA is not markedly affected by the nature or concentration of the additive, remaining at ~60 °C in agreement with previous studies [47]. Similarly, the Tm remained at ~170 °C, and the Xc at ~50% (as expected, given that the second heating/cooling cycle was considered and the thermal history of all the PLA composites was therefore the same). In contrast, we observed a significant additive-dependent difference in the Tc, which was 104 °C for pure PLA and composites containing the green and pink pigments. However, The Tc increased by more than 20 °C in the composites containing alizarin or the blue and yellow pigments, reaching maximum values of 129 °C (A1), 134 °C (B2) and 131 °C (Y1), respectively. Interestingly, although the Tc increased linearly with the weight percentage of indigo, there was a plateauing effect for the yellow pigment and no clear relationship between Tc and weight percentage for the other colorants (Figure 5, black rings). These results suggest that alizarin, indigo, and the blue and yellow pigments have a nucleating effect on PLA, a phenomenon also extensively observed for PP and colorants, including the blue pigment tested here [48]. The nucleating effect in PP reflects the fact that the blue pigment exists in different polymorphic forms, providing surfaces that match PP chains and thus enabling the epitaxial growth of PP crystals [49]. It is possible that the nucleation in PLA involves a similar mechanism, but this needs to be investigated in more detail to determine the exact mechanism.

The TGA thermograms of PLA and composites containing 3% (w/w) of each additive are presented in Figure 4.6 and the temperatures at which 5% and 50% weight loss occurred are compared in Figure 4.7. For pure PLA, we found that a 5% weight loss occurs at 350 °C and a 50% weight loss occurs at 378.0 °C, which is consistent with previous reports [50]. The lowest 5% weight loss temperature was 342 °C for composite G3, and the highest was 352 °C for composite A3. The lowest 50% weight loss temperature was 375 °C for composite I3 and the highest was 382 °C for composite A3. There was no significant difference in the degradation temperatures of PLA and composites containing 3% (w/w) of each additive.

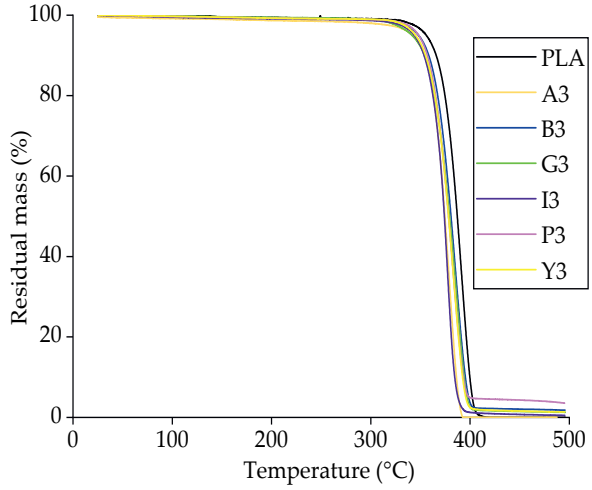

Figure 4.6: TGA thermogram of PLA and its composites containing 3% (w/w) of each additive, showing no significant difference between the degradation curves.

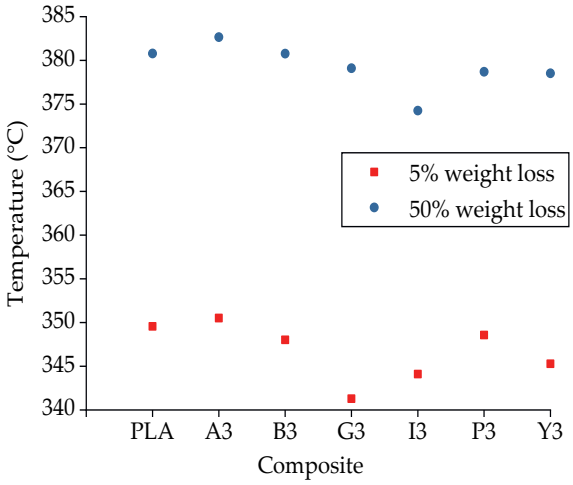

Figure 4.7: Comparison of 5% and 50% weight loss temperatures for PLA and composites containing 3% (w/w) of each additive.

4.3.2 Effect of Additives on Melt Viscosity

The rheogram of PLA and its composites containing 3% (w/w) of each additive is shown in Figure 4.8. Since the rheogram of composites containing other weight% of additives was similar to this, it is presented in the appendix (Figure 4.A3 and Figure 4.A4). All the samples exhibited non-Newtonian behavior (shear thinning). The viscosity was very high at low shear rates, and fell sharply with increasing shear rate. Although the viscosity increased following the incorporation of each additive, in most cases the composites showed similar rheological behavior to pure PLA. The increase in viscosity was the highest for the pink pigment.

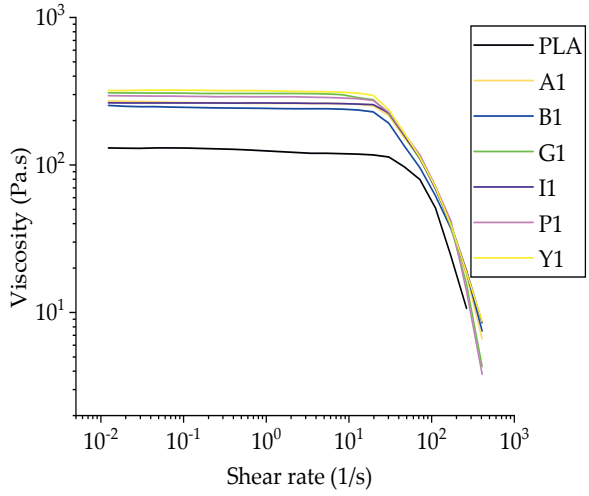

Figure 4.8: Rheogram of PLA and its composites containing 3% (w/w) of each additive

The incorporation of colorants significantly increased the viscosity of PLA, especially at the lower shear rate of 5 1/s (Figure 4.9).

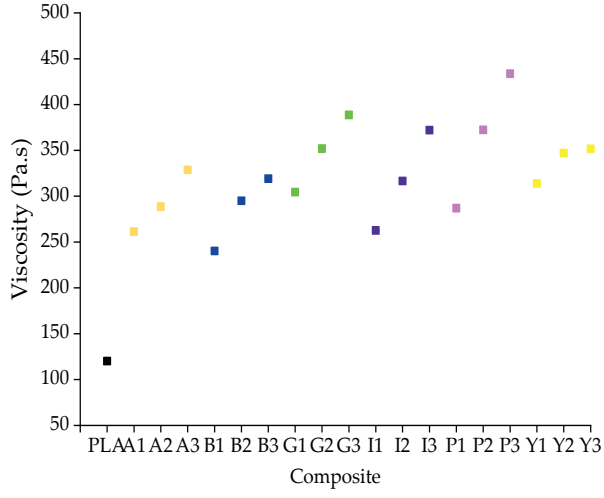

Figure 4.9: Viscosity of PLA and its composites containing 1%, 2% and 3% (w/w) of each additive at a shear rate of 5 rad/s. The colored squares indicate the different dyes/pigments for visual clarity.

Similarly, the viscosity of PLA was shown to increase when mixed with carbon black pigment [51]. Given that both PLA and the additives contain polar groups, it is likely that hydrogen bonds forming within the mixture inhibit the slippage of PLA chains [52]. This is more evident at lower shear rates, because the shear forces are not strong enough to break these interactions, leading to lower chain mobility and thus higher viscosity.

The viscosity of pure PLA at a shear rate of 5 1/s is 120 Pa·s. Adding 1% (w/w) alizarin increases the viscosity by >100% to 261 Pa·s, but the effect of increasing the additive concentration is less significant. The viscosity of A3 (328 Pa·s) is only 25% higher than that of A1. A similar trend was observed for the other composites, indicating that the type of additive affects the viscosity more than the concentration, as previously reported for PP composites with pigments [53].

The diameter of melt electrospun fibers can be reduced either by increasing the conductivity or reducing the viscosity of the polymer [54]. Because all the additives caused a significant increase in viscosity, any reduction in fiber diameter achieved by the PLA composites can only be attributed to an increase in electrical conductivity.

4.3.3 GPC Analysis of PLA and Its Composites

The relative Mw of extruded PLA was 150,940, the Mn was 96,977, and the PDI was 1.56. These values did not change significantly for the composites. The lowest Mw and Mn values were observed for P3 (148,860 and 92,850, respectively) and the highest were observed for G2 (167,900 and 103,760, respectively) as shown in Figure 4.10. The PDI for all composites varied between 1.55 and 1.65 (Figure 4.11). There was no significant change in any of these values caused by the additives, suggesting that none of the colorants induce the degradation of PLA.

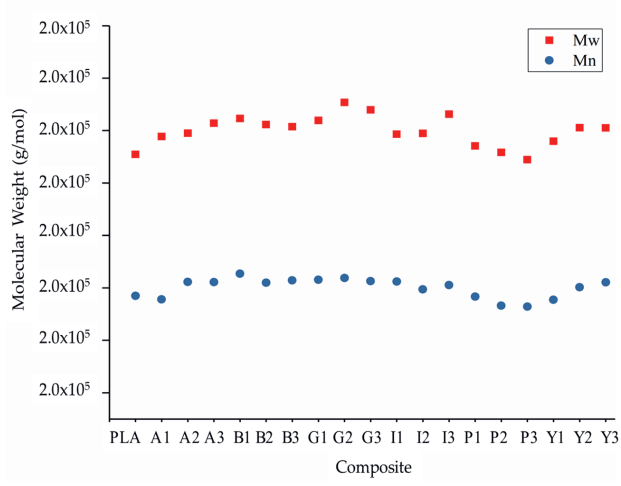

Figure 4.10: The weight average molecular weight (Mw) and number average molecular weight (Mn) of PLA and its composites containing 1%, 2% and 3% (w/w) of each additive.

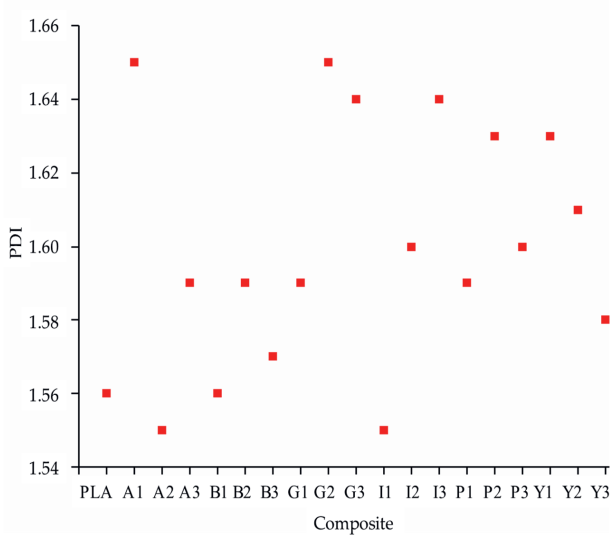

Figure 4.11: The polydispersity indices (PDI) of PLA and its composites containing 1%, 2% and 3% (w/w) of each additive.

4.3.4 Analysis of Additive Dispersion by SEM

The dispersion of the colorants was investigated by SEM. Images of PLA composite fibers containing 3% (w/w) of each additive are shown in Figure 4.12. No aggregates

were observed in the A3 and P3 fibers, but the distribution of alizarin was uniform whereas the pink pigment was not uniformly dispersed. The absence of aggregates suggests that the intermolecular interactions between PLA and these colorants are stronger than the intramolecular interactions between the colorant particles or molecules. Small colorant aggregates were observed on the Y3 fibers, but much larger aggregates, some up to 10 μm in diameter, were observed on the B3, G3 and I3 fibers. Accordingly, the intramolecular interactions between the colorant particles or molecules must be stronger in these fibers than the intermolecular interactions between the colorants and PLA. Aggregate formation is not favorable for electrospinning, because the electrical conductivity is enhanced by well-dispersed additives, allowing them to form a conductive network [55]. In our electrospinning setup (Figure 4.2), we use a glass syringe with a plunger for spinning. The composite is filled and melted inside the syringe, and the blue, green and yellow pigments, as well as indigo dye, could aggregate in the melt because no shear is applied and their movement is unrestricted. A possible optimization step would be the integration of a screw system to provide shear and thus improve the dispersion.

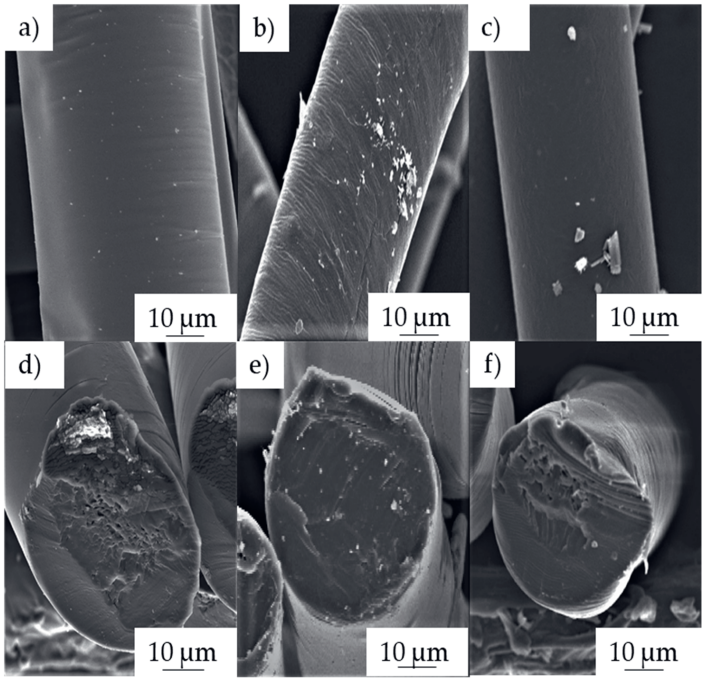

Figure 4.12: Scanning electron micrographs of PLA composite fibers: a) A3, b) B3, c) G3, d) I3, e) P3, and f) Y3.

4.3.5 Effect of Additives on Melt Conductivity

The electrical resistance of pure PLA and its composites was measured at a higher temperature than the spinning process (325 °C) to account for the heat energy lost over the larger surface of the beaker. Electrical conductivity requires mobile charge carriers, so the electrical resistance of pure PLA (5.0 GΩ) decreased at least by a factor of five in the presence of any of the colorants (Figure 4.13).

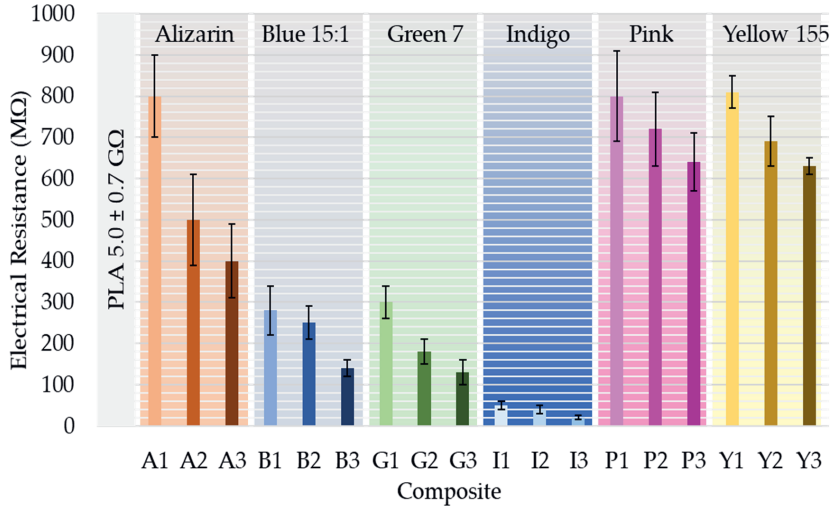

Figure 4.13: Electrical resistance of PLA and its composites containing 1%, 2% and 3% (w/w) of each additive.

For all composites, the electrical resistance decreased with the increasing additive concentration. The most significant decrease (~99%) was observed for the PLA/indigo composites. Alizarin and the pink and yellow pigments had similar moderate effects on electrical resistance at the lowest concentration of 1% (w/w), but alizarin had a stronger effect than either of the pigments at higher concentrations. The blue and green pigments had a stronger effect than alizarin and the pink and yellow pigments. In agreement with the SEM data, colorants that favor aggregate formation (indigo and the blue and green pigments) formed composites in which electrical resistance is less dependent on the additive concentration. The dispersion is poor at higher concentrations, and thus the additive's influence on electrical resistance is lower than expected. SEM showed that alizarin and the pink pigment were well dispersed, which can lead to the formation of a

conductive network and thus lower electrical resistance with increasing concentration [56].

4.3.6 Fiber Diameters Achieved Using Different PLA Composites

Next, we used our single-fiber melt electrospinning device to evaluate the processability of the PLA composites and determine how the colorants affected the fiber diameter. Taylor cone formation followed by typical fiber deposition was successful for pure PLA and all the composites at a temperature of 275 °C. The average fiber diameter of pure PLA (112.5 μm) was reduced by all the additives we tested (Figure 4.14).

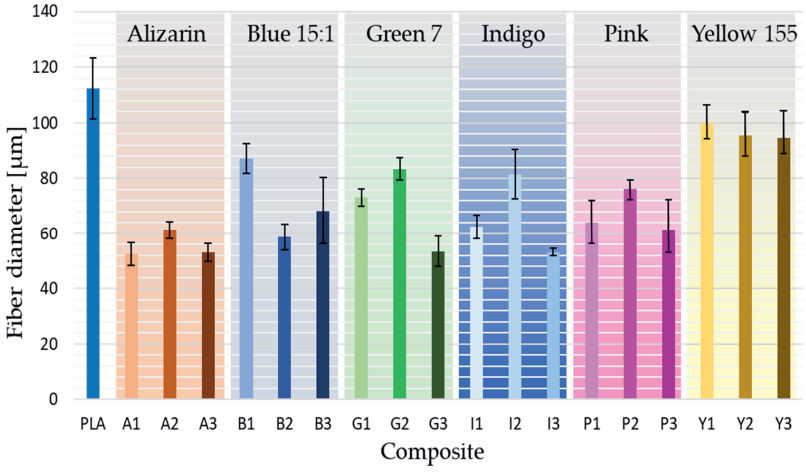

Figure 4.14: Fiber diameters and standard deviations of PLA and its composites containing 1%, 2% and 3% (w/w) of each additive produced by melt electrospinning at 275 °C using a single-nozzle laboratory device.

As stated above, narrower fibers can be produced by melt electrospinning if the viscosity of the melt is reduced and/or the electrical conductivity increased. Given that all additives increased the viscosity of the melt, and viscosity was driven more by the type of colorant than the weight percentage, it was apparent that the reduction in fiber diameter must reflect an increase in electrical conductivity. The finest fibers (52.5 μm, 53% narrower than pure PLA) were achieved for composite A1. However, even though the conductivity of the PLA/alizarin composites increased at higher alizarin concentrations, there was no significant difference in the diameters of the A1 and A3 fibers. Furthermore, the A1 and A3 fibers were also similar in thickness to the B2, G3, I3 and P3 fibers. Composites containing the pink pigment were more viscous than those

containing alizarin, whereas the electrical conductivity was almost the same, hence the fibers containing alizarin were marginally narrower. The B2, G3 and I3 fibers were among the finest despite the poor dispersion of the additives observed by SEM, suggesting the additives have higher conductivity than PLA. This means it should be possible to reduce the fiber diameter even further by improving the dispersion of additives using a melting unit that generates shear. Although the electrical conductivity of indigo-containing composites was the highest when measured in the beaker, this did not lead to the narrowest fibers, contrary to our expectations. We assume that the aggregation behavior in the beaker differs from that in the spinning device. Due to the greater space available in the beaker, colorant aggregation could lead to the formation of a network on the base of the vessel, making it easier for the applied load to flow. This possibility should be addressed in future investigations.

4.3.7 Color Measurement of Electrospun Fibers

The colorimetric analysis of fibers obtained from PLA and its composites is presented in Table 4.3. In the CIE-Lab color measurement system, L* represents lightness (L* = 100 for a perfectly reflective surface (white) and L* = 0 for a perfect black surface). Redness is represented by a*> 0, whereas greenness is represented by a*< 0. Similarly, b*> 0 represents yellowness, and b*< 0 represents blueness [57]. The presence of colorants caused the lightness index to decline compared to pure PLA, and in most cases, the lightness index fell further as the additive concentration increased. The exception was the yellow pigment, where increasing the concentration caused both L* and b* to increase, indicating the formation of a brighter yellow shade.

Table 4.3: Colorimetric values of PLA and its composites containing 1%, 2% and 3% (w/w) of each additive.

Composite	L*	A*	B*
PLA	67.22	–0.25	2.06
A1	40.42	–7.94	36.22
A2	37.69	–3.58	39.05
A3	31.42	–1.46	32.79

B1	19.45	6.01	–27.8
B2	16.95	5.14	–23.09
B3	13.53	7.5	–20.53
G1	36.27	–31.88	–0.42
G2	32.61	–32.28	–0.97
G3	25.16	–22.43	–1.84
I1	29.7	0.3	–15.54
I2	25.58	4.42	–22.78
I3	23.96	4.41	–20.86
P1	27.09	43.75	–5.42
P2	24.03	39.14	3.01
P3	22.35	36.95	2.92
Y1	50.9	–15.03	49.66
Y2	54.82	–9.52	61.13

4.4 Conclusion and further perspectives

We have investigated the effect of colorants (dyes and pigments) as conductive additives in the melt electrospinning of PLA, specifically their impact on fiber diameter. We produced electrospun fibers with diameters in the micrometer range. This environmentally friendly process could potentially replace conventional solution electrospinning to produce microfibers and nanofibers, which are used in textiles because of their superior breathability. This process is also advantageous because it allows inline dyeing to make colored textiles. All composites led to the formation of a Taylor cone in the melt electrospinning equipment, which was followed by the deposition of fibers on the collector plate. The diameter of the pure PLA fibers was > 100 μm, but this was reduced by at least 50% following the addition of all colorants except

the yellow pigment. The best result was achieved with composite A1, which formed fibers 52.5 μm in diameter (53% narrower than pure PLA). The composites containing alizarin dye and the pink pigment had similar electrical resistance, but the viscosity of composites containing the pink pigment was approximately three times higher than pure PLA, producing slightly thicker fibers. The composite containing yellow pigment showed similar electrical conductivity, but SEM analysis revealed the formation of small aggregates, which were not present in composites containing alizarin dye or the pink pigment. The electrical conductivity of a composite is inhibited by the non-homogenous dispersion of the additive, which probably explains the thickness of fibers containing the yellow pigment. Composites containing the indigo dye, blue pigment and green pigment had a lower electrical resistance than pure PLA—99% lower in the case of composites containing indigo dye. However, the diameter of the fibers was not as low as anticipated, probably due to the formation of large aggregates. Melt electrospinning is carried out using a syringe with a plunger, whereas electrical conductivity is tested in a beaker with a wide base, probably leading to different aggregation behaviors. The greater amount of space in the beaker may promote the formation of a conductive network that confers lower electrical resistance, which is not likely to occur in the melt electrospinning equipment. Taken together, our results suggest that dyes and pigments make useful functional additives, but their impact on fiber diameter must be evaluated on a case-by-case basis, to account for the conflicting effects on viscosity, conductivity and aggregate formation.

Acknowledgements

The authors acknowledge support from the students Niccolo Aldeghi, Matilde della Fontana, Celine Aarsen, and Joshua Verstappen from the Maastricht Science Program, Maastricht University, Maastricht, The Netherlands. We also acknowledge the Microscopy Department of the Institute for Textile Technology, RWTH Aachen University, Aachen, Germany. Finally, we thank our laboratory technician Henri Becker for the maintenance and modification of our equipment.

References

1. Brown, T.; Dalton, P.; Hutmacher, D.W. Melt electrospinning today: An opportune time for an emerging polymer process. Elsevier 2016, 56,116–166.
2. Huang, Z.-M.; Zhang, Y.Z.; Kotaki, M.; Ramakrishna, S. A review on polymer nanofibers by electrospinning and their applications in nanocomposites. Compos. Sci. Technol. 2003, 63, 2223–2253.
3. Greiner, A.; Wendorff, J.H. Electrospinning: A Fascinating Method for the Preparation of Ultrathin Fibers. Angew. Chem., Int. Ed. 2007, 46, 5670–5703.
4. Ma, B.; Xie, J.; Jiang, J. Rational design of nanofiber scaffolds for orthopedic tissue repair and regeneration. Nanomedicine (Lond) 2013, 8, 1459–1481.
5. Shin, S.-H.; Purevdorj, O.; Castano, O. A short review: Recent advances in electrospinning for bone tissue regeneration. J. Tissue Eng 2012, 3, 2041731412443530.
6. McClellan, P.; Landis, W.J. Recent applications of coaxial and emulsion electrospinning methods in the field of tissue engineering. Biores Open Access 2016, 5, 212–227.
7. Khajavi, R.; Abbasipour, M.; Bahador, A. Electrospun biodegradable nanofibers scaffolds for bone tissue engineering. J. Appl Polym Sci 2016, 133, 42883
8. Mani, M.P.; Jaganathan, S.K.; Ismail, A.F. Appraisal of electrospun textile scaffold comprising polyurethane decorated with ginger nanofibers for wound healing applications. J. Ind. Text. 2019, 49, 648–662.
9. Sundarrajan, S.; Tan, K.L.; Lim, S.H. Electrospun nanofibers for air filtration applications. Procedia Eng 2014, 75, 159–163.
10. Scholten, E.; Bromberg, L.; Rutledge, G.C. Electrospun polyurethane fibers for absorption of volatile organic compounds from air. ACS Appl Mater. Interfaces 2011, 3, 3902–3909.
11. Wang, J.; Li, Y.; Sun, X. Challenges and opportunities of nanostructured materials for aprotic rechargeable lithium–air batteries. Nano Energy 2013, 2, 443–467.
12. Wang, X.; Drew, C.; Lee, S.H. Electrospun Nanofibrous membranes for highly sensitive optical sensors. Nano Lett 2002, 2, 1273–1275.

13. Nan, N.; He, J.; You, X.; Sun, X.; Zhou, Y.; Qi, K.; Shao, W.; Liu, F.; Chu, Y.; Ding, B. A Stretchable, Highly Sensitive, and Multimodal Mechanical Fabric Sensor Based on Electrospun Conductive Nanofiber Yarn for Wearable Electronics. Adv. Mater. Technol 2019, 4, 1800338.

14. Bhat, G.S. Advances in polymeric nanofiber manufacturing technologies. J. Nanomater Mol Nanotechnol 2016, 5, 1800338.

15. Bhardwaj, N.; Kundu, S.C. Electrospinning: A fascinating fiber fabrication technique. Biotechnol Adv 2010, 28, 325–347.

16. Mehdi, M.; Mahar, F.K.; Qureshi, U.A.; Khatri, M.; Khatri, Z.; Ahmed, F.; Kim, I.S. Preparation of colored recycled polyethylene terephthalate nanofibers from waste bottles: Physicochemical studies. Adv. Polym. Technol. 2018, 37, 2820–2827.

17. Bubakir, M.; Li, H.; Yang, W. Handbook of Nanofibers (1st edition); Springer Nature: Basel, Switzerland, 2017, pp 125–156.

18. Qin, Y.; Cheng, L.; Zhang, Y.; Chen, X.; Wang, X.; He, X.; Yang, W.; An, Y.; Li, H. Efficient preparation of poly (lactic acid) nanofibers by melt differential electrospinning with addition of acetyl tributyl citrate. J. Appl. Polym. Sci. 2018, 135, 46554.

19. Nayak, R. Polypropylene nanofibers: Melt electrospinning versus Meltblowing; Springer International Publishing, Basel, Switzerland, 2017, pp 1-7.

20. Badami, A.S.; Kreke, M.R. Thompson, M.S.; Riffle, J.S.; Goldstein, A.S. Effect of fiber diameter on spreading, proliferation, and differentiation of osteoblastic cells on electrospun poly(lactic acid) substrates. Biomaterials 2006, 27, 596–606.

21. Casasola, R.; Thomas, N.L.; Trybala, A.; Georgiadou, S. Electrospun poly lactic acid (PLA) fibers: Effect of different solvent systems on fiber morphology and diameter. Polymer 2014, 55, 4728–4737.

22. Dalton, P.D.; Grafahrend, D.; Klinkhammer, K.; Klee, D.; Moller, M. Electrospinning of polymer melts: Phenomenological observations. Polymer 2007, 48, 6823–6833.

23. Zhao, F.; Liu, Y.; Yuan, H. Orthogonal design study on factors affecting the degradation of polylactic acid fibers of melt electrospinning. J. Appl Polym Sci 2012, 2652-2658.

24. Li, Q.; He, H.W.; Fan, Z.Z.; Zhao, R.H.; Chen, F.X.; Zhou, R.; Ning, X. Preparation and Performance of Ultra-Fine Polypropylene Antibacterial Fibers via Melt Electrospinning. Polymers 2020, 12, 606.

25. L., L.; R., S.J.M. Electrostatic fiber spinning from polymer melts. I. Experimental observations on fiber formation and properties. J. Polym Sci Polym Phys Ed. 19, 909–920.

26. Dalton, P.D.; Lleixà Calvet, J.; Mourran, A. Melt electrospinning of poly-(ethylene glycol-block-ε-caprolactone). Biotechnol J. 2006, 998-1006.

27. Yoon, K.; Hsiao, B.S.; Chu, B. Functional nanofibers for environmental applications. J. Mater. Chem 2008, 18.

28. Zhou, H.; Green, T.B.; Joo, Y.L. The thermal effects on electrospinning of polylactic acid melts. Polymer (Guildf) 2006, 7497-7505.

29. Brown, T.D.; Dalton, P.D.; Hutmacher, D.W. Direct writing by way of melt electrospinning. Adv Mater. 2011, 23, 5651–5657

30. Zhmayev, E.; Cho, D.; Joo, Y.L. Nanofibers from gas-assisted polymer melt electrospinning. Polymer 2010, 51, 4140–4144.

31. Yoon, Y.I.; Park, K.E.; Lee, S.J.; Park, W.H. Fabrication of Microfibrous and Nano-/Microfibrous Scaffolds: Melt and Hybrid Electrospinning and Surface Modification of Poly(L-lactic acid) with Plasticizer. BioMed Res. Int. 2013, 309048.

32. Nayak, R.; Kyratzis, I.L.; Truong, Y.B.; Padhye, R.; Arnold, L. Melt electrospinning of polypropylene with conductive additives. J. Mater. Sci. 2012, 47, 6387–6396.

33. Hacker, C.; Fourné, R.; Rübsam, U.; Seide, G.; Gries, T. Challenges of the meltelectrospinning process: An economical and technical window of opportunity [Herausforderungen des Schmelzelektrospinns: Wirtschaftliche und technische Potentiale und Möglichkeiten]. In 52nd Dornbirn Man-Made Fiber Congress, Dornbirn, Austria, 11th September 2013.

34. Lee, K.S.; Lee, B.S.; Park, Y.H.; Park, Y.C.; Kim, Y.M.; Jeong, S.H.; Kim, S.D. Dyeing properties of nylon 66 nano fiber with high molecular mass acid dyes. Fibers Polym. 2005, 6, 35–41.

35. Wang, T.; He, Z.; Zheng, X.; Wang, Y.; Zhang, C.; Zhang, W. Electrical properties of Copper (II) phthalocyanine derivative thin films. Optoelectronics Letters 2007, 3, 43–46.

36. Sun, C.; Li, Y.; Qi, D.; Li, H.; Song, P. Optical and electrical properties of purpurin and alizarin complexone as sensitizers for dye-sensitized solar cells. J. Mater. Sci.: Mater. Electron. 2016, 27, 8027–8039.

37. T.; Luong, T.T.; Chen, Z.; Zhu, H. Flexible solar cells based on copper phthalocyanine and buckminsterfullerene. Sol. Energy Mater. Sol. Cells 2010, 94, 1059–1063.

38. Gsänger, M.; Bialas, D.; Huang, L.; Stolte, M.; Würthner, F. Organic Semiconductors based on Dyes and Color Pigments. Advanced Materials 2016, 28, 3615–3645.

39. Gabr, M. Electric and Dielectric Properties of Some Fluorescent Dye/PMMA Solar Concentrators. Int. J. Polym. Mater. Polym. Biomater. 2008, 57, 569–583.

40. Maqsood, M.; Langensiepen, F.; Seide, G. Investigation of melt spinnability of plasticized polylactic acid biocomposites-containing intumescent flame retardant. J. Therm. Anal. Calorim. 2020, 139, 305–318.

41. Koenig, K.; Balakrishnan, N.; Hermanns, S.; Langensiepen, F.; Seide, G. Biobased Dyes as Conductive Additives to Reduce the Diameter of Polylactic Acid Fibers during Melt Electrospinning. Materials 2020, 13, 1055.

42. Puzyn, T. Organic Pollutants Ten Years After the Stockholm Convention - Environmental and Analytical Update; InTechOpen Publishing: London, United Kingdom, 2017, pp. 55-88.

43. Sigma Aldrich. Available online: https://www.sigmaaldrich.com/catalog/product/sial/122777?lang=en&region =NL.(accessed on 20 August 2020).

44. Chemical Book. Available online: https://www.chemicalbook.com/ProductChemicalPropertiesCB7399460_EN.htm# MSDSA. (Accessed on 20 August 2020).

45. Jia, S.; Yu, D.; Zhu, Y.; Wang, Z.; Chen, L.; Fu, L. Morphology, Crystallization and Thermal Behaviors of PLA-Based Composites: Wonderful Effects of Hybrid GO/PEG via Dynamic Impregnating. Polymers 2017, 9, 528.

46. Su, Z.; Li, Q.; Liu, Y.; Hu, G.-H.; Wu, C. Multiple melting behavior of poly(lactic acid) filled with modified carbon black. J. Polym. Sci., Part B: Polym. Phys. 2009, 47, 1971–1980.

47. Lascano, D.; Quiles-Carrillo, L.; Balart, R.; Boronat, T.; Montanes, N. Toughened Poly (Lactic Acid)—PLA Formulations by Binary Blends with Poly (Butylene Succinate-co-Adipate)—PBSA and Their Shape Memory Behaviour. Materials 2019, 12, 622.

48. Broda, J. Structure of polypropylene fibers coloured with a mixture of pigments with different nucleating ability. Polymer 2003, 44, 6943–6949.

49. Broda, J. Nucleating activity of the quinacridone and phthalocyanine pigments in polypropylene crystallization. J. Appl. Polym. Sci. 2003, 90, 3957–3964.

50. Ohkita, T.; Lee, S.-H. Thermal degradation and biodegradability of poly (lactic acid)/corn starch biocomposites. J. Appl. Polym. Sci. 2006, 100, 3009–3017.

51. Wang, N.; Zhang, X.; Ma, X.; Fang, J. Influence of carbon black on the properties of plasticized poly (lactic acid) composites. Polym. Degrad. Stab. 2008, 93, 1044–1052.

52. Slark, A.T.; Hadgett, P.M. The effect of polymer structure on specific interactions between dye solutes and polymers. Polymer 1999, 40, 1325–1332.

53. Marks, A.F.; Orr, P.; McNally, G.M.; Murphy, W.R. Effect of Pigment Type and Concentration on the Rheological Properties of Polypropylene. Dev. Chem. Eng. Miner. Process. 2008, 127-136.

54. Nayak, R. Effect of viscosity and electrical conductivity on the morphology and fiber diameter in melt electrospinning of polypropylene. Text. Res. J. 2013, 83, 606.

55. Király, A.; Ronkay, F. Effect of filler dispersion on the electrical conductivity and mechanical properties of carbon/polypropylene composites. Polym. Compos. 2013, 34, 1195–1203.

56. Pan, Y.; Li, L.; Chan, S.H.; Zhao, J. Correlation between dispersion state and electrical conductivity of MWCNTs/PP composites prepared by melt blending. Composites, Part A 2010, 41, 419–426.

57. Baykuş, O.; Tugce Celik, I.; Dogan, S.D.; Davulcu, A.; Dogan, M. Enhancing the dyeability of poly(lactic acid) fiber with natural dyes of alizarin, lawsone, and indigo. Fibers Polym. 2017, 18, 1906–1914.

Chapter 5

Pilot-Scale Electrospinning of PLA Using Biobased Dyes as Multifunctional Additives

This chapter is based on the following publication:
Balakrishnan, N. K.; Ostheller, M.-E.; Aldeghi, N.; Schmitz, C.; Groten, R.; Seide, G. Pilot-Scale Electrospinning of PLA Using Biobased Dyes as Multifunctional Additives. Polymers 2022, 14(15), doi: 10.3390/polym14152989

Abstract

Fibers with diameters in the lower micrometer range have unique properties suitable for applications in the textile and biomedical industries. Such fibers are usually produced by solution electrospinning, but this process is environmentally harmful because it requires the use of toxic solvents. Melt electrospinning is a sustainable alternative but the high viscosity and low electrical conductivity of molten polymers produce thicker fibers. Here, we used multifunctional biobased dyes as additives to improve the spinnability of polylactic acid (PLA), improving the spinnability by reducing the electrical resistance of the melt, and incorporating antibacterial activity against Staphylococcus aureus. Spinning trials using our 600-nozzle pilot-scale melt electrospinning de-vice showed that the addition of dyes produced narrower fibers in the resulting fiber web, with a minimum diameter of ~9 μm for the fiber containing 3% (w/w) of curcumin. The reduction in diameter was low at lower throughputs but more significant at higher throughputs, where the diameter reduced from 46 μm to approximately 23 μm. Although all three dyes showed anti-bacterial activity, only the PLA melt containing 5% (w/w) curcumin retained this property in the fiber web. Our results provide the basis for the development of environmentally friendly melt electrospinning processes for the pilot-scale manufacturing of microfibers.

5.1 Introduction

Micro fibers, submicro fibers, and nano fibers have a large surface area to volume ratio, making them ideal for applications as textiles (e.g., material for filters), biomedical devices (e.g., wound dressings, tissue engineering constructs, and drug delivery vehicles) [1], and battery components for fuel and solar cells [1-6]. The unique properties of such fibers include better flexibility, waterproofing, and breathability compared to regular fibers [7-9]. Their production methods include melt blowing, electro-blowing, and centrifugal spinning, but the most widely used one is electrospinning [10].

Electrospinning involves the application of an external electrostatic field to a polymer liquid as they emerge from a nozzle [11]. The electrostatic repulsion caused by this charge is strong enough to overcome the surface tension of a droplet, and once a certain threshold is exceeded, it results in the formation of a Taylor cone [12,13]. If the liquid is viscous and cohesive, it does not break up into droplets (the principle of electro-spraying) but forms an electrically charged laminar jet, which elongates due to electrostatic repulsion. In solution electrospinning, the fiber is formed as the solvent evaporates; in melt electrospinning, it is formed as the polymer solidifies.

The diameter of the fibers is mainly dependent on the viscosity and electrical conductivity of the polymer solution or melt. Solution electrospinning is used most frequently because polymer solutions are less viscous and more conductive than molten polymers, leading to more interaction with the electric field and enhanced whipping behavior of the polymer jet, producing finer fibers. However, for polymers such as polylactic acid, commonly used solvents include chloroform, dichloromethane, and N, N-dimethylformamide. Furthermore, solvents make up the bulk of the raw material. The polymer content is therefore low (reducing productivity), and this is exacerbated by frequent nozzle blockages caused by solvent evaporation [11,14]. Furthermore, even trace amounts of solvents present in the fibers create problems during usage, especially in the medical field, and therefore extensive removal of solvent is necessary. Therefore, researchers are shifting towards the more sustainable melt electrospinning approach. However, the higher viscosity and lower electrical conductivity of molten polymers make the production of submicrofibers more challenging. This can be addressed in part by modifying the electrospinning equipment [1,15,16]. Examples include the use of multi-temperature control [15] and spot laser melt electrospinning to produce fibers in the submicrometer range [16]. Another approach is the use of additives that alter the properties of the molten polymer, such as salts to improve the conductivity of polymers

[17] or plasticizers to re-duce the viscosity of polymers [10]. We have previously used dyes and pigments as additives to increase the conductivity of molten PLA during electrospinning and successfully reduced the diameter of the fibers [18,19]. However, the addition of salt has led to the degradation of PLA in the past.

One of the promising alternatives here is multifunctional colorants. They have been extensively used in the textile field for dyeing, but colorants can also confer other properties, such as conductivity and antibacterial activity. For example, the dye alizarin is used extensively in solar cells and is researched for other electronic applications [20]. The antibacterial activity of alizarin [21], quercetin [22], and curcumin [23,24] makes them suitable for applications such as food packaging [25] and wound dressings [26]. However, to the best of our knowledge, these additives have been used mainly in solution processing methods or as coatings, with only limited investigation of melt electrospinning. Furthermore, studies on electrospinning also involve single nozzles largely, and pilot-scale melt electrospinning studies are scarce.

In this study, we investigated the use of the multifunctional biobased dyes alizarin, curcumin, and quercetin as additives to reduce the diameter of PLA fibers produced using a 600-nozzle pilot scale melt electrospinning device. We studied the effect of these additives on the thermal and rheological properties of PLA, its degradation, electrical conductivity, and the diameter of the resulting fibers. Furthermore, we investigated the effect of thermal processing on the antibacterial properties of these dyes and the ability of the dyes to confer antibacterial properties on the PLA fibers. Our results provide the basis for the development of environmentally friendly melt electrospinning processes for the pilot-scale manufacturing of microfibers with diameters in the low micrometer range.

5.2 Experimental

5.2.1 Materials

We used PLA L130 (TotalEnergies|Corbion, Gorinchem, Netherlands), which has an L-PLA content >99%, a glass transition temperature (T_g) of 60 °C, a melting point (T_m) of 175 °C, and a melt flow index of 24 g/10 min at 210 °C/2.16 kg. The dyes alizarin, curcumin, and quercetin were purchased from Sigma-Aldrich (Zwijndrecht, The Netherlands). All materials were dried at 80 °C overnight before use. The chemical structures and the melting points of the dyes are presented in Table 5.1.

Table 5.1: Chemical structures and melting points of the dyes used in this study [19,27].

Additive	Chemical Structure	Melting Point (°C)
Alizarin	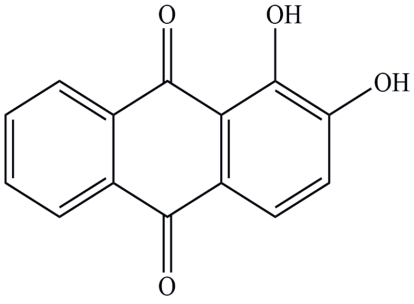	~280
Curcumin	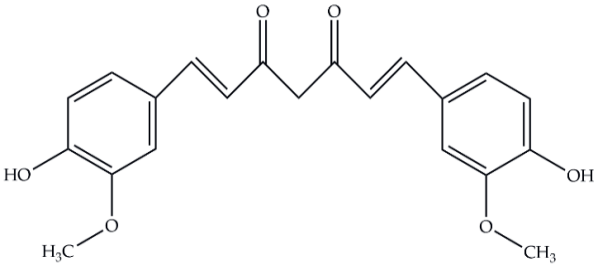	~175
Quercetin	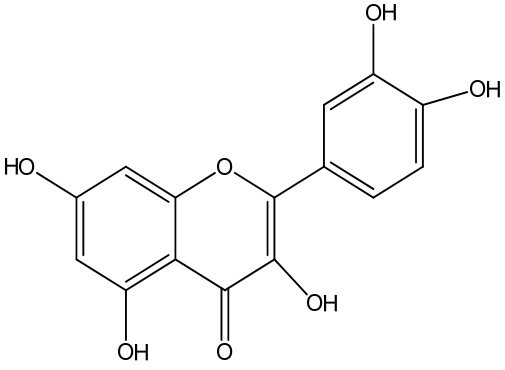	~320

PLA is typically melt-processed at less than 250 °C. Based on the melting points of the dyes used, we expected curcumin to be a melt during processing and the other two dyes to be solid particles. This could influence the viscosity of the PLA melt. Additionally, the

dyes used here also have functional polar groups and cyclic structures with double bonds, and we expected this to lead to improved electrical conductivity. PLA was dried at 80 °C under vacuum prior to all thermal processing step to reduce the water content below 100 ppm.

5.2.2 Methods

5.2.2.1 Compounding

We prepared the 5% (w/w) PLA/dye composites using a KETSE 20/40 twin-screw compounder (Brabender, Duisburg, Germany). The compounder featured six heating zones, all of which were set to 200 °C for the compounding trials. The extrudate was cooled in a water bath before granulation.

5.2.2.2 Pilot-Scale Melt electrospinning Equipment

Melt electrospinning was carried out using a pilot-scale machine from Fourne Polymertechnik (Alfter, Germany) with 600 0.3-mm nozzles (Figure 5.1) to obtain a nonwoven fiber web. We maintained a constant nozzle-to-collector distance of 7 cm and electric field strength of 60 kV. We used three different spin pump speeds (throughputs) of 2, 5, and 10 rpm to investigate the effect of throughput, dye, and the dye weight percentage on the diameter of the fibers. We mixed the 5% (w/w) PLA/dye composites with pure PLA to make fiber webs containing three different weight percentages of each additive (Table 5.2.) at a spinning temperature of 230 °C.

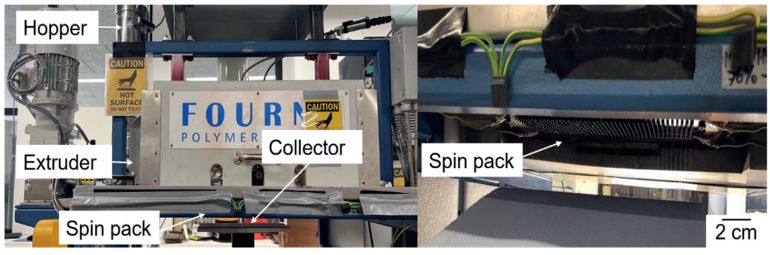

Figure 5.1: Our 600-nozzle pilot-scale electrospinning machine.

Table 1: PLA/dye composites used for the spinning trials.

Composite Abbreviation	Colorant Name	% (w/w) of Colorant
PLA	–	-
A1	Alizarin	1
A3		3
A5		5
C1	Curcumin	1
C3		3
C5		5
Q1	Quercetin	1
Q3		3
Q5		5

5.2.2.3 Characterization of Raw Materials

The rheological properties of PLA were determined using a plate–plate Discovery HR1 hybrid rheometer (TA Instruments, New Castle, DE, USA). The optimal melt electrospinning temperature for PLA was identified in a time sweep with a 25-mm plate for 60 min at an angular frequency of 10 rad/s, applying a strain amplitude of 5% at 210, 230, and 250 °C.

We determined the thermal stability of the dyes by thermogravimetric analysis (TGA) using a Q500 device (TA Instruments). We tested the dyes by heating from 35 to 230° C and then applied an isothermal run for 60 min to investigate weight loss under nitrogen purge. We also visually inspected the dye color after thermal treatment.

The antibacterial activity of the dyes was tested against Gram-negative Escherichia coli ATCC 25922 and Gram-positive Staphylococcus aureus ATCC 6538 by assessing the number of colony-forming units. We inoculated five tubes containing 5 mL of lysogeny

broth (LB) liquid medium, using 10 μL from the saturated bacterial starting culture as an inoculum before adding 100 μL of each dye at various concentrations (2, 5, 10, 15, and 20 mg/mL) in DMSO. After incubation at 37 °C and 180 rpm for 24 h, we prepared serial dilutions to achieve a bacterial concentration of ~105/mL, and 100-μL aliquots were plated on a tryptic soy agar solid medium. We counted the colonies after incubating the plates at 37 °C for 24 h. We used an untreated culture and a culture containing 100 μL of DMSO as controls.

We investigated physical changes (phase changes/melting) in the dyes within the processing window by differential scanning calorimetry (DSC) on a DSC 214 Polyma device (NETZSCH, Selb, Germany). We tested 5-mg samples by applying a temperature sweep from 25 to 250 °C at a heating rate of 10 °C/min and report the information from the first heating cycle.

5.2.2.4 Characterization of Composites

Potential interactions between PLA and the dyes were evaluated by Fourier transform infrared spectroscopy (FTIR) using a Perkin Elmer Spotlight 400 FTIR instrument equipped with a diamond crystal in ATR mode. We swept the wavenumber range from 4000 to 600 cm^{-1} at a resolution of 2 cm^{-1} using an average of 64 scans. The background was recorded before composite analysis.

The effect of dyes on the molecular weight of the manufactured masterbatches was determined by gel permeation chromatography (GPC) using a 1260 Infinity System (Agilent Technologies, Santa Clara, CA, USA). We tested pure PLA and PLA composites containing 5% (w/w) of each dye, with hexafluor-2-isopropanol (HFIP) containing 0.19% sodium trifluoroacetate as the mobile phase at a flow rate of 0.33 mL/min. Solutions were prepared by dissolving 5 mg of each sample in HFIP for ~2 h and passing them through a 0.2-μm polytetrafluoroethylene filter before injecting them into a modified silica column filled with 7-μm particles (Polymer Standards Service, Mainz, Germany). The relative weight, average molecular weight (Mw), number average molar mass (Mn), and polydispersity index (PDI) were determined using detectors calibrated with poly(methyl methacrylate) standards (1.0×10^5 g/mol).

The effect of dyes and processing on the thermal properties of PLA was tested by DSC, applying a heating and cooling cycle from 25 to 250 °C at a rate of 10 °C/min. We

recorded the T_m, T_g, cold crystallization temperature (T_{cc}), and crystallization temperature (T_c) of PLA and the composites from the first heating and cooling cycle.

We determined the thermal stability of the composites by thermogravimetric analysis (TGA), as mentioned above. Additionally, we also performed a time sweep at 230 °C using the HR1 rheometer on the PLA composites to investigate their thermal stability, as mentioned above. After the isothermal run, we heated the materials up to 500 °C to investigate the effect of the addition of dyes on the 50% weight loss temperature.

5.2.2.5 Characterization of Melt electrospun Fiber Webs

We measured the effect of dyes on PLA viscosity using the HR1 rheometer described above. We used a 25-mm plate (gap = 1000 μm) and varied the angular frequency from 10 to 628 rad/s while maintaining the strain amplitude at 5% in a constant environment with a nitrogen atmosphere at 230 °C. The equilibration time was 1 min. To facilitate comparison, we compared the complex viscosity of PLA webs with and without dyes at an angular frequency of 10 rad/s. We recorded the electrical resistance of PLA and PLA/dye composite webs at a temperature of 230 °C using a Keithley 617 electrometer (Tektronix, Beaverton, OR, USA), including band heaters to melt the polymer and two electrodes connected to the electrometer in the melt (6 mm apart). We placed a temperature sensor on the polymer melt to measure the melt temperature. We used a 10 MΩ resistor for calibration and applied a potential difference of 10 V between the electrodes (Figure 5.2).

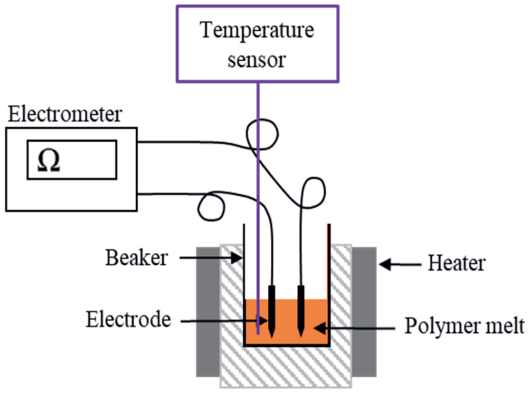

Figure 5.2: Schematic illustration of our electrometer setup.

We measured fiber diameters by reflected light microscopy using a BA310 microscope equipped with Moticam5 + 5.0MP (Motic, Wetzlar, Germany) at 400× magnification.

Diameters were measured in 100 images representing different areas of each web and the average value is presented. The webs were also analyzed by DSC in the temperature range 25–250 °C at a heating rate of 10 °C/min. We analyzed all fibers prepared with different throughputs and calculated the crystallinity of the web from the first heating cycle using Eq. 5.1 [28]:

$$X_c = {\Delta H_m - \Delta H_c * 100}\Big/{\Delta H_m^0} \qquad \textbf{Eq. 5.1}$$

H_m^0 is the melt enthalpy of the material at 100% crystallinity, H_m is the melting enthalpy at T_m and H_c is the enthalpy of cold crystallization at T_{cc}.

We tested the antibacterial properties of the fiber webs against *S. aureus* using the colony counting method discussed above.

5.3 Results and discussion

5.3.1 Overall Experimental Approach

Our experimental approach is summarized in Figure 5.3. First, we analyzed PLA and the dyes separately to determine the melt electrospinning temperature. Then, we prepared PLA containing 5% (w/w) of each dye as composites using a twin-screw compounder and analyzed the effect of the dyes on the thermal properties and thermal stability of PLA. Next, we dry-mixed pure PLA with the PLA dye composites to prepare composites with different weight ratios of each additive (Table 5.2.). Finally, we prepared fibers from the composites using our pilot-scale melt electrospinning machine. Our primary goal was to reduce the diameter of the fibers by increasing the electrical conductivity and/or reducing the viscosity of the melt. The secondary goal was to incorporate the antibacterial property of the dyes into the melt electrospun fibers. Other process parameters, such as temperature, electrical field, throughput, and nozzle-to-collector distance, were kept constant so that any change in fiber diameter could be attributed to the dye.

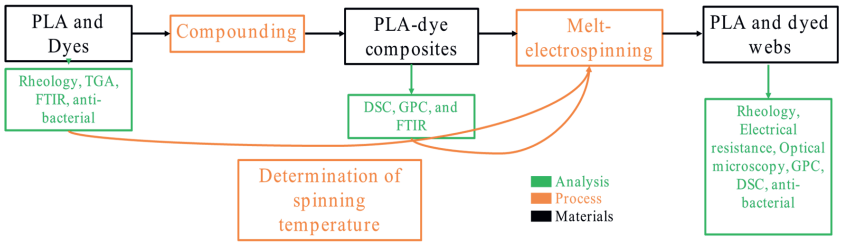

Figure 5.3: Overview of the experimental approach.

5.3.2 Characterization of Materials

5.3.2.1 Rheological Analysis of PLA

The rheograms of PLA at 210, 230, and 250 °C are presented in Figure 5.4. The complex viscosity of PLA was lower at 250 °C than at 210 °C, as expected because the polymer chains become more mobile and therefore the viscosity falls at higher temperatures. The complex viscosity remained constant over time at 210 °C. At 230° C, we observed a slight reduction in the viscosity towards the end of the isothermal run, whereas the reduction was more significant at 250 °C. This suggests that PLA degradation is significant at 250 °C but only marginal at 230 °C. A lower viscosity is preferred for melt electrospinning be-cause whipping behavior increases at lower viscosities. The reduction in complex viscosity was insignificant at 230 °C, so we selected this temperature for the melt electrospinning experiments.

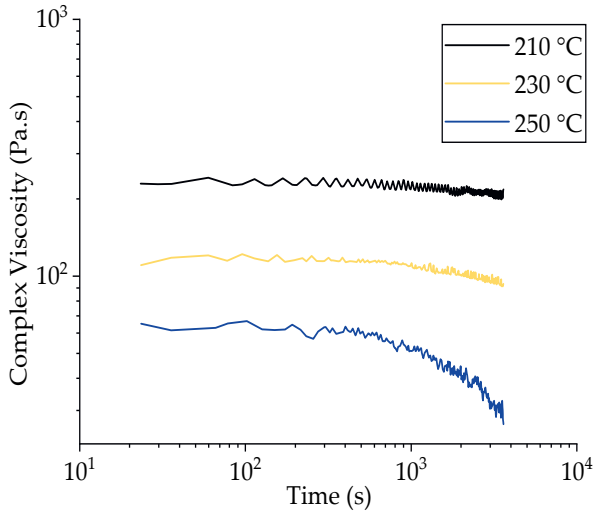

Figure 5.4: Rheograms representing a time sweep of PLA at different temperatures, showing a loss of complex viscosity at 250 °C.

5.3.2.2 Thermal Stability of the Dyes

The TGA thermogram of the dyes (Figure 5.5) indicated negligible weight loss during the heat ramp to 230 °C. Quercetin showed no weight loss even during the isothermal run. However, alizarin and curcumin both lost ~5% during the isothermal run at 230 °C. There was no color change in any of the three dyes following TGA, so we assume that the observed weight loss reflects the loss of water bound in the crystalline region of the dyes. This was not expected to affect the processing of the melt because we dried the dyes prior to the spinning and compounding trials.

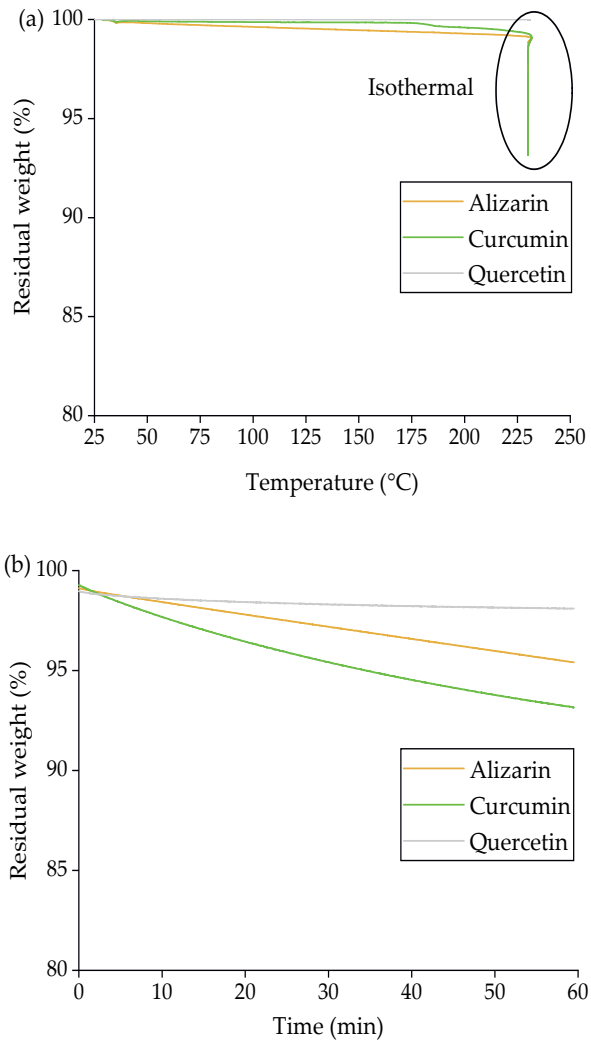

Figure 5.5: TGA thermogram of dyes during (a) the heating ramp to 230 °C and (b) the isothermal step at 230 °C for 60 min.

5.3.2.3 Antibacterial Activity of the Dyes

The antibacterial activity of the three dyes was tested using the colony counting method against E. coli (Figure 5.6) and S. aureus (Figure 5.7). The negative control and DMSO had no influence on the bacteria, so any reduction in the number of colonies was attributed to the antibacterial activity of the dyes. Alizarin was active against E. coli after treatment at 230 °C, but only at concentrations exceeding 10 mg/mL (Figure 8.6). The

other two dyes showed no activity against E. coli. One possible explanation for the heat-dependent behavior of alizarin is its ability to undergo keto-enol tautomerization, resulting in a different chemical structure [29]. However, a more plausible reason is the ability of alizarin to form polymorphic crystals [30]. Given that the thermal treatment is close to the melting point of alizarin, a change in crystal structure is likely. Further experiments are needed to determine which feature of alizarin underlies the variable antibacterial activity against E. coli.

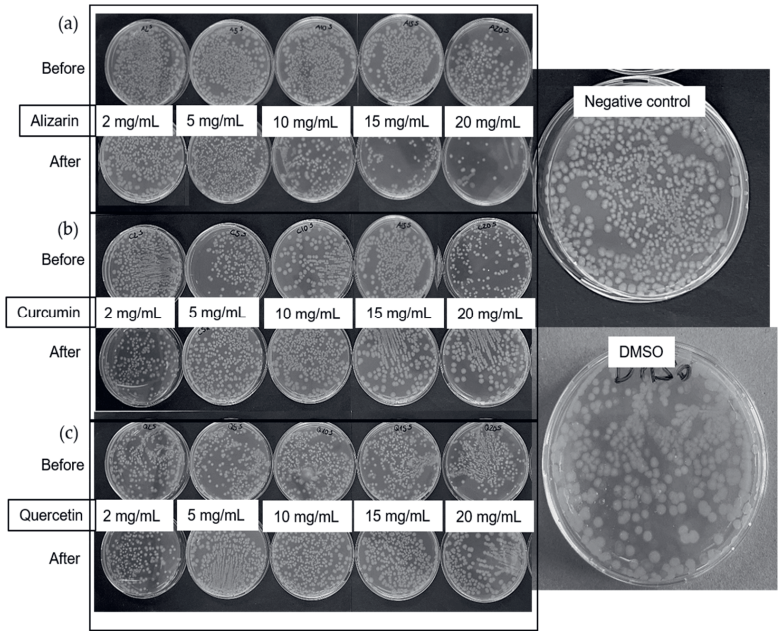

Figure 5.6: Antibacterial activity testing of (a) alizarin, (b) curcumin, and (c) quercetin against E. coli before and after thermal treatment of the dyes at 230 °C.

In contrast to the E. coli experiments, all three dyes were active against S. aureus (Figure 5.7). Before thermal treatment, alizarin showed antibacterial activity at the lowest tested concentration of 2 mg/mL. Curcumin was active at concentrations exceeding 5 mg/mL, and quercetin was active at concentrations exceeding 2 mg/mL, in agreement with earlier reports [24]. However, the activity of alizarin and curcumin was diminished by heat treatment, and post-treatment concentrations of more than 15 mg/mL were required to exert an antibacterial effect. Curcumin is also prone to keto-enol tautomerization and it is more active in its keto form [31]. Furthermore, we melted the curcumin and crystallized it again during the thermal treatment, and this could

produce a different crystalline form, as discussed above for alizarin. Quercetin appeared to be unaffected by thermal treatment. Given the limited activity of the dyes against E. coli, the antibacterial testing of fiber webs was restricted to S. aureus.

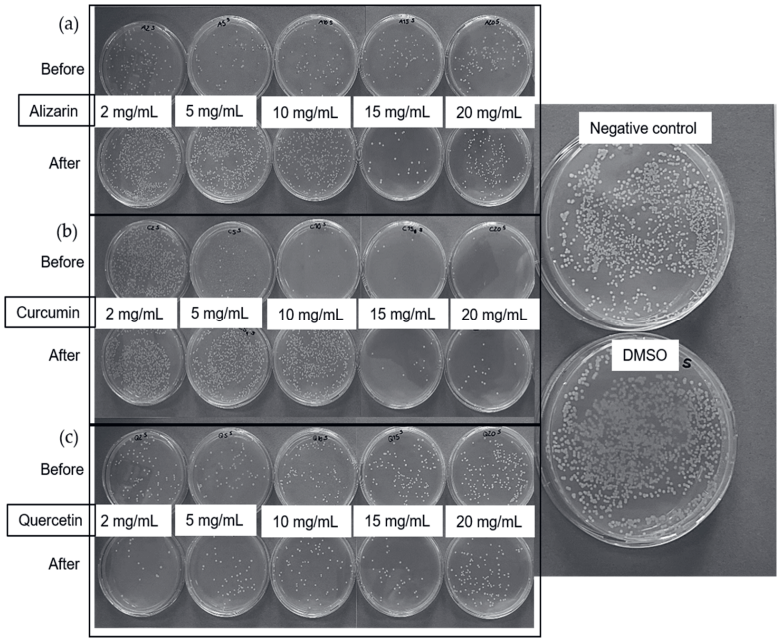

Figure 5.7: Antibacterial activity testing of (a) alizarin, (b) curcumin, and (c) quercetin against S. aureus before and after thermal treatment of the dyes at 230 °C.

5.3.2.4 Thermal Analysis of the Dyes

The DSC thermogram of the dyes (Figure 5.8) reveals an endothermic peak at ~175 °C for curcumin, which corresponds to its melting peak. The melting points of alizarin and quercetin fall outside our selected temperature range. Curcumin is a smaller molecule than PLA and its melting point falls below the selected processing temperature of 230 °C, so it could act as a plasticizer, thus reducing melt viscosity. No other thermal transitions were observed for any of the dyes in the selected temperature range, indicating that alizarin and quercetin remained as solid particles in the PLA melt during processing.

They could potentially act as anchor points to increase the viscosity of the melt, increasing the viscosity of the PLA compounds.

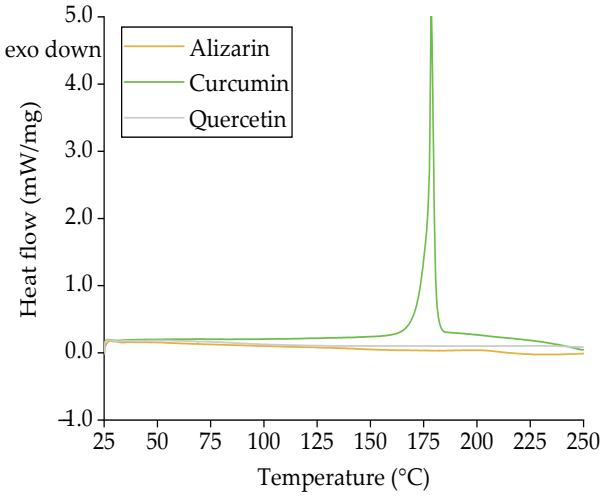

Figure 5.8: DSC thermogram representing dyes at different temperatures, showing an endothermic peak for curcumin.

5.3.3 Characterization of Composites

5.3.3.1 Analysis of PLA and Its Composites by GPC

The GPC elugram of PLA and its composites indicates that the average molecular weights (Mw, Mn) of PLA are similar to those of the PLA compounds containing 5% (w/w) dyes (Figure 5.9). The values are summarized in Table 5.3. The highest Mn (~58,700 g/mol) and highest Mw (~108,000 g/mol) were observed for compound Q5. The lowest Mn (~53,000 g/mol) and Mw (~99,000 g/mol) were observed for compound C5. The polydispersity in-dices (PDIs) were also similar. We concluded that the addition of dyes did not lead to the degradation of PLA during processing.

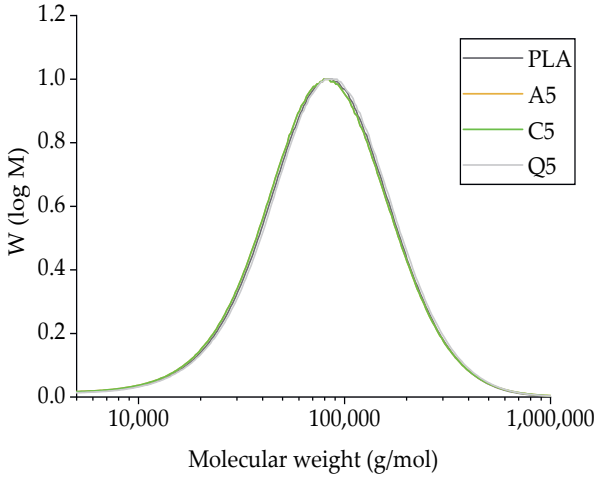

Figure 5.9: GPC elugram and the M_w, M_n, and PDI of pure PLA and its composites containing 5% (w/w) of alizarin (A5), curcumin (C5), or quercetin (Q5).

Table 5.3: Average molecular weights and PDI of PLA and its composites.

Sample	M_n (g/mol)	M_w (g/mol)	PDI
Pure PLA	55,000 ± 5,000	105,000 ± 10,500	1.89 ± 0.3
Alizarin A5	54,400 ± 5,340	105,000 ± 9,800	1.92 ± 0.2
Curcumin C5	53,000 ± 5,200	99,000 ± 96,00	1.87 ± 0.4
Quercetin Q5	58,700 ± 5,570	108,000 ± 10,000	1.84 ± 0.3

5.3.3.2 Analysis of PLA and Its Composites by FTIR Spectroscopy

The FTIR spectra of PLA and its composites containing 5% (w/w) of each dye were al-so very similar (Figure 5.10). We observed the characteristic C-O bending at 1184 cm^{-1}, the -CH_3 asymmetric and symmetric stretching bands at 1452 cm^{-1} and 1361 cm^{-1}, respectively, and the C-O-C stretching band at 1180 cm^{-1}. We did not observe a significant change in the positions of these bands in the presence of the dyes [32]. However, the C=O stretching vibration shifted from 1749 cm^{-1} for pure PLA to 1752 cm^{-1} for composite A5 and to 1751 cm^{-1} for composites C5 and Q5. This may indicate hydrogen bonding between the C=O in PLA and the functional groups of the dyes, as

observed when PLA was compounded with Kenaf fibers [33]. The presence of hydrogen bonds could increase the melt viscosity by hindering the movement of PLA chains, which we investigated by rheological analysis.

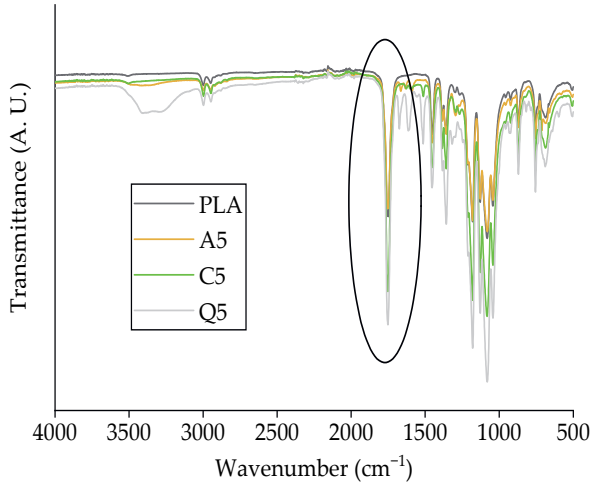

Figure 5.10: FTIR spectra of pure PLA and its composites containing 5% (w/w) of alizarin (A5), curcumin (C5), or quercetin (Q5).

5.3.3.3 Thermal Stability of PLA and Its Composites

TGA thermograms of PLA and its composites containing 5% (w/w) of each dye indicated no loss of weight during the heating ramp up to 230 °C (figure 5.11a). Furthermore, PLA and composite Q5 showed negligible weight loss during the isothermal step, where-as composite A5 lost 3% of its weight and composite C5 lost 5% (figure 5.11b). We expect this to come from loss of water and these results are similar to the thermal stability analysis of the dyes, and the minimal loss of weight should not affect the processability of PLA. Furthermore, the color of the masterbatch also remained the same before and after the thermal analysis. It was also observed that PLA has a 50% weight loss temperature of 372 °C and the thermal stability was reduced upon the addition of alizarin and curcumin. The 50% weight loss temperature was reduced to 340 °C for the PLA dye composites. As explained previously in the TGA of dyes, this could be the accelerated degradation occurring because of the release of bound water at higher

temperatures. Therefore, it can be concluded that the addition of dyes accelerates the degradation of PLA at higher temperatures when an isothermal step is involved.

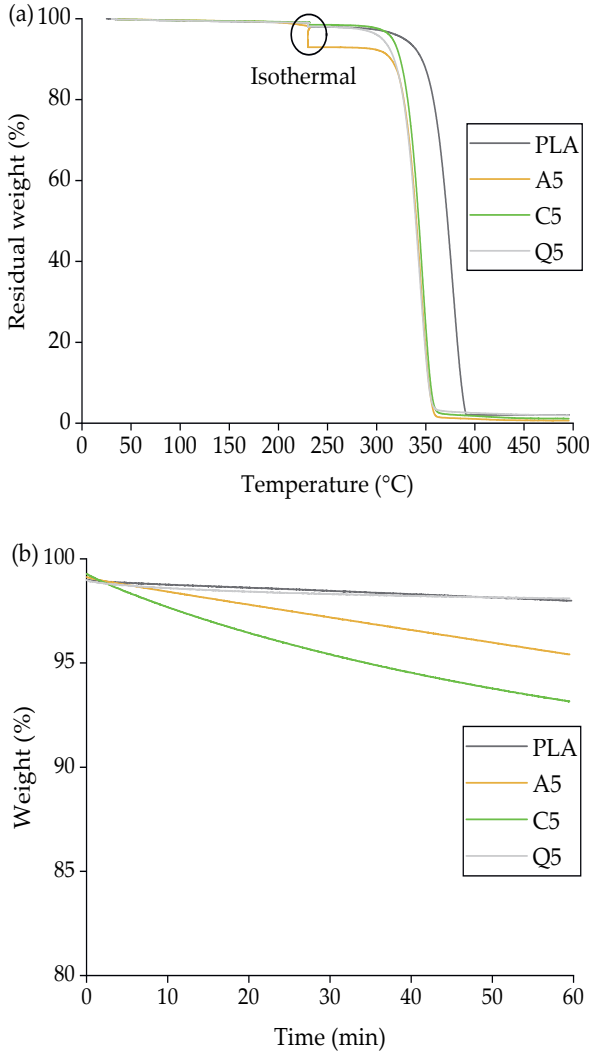

Figure 5.11: TGA thermogram of PLA and its composites containing 5% (w/w) of alizarin (A5), curcumin (C5), or quercetin (Q5) during (a) the heating ramp from 25 to 230 °C and (b) the isothermal step for 60 min at 230 °C.

The isothermal rheogram of PLA and its composites is presented below in (Figure 5.12).

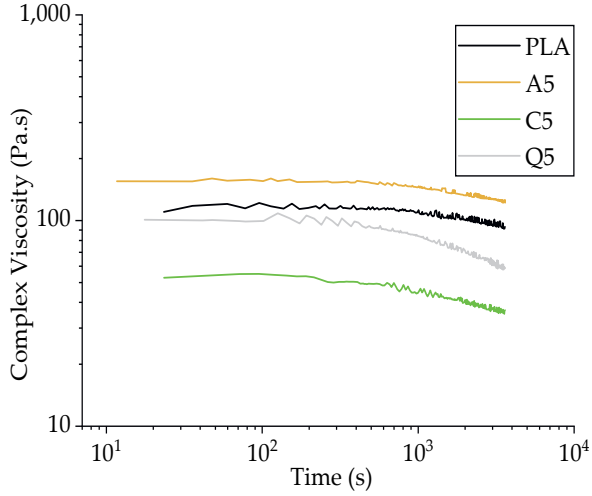

Figure 5.12: Isothermal rheogram of PLA and its composites containing 5% (w/w) of alizarin (A5), curcumin (C5), or quercetin (Q5).

It showed that the complex viscosity of PLA and composite A5 remained mostly constant during the isothermal testing at 230 °C, with only a slight degradation toward the end of the isothermal cycle, whereas the complex viscosity of composites Q5 and C5 declined toward the end of the isothermal testing. The complex viscosity of C5 fell from ~50 to ~36 Pa.s, whereas that of Q5 fell from ~100 to ~58 Pa.s. This indicates the slight degradation of PLA in the presence of curcumin or quercetin, but the effect was only marginal and was not expected to affect the melt electrospinning trials at 230 °C.

5.3.3.4 Thermal Analysis of PLA and Its Composites

The DSC thermograms of PLA and all three composites (figure 5.13a) included the glass transition temperature (Tg), a cold crystallization peak (Tcc), a recrystallization peak (Trc), and a melting peak (Tm). During the compounding experiments, the extrudate was quenched with water after mixing, and this did not give PLA sufficient time to crystallize. However, this crystallization process occurs during the DSC heating cycle above the Tg and is observed as the cold crystallization peak (Tcc). The formation of imperfect crystals results in subsequent recrystallization (Trc) [34]. The transition temperatures are summarized in Table 5.4 and remained constant even in the presence of the dyes. However, a significant change in the crystallization temperature was

observed during the cooling cycle, increasing from 98.70 to 117.10 °C following the addition of alizarin (Figure 5.13b). Alizarin therefore appears to act as a nucleating agent, in agreement with our earlier studies [18,19].

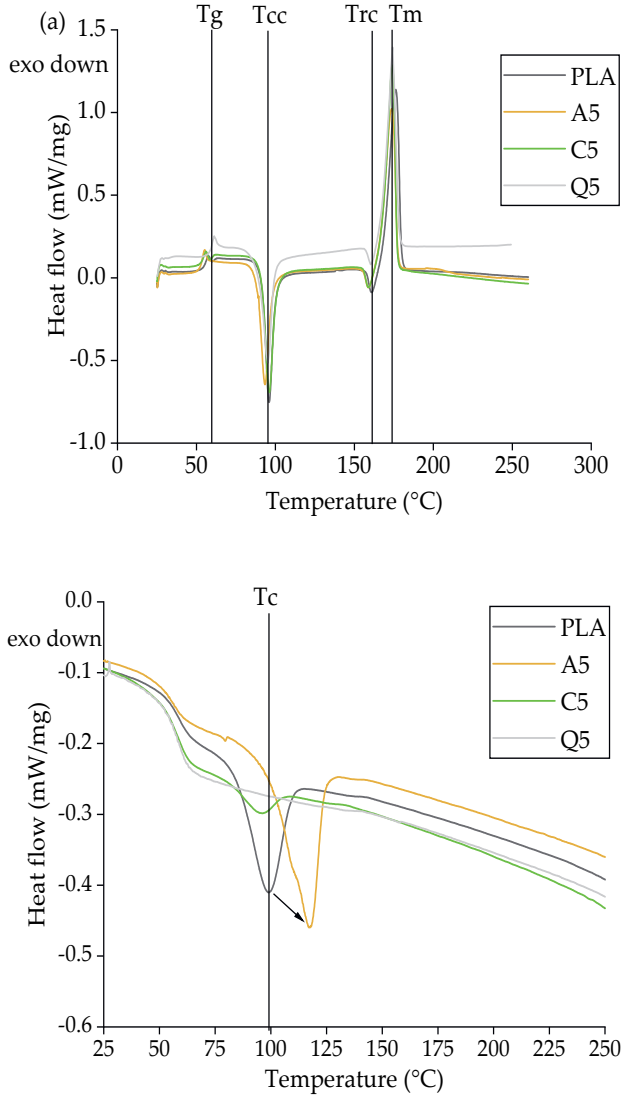

Figure 5.13: DSC thermograms of PLA and its composites containing 5% (w/w) of alizarin (A5), curcumin (C5), or quercetin (Q5) during (a) the heating cycle and (b) the cooling cycle.

Table 5.4: Thermal transition temperatures of PLA and its composites containing 5% (w/w) of alizarin (A5), curcumin (C5), or quercetin (Q5).

Material	Tg [°C]	Tcc [°C]	Trc [°C]	Tm [°C]	Tc [°C]
PLA	59.70	95.90	160.90	176.10	98.70
A5	60.10	93.30	158.80	173.60	117.10
C5	60.70	96.10	158.80	174.00	-
Q5	62.50	95.80	157.00	174.10	-

5.3.4 Characterization of the Fiber Webs

5.3.4.1 Effect of Dyes on the Viscosity of PLA

The rheogram of PLA and its composites in the fiber web showed evidence of shear thinning behavior, where the complex viscosity falls with increasing angular frequency (Figure 5.14). The increase in shear force breaks the chain interactions and entanglements, causing the polymer chains to align in the direction of the applied force and making it easier for the polymer melt to flow.

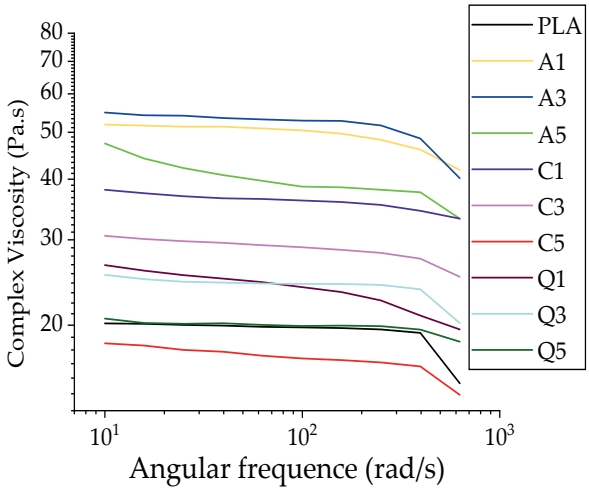

Figure 5.14: Rheogram of melt electrospun fibers formed of PLA and its composites containing 1%, 3%, or 5% (w/w) of alizarin (A1, A3, A5), curcumin (C1, C3, C5), or quercetin (Q1, Q3, Q5).

For ease of comparison, the complex viscosities of all fibers are shown at an angular frequency of 10 rad/s (Figure 5.15). The complex viscosity increases (almost twofold) following the addition of alizarin, reflecting its existence as solid particles in the composite and the possibility of hydrogen bonding with PLA, hindering the mobility of PLA chains. The forces at low shear rates are not strong enough to break these bonds, resulting in a high complex viscosity, but higher shear causes these interactions to break. Quercetin caused a marginal increase in the viscosity of PLA but not as significant as alizarin, in agreement with our earlier results [19]. The addition of curcumin initially led to an increase in viscosity but this effect was reversed at higher curcumin concentrations. Curcumin may therefore act as a plasticizer at higher concentrations, or it may promote the degradation of PLA, which we tested by GPC analysis (Section 5.3.4.5). Although the addition of dyes in-creased the viscosity of the melt, the opposite of the effect that we

sought, it only increased by 50 Pa.s. Therefore, if the dyes reduce the electrical resistance of the melt, this could still promote the formation of narrower fibers.

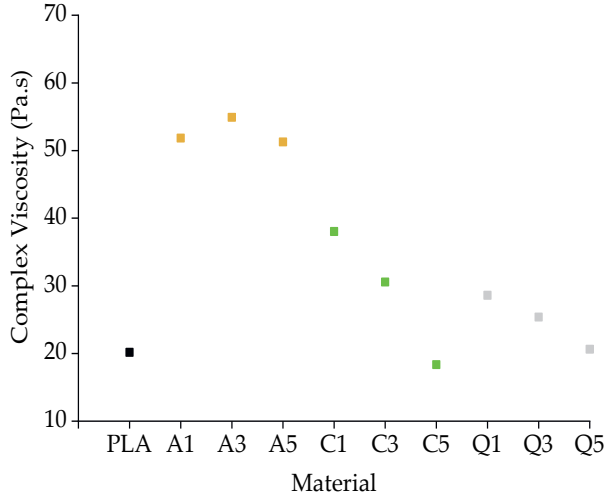

Figure 5.15: Complex viscosity of melt electrospun fibers formed of PLA and its composites containing 1%, 3%, or 5% (w/w) of alizarin (A1, A3, A5), curcumin (C1, C3, C5), or quercetin (Q1, Q3, Q5) at an angular frequency of 10 rad/s.

5.3.4.2 Effect of Dyes on the Electrical Resistance of PLA and Composite Fibers

The electrical resistance of PLA was much higher than that of its composites (Figure 5.16).

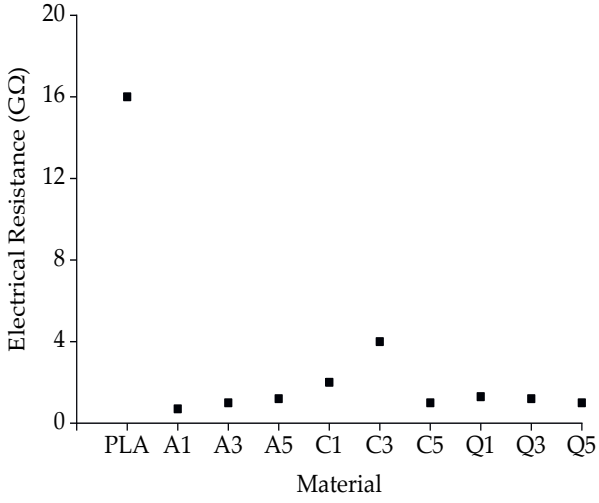

Figure 5.16: Electrical resistance of PLA and its composites containing 1%, 3%, or 5% (w/w) of alizarin (A1, A3, A5), curcumin (C1, C3, C5), or quercetin (Q1, Q3, Q5).

Even the presence of 1% alizarin or quercetin reduced the resistance to below 1 GΩ as compared to PLA, which has an electrical resistance of approximately 16 GΩ. The functional groups and double bonds present in the aromatic structures of the dyes may increase the electrical conductivity of the composites, thus favoring the formation of narrower fibers.

5.4.3 The Diameter of PLA and Composite Fibers

We assessed the diameters of PLA fibers in webs prepared by melt electrospinning at pump speeds of 2, 5, and 10 rpm (Figure 5.17).

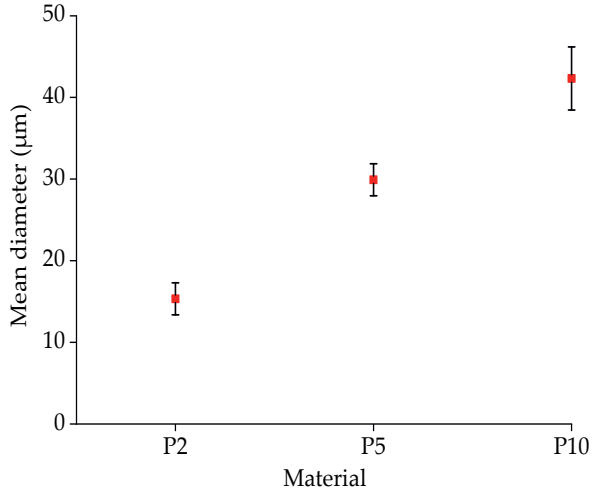

Figure 5.17: Mean diameter of fibers in webs prepared from pure PLA at different pump speeds of 2 rpm (P2), 5 rpm (P5), and 10 rpm (P10).

The mean fiber diameter increased at the higher pump speeds due to the higher volume of polymer melt passing through the spinneret in a shorter time, providing less opportunity for the polymer to interact with the electric field. The resulting coarseness of the fibers agrees with our earlier results [10].

Almost all fibers containing dyes were finer than pure PLA fibers prepared at the same pump speed (Figure 5.18). The highest mean fiber diameter at 2 rpm was 15 μm (pure PLA) and the lowest was 9 μm for composite C3 containing 3% (w/w) curcumin, which was also the lowest diameter that we achieved across all tests. The difference in diameter between pure PLA and its composites became more exaggerated at higher pump speeds. The highest mean fiber diameter at 5 rpm was 30 μm (pure PLA) and the lowest was 12 μm for composite A1 containing 1% alizarin, whereas the highest mean fiber diameter at 10 rpm was 46 μm (pure PLA) and the lowest was 22 μm for composite A3 containing 3% alizarin. At higher throughputs, the polymer jet flows quicker, giving it a smaller amount of time to interact with the electric field. Furthermore, the jet is also thicker and the surface area that interacts with the electric field is more limited, which inhibits the whipping of the PLA polymer jet. However, the addition of dyes led to an increase in electrical conductivity, which should counteract this effect and promote whipping, ultimately reducing the fiber diameter. As with alizarin, curcumin and quercetin also reduced the diameter of the PLA fibers. These results suggest that the increase in melt

viscosity caused by the dyes is not significant enough to affect the fiber diameter and the decrease in electrical conductivity plays a greater role. It was also observed that although the diameter of the fibers was reduced in most cases upon the addition of dyes, the standard deviation seemed to have increased. In the melt electrospinning equipment, we have a single-screw extruder followed by a large spin plate through which the fibers are made, and there is no mixing happening in the spin plate. We hypothesize that the agglomeration of the dyes can take place in the spin plate during spinning and this could lead to more non-uniformity in the fiber, therefore leading to a higher standard deviation. However, this needs to be investigated and optimized further.

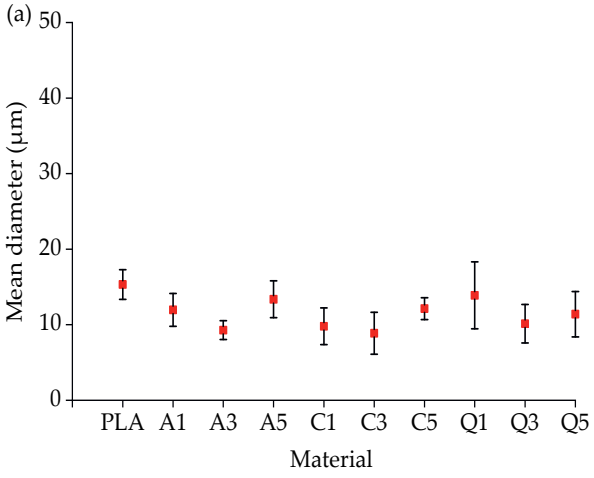

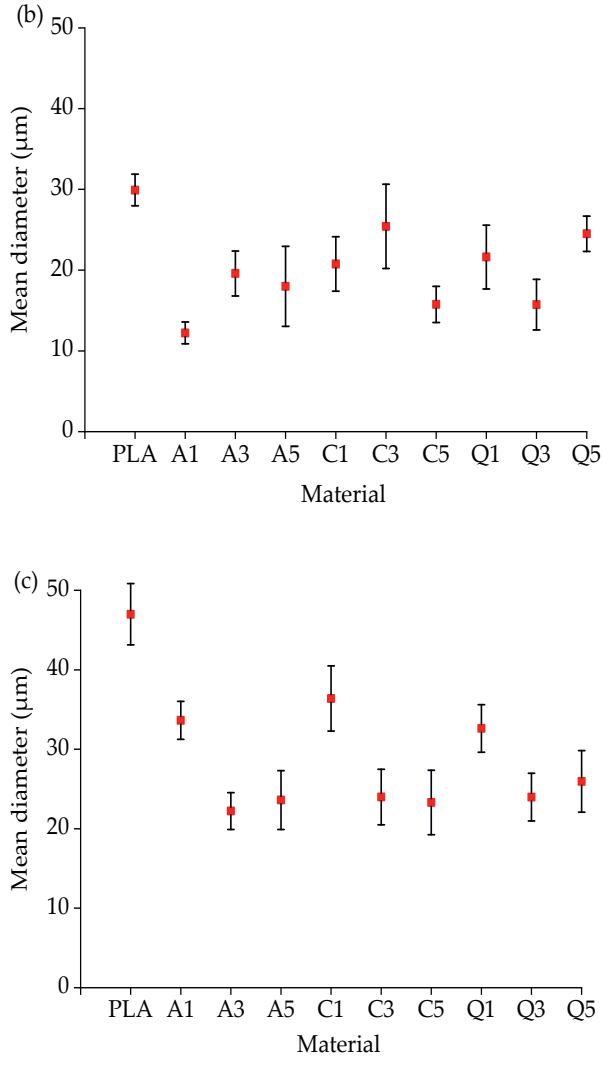

Figure 5.18: Mean diameters of fibers prepared from pure PLA and composites containing 1%, 3%, or 5% (w/w) of alizarin (A1, A3, A5), curcumin (C1, C3, C5), or quercetin (Q1, Q3, Q5) at pump speeds of (a) 2 rpm, (b) 5 rpm, and (c)10 rpm.

We observed a similar reduction in the diameter of melt electrospun PLA fibers when we added alizarin in a laboratory-scale process [10,19]. However, the dwell time was higher in the pilot-scale process, which caused slight polymer degradation that was not observed at the smaller scale. The fiber diameter is affected by dyes to a greater degree at higher throughputs. Since the throughputs used in the pilot scale and the lab scale are

different from each other, the extent to which the dyes affect the diameter is also different. Furthermore, the nozzle-to-collector distance in the laboratory-scale process is greater (10 cm) than in the pilot-scale device (7 cm). Our results show that melt electrospinning is scalable but each parameter affecting the properties of the fiber must be optimized.

We observed the uniform deposition of fibers regardless of the composition, but alizarin and curcumin achieved a higher dyeing efficiency than quercetin (Figure 5.19). The quercetin powder has a light-yellow color but the electrospun webs were much paler, suggesting that quercetin has lower dyeing power.

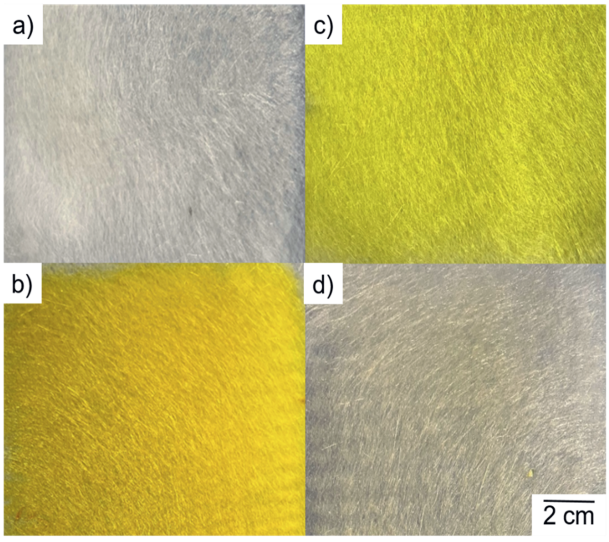

Figure 5.19: Visual appearance of melt electrospun fiber webs prepared from (a) pure PLA and composites containing 5% (w/w) of (b) alizarin, (c) curcumin, and (d) quercetin.

5.3.4.4 Analysis of Melt electrospun Webs by DSC

The DSC thermogram of the electrospun webs revealed a glass transition at ~60 °C, cold crystallization at ~95 °C, and a Tm of ~173 °C (Figure 5.20). The values are summarized in Table 5.5. In a typical melt spinning process, mechanical drawing of the fiber reduces the fiber diameter while aligning the polymer chains, increasing the crystallinity. During melt electrospinning, the electric field is used to draw the fibers and therefore we expected a similar phenomenon. The fiber diameter was much lower at a pump speed of 2 rpm compared to 10 rpm, so we also expected higher crystallinity at the lower speed.

However, the change in fiber diameter did not appear to affect the crystallinity of the PLA webs, with similar values of ~11% in each case. The crystallinity values of all fiber webs prepared from PLA composites were also similar, suggesting that varying the process parameters can reduce the fiber diameter, but the stress induced here was not sufficient to induce crystallization. Our crystallinity values were also similar to a low oriented yarn pre-pared by melt spinning [35,36]. Our results show that pilot-scale electrospinning requires further optimization to achieve well-oriented fibers.

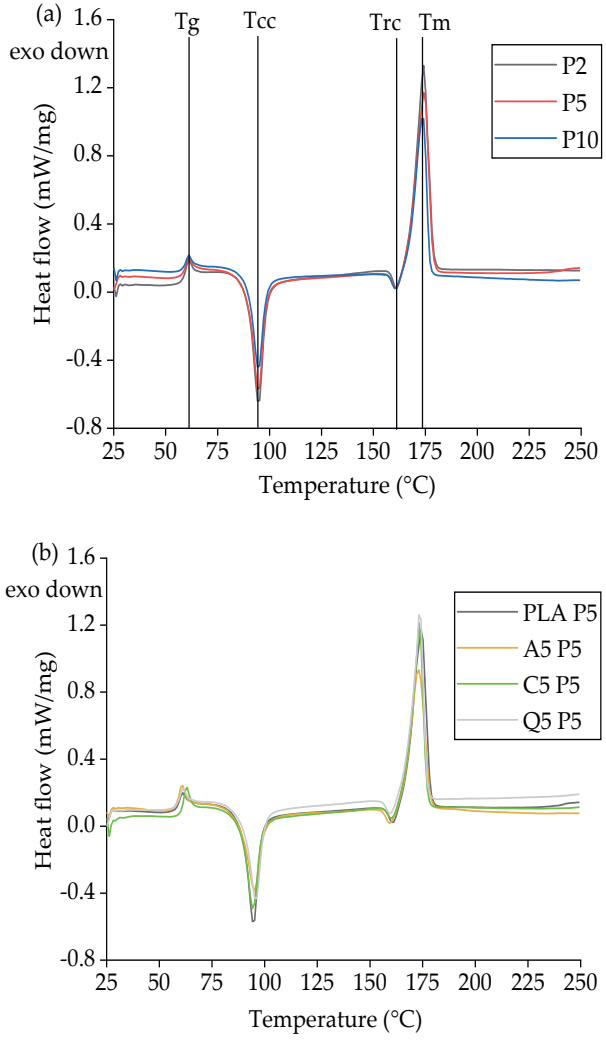

Figure 5.20: DSC thermograms of (a) PLA webs spun at different pump speeds (P2, P5, and P10 = 2, 5, and 10 rpm, respectively) and (b) PLA and PLA composite webs spun at a pump

speed of 5 rpm (A5, C5, and Q5 = composites containing 5% (w/w) alizarin, curcumin, and quercetin, respectively).

Table 5.5: Tg, Tcc, Tm, and Xc values of melt electrospun fiber webs.

Material	Tg [°C]	Tcc [°C]	Tm [°C]	Xc [%]
PLA P2	59.50	94.70	174.10	12.39
PLA P5	60.00	94.70	174.50	13.47
PLA P10	59.40	94.60	173.50	10.70
A5 P5	59.60	95.10	173.00	11.17
C5 P5	62.00	94.40	173.40	11.18
Q5 P5	60.00	95.80	173.90	12.27

5.3.4.5 Analysis of Melt electrospun Fiber Webs by GPC

The GPC elugram of melt electrospun fiber webs containing 5% (w/w) of each dye revealed similar molecular weights (Figure 5.21). The average molecular weight and PDI values are summarized in Table 5.6. The PLA and Q5 fiber webs showed little evidence of degradation during processing, matching the values of the composites after compounding (Table 5.3). However, the average molecular weights of the A5 and C5 fiber webs fell below those of the A5 and C5 composites, suggesting some degradation during processing (Table 5.3). Even so, the amount of degradation was not sufficient to hinder the electrospinning process, allowing the continuous formation of fibers. We observed weight loss for composites containing alizarin and curcumin during the isothermal TGA step, which may reflect the release of bound water from the dyes. This may also explain the degradation of PLA during melt electrospinning. GPC analysis showed that the reduction in viscosity noted for the curcumin composites might reflect the degradation of PLA rather than the ability of curcumin to act as a plasticizer.

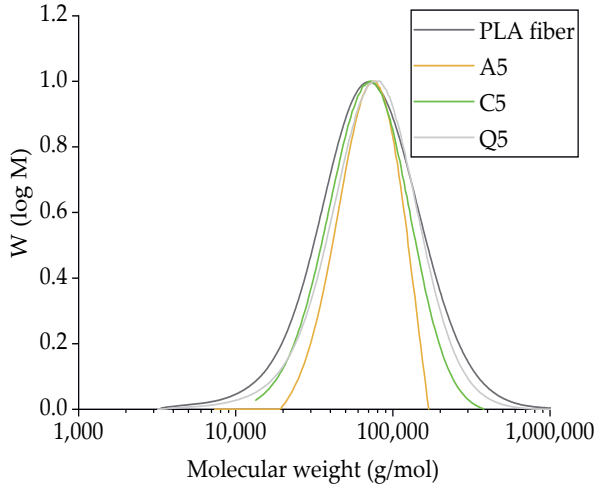

Figure 5.21: GPC elugram of melt electrospun fiber webs formed of pure PLA or PLA composites containing 5% (w/w) of alizarin (A5), curcumin (C5), or quercetin (Q5).

Table 5.6: The average molecular weight and PDI values of melt electrospun fiber webs formed of pure PLA or PLA composites containing 5% (w/w) of alizarin (A5), curcumin (C5), or quercetin (Q5).

Sample	**M_n (g/mol)**	**M_w (g/mol)**	**PDI**
PLA	51,100 ± 3,000	94,000 ± 9,000	1.84 ± 0.2
A5	62,400 ± 5,000	74,300 ± 6,000	1.19 ± 0.3
C5	57,500 ± 5,200	80,600 ± 7,000	1.40 ± 0.4
Q5	56,900 ± 4,000	91,800 ± 9,000	1.61 ± 0.2

5.3.4.6 Antibacterial Properties of Melt Electrospun Fiber Webs

The antibacterial properties of the PLA and composite fiber webs were tested against *S. aureus* to determine whether the properties of the dyes were retained (Figure 5.22). The A5 and Q5 fiber webs showed little antibacterial activity, whereas the C5 fiber web retained some antibacterial properties but was not as potent as the pure dye. Furthermore, the propagation of a potentially fungal contamination was observed using the C5 fiber web that might originate from material processing and handling. For the assessment of the antibacterial potential of the C5 fiber web, these fungal colonies were

neglected. This reduction in the antibacterial activity is likely to reflect the distribution of the dye in the polymer, with only those molecules presented on the fiber surface being able to kill the bacteria [24]. Similarly, quercetin-loaded PLA fibers were previously shown to lack the leaching of quercetin while retaining antibacterial activity [26]. Since there is no leaching, there is no possibility of the dye molecule stuck inside the fiber to provide any activity. Alizarin and curcumin also lost some of their antibacterial activity after thermal treatment, which would influence the final properties of the resulting fibers. A higher concentration of dye therefore appears necessary to ensure that the antibacterial activity is retained in melt electrospun fibers.

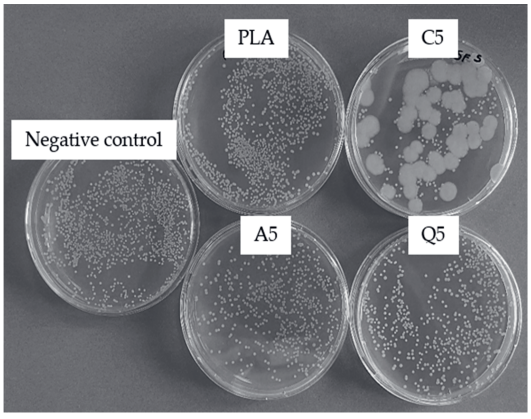

Figure 5.22: Antibacterial activity of melt electrospun webs of pure PLA or PLA composites containing 5% (w/w) of alizarin (A5), curcumin (C5), or quercetin (Q5) against S. aureus at a 10^{-5} dilution.

5.4 Conclusion

We investigated the effects of three dyes (alizarin, curcumin, and quercetin) on the pilot-scale melt electrospinning of PLA. We first analyzed the thermal stability of pure PLA and pure dyes at processing temperatures over a prolonged duration. We then tested the antibacterial activity of the dyes against E. coli and S. aureus. The dyes were effective against S. aureus at concentrations as low as 5 mg/mL, but the activity of alizarin and curcumin was reduced by thermal treatment and the concentration had to be increased to more than 15 mg/mL to achieve the same effect. This may reflect either keto-enol tautomerization or a change in the crystal structure of alizarin and curcumin during thermal treatment. After compounding, we analyzed the thermal stability of the PLA composites. FTIR spectroscopy revealed the possibility of hydrogen bonding between

PLA and the dyes. Based on these results, we selected a melt electrospinning temperature of 230 °C and produced electrospun fiber webs with diameters in the lower micrometer range. The finest pure PLA fibers that we produced were 15.3 μm in diameter, but this was reduced to 9.3 μm by adding 3% (w/w) curcumin, the lowest diameter that we achieved overall. Increasing the throughput led to an increase in diameter, but all three dyes reduced the fiber diameter at all three concentrations tested. At higher throughputs, the addition of dyes led to a greater reduction in diameter. DSC analysis of the melt electrospun fiber webs revealed that neither the additives nor the process parameters affected the (generally low) crystallinity of the fibers. GPC analysis indicated the slight degradation of PLA fiber webs containing alizarin or curcumin. Antibacterial analysis showed that only the fiber web containing 5% (w/w) curcumin retained some antibacterial activity against *S. aureus*. This is likely to reflect the small proportion of dye molecules available on the fiber surface compared to the larger proportion buried inside. More of the additive would therefore be necessary to achieve the antibacterial potency of the uncompounded dye. Our work provides insight into the scaling up of a melt electrospinning process from the laboratory to pilot scale, and provides an environmentally friendly alternative to replace conventional solution electrospinning for the production of microfibers with antibacterial properties.

Acknowledgments

The authors acknowledge support from the Konrad Buekenberg and Abdelrahman M. Abdelgawad. We would also like to thank our laboratory technician, Henri Becker, for the maintenance and modification of our equipment. We extend our thanks to Richard M Twyman for his extensive support with making necessary lingual corrections.

References

1. McClellan, P.; Landis, W.J. Recent Applications of Coaxial and Emulsion Electrospinning Methods in the Field of Tissue Engineering. Biores Open Access 2016, 5, 212-227, doi:10.1089/biores.2016.0022.
2. Brown, T.D.; Dalton, P.D.; Hutmacher, D.W. Melt electrospinning today: An opportune time for an emerging polymer process. Progress in Polymer Science 2016, 56, 116-166, doi:10.1016/j.progpolymsci.2016.01.001.
3. Shin, S.H.; Purevdorj, O.; Castano, O.; Planell, J.A.; Kim, H.W. A short review: Recent advances in electrospinning for bone tissue regeneration. J Tissue Eng 2012, 3, 2041731412443530, doi:10.1177/2041731412443530.
4. Khajavi, R.; Abbasipour, M.; Bahador, A. Electrospun biodegradable nanofibers scaffolds for bone tissue engineering. Journal of Applied Polymer Science 2016, 133, n/a-n/a, doi:10.1002/app.42883.
5. Mani, M.P.; Jaganathan, S.K.; Ismail, A.F. Appraisal of electrospun textile scaffold comprising polyurethane decorated with ginger nanofibers for wound healing applications. Journal of Industrial Textiles 2018, 49, 648-662, doi:10.1177/1528083718795911.
6. Ma, B.; Xie, J.; Jiang, J.; Shuler, F.D.; Bartlett, D.E. Rational design of nanofiber scaffolds for orthopedic tissue repair and regeneration. Nanomedicine (Lond) 2013, 8, 1459-1481, doi:10.2217/nnm.13.132.
7. Nan, N.; He, J.; You, X.; Sun, X.; Zhou, Y.; Qi, K.; Shao, W.; Liu, F.; Chu, Y.; Ding, B. A Stretchable, Highly Sensitive, and Multimodal Mechanical Fabric Sensor Based on Electrospun Conductive Nanofiber Yarn for Wearable Electronics. Advanced Materials Technologies 2019, 4, doi:10.1002/admt.201800338.
8. S Bhat, G. Advances in Polymeric Nanofiber Manufacturing Technologies. Journal of Nanomaterials & Molecular Nanotechnology 2016, 05, doi:10.4172/2324-8777.1000e108.
9. Mehdi, M.; Mahar, F.K.; Qureshi, U.A.; Khatri, M.; Khatri, Z.; Ahmed, F.; Kim, I.S. Preparation of colored recycled polyethylene terephthalate nanofibers from waste bottles: Physicochemical studies. Advances in Polymer Technology 2018, 37, 2820-2827, doi:10.1002/adv.21954.

10. Koenig, K.; Beukenberg, K.; Langensiepen, F.; Seide, G. A new prototype meltelectrospinning device for the production of biobased thermoplastic submicrofibers and nanofibers. Biomater Res 2019, 23, 10, doi:10.1186/s40824-019-0159-9.

11. Bhardwaj, N.; Kundu, S.C. Electrospinning: a fascinating fiber fabrication technique. Biotechnol Adv 2010, 28, 325-347, doi:10.1016/j.biotechadv.2010.01.004.

12. Suvorov, V.G.; Zubarev, N.M. Formation of the Taylor cone on the surface of liquid metal in the presence of an electric field. Journal of Physics D: Applied Physics 2004, 37, 289-297, doi:10.1088/0022-3727/37/2/019.

13. Yarin, A.L.; Koombhongse, S.; Reneker, D.H. Taylor cone and jetting from liquid droplets in electrospinning of nanofibers. Journal of Applied Physics 2001, 90, 4836-4846, doi:10.1063/1.1408260.

14. Góra, A.; Sahay, R.; Thavasi, V.; Ramakrishna, S. Meltelectrospun Fibers for Advances in Biomedical Engineering, Clean Energy, Filtration, and Separation. Polymer Reviews 2011, 51, 265-287, doi:10.1080/15583724.2011.594196.

15. Zhou, Y.; He, J.; Wang, H.; Qi, K.; Nan, N.; You, X.; Shao, W.; Wang, L.; Ding, B.; Cui, S. Highly sensitive, self-powered and wearable electronic skin based on pressure-sensitive nanofiber woven fabric sensor. Sci Rep 2017, 7, 12949, doi:10.1038/s41598-017-13281-8.

16. Ogata, N.; Yamaguchi, S.; Shimada, N.; Lu, G.; Iwata, T.; Nakane, K.; Ogihara, T. Poly(lactide) nanofibers produced by a meltelectrospinning system with a laser melting device. Journal of Applied Polymer Science 2007, 104, 1640-1645, doi:10.1002/app.25782.

17. Nayak, R.; Kyratzis, I.L.; Truong, Y.B.; Padhye, R.; Arnold, L. Meltelectrospinning of polypropylene with conductive additives. Journal of Materials Science 2012, 47, 6387-6396, doi:10.1007/s10853-012-6563-3.

18. Balakrishnan, N.K.; Koenig, K.; Seide, G. The Effect of Dye and Pigment Concentrations on the Diameter of Meltelectrospun Polylactic Acid Fibers. Polymers (Basel) 2020, 12, doi:10.3390/polym12102321.

19. Koenig, K.; Balakrishnan, N.; Hermanns, S.; Langensiepen, F.; Seide, G. Biobased Dyes as Conductive Additives to Reduce the Diameter of Polylactic Acid Fibers during Melt Electrospinning. Materials (Basel) 2020, 13, doi:10.3390/ma13051055.

20. Abubakari, I.; Babu, N.S.; Vuai, S.; Makangara, J. Optical and photovoltaic properties of substituted alizarin dyes for dye-sensitized solar cells application. Energy Sources, Part A: Recovery, Utilization, and Environmental Effects 2020, 43, 2569-2582, doi:10.1080/15567036.2020.1836083.

21. Cui, L.; Hu, J.-j.; Wang, W.; Yan, C.; Guo, Y.; Tu, C. Smart pH response flexible sensor based on calcium alginate fibers incorporated with natural dye for wound healing monitoring. Cellulose 2020, 27, 6367-6381, doi:10.1007/s10570-020-03219-1.

22. Pandey, S.K.; Patel, D.K.; Thakur, R.; Mishra, D.P.; Maiti, P.; Haldar, C. Anti-cancer evaluation of quercetin embedded PLA nanoparticles synthesized by emulsified nanoprecipitation. Int J Biol Macromol 2015, 75, 521-529, doi:10.1016/j.ijbiomac.2015.02.011.

23. Perumal, G.; Pappuru, S.; Chakraborty, D.; Maya Nandkumar, A.; Chand, D.K.; Doble, M. Synthesis and characterization of curcumin loaded PLA-Hyperbranched polyglycerol electrospun blend for wound dressing applications. Mater Sci Eng C Mater Biol Appl 2017, 76, 1196-1204, doi:10.1016/j.msec.2017.03.200.

24. Ostheller, M.E.; Abdelgawad, A.M.; Balakrishnan, N.K.; Hassanin, A.H.; Groten, R.; Seide, G. Curcumin and Silver Doping Enhance the Spinnability and Antibacterial Activity of Meltelectrospun Polybutylene Succinate Fibers. Nanomaterials (Basel) 2022, 12, doi:10.3390/nano12020283.

25. Roy, S.; Rhim, J.W. Preparation of bioactive functional poly(lactic acid)/curcumin composite film for food packaging application. Int J Biol Macromol 2020, 162, 1780-1789, doi:10.1016/j.ijbiomac.2020.08.094.

26. Kost, B.; Svyntkivska, M.; Brzezinski, M.; Makowski, T.; Piorkowska, E.; Rajkowska, K.; Kunicka-Styczynska, A.; Biela, T. PLA/beta-CD-based fibers loaded with quercetin as potential antibacterial dressing materials. Colloids Surf B Biointerfaces 2020, 190, 110949, doi:10.1016/j.colsurfb.2020.110949.

27. Ghorai, S.; Laskin, A.; Tivanski, A.V. Spectroscopic evidence of keto-enol tautomerism in deliquesced malonic acid particles. J Phys Chem A 2011, 115, 4373-4380, doi:10.1021/jp112360x.

28. Zhang, C.; Lan, Q.; Zhai, T.; Nie, S.; Luo, J.; Yan, W. Melt Crystallization Behavior and Crystalline Morphology of Polylactide/Poly(epsilon-caprolactone) Blends Compatibilized by Lactide-Caprolactone Copolymer. Polymers (Basel) 2018, 10, doi:10.3390/polym10111181.

29. Preat, J.; Laurent, A.D.; Michaux, C.; Perpète, E.A.; Jacquemin, D. Impact of tautomers on the absorption spectra of neutral and anionic alizarin and quinizarin dyes. Journal of Molecular Structure: THEOCHEM 2009, 901, 24-30, doi:10.1016/j.theochem.2008.12.032.

30. Cyrański, M.K.; Jamróz, M.H.; Rygula, A.; Dobrowolski, J.C.; Dobrzycki, Ł.; Baranska, M. On two alizarin polymorphs. CrystEngComm 2012, 14, doi:10.1039/c2ce06063a.

31. Rege, S.A.; Arya, M.; Momin, S.A. Structure activity relationship of tautomers of curcumin: a review. Ukrainian Food Journal 2019, 8, 45-60, doi:10.24263/2304-974x-2019-8-1-6.

32. Mofokeng, J.P.; Luyt, A.S.; Tábi, T.; Kovács, J. Comparison of injection moulded, natural fiber-reinforced composites with PP and PLA as matrices. Journal of Thermoplastic Composite Materials 2011, 25, 927-948, doi:10.1177/0892705711423291.

33. Ochi, S. Mechanical properties of kenaf fibers and kenaf/PLA composites. Mechanics of Materials 2008, 40, 446-452, doi:10.1016/j.mechmat.2007.10.006.

34. Cuiffo, M.A.; Snyder, J.; Elliott, A.M.; Romero, N.; Kannan, S.; Halada, G.P. Impact of the Fused Deposition (FDM) Printing Process on Polylactic Acid (PLA) Chemistry and Structure. Applied Sciences 2017, 7, doi:10.3390/app7060579.

35. Mai, F.; Tu, W.; Bilotti, E.; Peijs, T. The Influence of Solid-State Drawing on Mechanical Properties and Hydrolytic Degradation of Melt-Spun Poly(Lactic Acid) (PLA) Tapes. Fibers 2015, 3, 523-538, doi:10.3390/fib3040523.

36. Siebert, S.; Berghaus, J.; Seide, G. Nucleating Agents to Enhance Poly(l-Lactide) Fiber Crystallization during Industrial-Scale Melt Spinning. Polymers (Basel) 2022, 14, doi:10.3390/polym14071395.

5

Chapter 6

Comparison of melt spinning and melt electrospinning: An insight into the two processes

Comparison of melt spinning and melt electrospinning: An insight into the two processes

6.1 Introduction

Melt spinning and melt electrospinning are two techniques used for the manufacture of polymer filament yarn and low micrometer/nanometer fibers, respectively. Melt spinning was first carried out in 1969 and has since undergone various improvements [1]. On the other hand, melt electrospinning was patented in 1936, but its research into commercial use started in 1988 [2,3,4]. Both melt spinning and melt electrospinning work with polymer melts. They make use of drawing to stretch the filament thin, impart molecular orientation and mechanical properties, but there are significant difference in the functioning principals of both the processes. A schematic of both the processes is presented below in Figure 6.1.

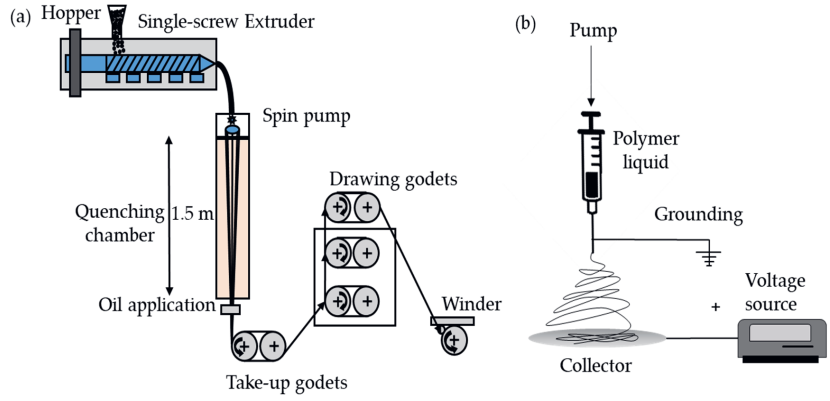

Figure 6.1: Schematic representation of a) melt spinning and b) melt electrospinning

Through various optimizations, high productivity with a high throughput of several kg/hour is possible in melt spinning making it profitable but melt electrospinning still has low throughputs of only a few grams/min to achieve low fiber diameters since higher throughput means the fiber coming out will be thicker and the influence of the electric field must be very high to stretch them thin enough to reach diameter in the submicrometer range [5]. Furthermore, the fiber web obtained from melt electrospinning

at this moment seem to be weak with low mechanical properties. The mechanical properties are much higher in melt spinning due to strain induced orientation happening because of drawing at high take up speeds. The temperature profile and process parameters used for drawing filaments during melt spinning has been studied and optimized for several polymers and this enables the high drawing and production rates. However, the corresponding drawing values and conditions are not known for the melt electrospinning. These factors are quintessential to develop melt electrospinning further to make fibers with good mechanical properties and to increase productivity. To support this improvement of melt electrospinning, this chapter provides insights into melt spinning and melt electrospinning by comparing both the processes and gives recommendations for the development of the novel melt electrospinning process.

6.2 Insights into Melt spinning

The mechanical properties of the multifilament yarn come from the drawing ratio and drawing rate applied during the process. Therefore, high take up speeds of more than 5000 m/min are used here to have a high melt draw ratio of over 300 [1]. Quenching lengths of at least 1.5 m are used for melt spinning to ensure that the yarn is sufficiently cold before they are wound. During melt spinning, a polymer droplet is first formed, which undergoes necking deformation during drawing. A schematic overview of the structure development in a melt spinning process is presented below in Figure 6.2.

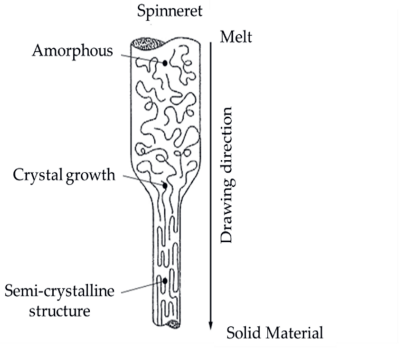

Figure 6.2: Structure development in melt spinning (through necking) [1]

It was reported by Kohler et. Al that during melt spinning of PLA, when a quenching length of about 3 m is used, maximum orientation occurs at about 1.5 m below the spinneret [6]. The stress developed during spinning, which induces orientation, also

leads to crystallization and maximum crystallization is observed at about the same length. Considering the take up speeds used during melt spinning, it takes less than 1 second before this process is completed and the filament cools down. This also corresponds to cooling rates in melt spinning reaches up to >200 °C/s. During melt spinning, crystallization can occur primarily due to two reasons. The first one is because of the polymer melt cooling down and the second one is the crystallization induced due to drawing stress applied. Crystallization due to cooling down even at such high cooling rates occurs in fast crystallizing polymers such as polyamides (PA 6, PA 66), whereas in case of slow crystallizing polymers such as PLA, it occurs largely due to stress induced crystallization [7]. It was observed that stress induced crystallization in PLA is more evident at take up speeds of over 1400 m/min [8]. In this work (chapter 2), a drawing stress was applied during melt spinning and its effect on crystallinity was investigated, however, the effect of cooling rate on crystallization of PLA in the presence of colorants but absence of drawing stress is unknown and is therefore discussed below.

6.2.1 Effect of cooling rate on crystallinity

During our study (Chapter 2), we observed that some colorants, namely, pigment blue 15:1, pigment yellow 155, and alizarin functioned as nucleating agents in PLA at lower cooling rates of 10 °C/min tested in DSC (as described in section 2.3.3.2). However, the effect of these nucleating agents during melt spinning was nonexistent. To get a better understanding about this, DSC was performed with PLA and its compound containing 0.3% (w/w) of pigment blue 15:1 (using the same device as in section 2.2.6). The materials were heated from 25 °C to 200 °C at a heating rate of 10 °C/min, and then kept isothermal at 200 °C for 5 minutes to erase their thermal history. Later 3 different cooling rates of 10 °C/min, 30 °C/min, and 60 °C/min were applied to these materials to investigate the effect of cooling rate on crystallization of PLA and its compound. The materials are named using the convention Cxx.y, wherein C is the first letter of the colorant name, xx is the weight percentage, and y is the cooling rate. For example, PLA.10 refers to the pure PLA yarn drawn cooled down with a cooling rate of 10 °C/min B03.30 refers to the yarn dyed with 0.3% (*w*/*w*) of pigment blue 15:1 and cooled with a cooling rate of 30 °C/min. The DSC cooling thermograms are presented below in Figure 6.3.

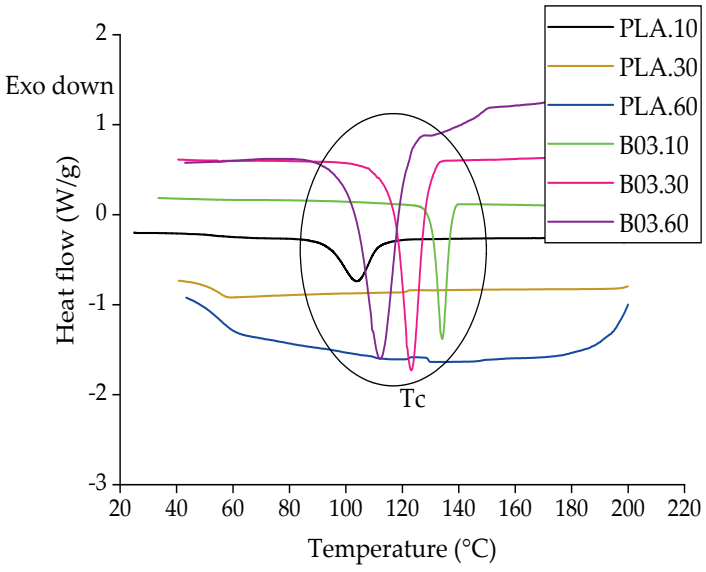

Figure 6.3: DSC cooling thermogram of PLA and its compound with 0.3% (w/w) of blue pigment cooled at different cooling rates

As observed from Figure 6.2, PLA normally crystallizes around 100 °C when crystallized at a cooling rate of 10 °C/min but the compounds containing 0.3% (w/w) of blue pigment crystalizes already at about 135 °C. This is a clear indication that at the tested cooling rate, the blue pigment acts as a nucleating agent. However, the crystallization temperature goes down with increasing cooling rates. PLA does not seem to crystallize at cooling rates of 30 °C/min and 60 °C/min. At a cooling rate of 30 °C/min, it is observed at 123 °C and at a cooling rate of 60 m/min, it occurs at 112 °C. It is clear from the observation that at higher cooling rates, the efficiency of the blue pigment as a nucleating agent goes down. This is also backed by the experimental observation that the blue pigment did not affect the crystallinity of yarn produced during melt spinning. Therefore, it can be concluded that in the absence of nucleating agents that work at very high cooling rates, during melt spinning, crystallization in slow crystallizing polymers such as PLA occurs primarily through stress-induced crystallization.

Another important parameter to take care of during melt spinning is the relaxation of the multifilament. Since the process is fast and stress driven, there is residual stress left in the multifilament after the drawing process. Unless allowed to relax properly, the polymer start to relax or post crystallize in the bobbin after winding and shrink. This

causes damage to the multifilaments in the bobbin making them unusable and in extreme cases, can lead to complete collapse of bobbin during spinning as shown in Figure 6.4. In other cases, it may lead to filaments sticking to each other making unwinding impossible. Therefore, improving the crystallization speed of PLA during melt spinning with the help of nucleating agent would come in handy to increase production rates of PLA yarn but this area of research needs to be investigated further.

Figure 6.4: Broken filaments in bobbin

6.3 Insights into Electrospinning

Fiber formation in electrospinning occurs when the polymer jet (after formation of Taylor cone) is ejected from the nozzle interacts with the electric field. In Figure 6.5, a schematic of fiber formation during melt electrospinning is presented.

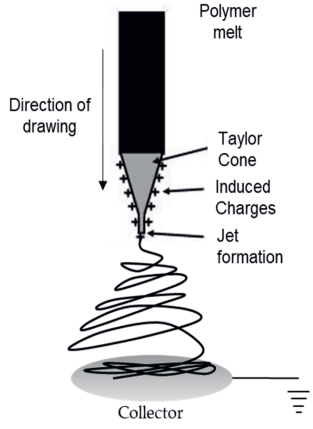

Figure 6.5: Schematic of fiber formation in melt electrospinning (through Taylor Cone)

For the success of melt electrospinning, two material properties are quintessential. The first one is the electrical conductivity of the polymer and the second one is the viscosity of the polymer. Both the properties depend on the temperature. A brief discussion on the effect of temperature on the important material parameters is given below.

6.3.1 Effect of temperature on material properties

For melt electrospinning, a low polymer viscosity and a high electrical conductivity are favored. Ostheller et. Al recently published that the electrical resistance of polybutylene succinate (PBS) can increase multiple fold from about 20 MΩ at 265 °C to about 8 GΩ at 145 °C [10].

To determine the effect of temperature on polymer melt viscosity, we performed a temperature sweep using a plate plate rheometer (as described in methods section in chapter 5-section 5.2.2.4) from 200 °C at a cooling rate of 5 °C/min. The test was performed on PLA and the PLA masterbatch containing 5% (w/w) of blue pigment to investigate if adding a nucleating agent can benefit melt electrospinning. The change in complex viscosity with temperature is presented below in Figure 6.6.

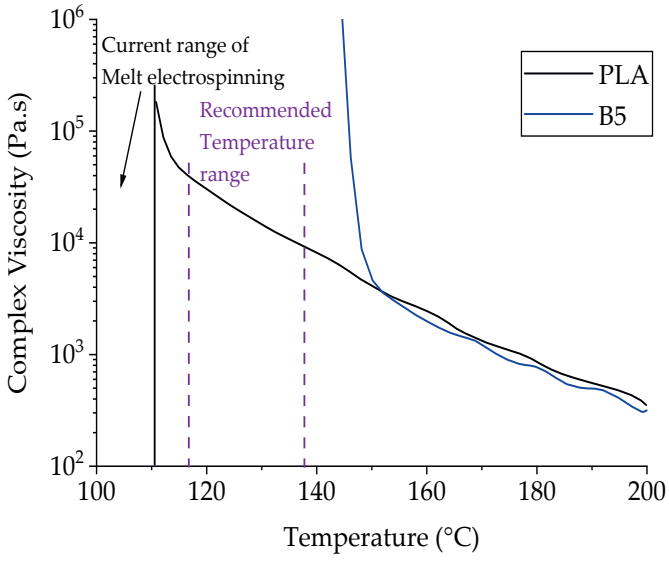

Figure 6.6: Effect of temperature on viscosity of PLA and the blue pigment masterbatch

The sharp increase in viscosity when the temperature goes down corresponds to the start of crystallization. It is observed from Figure 6.5 that the viscosity increases sharply already below 150 °C in case of the B5 masterbatch because of the nucleating effect of the blue pigment, whereas it happens first below 110 °C for pure PLA. Similar results were observed for crystallization temperatures from DSC thermogram in Figure 6.3. Formation of thinner fibers is possible in melt electrospinning only when the polymer melt has lower viscosity and higher electrical conductivity. As the polymer melt flows through the nozzle, it begins to cool down and crystallize. But the interaction with the electric field and the resultant whipping also occurs simultaneously. At this point, if the viscosity is too low, the polymer melt forms droplets and if it is too high, no whipping occurs. Therefore, the viscosity needs to be maintained in the correct rage to get optimal results and a typical range for this could be between 115 and 135 for PLA since the viscosity is not as low as the melt and not as high as the crystalline sample here. However, more research is necessary to know the exact optimal range. The addition of nucleating agents leads to crystallization happening much earlier and therefore, the viscosity increases earlier and this could have a negative influence on the melt electrospinning process. However, as observed from section 6.1.1, the cooling rates in the spinning processes are much higher than 5 °C/min and the efficiency of the nucleating agent goes down at higher cooling rates. So, there is a possibility that the blue pigment did not affect the process but in case a nucleating agent that is efficient at higher cooling rate is used, that could affect the melt electrospinning process negatively. A potential solution for this could be an integration of a climate chamber to keep the fiber warm for longer duration and prevent crystallization to allow better interaction with the electric field.

6.4 Melt spinning vs melt electrospinning: An insight into the processes

In melt spinning, the drawing force is directly applied to the filaments by contact through the godets rotating at high speeds. Friction is also experienced by the filaments when they come in contact with the godets. A higher melt strength or viscosity of the polymer is essential to draw the filaments. However, in contrast to this, the fibers in melt electrospinning experience indirect drawing with the help of an electric field and no friction is present. Furthermore, a lower viscosity is preferred here to facilitate drawing by electric field. Polymers having good electrical conductivity are also preferred for melt electrospinning, whereas, this is not an important factor for melt spinning. The polymer

melt coming out of the spinneret in melt spinning undergoes necking deformation when it gets stretched, whereas, in melt electrospinning, a Taylor cone is formed due to the forces of electrostatic repulsion and a jet is ejected from the cone depending on the strength of the electric field applied.

During the melt electrospinning trials, we used spin pump speeds of 2, 5, and 10 rpm. The lowest diameter was achieved with a spin pump speed of 2 rpm with a spin pump capacity of 0.32 mL/revolution. In case of melt spinning, a spin pump speed of 12 rpm with a spin pump capacity of 2.5 mL/revolution was used to produce the PLA.1 yarn. The take up speed was 1100 m/min and the winding was done at 1200 m/min. Here very low solid-state drawing was applied and this was done only to have enough tension in the yarn to pass them through the godets. Therefore, any orientation/crystallinity obtained must come from melt drawing. Since in melt electrospinning, only melt drawing occurs, a comparison between both the process is done based on these two filaments. A quenching length of 1.5 m was used for melt spinning and a nozzle to collector distance of 10 cm was used in melt electrospinning.

The extrusion speed at the nozzle was calculated based on Eq.1. The throughput in g/min was measured by collecting the material flowing from the respective devices for 1 minute and measuring the weight. Since the device has 600 nozzles and the overall throughput is measured, the value is divided by 600 to measure the throughput per nozzle.

$$Extrusion\ speed\ at\ nozzle\left(\frac{m}{min}\right) = \frac{Throughput\ \left(\frac{g}{min}\right)}{Density\ \left(\frac{g}{cm^3}\right) * area\ of\ the\ capillary\ (mm^2) * 600} \quad \textbf{Eq.1}$$

In Table 6.1 below, the throughput and extrusion speeds corresponding to these spin pump speeds are presented.

Table 6.1: Spin pump speeds and the corresponding throughputs of melt and melt electrospinning

Process	Spin pump speed (rpm)	Throughput (g/min)	Throughput per nozzle (g/min)	Extrusion speed at nozzle (m/min)
Melt spinning (48 nozzles)	12	36	0.75	15.28
Melt electrospinning (600 nozzles)	2	0.8	0.0013	0.02

It is observed, as previously stated, from Table 6.1 that melt electrospinning is much slower than melt spinning. The diameter obtained from both the processes were also measured using an optical microscope (as explained in chapter 5, section 5.3.4). The take up (1100 m/min) and winding speeds were known in case of melt spinning and in case of melt electrospinning, the equivalent take-up speed was calculated back from the fiber diameter, the throughput used, and nozzle diameter using Eq.2, Eq.3, Eq.4 and Eq.5 [11].

$$Fiber\ diameter\ (\mu m) = 11.3 * \sqrt{\frac{Singele\ Filament\ fineness\ (dtex)}{Density(g/cm^3)}} \quad \textbf{Eq.2}$$

$$Single\ filament\ fineness\ (dtex) = (\frac{Fiber\ diameter\ (\mu m)}{11.3})^2 * Density\ (g/cm^3) \quad \textbf{Eq.3}$$

$$Single\ filament\ fineness\ (dtex) = \frac{Throughput\ per\ nozzle\ (g/min)}{Take-up\ speed\ (m/min)} * 10{,}000 \quad \textbf{Eq.4}$$

$$Take-up\ speed\ (m/min) = \frac{Throughput\ per\ nozzle\ (g/min)}{Single\ filament\ fineness\ (dtex)} * 10{,}000 \quad \textbf{Eq.5}$$

The melt draw ratio was calculated based on Eq.6.

$$MDR = \frac{Take-up\ speed\ (m/min)}{Extrusion\ speed\ (m/min)} \quad \textbf{Eq.6}$$

The second parameter that affects the crystallinity and property of the fiber obtained is the melt drawing rate. In case of melt spinning, a quenching speed of 1.5 m is used and

in melt electrospinning, a quenching length (nozzle to collector length) of 10 cm is used. Considering the take up speeds of both the processes and the distance between take up and nozzle, melt drawing rate was calculated based on Eq. 7. Since the take up speed is measured as m/min and the MDR is measured in 1/s, the take up speed is divided by 60 to get the value in m/s.

The melt draw ratios are tabulated below in Table 6.2.

Table 6.2: Extrusion speed, diameter and melt draw ratio obtained during melt and melt electrospinning

Process	Diameter (μm)	Extrusion speed at nozzle (m/min)	Single filament fineness (dtex)	Take up speed (m/min)	Melt draw ratio
Melt spinning	25.80	15.28	6.25	1100.00	72.00
Melt electrospinning	9.30	0.02	0.84	15.47	773.50

It is observed from Table 6.2, that the melt draw ratio applied in case of melt electrospinning is much higher than melt spinning in the processing window considered in this research work. The % crystallinity (X_c) results of the corresponding melt spun yarn and the melt electrospun fiber webs are is presented below in Table 6.3 (Results are taken from Chapter 2- section 2.3.3.2 and Chapter 5-section 5.3.4.4).

Table 6.3: Percentage crystallinity of melt spun filament and melt electrospun fiber webs.

Process	Percentage crystallinity Xc (%)
Melt spinning	29.8
Melt electrospinning	12.4

It is observed from Table 6.3 that even though the melt draw ratio in melt electrospinning was higher, the Xc in melt spinning seems to be higher. In slow crystallizing materials such as PLA, the crystallinity develops based on stress induced orientation [4]. Compared to melt electrospinning, melt spinning is carried out at significantly higher

rates. This could potentially lead to a higher drawing rate and therefore higher crystallinity. Since the crystallinity is higher in case of melt spun filaments, it is also expected that the orientation is higher here. Therefore, the mechanical properties of the filaments obtained from melt spinning is expected to be higher.

6.4 Conclusion

Melt electrospinning is currently being carried out at low throughputs to achieve smaller diameter. This is because, when the throughput is high, a very strong electric field is required to stretch the fiber thin. However, this leads to electric short circuits and formation of sparks. Due to absence of climate chamber underneath the spinneret in melt electrospinning, the polymer jet cools down too fast and the polymer jets electrical conductivity goes down and viscosity goes up. This limits its interaction with the electric field. As seen from the rheological and electrical conductivity measurements, if the polymer jet is maintained above the crystallization temperature, its viscosity and electrical resistance do not increase so abruptly. Therefore, incorporation of a climate chamber and maintaining a temperature above the crystallization temperature of the polymer could be a potential solution to make thin fibers. If this promotes interaction with the electric field, this could also lead to increased production rates since more drawing would be possible. Furthermore, this gives the possibility for the formation of nonwoven webs on the collector plate. However, care should be taken that the temperature is not too high to avoid droplet formation.

Nucleating agents can potentially lead to negative effects in melt electrospinning. Although delaying the crystallization is advantageous for melt electrospinning, this can be detrimental to melt spinning due to the previously explained problem of collapse of bobbin (Figure 6.3). Therefore the crystallization of the material needs to be studied and optimized individually for both the processes. It can be hypothized from these results that in order to obtain fiber webs with higher crystallinity and mechanical properties in melt electrospinning, higher production speeds (extrusion and take-up speeds) with high melt draw ratios would be necessary. Integration of a climate chamber to precisely control the temperature below the spinneret could pave way for this and lead to formation of thinner fibers with good mechanical properties.

References

1. Ziabicki, A. *Fundamentals of Fiber Formation*; Wiley Interscience Publishers: Cambridge, UK, 1976.
2. Cooley, J.F. Method of and apparatus for producing fibrous or filamentary material. 1899.
3. Norton, C.L. Method of and apparatus for producing fibrous or filamentary material. 1933.
4. Simon, E. NIH Phase I Final Report: Fibrous Substrates for Cell Culture; 1988.
5. Koenig, K. Melt electrospinning towards industrial scale nanofiber production: An in-depth material and parameter study based on polypropylene and polylactic acid. PhD, Maastricht University, Maastricht, The Netherlands, 2020.
6. Kohler, W. H.; Shrikhande, P.; Mchugh, A. J. Modeling Melt Spinning of PLA Fibers. Journal of Macromolecular Science Part B Physics 2005, 44, doi: 10.1081/MB-200049786.
7. Guan, X. Crystallization of Polyamide 66 Copolymers at High Supercoolings. PhD, University of Tennessee, Knoxville, USA, 2004.
8. Siebert, S.; Berghaus, J.; Seide, G. Nucleating Agents to Enhance Poly(l-Lactide) Fiber Crystallization during Industrial-Scale Melt Spinning. Polymers 2022, 14, doi:10.3390/polym14071395.
9. Guan, X. Crystallization of Polyamide 66 Copolymers at High Supercoolings. PhD, University of Tennessee, Knoxville, USA, 2004.
10. Ostheller, M.E.; Balakrishnan, N.K.; Groten, R.; Seide, G. Detailed Process Analysis of Biobased Polybutylene Succinate Microfibers Produced by Laboratory-Scale Melt Electrospinning. Polymers 2021, 13, doi: 10.3390/polym13071024.
11. Hasan, M. Useful Formulas for Determining Fiber Properties. Available online: https://www.textilecalculations.com/formulas-for-determining-fiber-properties/ (accessed on 02.01.2023).

Chapter 7

Summary and outlook

Summary

Innovative textile products and fabrication techniques are the need of the hour to make the textile field more sustainable. Although biobased polymers such as PLA is being investigated for various textile applications, the processes used currently in textile productions are not always sustainable. Conventional exhaust dyeing of PLA can lead to hydrolytic degradation and obtaining satisfactory color performance is therefore challenging. Furthermore, the effluents from the process are toxic and leads to water pollution.

Colorants are multifunctional meaning they can impart other functionalities like electrical conductivity, and anti-microbial properties, when the right ones are used. With the outburst of Covid-19 virus, the need for masks with very low fiber diameter and antibacterial functionality skyrocketed. Electrospinning is an upcoming way for producing such materials but solution electrospinning is commonly used now and this is not environmentally friendly because of the use of solvents. Melt electrospinning has shown potential but the low electrical conductivity and high viscosity of polymer melt makes it challenging.

To overcome both these challenges, in this thesis, a novel approach to use multifunctional colorants for manufacture of potentially sustainable PLA textiles was investigated and the following objectives were accomplished:

- Evaluation of dope dyeing process as a sustainable alternative to conventional exhaust dyeing of PLA
    - A dope dyed knitted fabric was successfully developed
        - It was observed that dope dyeing did not lead to loss in performance and no degradation happened, unlike exhaust dyeing, where degradation was observed
        - The properties of the filaments and knitted fabrics were influenced by process parameters more than the colorants used
    - The performance of the selected biobased and potential biobased colorants were comparable to fossil-based colorants
- Investigation of the effect of multifunctional colorants on rheological, and electrical properties of PLA and the diameter of the fibers fabricated in melt electrospinning
    - Addition of colorants led to reduction of fiber diameter

- A prototype of melt electrospun PLA fiber web with antibacterial properties was produced using the 600 nozzle pilot-scale melt electrospinning device

- A comparison of melt spinning and melt electrospinning process was performed and the key similarities and differences between the processes were identified

The colorant used and its weight percentages influenced the diameter of the fiber obtained from the melt electrospinning process, whereas the colorant used did not influence the properties of the melt spun yarn. Overall, the potential of colorants to perform as multifunctional additives that impart color, antibacterial properties and work as a nucleating agent in PLA was demonstrated and a short overview is given in the following summary.

The various textile production techniques used to produce fibers with different diameters was presented in **Chapter 1,** the current state of the art on important processes (melt spinning and electrospinning) involved in production of fibers for conventional textile applications and submicron, and nanofibers for filtration application were discussed.

In **Chapter 2**, the dope dyeing of PLA was focused on. The low thermal stability of PLA and its hydrolytic degradability posed challenges for its conventional exhaust dyeing. Therefore, dope dyeing was proposed as a more sustainable and suitable alternative. The impact of colorants on thermal, rheological, and mechanical properties of PLA multifilaments and fabrics were investigated. A mix of fossil-based, potential biobased, and a biobased colorants (a total of 5 colorants) were used to perform dope dyeing. It was observed that three of the colorants used worked as a nucleating agent to promote crystallization in PLA at lower cooling rates. However, they did not affect the mechanical properties and crystallinity of the melt spun yarn and the draw ratio used played a more dominant role in determining these. It was demonstrated that unlike exhaust dyeing, dope dyeing using the selected colorants did not lead to hydrolytic degradation of PLA. Color stability tests (BWS, UV-stability) tests performed on the dyed yarn and the fabric revealed that the potential biobased and actual biobased colorants performed as good as the fossil-based colorants. The results obtained in the study show the potential of dope dyeing as a sustainable dyeing technique for dyeing PLA to produce conventional textiles.

Chapter 3 was a proof-of-concept study designed to investigate the effect of colorants on electrical conductivity of PLA. Lab-scale melt electrospinning of PLA was performed

using potential biobased dyes at different concentrations. The electrical conductivity of PLA increased upon addition of colorants. Addition of quercetin, and alizarin did not lead to any degradation of PLA. However, addition of hematoxylin led to degradation but the finest fibers (16.04 μm in diameter) were produced by adding 2% (w/w) hematoxylin, reducing the average fiber diameter by 77% compared to pure PLA. The crystallinity of the lab-scale melt electrospun fiber was measured to be very low (8.87%), meaning the orientation was low in the fiber. Although the crystallinity was low, the study revealed the potential of biobased dyes as additives to increase the electrical conductivity of PLA.

In **Chapter 4,** the effect of dyes and pigments on the melt electrospinning performance of PLA was investigated. Pigments such as copper pthalocyanine are expected to have higher electrical conductivity than the dyes but are harder to disperse in the polymer and dyes are easier to disperse. Since when conductive additives are added, the electrical conductivity of the polymer compound depends on the additive and the degree of dispersion, the potential of dyes and pigments were compared here. It was observed that the addition of pigments led to higher electrical conductivity compared to the selected dyes. However, the diameter was lower with fibers containing dyes. This was attributed to the aggregate formation, which was observed through SEM images in case of pigments. The diameter of the pure PLA fibers was > 100 μm, and the best result was achieved with composite A1, which formed fibers 52.5 μm in diameter. Based on the results, it was determined that, among the colorants tested, dyes performed better and a scale-up was therefore performed with dyes.

Chapter 5 focused on scaling up the melt electrospinning of PLA with colorants to the 600-nozzle pilot scale device. Curcumin, alizarin, and quercetin were the dyes used since dyes were observed to perform good in lab scale and they offered an additional antibacterial functionality. Spinning trials showed that the addition of dyes produced narrower fibers in the resulting fiber web, with a minimum diameter of ~9 μm for the fiber containing 3% (w/w) of curcumin. Furthermore, it was also observed that the PLA fiber web containing 5% (w/w) curcumin was antibacterial against *S. Aureus*. Our work provides insight into the scaling up of the melt electrospinning process from the laboratory to pilot scale, and shows the potential of multifunctional colorants to develop environmentally friendly microfiber webs with antibacterial properties for filtration and biomedical applications.

In **Chapter 6,** an insight into similarities and differences between melt spinning and melt electrospinning was pondered. It was observed from DSC studies, that although the pigments acted as nucleating agents at a cooling rate of 10 °C/min, the nucleation efficiency started to decrease once the cooling rate was increased to 30 °C/min and it was even lower at a cooling rate of 60 °C/min. The cooling rates in melt spinning exceed 200 °C/min and it was observed that the nucleating agent did not have sufficient time to promote crystallization. Drawing applied during the process led to stress induced crystallization and proved more effective. In case of melt electrospinning, it was observed that having nucleating agent could be detrimental to the process. When the polymer crystallizes, its viscosity increases multiple-fold and the electrical conductivity decreases. Both have negative influence on melt electrospinning process and since nucleating agent speeds up the crystallization process, it could reduce the time the polymer jet has for whipping during processing. Therefore, performing the process without nucleating additives could be more beneficial. Based on calculation of the processing parameters, it was observed that the melt drawing ratio was higher in melt electrospinning but the drawing rate was higher in melt spinning than melt electrospinning. Furthermore, the results showed that the crystallinity of yarn obtained from melt spinning was higher leading to the hypothesis that in order to obtain melt electrospun fibers with good mechanical properties, both high melt draw ratio and drawing rates are necessary. Integration of a climate chamber could be the next step in achieving this.

Outlook

Dope dyeing is generally expected to be more sustainable than exhaust dyeing since lesser amount of water and chemicals are used for processing. However, high temperatures are needed to perform the mixing process and large amounts of materials are required to clean the extruder, when the color needs to be changed. Taking this into account, dope dyeing would be suitable for producing yarns in larger quantities and exhaust dyeing would be suitable to produce dyed yarns at lower quantities. Although, no toxic chemicals are used in dope dyeing, cleaning the extruders to change the color of the yarn is challenging and a lot of polymer and cleaning materials are required for this. In order to get a clear idea on how sustainable this can be, a life cycle assessment (LCA) study would be necessary. Since the colorants are extracted from different resources, and have different toxicity levels, it would be necessary to perform LCA for each individual scenario to identify the hotspots. In the current research work, potential

biobased colorants were used. Together with colleagues, we also performed a LCA study on extraction and dyeing with a biobased colorant. A madder root extract was prepared and we performed dyeing with this extract. It was observed during this study that the extraction of the colorant was a major hotspot that needed to be optimized to make the biobased colorants more sustainable. Furthermore, when the sugars presented in the extract are not fully removed, exhaust dyeing still worked but dope dyeing did not work. It led to burnt brown color. Therefore, more research to improve the yield of biobased colorants during extraction is necessary to bring them to the market. Nucleating agents, based on colorants, have been shown to influence the crystallinity in PP even when melt spinning at higher speeds. Even though the colorants used in this thesis proved to be nucleating at lower cooling speeds, it was not the case during melt spinning. In this thesis, we used colorants that melt during melt spinning of the polymer and colorants (with higher melting point) that do not melt during melt spinning. When using colorants that melt during processing, we observed that there was plasticizer effect on the polymer melt. However, for the colorant to act as a nucleating agent, they need to crystallize very fast under melt spinning conditions and then nucleate the crystallization of PLA. This can be quite challenging. Therefore, using colorants that do not melt during melt spinning could have more potential to work as nucleating agents at these higher cooling speeds. Further investigation is necessary into the crystallization and crystal structure of colorants to determine what characteristics of a colorant are necessary for them to function as nucleating agents and improve the mechanical properties of melt spun PLA filaments. Apart from process optimization, next steps could be investigating the performance of PLA based textiles. Tailoring the crystallization of PLA and heat setting can help influence the biodegradation of PLA. This can lead to very interesting textile products, where the age of the product could potentially be tailored.

Melt electrospinning is still under developmental stage. Our research showed that the use of colorants had a positive influence on the diameter of the fiber web. In future attempts, a combination of more than one colorant can be used to investigate a potential synergetic effect. One more alternative could be use of an antibacterial colorant and a nanoadditive such as graphene to improve the electrical conductivity even further. Colorants such as curcumin, and alizarin are also pH sensitive. Their color changes based on the pH they are used in. Since wounds have different pH during the healing process, melt electrospun anti-bacterial wound dressing made with these colorants could serve as smart wound dressing materials. A second optimization step can come from the machine modification. For ex., an integration of a climate chamber to control

the temperature below the spinneret could promote production of thinner fibers through melt electrospinning. Optimizing the design of the current spinning nozzle to reduce the dwell time of the polymer inside can reduce thermal degradation and make the process more versatile for other polymers. A two-side approach to modify the material and the machine simultaneously can help make more innovative sustainable melt electrospun textile materials. Although, melt electrospinning shows a lot of promise for producing fibers suitable for filtration application, to the best of our knowledge, no such filter exists in the market currently. Investigating the performance of melt electrospun nonwovens as filters can be a good follow-up to the current results of the thesis. Using colorants as multifunctional additives to make anti-bacterial filters has great potential in the field of air filtration for hospitals and also medical masks. During Covid pandemic, disposal of filters was a big challenge and using biopolymers such as PLA to produce one material filters can be a positive step towards solving this issue. Overall, this thesis showed the potential of using colorants to make PLA based textiles. Further investigation in this field could lead to new interesting textile products based on PLA.

Chapter 8

Impact Chapter

Impact Chapter

The social and economic impact that can be generated by the current research work is discussed in this chapter. The application of multifunctional colorants for improving the properties of PLA to make more sustainable textile products is focused on this dissertation. The textile industry is heavily dependent on fossil-based polymers, especially PET with a market of about 48 million tons and to battle against climate change and CO2 production, it is aiming to shift towards more sustainable polymers such as PLA [1]. It is a biobased material made from sustainable feedstock and the production of 1 tons of PLA consumes 42 GJ of energy and releases 1.3 tons of CO2, ~40% less than PET [2]. Apart from the polymer used, the textile industry depends a lot on colorants also since appearance influences the buying decision. The global market of colorants is huge and growing and is expected to reach €98 Billion by 2030 [3]. Vast majority of these colorants are fossil-based but the market is also shifting towards more biobased colorants to make the industry more sustainable. However, due to low yield, thermal stability of these biobased colorants, it is still a bit challenging.

Even though a lot of focus has been put on shifting towards more sustainable materials, development of corresponding sustainable processing is still lacking. For ex., exhaust dyeing is the most common process used to dye conventional textiles and during this process, the toxic effluents released leads to contamination of water bodies and is also not the best choice for PLA because of its low heat stability and hydrolytic degradation [4,5]. Although the Covid-19 outburst led to significant improvement in the filter (nonwoven) market, it did not seem to accelerate the use of sustainable materials and methods to produce these filters [6]. Melt electrospinning is an upcoming and a potentially sustainable way to produce such materials but the required functionalities and fiber diameters are challenging to reach with this process.

In this dissertation, we have proposed the use of multifunctional colorants to address these shortcomings. Here we proposed the use of sustainable dope dyeing to dye PLA filaments to avoid the degradation that happens during exhaust dyeing. This not only gives filaments with better properties but also reduces waste production considerably since in exhaust dyeing, upto 20% of the dye used can stay behind in the dye bath and when these effluents are thrown away, it causes water pollution [7]. Melt electrospinning, although promising, has been limited mostly to lab scale until now. In this research, we proposed the use of colorants as multifunctional additives for pilot-scale melt electrospinning of PLA and produced antibacterial nonwoven fiber

webs. The trials in this dissertation were carried out in pilot scale and therefore, the findings reported especially in chapter 2 and chapter 5, are very promising for industrial scale up and valorization.

The first part of the thesis dealt with dope dyeing of PLA for conventional textile applications. One of the targeted applications for the developed product are the apparels. After discussion with industrial partners, we observed that the properties of the yarn developed in this dissertation are comparable to the properties of the ones used for sock manufacture in the market. The UV fastness obtained from the biobased and potential biobased colorants in this dissertation are comparable to fossil-based colorants. This gives potential for the manufacture of fully biobased socks that can be potentially sustainable. Furthermore, the superior wicking property of PLA improves comfort of the sock [8]. Similar to sock, the yarn developed here can potential be used for other apparel applications such as sports T-shirts. A Belgian company called Noosa is developing this technology and are working on developing PLA based apparels. Starsock, a sock manufacturer in the Netherlands, are also interested in developing sustainable PLA based socks. Currently, as an extension of the thesis, work is being carried out under the framework of Biotexfuture project "Biobase" in Germany with several industrial partners to explore the possibility of using biopolymers for several textile applications.

Apart from apparels, the European flooring industry is looking for sustainable alternatives. The bulk continuous filament or commonly known as carpet yarn is typically dope dyed. Therefore, the results of this dissertation can be very interesting for the carpet industry. The Dutch and Belgian companies such as Low & Bonar, TWE Meulebeke BCBA can make use of the results of this dissertation to make potentially sustainable carpets.

The second part of the thesis focused on developing fiberwebs with low diameters using pilot-scale melt electrospinning for potential filtration applications. Antimicrobial filters have gained a lot of importance since 2020 and the market was estimated to reach €32 billion in 2022 but fossil-based PP and polyethylenesulfone are the major players here [9]. Fibers with low diameter in the low-micro and nanoranges are necessary to function as effective filters to filter viruses, bacteria, also fine dust [10]. Inorganic additives such as silver are generally used to impart anti-microbial functionalities on these filters and fossil-based polymers are used here making this industry unsustainable. The approach proposed in this dissertation for the use of multifunctional colorants to

reduce the diameter of PLA fibers in meltelectrospinning and to impart anti-microbial functionality at the same time can be very interesting for filtration applications. These results can be made use of develop more sustainable HEPA filters and air filters for airplanes and hospitals.

The antibacterial PLA fiber web developed in this dissertation can be a sustainable alternative for the wound dressing market. Apart from being antibacterial, colorants such as curcumin and alizarin used in the study are pH responsive. The pH of a wound changes through the healing process and because of the anti-bacterial properties and the pH responsive nature, the fiber webs developed here can support the healing process and function as smart wound dressing to show the status of the wound healing. This could be hugely beneficial for the patient with the wound.

In addition to textile applications, the antibacterial nature of the potentially biobased colorants used in this work can also be beneficial for food packaging. The antibacterial PLA composite developed in this dissertation can potentially be used to create sustainable anti-bacterial packaging material. The slow crystallization rate of PLA can be a hindrance to achieve high production rates during injection molding of products such as cutleries, plates. Here we demonstrated the performance of colorants as nucleating agents for PLA. The developed composite can be used in injection molding to improve the production rates. With nucleating agents, the crystallization process occurring during molding can be accelerated and thus the production time can be reduced.

Although some questions, such as washing stability of the colorants, filtration efficiency of the fiber webs, need to be investigated, this dissertation showed the potential of multifunctional colorants to improve the properties of PLA. Production of PLA is observed to emit lower amounts of CO_2 compared to PET. Apart from this, the processing temperatures of PLA are lower than that of PET, which could also lead to lower energy consumptions on the long run. Furthermore, the wicking behavior of PLA is better than PET giving consumers' textile materials that can be more comfortable to wear. The reduction of effluents by the use of dope dyeing reduces water pollution. Mixing colorants and PLA can also lead to production of smart wound dressing materials and anti-bacterial filters. By exploring these benefits, the results of this dissertation can be used to make the world potentially more sustainable through development of functional PLA based textiles.

References

[1] Pulidini, K.B., S. Polyester Fiber Market Size. Available online: https://www.gminsights.com/industry-analysis/polyester-fiber-market (accessed on 02.05.).

[2] Chen, G.Q.; Patel, M.K. Plastics derived from biological sources: Present and future: A technical and environmental review. Chem. Rev. 2012, 112, 2082–2099. Doi: https://doi.org/10.1021/cr200162d.

[3] Colorants Market Overview. Available online: https://www.marketresearchfuture.com/reports/colorants-market-3215 (accessed on 26.03.2023).

[4] Carmen, Z.; Daniela, S. Textile Organic Dyes—Characteristics, polluting effects and separation/elimination procedures from industrial effluents—A critical overview. In Organic Pollutants Ten Years After the Stockholm Convention; Puzyn, T., Mostrag-Szlichtyng, A., Eds.; InTech: Rang-Du-Fliers, France, 2012; Volume 1, pp. 55–86.

[5] Xu, S.; Chen, J.; Wang, B.; Yang, Y. Sustainable and Hydrolysis-Free Dyeing Process for Polylactic Acid Using Nonaqueous Medium. ACS Sustain. Chem. Eng. 2015, 3, 1039–1046. Doi: https://doi.org/10.1021/sc500767w.

[6] Industrial Filtration Market. Available online: https://www.marketsandmarkets.com/Market-Reports/industrial-filtration-market-81304454.html#:~:text=%5B254%20Pages%20Report%5D%20The%20global,6.2%25%20from%202022%20to%202027 (accessed on 06.02.2023).

[7] Carmen, Z.; Daniela, S. Textile Organic Dyes—Characteristics, polluting effects and separation/elimination procedures from industrial effluents—A critical overview. In Organic Pollutants Ten Years After the Stockholm Convention; Puzyn, T., Mostrag-Szlichtyng, A., Eds.; InTech: Rang-Du-Fliers, France, 2012; Volume 1, pp. 55–86.

[8] Abdrabbo, A.; El-Dessouky, H.M.; Fotheringham, A.F. Treatment of polylactic acid fiber using low temperature plasma and its effects on vertical wicking and surface characteristics. J. Text. Inst. 2013, 104, 28–34. Doi: https://doi.org/10.1080/00405000.2012.693699.

[9] Pleated Membrane Filtration Market Size, Share, Growth and Industry Analysis by Type, Application. Available online:

https://www.businessresearchinsights.com/market-reports/pleated-membrane-filtration-market-100964 (accessed on 28.12.2022).

[10] Chase GG, Swaminathan S, Raghavan B, Wei Q. 7 - Functional nanofibers for filtration applications. Functional Nanofibers and their Applications: Woodhead Publishing; 2012. p. 121-52.

8

Appendix

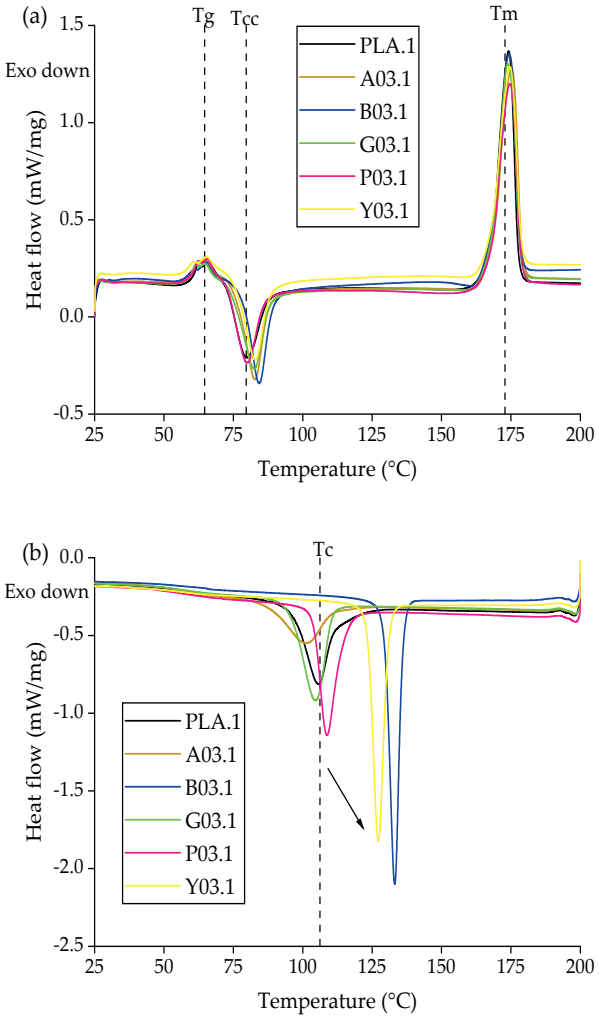

Figure 2.A1: DSC thermograms of PLA and dyed yarns containing 0.3% (w/w) of each colorant at an SSD ratio of 1 during (a) the heating cycle and (b) the cooling cycle.

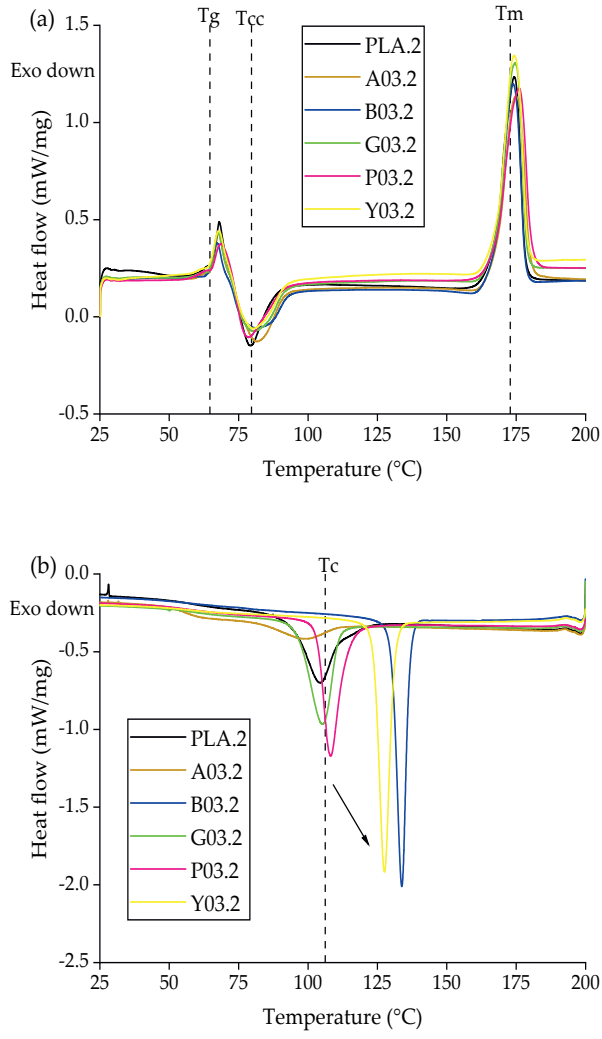

Figure 2.A2: DSC thermograms of PLA and dyed yarns containing 0.3% (w/w) of each colorant at an SSD ratio of 2 during (a) the heating cycle and (b) the cooling cycle.

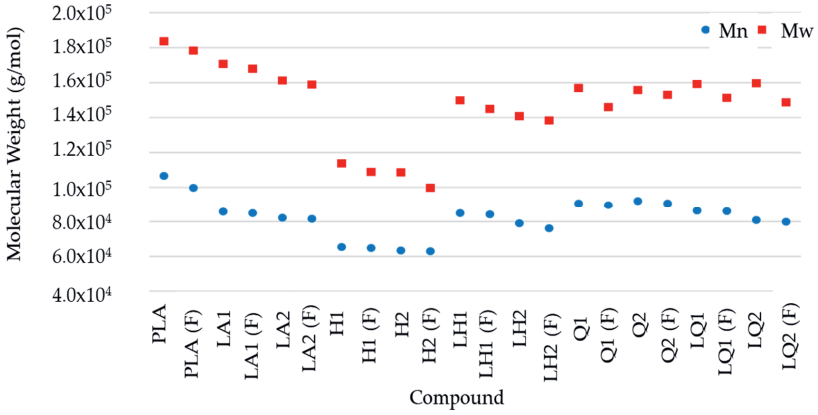

Figure 3.A1: Molecular weight of PLA, PLA/dye compounds and the melt-electrospun fibers (F).

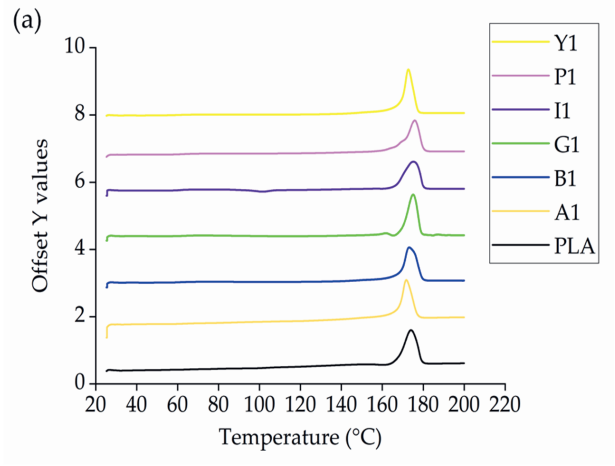

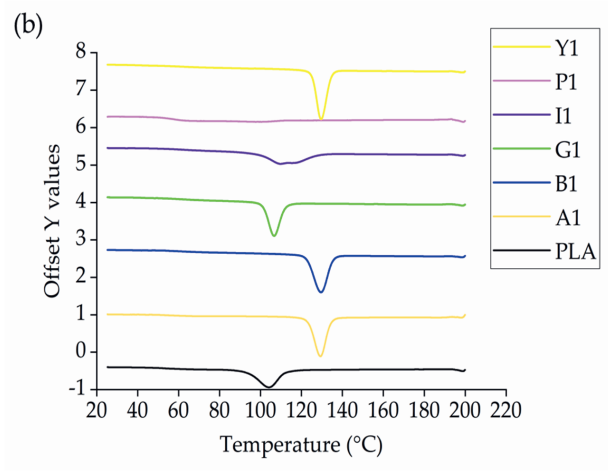

Figure 4.A1: DSC thermograms of PLA and composites containing 1% (w/w) of each additive during **(a)** the heating phase and **(b)** the cooling phase.

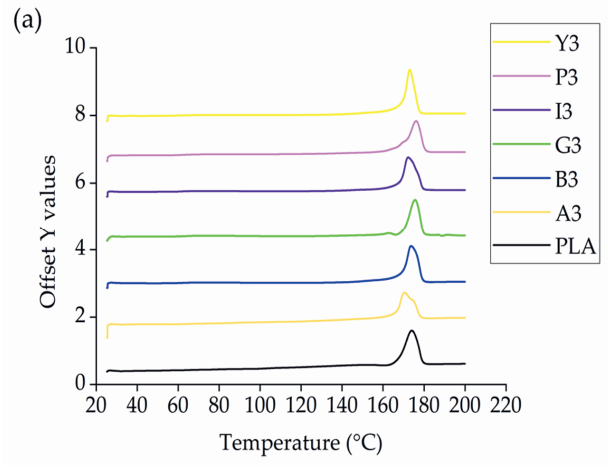

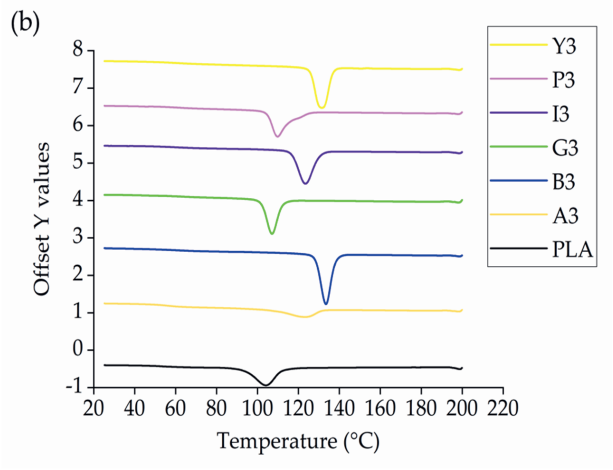

Figure 4.A2: DSC thermograms of PLA and composites containing 3% (w/w) of each additive during (a) the heating phase and (b) the cooling phase.

List of Publications

Journal publications:

Chapter 2: Koenig, K. [†]; Balakrishnan, N. K. [†], Hermanns, S.; Langensiepen, F.; Seide, G. Biobased dyes as conductive additives to reduce the diameter of polylactic acid fibers during melt electrospinning. *Materials* **2020**, 13 (5), doi: 10.3390/ma13051055.
[†] Both authors contributed equally to the work.

Chapter 3: Balakrishnan, N. K.; Koenig, K.; Seide, G. The Effect of Dye and Pigment Concentrations on the Diameter of Melt electrospun Polylactic Acid Fibers. *Polymers* **2020**, 12(10), doi: https://doi.org/10.3390/polym12102321.

Chapter 4: Balakrishnan, N. K.; Ostheller, M.-E.; Aldeghi, N.; Schmitz, C.; Groten, R.; Seide, G. Pilot-Scale Electrospinning of PLA Using Biobased Dyes as Multifunctional Additives. *Polymers* **2022**, 14(15), doi: 10.3390/polym14152989.

Chapter 5: Balakrishnan, N. K.; Siebert, S.; Richter, C.; Groten, R.; Seide, G. Effect of Colorants and Process Parameters on the Properties of dope dyed Polylactic Acid Multifilament Yarns. *Polymers* **2022**, 14, doi: https://doi.org/10.3390/polym14225021.

Other journal publications:

Haan, M. P.; Balakrishnan, N.K.; Kuzmyn, R. A.; Li, G.; Willemen, H. <.; Seide, G.; Derksen, C. H. D.; Albada, B.; Zuilhof, H. Alizarin Grafting onto Ultra-Small ZnO Nanoparticles: Mode of Binding, Stability, and Colorant Studies. Langmuir 2021, 37, doi: https://doi.org/10.1021/acs.langmuir.0c02981.

Ostheller, M.E.; Balakrishnan, N.K.; Groten, R.; Seide, G. Detailed Process Analysis of Biobased Polybutylene Succinate Microfibers Produced by Laboratory-Scale Melt Electrospinning. Polymers 2021, 13, doi: 10.3390/polym13071024.

Ostheller, M.E.; Abdelgawad, A.M.; Balakrishnan, N.K.; Hassanin, A.H.; Groten, R.; Seide, G. Curcumin and Silver Doping Enhance the Spinnability and Antibacterial Activity of Meltelectrospun Polybutylene Succinate Fibers. Nanomaterials 2022, 12, doi: 10.3390/nano12020283.

Ostheller, M.E.; Balakrishnan, N.K.; Groten, R.; Seide, G. The Effect of Electrical Polarity on the Diameter of Biobased Polybutylene Succinate Fibers during Melt Electrospinning. Polymers 2022, 14, doi: 10.3390/polym14142865.

Journal Cover:

The journal article titled "**Pilot-Scale Melt-Electrospinning of PLA with Multifunctional Biobased Dyes**" was published as a cover in the **Polymers** Journal.

Cover story:

Fibers with diameters in the lower micrometer range for textile and biomedical applications are produced by solution electrospinning, but this process is environmentally harmful because toxic solvents are used. Melt electrospinning is a sustainable alternative but the high viscosity and low electrical conductivity of molten polymers produce thicker fibers. Here, we used multifunctional potentially biobased dyes as additives to produce antibacterial fibers in the lower micrometer range using pilot-scale melt electrospinning for interesting applications in the biomedical field.

Cover image:

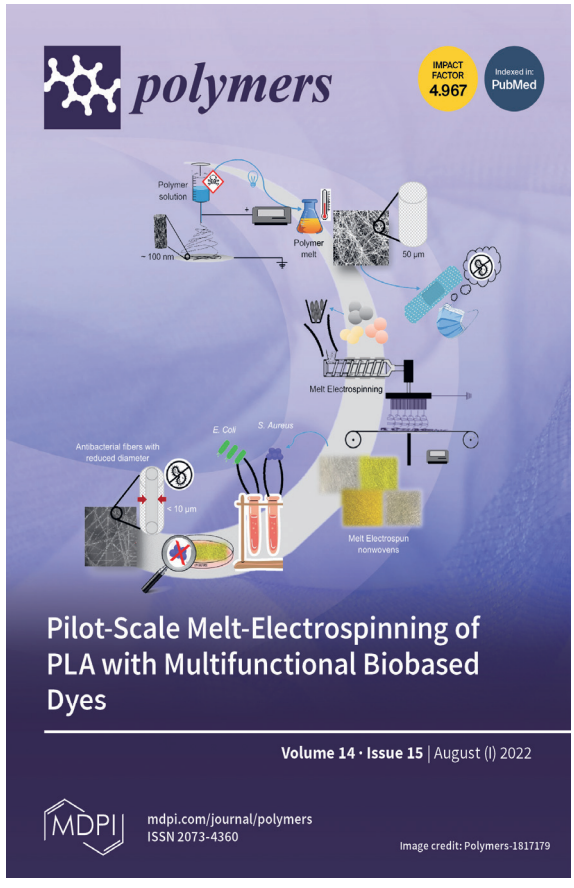

Magazine articles:

Balakrishnan, N. K.; Siebert, S.; Schmitz, M. False-twist texturing of bio-dyed PLA yarns. Bioplastics Magazine 2021. Textile Network 2018*.

Oral presentations:

Balakrishnan, N. K.; Seide, G. Potential biobased additive as conductivity promoter for melt electrospinning of PLA. Scientific Online Conference on Advanced Materials 2020.

Balakrishnan, N. K.; Ostheller, M. –E.; Oikonomidi, C.; Seide, G. Biopolymers-A look into sustainability. Dutch Design Week 2022.

Balakrishnan, N. K.; della Fontana, M.; Samani, P.; Derksen, D.; Seide, G. Sustainable dyeing of PLA fibres using natural colourants. International Federation of Associations of Textile Chemists and Colourists 2021.

Other oral presentations:

Manvi, P. K.: Balakrishnan, Pratiwi, J.; Gries, T. Plants to products: starch, a low cost and biodegradable raw material in textile process chain. ADDITC 2016*

Della Fontana, M.; Samani, P.; Balakrishnan, N.K.; Derksen, D. Sustainability assessment of biobased colorants in the textile value chain. International Federation of Associations of Textile Chemists and Colourists 2021.

*The publication does not constitute a part of this work.

Acknowledgements

I would like to thank everyone who had supported me directly or indirectly to the doctoral thesis. I would like to express my gratitude to **Prof. Gunnar Seide** for giving me the opportunity to work in his research group. I would like to thank **Prof. Gunnar Seide** and **Prof. Robert Groten** for their supervision, recommendation, and insights on this dissertation. Thanks for helping me grow as an independent researcher. I extend my gratitude to **Prof. Stefan Jockenhövel, Prof. Kim Ragaert, Prof. Christian Hopmann,** and **Dr. Roy Dolmans** for assessing my PhD Thesis. Your insights and feedback on my thesis enhanced the quality of my thesis. I would like to thank **Prof. Romano Orrù** and **Prof. Jörg Meyer** for taking time to be a part of my Defence Committee.

I am thankful to be a part of Aachen Maastricht Institute for Biobased Materials. It is really a cross-border institute with great colleagues from all over the world. The rich international culture and views have helped me grow a lot as a person and build good long-lasting relationship with my colleagues. A big thank you to all my colleagues**. Hay Becker, Stefan Siebert, Maike-Elisa Ostheller, Kylie König, Muhammad Maqsood, Konrad Beukenberg, Fabian Langensiepen, Bhavidharan Kalaiselvan, Chrysanthi Oikonomidi, Monika Oleksy, and Fariha Sehar** I thank you for putting up with me in the lab and being supportive when the lab was literally not usable after my trials ☺ **Stefan and Hay**, a special thanks to you guys for making all the out-of-the box ideas possible with your smartness and hands-on expertise**. Maike and Kylie** thank you for the support with finishing the papers. Without the support of you all, I wouldn't have managed to finish my thesis. I needed the push in the back. I sincerely thank **Monika Jedrzejczyk, Anne Coenen, Jules Stouten, Matin Rostami Tabar, Vahid Ansari, Jurrie Noordijk, Christian van Slagmaat, Enzo Pichon, Sofiya Vynnytska, Abdelrahman Abdelgawad, Peter Lijnen, Pouya Samani, and Nils Leone. Pouya, Jurrie, Christian** thank you for making sure there are no boring days at the office and keeping everything cheerful. **Monika, Anne, Jules, Jurrie** thanks guys for helping me integrating easily. I will never forget the movie evenings and the Game of Thrones finale. I would like to thank **Jules Harrings** for the insightful discussion about my results and support in planning experiments. **Christian Schmitz**, you are one of the most friendly and supportive person in AMIBM and I want to thank you for all the support in the Bio lab. I want to thank **Pavan Kumar Manvi**, who supported me like a brother at the start of my journey at ITA. I want to thank **Dorien Derksen** from AVANS Hogeschool for her support and insight with the colorants project.

Thank you for the support and motivation during the final stages of the PhD, **Ermo Daniels**. **Marcelle**, a special thanks to you for the support in organizing all the letters and bureaucracy for the defence. I thank **Christoph Richter** for the support with the experimental trials. I am also grateful to my Professors from my Bachelors and Masters, who have put me in this path of research. I want to extend my gratitude to all the students, who have worked with me during my thesis: **Ellen, Kristin, Niccolò, Joshua, Mathilde, Jennifer, Sebastian, Elias, Mariah, Thalia,** and **Celine.**

I want to thank all my family and friends for their relentless support. I want to thank **Subramani, Annamalai, Shalini, Ashwini, Sujeeth, Captain Anand, Priyanka, Siva, Arjun, Siddharth, and Harish** for all the motivation, support and listening to my never ending stories. Special thanks to the Liquid group (**Ranjith, Arjun, Rakesh, Deepak, Sundar, and Raghu**) and Soulmates group (**Sukanya, Tarini, Karthik, and Mithun**) for all the good times and support. A quick call with you all meant all the stress went away and it lightened the mood and helped me focus better.

Thanks to my extended family members (**Sekar, Saraswathy, Babu, Veena, Srinivasan, Suneetha, Harini, Vinay, Rogith, Praneeth, Vani, Chaithanya**) for all their support. Special thanks to my Grandma **Prabakareeshwari** for always believing in me.

Last but not least, my sincerest thanks to my parents (**Balakrishnan and Raja Rajeswari**) for their unconditional love and relentless support, which made this PhD possible. Thanks to my brother **Gokul** for all the late night calls whenever I was feeling down. You have been a great inspiration for me and a target to reach. You three are the main reasons I even started a masters, which led to this PhD life. I also want to thank my sister-in-law **Samanvitha** for listening to my non-stop nonsense all the time. Special thanks to my father-in-law **Srinivasan**, and mother-in-law **Kamakshi** for their trust and confidence in me. Thank you **Abishai** for all the intellectual conversations and positive vibes. Lastly, thank you my pillar of support, my wife **Sandhiya** (alias **Keerthana**) for being there for me during this journey. You had to put up with me working all night to finish my thesis. Your motivation and never ending support helped me through the difficult times. You made sure that I got the drive to finish my thesis and I am ever grateful for that.

A big heart-felt thank you all ☺

Naveen

Biography

Naveen Kumar Balakrishnan was born in Chennai (India) on December 22, 1992. He obtained his B. Tech in Rubber and Plastics Technology from Anna Univerisity (India) in 2014. He did his bachelor thesis in an industry on Development of seal cone and seal kidney used in a cement pump with a blend of Nitryl rubber and Styrene Butadiene rubber. During his bachelors, he also performed an additional project sponsored by the Anna University, where with a team of 3 students, he developed a working Tyre Wear Test Rig. For this project, the project team won the best project award among 75 projects that entered the competition.

He was later awarded full scholarship to pursue his M. Tech in Materials Science Engineering from Indian Institute of Technology, Kharagpur (India) between 2014-2016. During his masters, he got selected for the DAAD scholarship and did his master thesis at the Institute of Textile Technology (ITA) of RWTH University. During his master thesis, he worked on Fabrication of flexible twisted yarn supercapacitor using Nano additives in the melt-spinning process under the supervision of Prof. Dr.-Ing. habil. Dipl.-Wirt. Ing. G.H. (Gunnar) Seide. He later joined ITA as a part time research assistant from August 2016 to June 2017 and pursued German language course simultaneously. During his time as research assistant, he worked on developing the melt spinning process of thermoplastic starch and starch based blends.

He joined the Maastricht University in July 2017 to pursue his Doctoral degree on sustainable dope dyeing of PLA in the Polymer Engineering Research group under Prof. Dr.-Ing. habil. Dipl.-Wirt. Ing. G.H. (Gunnar) Seide. The focus of his PhD study is on the use of multifunctional colorants for dope dyeing of PLA for conventional textile applications and development of submicro and nano fibers using the pilot scale melt electrospinning device for an upscaled melt electrospinning process for an industry-related production of nanofibers. During his tenure as a PhD, he published eight peer reviewed articles in collaboration with his colleagues. Apart from his PhD, he also worked on other research projects.

He worked on two different public funded projects: 1. Beauti-fully Biobased Fibers Project, funded by NWO under RAAK-PRO program. The goal of the project was to develop biobased colorants for application in textiles. 2. Biotexfieldlab: Funded by the

Limburg government with the aim to co-create the development of new textile products, based on innovative fibers from biobased polymers. Apart from this, he also worked on several industrial research projects and also supported in developing the lab infrastructure for future researchers. He also supervised several internship and master students.

As of July 2021, he joined AMIBM e.V. as a scientific researcher and has been working on a Bundesministerium für Bildung und Forschung (BMBF) funded project to develop biobased yarn for various textile applications. In September 2022, he became the group leader and started supporting in project management, funding acquisition and the daily supervision of PhDs of the Polymer Engineering group.